Department of Petroleum Engineering

Experimental Study of Cuttings Transport in Coiled Tube Micro-Borehole Drilling

Hongyang Zhang

This thesis is presented for the Degree of
Doctor of Philosophy
of
Curtin University

April 2018

Declaration by author

To the best of my knowledge and belief this thesis contains no material previously published by any other person except where due acknowledgement has been made.

This thesis contains no material which has been accepted for the award of any other degree or diploma in any university.

Signature: 

Date: 5 April, 2018

Abstract

The new discovery of mineral deposits at shallow depths is declining. To address this challenge, coiled tubing drilling has been proposed for the mineral exploration by Deep Exploration Technologies Cooperative Research Centre (DET CRC). Coiled tube drilling decreases the drilling cost, which facilitates further mineral exploration. In this technology, the interpretation of the geochemistry and mineralogy relies on the cuttings. In this context, it is essential to determine the depths of cuttings to map the cuttings information in the spatial domains.

The objective of this thesis is to study the transport velocity of the mineral cuttings in the micro borehole drilled by the coiled tubing drilling technology. This research provides fundamental understanding of cuttings transport in micro borehole, which is the basis of cutting assay analysis. After review of literature review, and explaining the experimental methodology, the thesis was followed by three main studies of settling velocity, cuttings transport velocity and field tests.

The first part of the thesis studied the settling velocity of the drilled cuttings. In previous study the cuttings velocity is often assumed to be equal to the difference of the fluid velocity and the cuttings slip velocity, where the slip velocity is assumed to be equivalent to the cuttings settling velocity. The parametric analysis was performed to investigate the effects of fluids rheology, cuttings size, concentration and annulus wall effect on the cuttings settling velocity. Based on the experimental results, the correlation of the particle Reynolds number and drag coefficient was obtained, and the results presented as the "standard drag curve" for the cuttings in the micro borehole annulus (45-60 mm).

In the second part of the thesis, the cuttings transport velocity in an upward flow was studied using a state of the flow loop equipped with particle tracking velocimetry (PTV) system. The experimental results showed that the cuttings transport velocity distributed in a range, which is affected by the fluids rheology and flow rates. It was also found that the cuttings transport velocity can be higher than the fluid average velocity due to the fluid velocity distribution. The parametric analysis on the cuttings transport velocity has been investigated including various cuttings (size and concentration) and fluids properties (rheology and flow rate). By comparing the cuttings transport velocity and settling velocity, this study found that it is inaccurate to predict the cuttings transport velocity based on the slip velocity obtained from the cuttings settling, as the effects of these parameters are different and in some cases contrary. The cuttings

slip velocity was quantified for different circulating conditions such as flow rate, fluid rheology, concentration and size of the cuttings.

In addition to laboratory studies, a series of field tests were conducted using drilling rigs on a mine site located in South Australia. The cuttings transport velocity was obtained for various cuttings and fluids conditions, and it was found that the results of the field tests were in agreement with the cuttings transport velocity from PTV measurements. Other parameters such as cuttings density, drill pipe rotation and higher range flow rate were investigated in the field tests, and the results were characterised using lag time analysis of cuttings and the weight distribution on the arrival time. Furthermore, the cuttings transport experiments were performed on the coiled tube to investigated the pipe geometry effect on the cuttings velocity for the condition of coiled tube reverse circulation drilling. It was found that the cuttings size impact on the cuttings velocity was significantly different from the straight annulus.

Acknowledgements

I would like to appreciate the support of all the people in my PhD study.

I would like to express my most sincere thanks to my supervisor, Dr Masood Mostofi, who have guided me on both study and life throughout my PhD. This work would not have been completed without his supports and encouragement. His passion and hardworking as well as nice personality will always be an inspiration in my future work.

I also appreciate the help from my associate supervisor, Prof Brian Evans, for the language revision of thesis and his guidance during my PhD.

I would like to acknowledge Deep Exploration Technologies Cooperative Research centre (DET CRC) for the financial support. I learned a lot about the industrial practice and experience during the field work and conferences. This is DET CRC document 2018/1095.

Finally, special thanks to my wife for her love in everyday of my past eight years. I express my deep gratefulness to my parents and parents-in-law.

Contents

List of Figures

List of Tables

Nomenclature

F_{drag}	drag force
V_s	particle settling velocity
V_C	cuttings transport velocity
V_{slip}	cuttings slip velocity
V_f	fluid velocity
Q	flow rate
C_D	drag coefficient
Re_P	particle Reynolds number
D_P	particle diameter
D_{Sieve}	particle sieve size
D_C	cuttings depth
f	wall factor
μ	fluid viscosity
K	consistency index
n	flow behaviour index
ϕ	particle volume fraction
Ψ	particle sphericity
PTV	particle tracking velocimetry
PIV	Particle Image Velocimetry
VSD	Variable Speed Drive
DAQ	data acquisition

CCD	charge coupled device
HID	high intensity discharge
PSD	particle size distribution

Chapter 1. Introduction

1.1. Background

New discoveries of mineral deposits at shallow depths are declining in Australia [1]. In order to sustain mineral production, it is essential to develop new exploration techniques to uncover the mineral resources at deeper depths. Exploration for deeper minerals is associated with high expenses of drilling, and therefore there has been limited discoveries at higher depths in Australia [2].To address this challenge, an innovative technology of coiled tubing drilling has been developed by the Deep Exploration Technologies Cooperative Research Centre (DET CRC).

The new drilling technology is aimed at a cost effective, faster and safer drilling operation. Coiled tubing has been employed to decrease the non-production time with no requirement for the drill pipe connections and also reduces the time to retrieve the cores using wireline compared with conventional drilling. Furthermore, the drilling fluid circulation in coiled tubing drilling is continuous while drilling, which results in a more stable borehole. In the workflow of such exploration, the geochemistry and mineralogy information are analysed from the cuttings collected at the surface as opposed to the conventional method, where the core samples are collected at every rod length (typically 3m). Figure 1.1 shows the conventional rotary drilling rig that is commonly used for mineral exploration and the proposed coiled tubing drilling rig.

The main components and workflow of the coiled tubing drilling rig in DET CRC is shown in Figure 1.2. The rig is composed of a 500m coiled tube which is stored on a reel. The reel is mounted at the top of the rig to minimise additional fatigue on the coil. The bottom hole assembly (BHA) is composed of drill collars (weighting rods) and a bottom hole motor is connected to the bottom of the coiled tube. The drilling fluid is circulated through the coiled tube and drives the downhole motor to provide two modes of rotary or percussive drilling. The rotary mode is used for drilling both soft and hard formations, while the percussive drilling is deployed only for hard rock drilling.

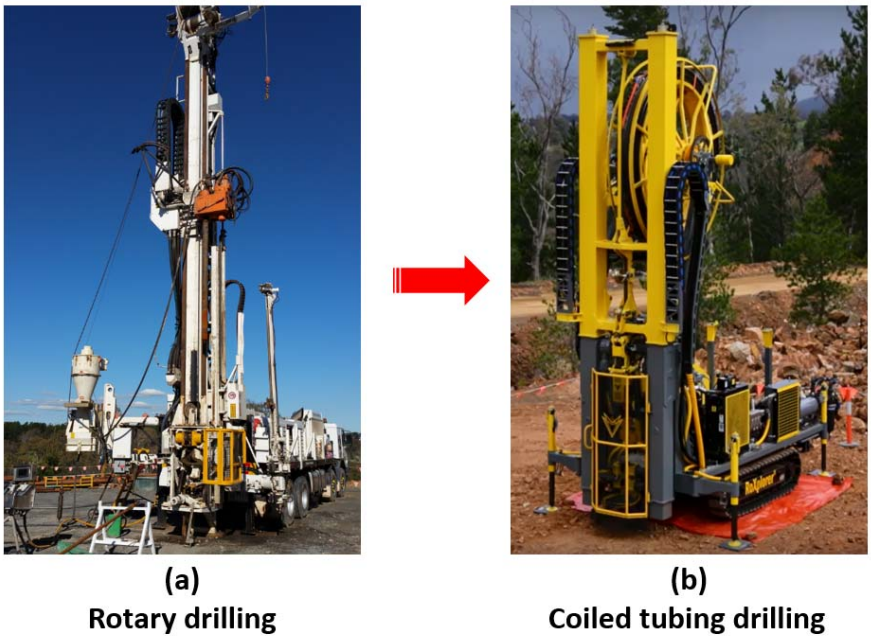

Figure 1.1 Different drilling method used for mineral exploration, (a) Rotary drilling, (b) Coiled tubing drilling [3].

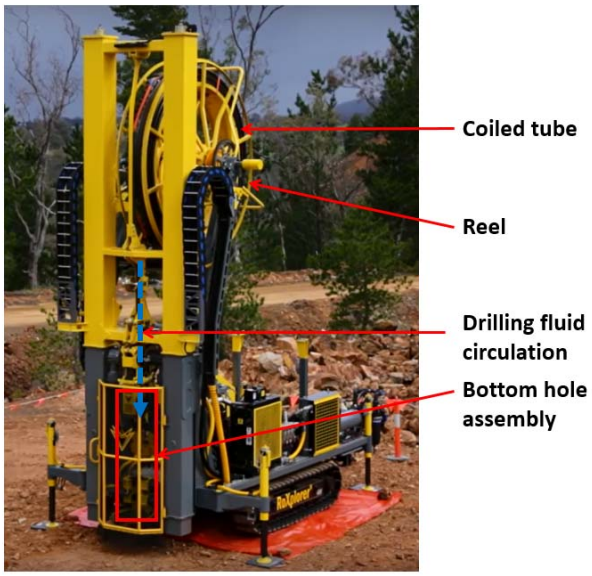

Figure 1.2 Coiled tubing drilling rig for mineral exploration: various components of the rig [3].

In the case of drilling soft formations, a positive displacement motor (PDM) is used to drive the blade bit. However for hard rock drilling, the rotary drilling mode is achieved using turbines bottom hole motors, where the hydraulic energy of the drilling fluid produces high angular velocities to provide the required angular velocity and torque for impregnated diamond bits.

Percussive drilling is achieved using a PDM to provide high torque and low rpm rotation and also a water percussive hammer to produce the percussion movement.

As there is no core recovered from the coiled tube drilling operations, the interpretation of the geochemistry and mineralogy relies on the cuttings retrieved at the surface. The cuttings are collected at surface by sampling of about 20 percent of the return using a specially designed sample splitter, while the remaining return flow is directed to solid removal units such as shale shakers, hydro-cyclones and centrifuge decanters to clean the fluid. The cuttings are separated from the sampled fluid and dried and introduced to various sensors such as XRD and XRF to infer mineralogy and geochemistry information of drilled formations.

In this context, it is essential to determine the depth location of cuttings to build a spatial domain, i.e. attributing the collected data to the depth of cuttings. This process can be performed using a depth matching process, where drilling data is used to determine the position of the bit at different depths, and fluid and cuttings properties are incorporated to estimate the cuttings transport velocity to obtain the lag time, and then the depth of cuttings.

The cuttings transport velocity has an important role in the success of determining the cuttings depths. Depending on the formation and also the drilling technique, the cuttings will have different size and densities, and as a result they will exhibit different transport velocities. Therefore, it is expected that the produced cuttings become spread (smeared) in the annulus and therefore arrive at surface at different times. Due to continuous drilling condition, where the circulation is not stopped every three meters, it can further impact the cuttings smearing. The cuttings smearing results in errors in assay interpretation. The cuttings smearing leads to attributing imprecise depths to the collected cutting, and subsequently inaccurate analysis of the concentration of minerals in the cuttings.

In addition to cuttings transport, the drilling fluid hydraulics is an important issue in the micro-borehole drilling. The fluid velocity is larger compared to conventional drilling: the borehole geometry is smaller, and the flow rate is larger than conventional mining drilling operations to provide sufficient hydraulic energy to drive the downhole motor. The smaller annulus results in higher a magnitude of friction in the annulus inducing higher pressure drop. Furthermore, the cuttings are smaller especially in the case of impregnated diamond drilling, and therefore, it is more likely to increase the fluid rheology.

In summary, several major problems have to be considered due to the change of the drilling method.

First, full-faced bits are used instead of the coring bits as. For lack of the cores, the mineral analysis including geological and depths information has to rely on the drilled cuttings, and therefore it is significant to determine the formation depths where the cuttings are originally from. The proposed solution is to calculate the cuttings original depths based on the cuttings and fluids property, cuttings transport velocity and cuttings residence time along the borehole. Since the cuttings size and density are readily obtained from the cuttings returned to the surface, and the cuttings transport time can be achieved combining the drilling data and the arrival time to the solid removal unit, the cuttings transport velocity becomes a fundamental element for determining the cuttings original location.

Second, the borehole size in traditional oil and gas drilling and mineral drilling is relatively larger, but the annulus size of the coiled tubing drilling in this research is much narrower (annulus size 45mm-60mm). Therefore it is necessary to study the cuttings transport in the micro borehole as the cuttings are more likely to get stuck compared with previous drilling.

On the other hand, since the drill pipe of coiled tubing is unable to rotate which cannot provide power to the bits, the downhole turbine must be used which needs to maintain a high flow rate. In addition, the coiled tubing is incapable of exerting large weight on the bit, and to achieve faster rate of penetration (ROP), a higher flow rate is essential in the coiled tubing drilling than conventional drilling. Although the high flow rate in the micro borehole is beneficial for the carrying capacity of the drilling fluid, it may cause more pressure losses. Thus it is also significant to study the hydraulics aspects of the cuttings transport in the coiled tubing drilling.

Another concern in mineral drilling is the cuttings smearing problem during the cuttings transport in the wellbore. The cuttings smearing refers to the phenomenon that the mineral particles produced from the same layer of the formation may not arrive to the surface simultaneously as the mineral cuttings from different formations may mix together. So the mineral content analysis based on the cuttings can generate inaccurate results because of the cuttings smearing, and therefore it is significant to study the cuttings residence time in the wellbore and the cuttings distribution on arrival time which is a function of the cuttings transport mechanism.

Furthermore, the cuttings property is also different from the oil and gas drilling cuttings which have been investigated extensively in previous research. The minerals contents usually result in larger cuttings density, while the cuttings from oil and gas drilling has the density close to the shale. The cuttings size also has an important impact on the cuttings transport. If diamond bit is selected for the coiled tubing drilling, the produced cuttings size is mostly below 500 microns, and then the fine particles can change the slurry rheology. Thus investigation about the effect of the fine cuttings on the slurry rheology is prerequisite before studying the cuttings transport through the annulus. On the other hand, when the hammer bit is chosen for the coiled tubing drilling, there is a wider cuttings size distribution, and it is critical to study the particle size influence on the cuttings motion in the solid-liquid two phase flow.

From the above discussion it can be seen that the challenge of using coiled tubing for mineral drilling has two main issues. First, the cuttings is the only representative sample of the formation, and the determination of the mineral depths location has to rely on the cuttings depths. Thus measurement of cuttings transport velocity is essential for the cuttings transport. Second, the drilling fluid and cuttings properties are different from those of conventional drilling, so understanding the hydraulics in the micro borehole is fundamental before using coiled tubing for mineral drilling.

In order to ensure the success of the new drilling technology and provide reliable quality cuttings samples, this research embarked on better understanding the cuttings transportation in micro borehole and in particular to characterise the cuttings transport velocity. The Particle Tracking Velocimetry method using a high speed camera is used to measure the cuttings transport velocity. Various parameters will be investigated including fluids properties (fluid rheology, flow rate), cuttings property (particle size, density, particle shape, cuttings concentration) and wellbore conditions (annulus wall effect, curved pipe). A series of field tests of particle tracking are conducted as well to study the cuttings residence time and distribution affected by the cuttings and fluids properties.

1.2. Shortcomings of previous studies

Although extensive research has been carried out over the last few decades on the cuttings transport and hole cleaning [4-7], further fundamental study is essential to better understand the cuttings transport in micro borehole. In particular, further study is required to investigate the cuttings transport velocity affected by a series of drilling operation parameters to determine

the cuttings depths in the spatial domain for geological and geochemistry analysis and optimise the drilling operation to provide reliable cuttings samples with minimum cuttings smearing.

The cuttings transport velocity has been used for the cuttings lag time and drilling fluid carrying capacity using parameters such as cuttings transport ratio. However, there is limited understanding of the particles travelling velocity in flowing fluids. Most of the previous study has been devoted towards the cuttings transport patterns and cleanout effect which is not necessarily related to the direct measurement of the cuttings transport velocity. In addition, the cuttings transport velocity is regarded as the difference between the fluid superficial velocity and the cuttings slip velocity, however the cuttings slip velocity is assumed to be approximately equal to the cuttings settling velocity [8, 9]. The influence of the flowing fluid on the cuttings slip velocity has been mostly neglected. The transport velocity obtained from various studies such as the cuttings lag and slip velocity even show controversial conclusions.

Furthermore, even in the field of particle mechanics, further research is required to study the effect of the fluid rheology, cuttings concentration and borehole geometry on the cuttings movement. The relationship of particle drag coefficient and Reynolds number is usually obtained from empirical correlations based on single particle settling experiments. But the impact of fluid velocity, fluid rheology and borehole geometry on the particle drag coefficient has been rarely studied.

Finally, the cuttings transport has been rarely studied on such small sized wellbore, and therefore it is critical to better understand the mineral cuttings transport in micro borehole. The cuttings in this research are quite different from that of oil and gas drilling, and the fluid velocity is drastically higher than conventional boreholes. Therefore it is essential to study the effect of fluid and cuttings properties on the cuttings transport.

1.3. Objective of the thesis

The main objective of this thesis is to investigate the cuttings transport in micro borehole coiled tubing drilling for mineral exploration.

This study especially focuses on the measurement of cuttings transport velocity, aiming at characterising the variation of cuttings transportation velocity with fluid and cuttings properties, and develop the required engineering knowledge for determining the cuttings depths location in coiled tubing drilling.

To achieve the objectives above, specific objective is accomplished in this thesis as follows:

1. To develop an effective "Particle Tracking Velocimetry" method that can measure the particle travelling velocity during the cuttings transport. The experimental setup will be used to study the effect of flow rate, fluid rheology, cuttings property, particle concentration and wellbore geometry on the cuttings transport velocity. Similar experiments will be designed and implemented on field scale where the cuttings velocity is characterised by timing the arrival of cuttings in a 130 m borehole.
2. To study the cuttings concentration effect on the fluid viscosity, which has influence on both hydraulics of micro borehole and the cuttings transport velocity.
3. To establish the relationship of the drag coefficient and particle Reynolds number based on the conventional method by studying the particle settling velocity as the slip velocity, and also to investigate the influence of the fluid rheology and wall effect on the settling velocity and drag coefficient.
4. To quantify the variation of cuttings transportation velocity under various drilling conditions such as fluid rheology, flow rate, cutting concentration and size. The investigation was carried out on both geometries of straight annulus and curved pipe (curved pipe has application for reverse circulation using coiled tube drilling technique).

1.4. Organization of the thesis

Chapter 1 introduces the background of the thesis and an overview of the proposed topic. The significance of this work, the objectives and thesis structure are presented.

In Chapter 2 a literature review of multi-disciplinary research is presented. Since the topic of the cuttings transport velocity covers extensive aspects of work, this chapter illustrates a comprehensive summary including cuttings transport, particle mechanics, fluid rheology and flow visualisation technique and particle velocity measurement. The review of the cuttings transport includes the cuttings movement pattern and various parameters affecting the minimum flow rate and pressure drop. For particle mechanics, the motion of the particles in fluids is briefly analysed, and the effect of the particle property, fluid rheology and wall effect is presented. A series of techniques used for measuring the solid-liquid two phase flow are analysed and compared, and finally the Particle Tracking Velocimetry (PTV) is selected as the measurement method for this research.

Chapter 3 introduces the experimental setup for the cuttings transport and the PTV system for the particle tracking tests. Detailed specifications of the experimental apparatus are presented. The method of preparing the test fluid and solid particles is illustrated. This chapter also introduces the method of validation and calibration for the PTV system.

Chapter 4 is focused on the cuttings settling. Experiments are performed to measure the cuttings settling velocity using PTV to establish the relationship of drag coefficient and particle Reynolds number. The parameters are investigated including the effect of the Newtonian fluid viscosity and power law fluid rheology, particle property, wall effect of annulus and cylinder pipe.

Chapter 5 extends the PTV measurement from particle settling in stationary fluid to the cuttings transport. The cuttings transport velocity is measured under the same parameters influence as Chapter 4. In addition, this chapter also studies the effect of the cuttings concentration on the fluid rheology. The slip velocity obtained in Chapter 4 are compared with the slip velocity from the cuttings transport velocity.

In Chapter 6 the work of particle tracking field tests is presented. The flow rate and particle property effect on the cuttings transport velocity is studied, and the results are compared with the experimental work. The drill pipe rotation effect on the cuttings is analysed. In addition to straight annulus experiments, a series of tests were conducted to study the transportation of cuttings in curved pipes simulating the reverse circulation condition in coiled tube drilling.

Finally Chapter 7 summarises the main conclusion of this thesis and recommendations for future work.

Chapter 2. Literature review

The topic in this research covers both conventional study on the cuttings transport and the particle velocity in the solid-liquid two phase flow. For this purpose, a literature review is presented in this chapter summarising the knowledge from multiple discipline. The study involving the solid particle movement from the cuttings transport in oil and gas drilling is reviewed, and considering the influence of the coiled tubing and mineral cuttings, previous study on the cuttings transport in coiled tubing drilling is discussed. The particle mechanics in the two phase flow is briefly introduced including particle settling, particle travelling conveyed by flow fluid and the relationship of drag coefficient and Particle Reynolds number.

2.1. Cuttings transport

2.1.1. Introduction

One of the important functions of the drilling fluid in drilling is to suspend and carry the rock fragments produced by the drill bits along the wellbore to the surface. The rock fragments are usually called cuttings, and the process of the cuttings movement in the wellbore is called cuttings transport.

Although a considerable amount of work has been conducted in the past decades, most studies on the cuttings transport were focused on the issues such as carrying capacity of drilling fluid, minimum fluid velocity for hole cleaning, and layer models of the cuttings bed movement. Limited attempts have been performed to study the particle velocity in the cuttings transport and the cuttings movement in the micro borehole.

Pigott (1941) [10] was one of the first researchers studying the cuttings transport. The viscosity of the muds were investigated for the turbulent flow. The experiments of cuttings settling was conducted to estimate the mud capacity, and the cuttings size effect was studied.

The carrying capacity of the drilling fluid was studied after it was realised that the flow rate and fluid rheology play a critical role in carrying the cuttings [11-14]. The cuttings settling velocity was investigated under various parameters condition such as cuttings size and fluid rheology. Williams and Bruce (1951) [12] studied the minimum annular velocity to remove the cuttings in vertical annulus, and investigated the influence of particle density, fluid viscosity and drill pipe rotation. It was found that the low viscosity fluid in turbulent flow was more

advantageous for cuttings removal, and the fluid carrying capacity was higher with drill pipe rotation.

The research centre in Tulsa University performed a series of experiments about the cuttings transport using a large scale flow loop [15-20]. The impacts of various parameter were investigated including drill pipe rotation, wellbore inclination and Non-Newtonian fluid and foam rheology. The hole cleaning effect such as the cuttings concentration and cuttings bed pattern was studied in these research.

Mechanical model and simulations were also performed to study the cuttings transport in vertical and horizontal wells under various drilling fluids [21-23]. The models were established from previous model of the solid liquid two phase flow, and were mostly used to analyse the cuttings patterns such as the cuttings bed height and movement velocity.

2.1.2. Flow patterns of cuttings transport

The characterization of the cuttings transport patterns arises from the investigation of the cuttings removal in inclined wellbores. The early research focused on the drilling parameters needed for the efficient hole cleaning, for example Ford (1990) [24] conducted a series of experiments studying the effect of the wellbore inclination angle and the annular fluid velocity on the borehole cleaning effect. During the hole cleaning process, it was found that the cuttings transport have various patterns of movement affected by flow rate and borehole inclinations. It was also found the cuttings movement have different mechanisms of motion including the rolling/sliding and suspension. The minimum transport velocity was proposed for the cuttings transport.

Various patterns of the slurry flow and the cuttings bed movement were identified and classified into a series of flow patterns. Previous researchers have studied the cuttings transport flow patterns for conventional drilling [24] and coiled tubing drilling [25, 26] respectively. Due to the micro borehole of coiled tubing drilling, the cuttings transport is inefficient when it is applied for high inclined or horizontal wells. And the non-rotation drill pipe makes it worse. Although there is a slight variation for the classification, most of the flow patterns defined from various work are consistent in spite of the narrow wellbore geometry of the coiled tubing.

The commonly used flow patterns of the cuttings transport are listed below summarized from the previous classification by the order of the desired borehole cleaning effect.

Homogeneous suspension

The flow rate is large enough and all of the cuttings are suspended by the drilling fluid. The cuttings are dispersed uniformly in the annular wellbore.

Heterogeneous suspension

The cuttings are still in suspension, but mostly on the lower side of the annulus. As the flow rate is not sufficient for the uniform distribution of the cuttings, the cuttings concentration appears as a gradient across the wellbore.

Moving bed

The cuttings moving bed is a general pattern containing several specific flow profiles. When the flow rate continues to decrease from the cuttings heterogeneous suspension, the cuttings begin to settle and accumulate on the lower side of the wellbore. A continuous cuttings bed is formed while the rest of the cuttings may still be in suspension, and this transition type between the cuttings suspension and the fully cuttings bed is called Suspension and Moving Bed.

With further decline of the flow rate, the cuttings in suspension will settle down thus all of the cuttings are formed as a bed covering the lower side of wellbore but moving forward, and this pattern is called the Moving Bed.

Dunes movement

The cuttings move as separated moving beds, and each part of the cuttings travels like dunes keeping a distance between each other. On each dune, the cuttings in the rear are carried by the fluid to move across the dune surface and settle down in the front, and the cuttings newly exposed to the fluids continue this kind of movement. In this way the whole dune looks like sliding and rolling simultaneously yet moving forward with the fluids, while the particles inside the dune may stay stationary.

Stationary bed

The cuttings bed is continuous settled down on the lower side of the wellbore, and the fluids flow rate is not sufficient to suspend any cuttings.

2.1.3. Cuttings transport in coiled tubing drilling

Coiled tubing has been used as a well intervention tool in oil and gas wells for cleanout and stimulation, and later has been applied as a reliable method for re-entry operations to deepen wellbores [27] and drilling underbalanced wells [28, 29].

The cuttings transport for the coiled tubing drilling is distinct due to the difference from rotary drilling. First, the annulus space is narrow compared to the conventional drilling. Although earlier research has discussed about the cuttings transport problems for slim holes or micro-borehole, the wellbore dimension is still much larger than that of the coiled tubing borehole for mineral drilling. For example, the diameters of the slim-hole wells are 6in [30], 124mm [31] and 4.75in [32] in the previous study for oil and gas drilling. However, the size of the wellbore in this thesis is only 45mm-60mm. In addition, the most critical aspect for the coiled tubing drilling is that the drill pipe cannot rotate, which provide extra carrying capacity in rotary drilling.

Limited studies have been carried out to address the cuttings transport especially for coiled tubing drilling. Most literatures on coiled tubing drilling presented the application for oil and gas [27, 28, 33-40].

The drilling fluid circulation in coiled tubing drilling has limits in hydraulics [41]. Minimum flow rate is decided by the pressure drop on the annulus, and is related with the hole cleaning problems. The cuttings transport was estimated by the minimum flow rate using annular velocity. The maximum flow rate is dependent on the downhole motor, resulting in more pressure loss. It was found that the pressure drop through the coiled tube is large than the straight annulus by 11-17% [42].

Kamyab [26, 43] conducted a series of experiments using flow loop and simulations to study the transportation of mineral cuttings in micro borehole. The effect of the cuttings size and drilling fluid rheology on the minimum transport velocity was investigated. The patterns of the cuttings transport including several types of cuttings bed were observed and categorised. The pressure drop on the annulus due to rheology change caused by the minerals was investigated.

The cuttings bed movement of two and three layers were also studied in other research for coiled tubing drilling [25]. Critical flow rate to move the cuttings bed was studied effected by the cuttings size and fluid rheology, and the corresponding shear stress on the annulus wall was

obtained [44]. It was found that the cuttings size impact was less significant than the fluid rheology.

In addition to the experiments, numerical simulations and various models were used to study the cuttings transport for coiled tube drilling. However, most studies still used the correlations based on the particle settling when establishing the models.

Cho et al (2002) [45] analysed the forces on the cuttings transport and developed a three layer model. However it was assumed that there is no slip between the fluid and the cuttings. The model was used to study the effect of fluid annular velocity and fluid rheology on the cuttings bed and the cuttings concentration in the annulus under various inclinations.

Leising and Walton (2002) [46] reviewed the hole cleaning problem in coiled tubing drilling. The hole cleaning model was proposed to estimate the carrying capacity of high low-shear-rate-viscosity muds in micro horizontal wellbores. Turbulent flow was estimated using annular velocity as well. A case study was performed and it was concluded that the low viscosity fluid in turbulent flow is more effective in terms of carrying the cuttings and hole cleaning than high-viscosity fluid in laminar flow.

Kelessidis (2003) [25] proposed two models of two layer and three layer for the steady cuttings transport in horizontal annulus for coiled tubing drilling. The cuttings are suspended in the upper layer. However the drag coefficient used in the models was based on the single particle settling. The minimum fluid velocity which can suspend the cuttings was obtained using the models. But the results were inaccurate due to various parameters such as the cuttings concentrations.

Kamyab and Rasouli (2016) [26] investigated the patterns of the cuttings transportation in coiled tubing drilling using CFD. The cuttings Boycott movement was observed. The cuttings concentration distribution and the cuttings velocity of the cuttings bed were studied for inclined annulus.

2.2. Cuttings transport velocity

The main objective of this research is to obtain the cuttings transport velocity in annulus. A number of studies have been reviewed related to the cuttings movement in fluid and solid liquid two phase flow. It was found that there were various topics indirectly related to the cuttings

transport velocity, which were controversial in some cases. Therefore this section summarises the study on the cuttings transport velocity from multi-disciplinary fields.

2.2.1. Particle settling velocity

The cuttings transport velocity is assumed to be the difference of the fluid annular velocity and the cuttings lip velocity, and the cutting slip velocity was usually assumed approximately to be equal to the cuttings settling velocity [8, 9]. The settling velocity of particle is presented below.

A particle settling through stationary fluid media will reach its constant terminal velocity. When the process is at balance, the sum of the forces exerted on the particle is zero, which is expressed as:

$$F_{drag} = W - F_b \quad \text{(Equation 2.1)}$$

where, W is the particle weight, F_b is the buoyancy force on the particle by fluid, and F_{drag} is the drag force on the particle by fluid acting opposite to the particle settling velocity, which is defined as [47]:

$$F_{drag} = \frac{C_D A \rho_f {V_s}^2}{2} \quad \text{(Equation 2.2)}$$

Where V_s is the particle settling velocity, C_D is the drag coefficient, A is the spherical area, and ρ_f is the fluid density.

Assuming the particle is a sphere, and combining Equation 2.1 and 2.2, then we have:

$$\frac{C_D \pi {D_P}^2 \rho_f {V_s}^2}{8} = \frac{\pi {D_P}^3}{6}(\rho_P - \rho_f)g \quad \text{(Equation 2.3)}$$

Then the particle settling is obtained as:

$$V_s = \sqrt{\frac{4D_P(\rho_P - \rho_f)g}{3C_D\rho_f}} \quad \text{(Equation 2.4)}$$

And the drag coefficient is written in another form:

$$C_D = \frac{4D_P(\rho_P - \rho_f)g}{3\rho_f {V_s}^2} \quad \text{(Equation 2.5)}$$

It can be seen from the equation 2.4, once the drag coefficient C_D is given, the particle settling can be easily calculated. However the drag coefficient is a function of Particle Reynolds

Number. The Particle Reynolds Number is:

$$Re_P = \frac{D_P V_s \rho_f}{\mu} \quad \text{(Equation 2.6)}$$

where D_P is the particle diameter, and μ is the Newtonian fluid viscosity.

For power law fluid, the viscosity of Newtonian fluid in Equation 2.6 is replaced with the viscosity corresponding to the characteristic shear rate on the particle, which can be approximately equal to the settling shear rate of the shear rate $\frac{V_s}{D_P}$. Thus Equation 2.6 is expressed as Equation 2.7 for power law fluid.

$$Re_P = \frac{\rho_f {V_s}^{2-n} {D_P}^n}{K} \quad \text{(Equation 2.7)}$$

Where *K* is the consistency index, and *n* is the flow behaviour index in the power law model $\tau = K\gamma^n$.

Tremendous experimental work has been performed in the last decades to study the particle settling in stationary fluid, and various parameter were investigated including the particle property, fluid rheology, particles concentration and the wall effect. The experimental results showed that the settling velocity at concentrations was reduced due to the hindered settling effect [48-53]. The research on the wall effect showed that the particle velocity decreased due to the confining effect of the cylindrical tube [54-57].

2.2.2. The relationship of drag coefficient and particle Reynolds number

Based on the particle settling velocity, the drag coefficient can be obtained, and there are three regimes roughly according to the range of the Particle Reynolds Number range.

Laminar regime:

For Re_P < 0.1, approximately, the particle is settling in creeping flow. For spherical particle, the drag force can be written using the Stokes' Law:

$$F_{drag} = 3\pi D_P \mu V_s \quad \text{(Equation 2.8)}$$

Then the particle settling velocity is:

$$V_s = \frac{{D_P}^2 (\rho_P - \rho_f) g}{18\mu} \quad \text{(Equation 2.9)}$$

The drag coefficient for laminar flow is:

$$C_D = \frac{24}{Re_P} \quad \text{(Equation 2.10)}$$

Intermediate regime:

When the particle Reynolds number is between 1 and 1000 approximately, the drag coefficient can't be expressed theoretically, and this regime is regarded as intermediate regime [47]. Prediction of the particle settling velocity in this regime mainly depend on the empirical correlations based on the huge amount of data from particle settling experiments [58].

Most particle settling process encountered in industrial application including drilling cuttings settling falls into the intermediate regime. Therefore numerous drag correlation have been proposed aiming at the different process considering the fluid, particle property and wall effect.

Various correlations of the drag coefficient have been proposed based on the particle settling [59-63].

Turbulent regime:

When the flow is turbulent, the drag coefficient is almost constant. This value is usually regarded as 0.44 for spherical particle [64].

Due to the particle shape of drill cuttings, Moore's experiments using shale cuttings in wellbore suggested that the drag coefficient is around 1.5 for particle Reynolds number larger than 2000 [65], and similarly, Chien recommended the used of 1.72 as drag coefficient for turbulent flow [8].

2.2.3. Particle transport velocity

2.2.3.1. Particle slip velocity

As mentioned earlier, particle slip velocity is defined as the difference of fluid velocity and particle transport velocity, and the slip velocity was often assumed to be approximately equal to the particle settling velocity. It might be accurate enough to evaluate the hole cleaning, but not precise to determine the cuttings transport velocity. The misuse of the settling velocity as slip velocity was pointed out explicitly by explaining that the slip velocity is only under the flowing fluid condition [13].

As it is difficult to directly measure the particle transport velocity in flowing fluid due to the experimental technique limitation, most previous research studied the particle settling. These research attempted to interpret the slip velocity based on the relative motion between the particle and fluid for stationary fluid.

For example, the experiment of Sample and Bourgoyne found that the slip velocity is independent of the fluid velocity when the fluid velocity is under 120ft/min [14]. The cuttings transport and hole cleaning in the annulus was estimated using Stokes' law [46], which is only accurate for the cuttings settling velocity of single particle for very fine particles.

As the new measurement technique has been used for the solid liquid two phased flow, some research investigated the particle slip velocity under dynamic conditions, i.e. the fluid is flowing.

Ghatage et al (2013) studied the slip velocity of particles and bubbles in fluidized bed. The particle concentrations impact on the slip velocity was studied [66]. It was found the slip velocity for hindered settling could be as low as 20% of the prediction. The study concluded that the drag coefficient increases for the particle slip velocity under fluid flowing condition due to the turbulence.

More experiments using camera measurement were conducted on the particles slip velocity when the fluid was flowing and carrying the particles. Although most research were performed especially for fluidized bed or the minimum flow rate to suspend the particle in pipe, which was not the case for the cuttings transport along with the carrying fluids, these research still proved that the characters such as turbulence of the flow in certain column and the particle concentration play a critical role in the particle slip velocity. The empirical equation of the particle slip velocity was proposed for fluidized bed, and the particles concentration was considered [67].

The experiments were conducted to study the particle slip velocity in pipe flow [68]. The fluid of both counter-current and co-current flow were investigated, and the wall effect on the particle velocity was studied. The results were compared with the particle settling, and the comparison showed that the slip velocity decreased with the increase of water velocity. The drag coefficient for the particle transport in upward flow was higher than the previous correlations of drag coefficient and Reynolds number from the particle settling. However, in

other research it was found that the drag coefficients of the particle in upward flow were in agreement with previous correlations [69].

It was realized that the impact of the flowing fluid is significant on the particle movement. More research was devoted to measuring the particle transport or slip velocity to develop new correlation of the particle drag coefficient and Reynolds number for various fluids and particle properties.

The drag coefficient was studied for spherical particles and it was found the results were higher by 50% than previous correlations, which was possibly due to the viscous flow effects [70]. The spherical particles suspended in vertical tube was studied, and the results showed that the drag coefficient was increased by the wall effect between the pipe wall and the particle surface [71]. The research concluded that the particles movement in cylindrical pipes were quite different from the particle settling, and the previous study based on the settling particles cannot be used for the particles transport. Similar work about the wall effect on the particle drag coefficient was also studied in other research [72]. The drag force was analysed for cubic particle in pipe flow [73]. It was found that the drag force was a function of the superficial fluid velocity.

The slip velocity in turbulent flow was studied using PIV. The fluid velocity distribution was obtained and compared with the particle velocity. It was found that the drag coefficient based on the experimental measurement could not match the previous correlations [74]. The particle slip velocity studied in solid liquid stirred tanks. It was found that the slip velocity was affected by the particle density. Also, the slip velocity decreased in the high shear region [75].

Some research studied the relative motion of particle and fluid using bubbles rising in stationary fluids, instead of the cuttings suspended in flowing fluids. The effect of Non-Newtonian fluid was investigated for the bubble rising in wellbore [76]. Similar study on the drag coefficient of rising particle was done in other research [77]. It was generally believed that the drag coefficient for rising follows the settling particles, however, some work concluded that the free rising particle did not obey the settling particles [78].

Some research were devoted to study the slip velocity in gas solid two phase flow. Early in 1974 the experiments were perform to study the particle transport slip velocity in vertical pipes [79]. It was found that for low flow rate of air, the particle slip velocity was almost the same as the settling velocity. But the slip velocity increased due to the wall effect and flow rate. The

slip velocity become lager for small diameter tubes. For a horizontal pipe, it was qualitatively concluded that the particle lag, i.e. the slip velocity was substantial, and affected by the particle shape [80]. The experiments of particle slip velocity and dispersion showed that the particles were significantly slow around the pipe bends [81]. The particle close to the pipe wall was found to have a bigger slip velocity, and the particle slip velocity was in agreement with previous correlations [82]. This result showed that the wall effect is important and the gas of fluid velocity distribution has impacts on the particle velocity.

A large quantity of work of both particles settling and particles movement in flowing fluid have been reviewed by Clift (2005) and Chhabra (2006) [59, 83]. In their review, the particle settling have been explained. The results from theoretical and experimental work were discussed about the various parameters impacts on the particle velocity and the drag coefficient, such as the influence of particles concentration and wall effect. However, the particle mechanics of the solid liquid flow was still not clear in some aspects.

2.2.3.2. Cuttings transport ratio

The cuttings transport ratio is defined as the ratio of the cuttings transport velocity to the average annular velocity of the drilling fluid:

$$F_{\mathrm{T}} = \frac{\bar{V}_C}{\bar{V}_f} = \frac{\bar{V}_f - V_{slip}}{\bar{V}_f} \qquad \text{(Equation 2.11)}$$

It's worthy to note that the average velocity is the flow rate divided by the cross section area which is $\bar{V}_f = \frac{Q}{A}$, but the maximum fluid velocity in the middle of the flow field is higher than the average velocity based on the fluid velocity distribution.

The cuttings transport ratio is commonly used as the evaluation of the drilling fluid carrying capacity, because the ratio decrease indicates an increase of the cuttings concentration in the annulus, which means the cuttings are not removed efficiently. Although the cuttings transport ratio by its definition is an indirect reflection of the particle transport velocity, the previous research seldom correlates it to the cuttings velocity.

The minimum annular velocity was suggested to be twice of the cuttings settling velocity, i.e the cuttings transport ratio was 0.5 [11]. The transport ratio obtained from the work of Sample and Bourgoyne [14] was linear with the reciprocal of the fluid velocity, which actually assumed that the cuttings slip velocity is constant. They summarized the work from other researchers

and then drew the data in the same plot. The enormous distinction illustrates that the fluid velocity and wellbore geometry have a significant effect on the ratio, and it is difficult to determine the cuttings transport velocity by referring to the relationship of transport ratio and fluid velocity.

Other researchers also involved the transport ratio in their studies related to the cuttings transport. For example, Sifferman et al. (1974) was among the first researchers that have experimentally investigated the cuttings transport ratio by measuring the particle concentration, and the influence was systematically studied by a series of parameters including the fluid annular velocity, fluid viscosity and density, cuttings size and drill pipe rotation RPM [9, 11]. Walker et al. (2000) used similar methods to study the ratio in coiled tube drilling with 15 degree from vertical and found the ratio is always smaller than 0.4 [84]. Tomren et al. (1986) in his experiment noticed that the transport ratio for turbulent flow is larger than 1, and the ratio increased to 1.4 for annulus inclination of 40 degree [85].

2.2.3.3. Cuttings lag

Cuttings lag is the application of the cuttings slip velocity in drilling, and the lag diagram has been analysed for determining the cuttings source [86]. Garcia-Hernandez et al. (2007) used a camera system to measure the travel time of the marked cutting through the annulus, and concluded that the cuttings lag was 40% of the fluid velocity [86]. The velocity of the cuttings moving bed was measured effected by the fluid velocity, fluid type and drill pipe rotation.

The determination of the cuttings original depth is analysed below. Figure 2.1 shows the cuttings transport in vertical well. The cuttings are produced at the depth of D_C, and transported to the surface at a constant velocity of V_C. When the cuttings are collected at the surface, the drill bit has reached the depth of D_{Bit}.

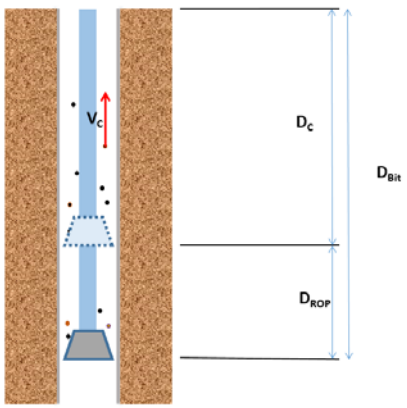

Figure 2.1 Determination of the cuttings depth.

The depth of the cuttings location is equal to the distance that the bit has moved, which can be expressed as

$$\frac{D_C}{V_C} = \frac{D_{ROP}}{\overline{ROP}} \quad \text{(Equation 2.12)}$$

where $\overline{ROP}$ is the average rate of the penetration, and D_{ROP} is the travel distance of the drill bit, which is

$$D_{ROP} = D_{Bit} - D_C \quad \text{(Equation 2.13)}$$

Combining Equation 2.13 and 2.14, the original depth of the cuttings is derived:

$$D_C = \frac{D_{Bit} \times V_C}{V_C + \overline{ROP}} \quad \text{(Equation 2.14)}$$

In this equation, the cuttings transport velocity V_C is a constant which is affected by the fluid and cuttings properties, and wellbore geometry.

2.3. Effect of solid particle on fluid rheology

One of the main drilling fluids function is to clean the cuttings out of the wellbore, and therefore the drilled cuttings and drilling fluid form a mixture. The particles will settle down in the slurry when the fluid is stationary, and aiming at the settling behaviour, experiments were conducted on the critical flow rate of various fluids to suspend the cuttings, which is review in last section. However, when the fluid viscosity is high enough and especially the cuttings is fine, the mixture will form a suspension. The solid settling velocity is extremely small in the suspension, thus it can be quite stable and uniform for a long time. The difference of the suspension from the slurry has a significant influence on the drilling fluids property and hydraulics.

The stability of the drilling fluid and cuttings mixture is different from the traditional suspensions stabilization, which usually deals with the nanoparticles and thus has to consider van der Waals forces and surfactant layer on solid surfaces. As the particle concentration increases, the surfactant molecules position would change, resulting in the suspensions property change such as yield stress and rheology [47].

As polymer is one of the main drilling fluid components used for the current CT drilling in DET CRC, so another problem need for consideration is the relationship of the particle and polymer solutions. Previous research has demonstrated that, when the polymer molecular weights are small, the polymer chain can't envelop the solid completely and the particles intend to form clusters with larger size [47], while the larger polymer molecular weights lead to small sized clusters due to the better coverage of the particles.

The main influence of the cuttings existence on the drilling fluid slurry or suspensions is the change of the rheology and the consequent pressure drop. Both the particle size and concentration have an effect on the mixture viscosity. For the cuttings transport in drilling, it's usually regarded that the coarse particles don't influence the bulk fluids viscosity much, and the slurry viscosity is assumed to be the same as the single-phased fluid [87]. But the small sized rock cuttings are found to have a significant impact on the fluids rheology [43].

Previous research on the particle effect on the fluids viscosity is focused on the concentrated fluids, in which the particles volume fraction is much higher than the cuttings concentration used in the drilling that is normally maintained below 5% [25]. For the concentrated solid liquid mixtures, as the shear rate increases, a shear thinning behaviour is observed at first and then switches into shear thickening. The experiments of polymer solution and particle demonstrates that the apparent viscosity of the mixture keeps unchanged for low shear rate, and for high shear rate the viscosity stays a constant with the variation of the shear rate, like Newtonian fluid [47].

The viscosity of the suspensions is sensitive to the particles concentration, and can be expressed by Einstein equation listed below. In 1906 Einstein obtained the viscosity change of dilute suspensions affected by spherical particles based on the Newtonian fluid. Einstein equation assumes no interaction between the particles within the fluids, so it is only applicable for low volume fraction.

$$\eta = \mu_0(1 + 2.5\phi) \qquad \text{(Equation 2.15)}$$

Where, η is the viscosity of the suspension, μ_0 is the viscosity of the original fluid, and ϕ is the volume fraction of the solid particles.

Experimental results often deviate from the theory, and more empirical correlations are proposed. The Krieger-Dougherty equation showed its applicability for a wide range of suspensions [88].

$$\eta_{\mathrm{r}} = (1 - \frac{\phi}{\phi_{\mathrm{m}}})^{-[\eta]\phi_{\mathrm{m}}} \quad \text{(Equation 2.16)}$$

In which, $\eta_{\mathrm{r}} = \eta/\mu_0$ is called the relative viscosity defined, ϕ_{m} is the maximum fraction allowed by the suspension, and is a function of the particle shape and size distribution, $[\eta]$ is called the intrinsic viscosity, which is 2.5 for spherical particles.

Similar models are suggested by Quemada [89], which is

$$\eta_{\mathrm{r}} = (1 - \frac{\phi}{\phi_{\mathrm{m}}})^{-2} \quad \text{(Equation 2.17)}$$

Various research have been performed to investigate the rheology of the concentrated suspensions aiming at different fluids [90-94]. Rotational cylinder rheometer is often used to study the influence of the particle size and volume fraction on the suspensions viscosity [95]. However none of the studies meets the requirement of the cuttings effect on the polymer drilling fluids viscosity due to the cuttings unique property and fluids components difference. Although in the field of drilling, the cuttings size has been investigated together with the fluid viscosity, these research is more focused on the effect on the cuttings transport, for example the minimum flow rate to initiate the cuttings movement [84] or the cuttings removal problem [96].

Chapter 3. Methodology

3.1. Introduction

This chapter mainly introduces the research methodology for the cuttings transport in the annular wellbore and the measurement of the cuttings transport velocity.

To better understand the cuttings transport velocity, a series of experiments were conducted in this research to study the impact of fluids and cuttings properties on the transportation of cuttings. The experiments mainly contain two aspects of investigation, which is particle velocimetry and cuttings transport. Particle velocimetry refers to the measurement of the particle velocity in stationery fluids (particle settling velocity) and particle travelling velocity conveyed by moving fluid, i.e. during the process of the cuttings transport.

A flow loop was designed and modified to conduct experimental work on the cuttings transport with an online non-intrusive measurement system using a high speed camera. Online particle feeding devices were installed, enabling the flow loop to adjust the particle volume fraction or concentration accurately. The method of preparing the test materials and measuring the particles and fluids properties are provided as well. As the experimental results are highly dependent on the accuracy of the high speed camera measurement, the calibration method is provided as well in the end of the chapter.

3.2. Experimental setups

The cuttings transport experiments are conducted in the transparent conduits on flow loop, where the cuttings travelling velocity is measured with the high speed camera using and particle tracking velocimetry (PTV).

A detailed description of the apparatus is presented below.

3.2.1. Flow loop

The flow loop is a large scale slurry system which simulates the flow of various types of fluids and particles under different experimental conditions.

Figure 3.1 shows the schematic diagram of the flow loop. The flow loop consists of: 1) pump and piping system, 2) cuttings injection and separation system, 3) test section, 4) data acquisition and control system. The main valves positions are marked in the figure as well to

explain the experimental procedure in later sections. An overview of the flow loop is demonstrated in Figure 3.2.

Figure 3.1 presents the overall circulation of the cuttings transport. The fluid is prepared in the storage tank, and pumped into the pipeline system using the centrifugal slurry pump. The cuttings are introduced to the fluid stream using cuttings injection system. The flow rate of the slurry mixture is measured using a magnetic flow meter. When the slurry flows through the test section, the pressure drop is measured using two precise pressure sensors and transportation of cuttings is captured by the high speed camera. The test section can have different inclinations from vertical to horizontal. The return fluid before flowing back to the tank is passed through a set of hydro-cyclones and filter to separate the solid particle. The collected cuttings are used for cuttings concentration measurement. At the end, the fluid returns to the storage tank for the next circulation round.

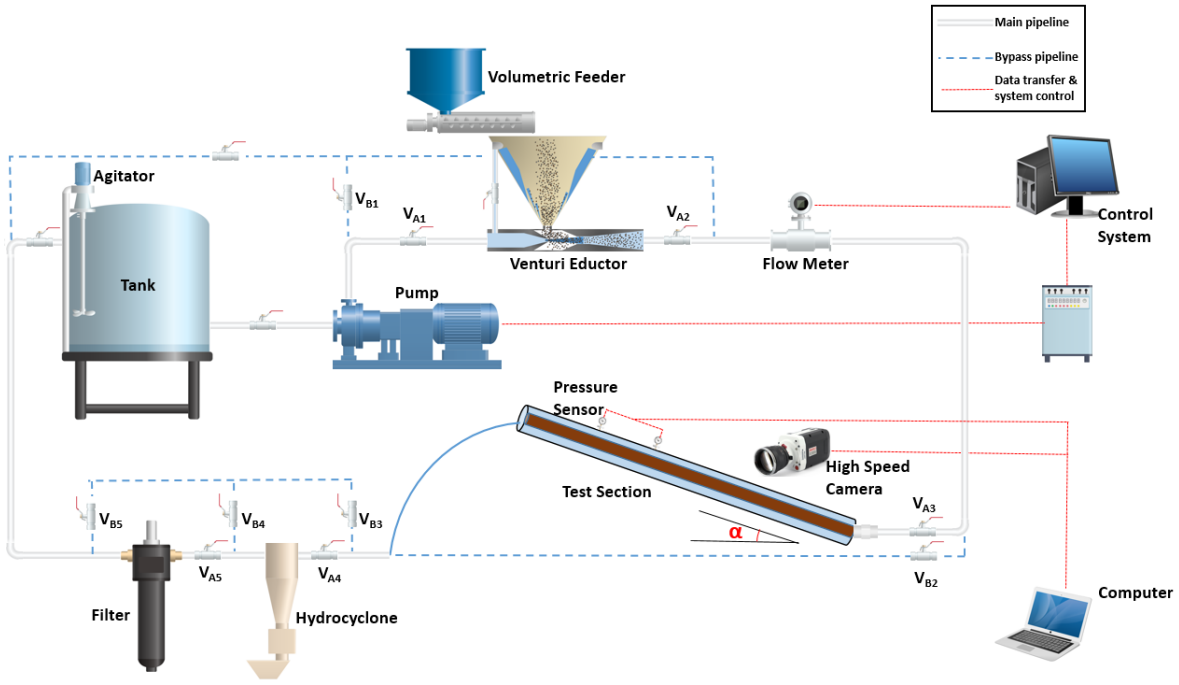

Figure 3.1 Schematic diagram of the flow loop.

Figure 3.2 Overview of the flow loop.

Pump and piping system

Pump and piping system is used for circulating the test fluids and adjusting the flow rate by control of the valves and bypass combination.

Figure 3.3 shows the storage tank with a capacity of 1200 L. A 1.5kW agitator is installed on top of the tank which is used to prepare the test fluid.

Figure 3.3 The storage tank with the agitator.

A slurry centrifugal pump is used to pump the test fluid in the system (Figure 3.4). A Variable Speed Drive (VSD) is used to control the frequency of the pump to adjust the flow rate.

Figure 3.4 Centrifugal pump and VSD.

The pipeline between the pump and the test section is made of PVC pipes with an inner diameter (ID) of 40mm. The pipe internal diameter is specially selected to establish a similar average fluid velocity in the pipeline as the test section (annulus 45-60 mm) to minimise the entrance effect and particles settlement.

A Siemens magnetic flowmeter is installed before the test section, see Figure 3.5. The sensor accuracy is 0.5% of the full range from 0 to 1500 l/min. The flowmeter can measure the total flow rate of the fluids including the cuttings.

Figure 3.5 The magnetic flow meter.

Cuttings injection and separation system

In order to accurately control the particles injection rate, the particles are injected using a system consisting of a volumetric auger feeder and Venturi eductor with a funnel.

Figure 3.6 illustrates the volumetric feeder and the eductor. The system is installed before the flow meter so that it can measure the total flow rate including the solid phase. The feeder is set above the funnel of the eductor. The particles are loaded into the storage box of the feeder, and then a horizontal auger will transfer the particles through a tube to the top of the funnel. The cuttings feeding rate is adjusted by changing the auger rotation speed, which will be set for each sized particle. The funnel has a capacity of 50 litres, which is large enough for sufficient cuttings and fluids required for one test.

Figure 3.6 Volumetric auger feeder and Venturi eductor.

When the particles are fed into the funnel, the eductor introduces them into the fluid passing it. As shown in Figure 3.7, the working principle of the Venturi eductor is that when a fluid is flowing through the nozzle inside the eductor, based on the Bernoulli Principle the pressure in the chamber is lower than the atmospheric pressure, and therefore the particles will be sucked into the eductor. Three fluid bypasses are connected to the funnel to facilitate the flow of cuttings to the stream, and also to prevent adding air to the system by maintaining a level of fluids in the funnel.

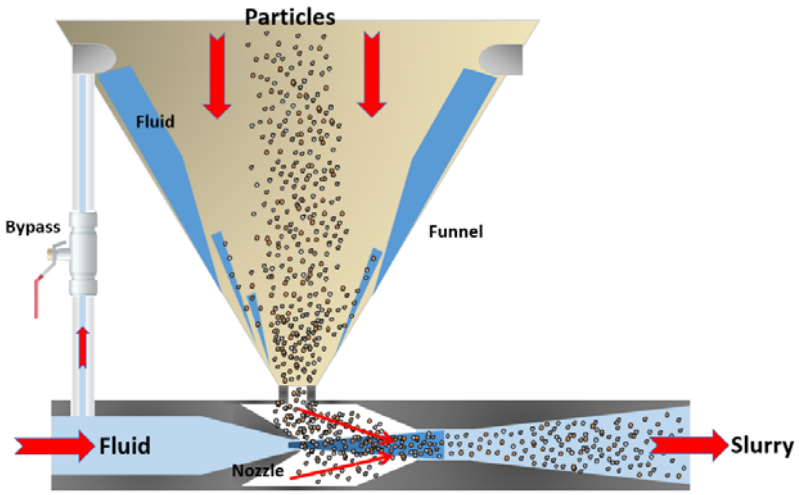

Figure 3.7 Working principle of the Venturi eductor.

After the test section, the cuttings are separated by the combination of hydrocyclones and filters, shown in Figure 3.8. The advantages of the particles removal are: 1) the particles are removed before entering the storage tank to avoid them being introduced into the flow loop again to cause interference for the cuttings concentration. 2) The field cuttings can be recycled using drying and sieving. The particle size distribution and weight are measured. Measurement of the cuttings weight is used to determine the overall particle concentration for comparison with the cuttings injection rate. The weight is also used to calculate the cuttings bed amount in the test section during the cuttings transport experiment.

Figure 3.8 Hydrocyclons and filters.

Test section

The test section is removable and can be installed on the flow loop depending on the experimental objective. There are annular and cylindrical pipes to choose to investigate the

wall effect. The annular configurations are 45 mm-60 mm and 45 mm-80 mm, and the ID of cylinder pipe are 60mm and 80mm.

The 45 mm-60 mm annulus is the main interest of this research because it has exactly the same size as the real coiled tubing used in the DET CRC project. The inner pipe of the annulus can be PVC or the real coiled tubing pipe with an outer diameter (OD) of 45mm, shown in Figure 3.9. PVC pipe is usually installed for particle velocity measurements as PVC provides a more transparent flow condition, unlike the steel pipe which produces lots of rust due to corrosion. On the other hand, the coiled tubing inner pipe is more for testing the cuttings transport because it simulates a more real flow condition by providing the same roughness. The outer pipe of the annulus has an ID of 60mm and is made by acrylic. The transparent wall of the outer pipe is convenient for the high speed camera measurement of the particle movement inside the annulus during the particle tracking experiment, and also it allows for the observation of the cuttings movement pattern, such as cuttings bed for the cuttings transport test.

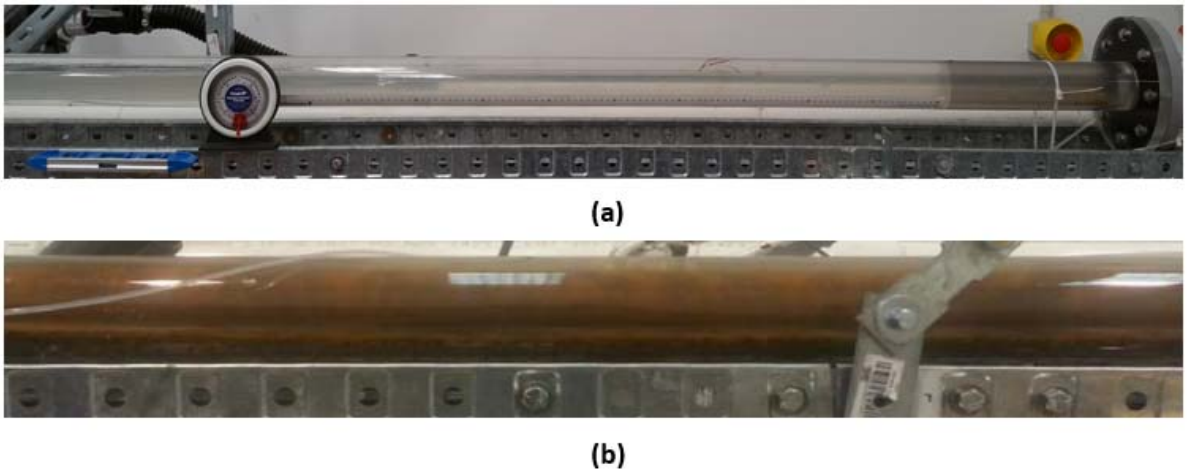

Figure 3.9 Annular test section, (a) PVC inner pipe, (b) coiled tubing inner pipe.

Figure 3.10 demonstrates the cross section of the annulus entrance. It can be seen that the fluid enters the annulus straight from the pipe connecting the annulus. This entrance design can relieve the entrance effect most, so the particles can go through the openings without changing movement direction. The way of particle entering ensures that the cuttings will reach the stable terminal transport velocity in minimum time, reducing the measurement error of particle velocity.

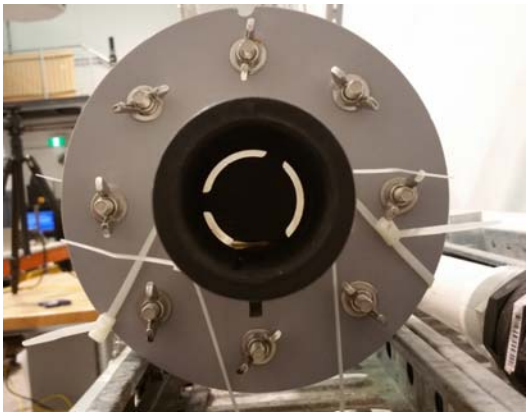

Figure 3.10 The cross section of annulus inlet.

The test section can be adjusted at different angles from horizontal (0°) to vertical (90°) to investigate the influence of borehole inclination on the slurry pattern. A protractor is attached on the frame of the test section. A precise ruler is fixed on the annulus to determine the particle movement displacement and calibration of the accurate length standing for each pixel in the images.

The test section of both annular and cylindrical pipe has a length of 4 meters, which is long enough to obtain a fully developed flow for the slurry. As shown in Figure 3.11, the location of the high speed camera and the pressure sensors on the test section is marked. According to the entrance effect [97], the length required for stable flow is 0.37 m for water flow of 2m/s, and the transition influence at the entrance is less for viscos fluids.

Two pressure sensors with an accuracy of 0.1% of the full range are installed on the rear part of the test section with a distance of 1m, where the flow is fully developed and the entrance effect can be ignored. The sensors are used to determine whether the slurry flow has reached steady and to measure the differential pressure of the cuttings transport. Two sets of sensors with 1Bar and 5Bar are used depending on the fluid pressure in the test section. The bios of sensors are measured before and after each test to accurately measure the pressure drop.

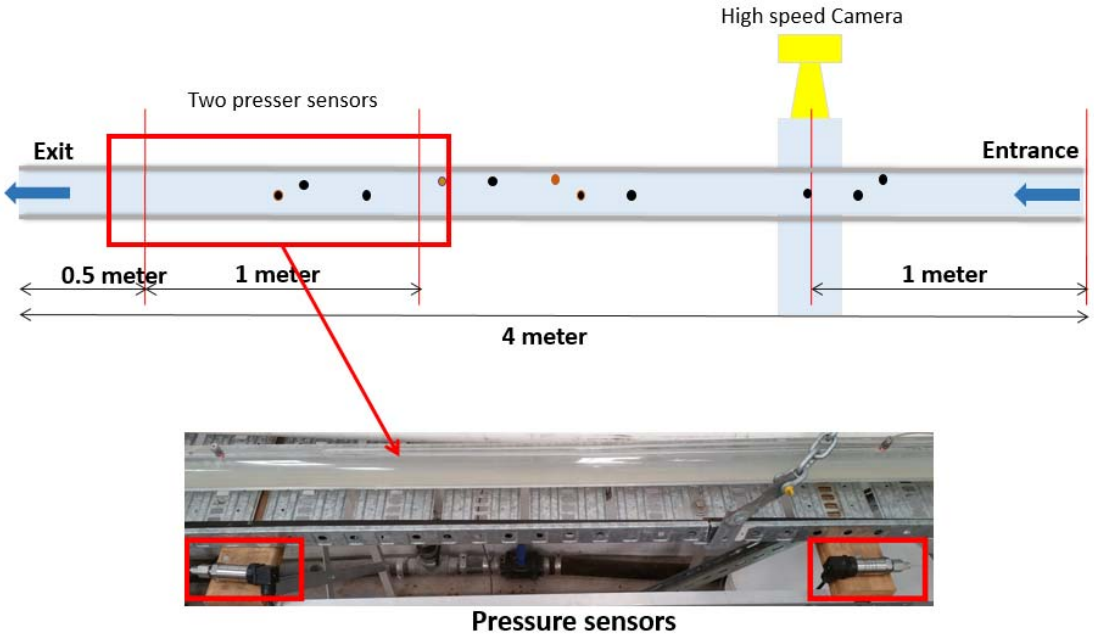

Figure 3.11 Pressure sensors on the flow loop.

Data acquisition and control system

Two sets of data acquisition (DAQ) systems are installed on the flow loop. One is connected to the pump VSD device to read the pump pressure, flow rate and pressure drop. Another set of HBM Quantum data acquisition instruments is installed on a laptop which is able to receive the data and control the high speed the camera at the same time.

The pump frequency can be directly adjusted by the VSD Local Mode, or the DAQ system can remotely control the pump. The pump start/shut off can be performed through VSD, and a threshold pressure value can be set to automatically stop the pump in case that the pressure in the flow loop is too high. The data acquisition and pump control are integrated in one system.

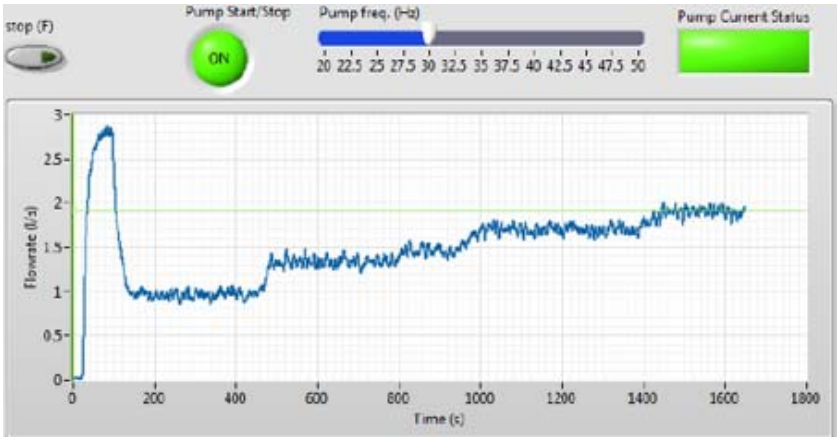

Figure 3.12 Data acquisition system.

Figure 3.12 shows the set of the data acquisition which is also used to receive the signals from flow meter and pressure sensors. Its advantage is that the data software is installed on a laptop set next to the annular test section, which makes it convenient to observe the cuttings transport in the test section and operate the DAQ system at the same time. All the data from the DAQ is saved in Matlab format for later analysis. A timing line set in the software of the DAQ can help to match the time of conducting experiments, for example the differential pressure or flow rate when the video of particle tracking is captured.

3.2.2. Particle Tracking Velocimetry (PTV) setup

A PTV setup is established on the flow loop to measure the cuttings transport velocity. The system is composed of a high speed camera, light source and image analysis software. Figure 3.13 illustrates the schematic diagram of the experimental setup.

Two test columns are used in the PTV. One is the annular or cylinder pipe installed on the flow loop which is used to test the cuttings conveyed by the upward flowing fluids. The other is set independently for the single particle settling tests.

It is worth pointing out that a High Intensity Discharge light is employed in this research other than the laser which is usually used in conventional PIV or PTV. The specification details of the facilities are presented below. Figure 3.14 presents the PTV setup for measurement of the cuttings transport velocity on the flow loop.

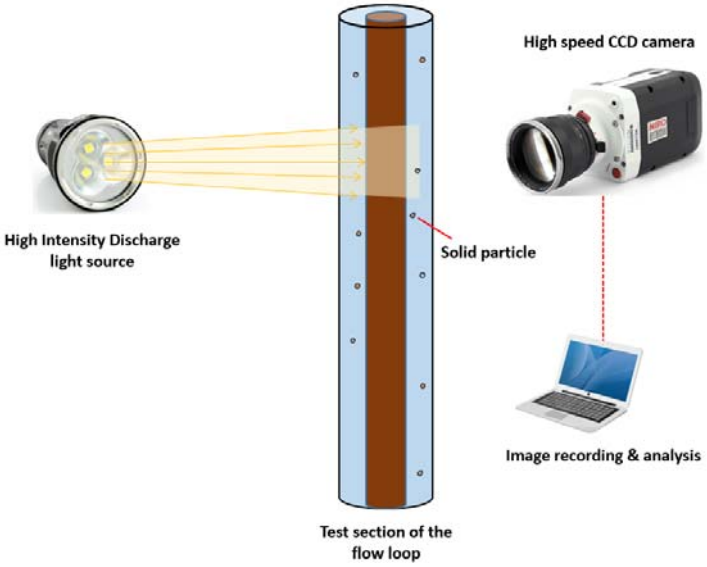

Figure 3.13 Schematic diagram of PTV system.

Figure 3.14 PTV system for measuring cuttings transport velocity.

High speed camera

A Phantom charge coupled device (CCD) camera is used in the PTV setup to capture the images of moving particles. The maximum frame rate is 2000 frames per second (fps). The resolution can reach 1440×1080 pixels. The minimum digital exposure time is 2 μs. The camera specification is adjusted depending on experimental condition such as the particle size or light source to capture clear images of cuttings. The camera recoding time varied from minimum 3 seconds to a few minutes during the experiments. The camera control is conducted by the Phantom software. Figure 3.15 demonstrates the camera setup and the software panel.

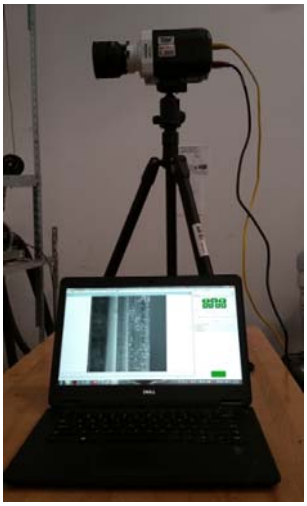

Figure 3.15 High speed camera and controlling computer.

High Intensity Discharge (HID) Light

Two types of light source are employed in the PTV system, illustrated in Figure 3.16. One is the alternating current (AC) LED light, which can emit a flux of 2000 lumens. This light is mainly used for illuminating the background of the test section. Sometimes it is also used as the main light source for the particle settling test, in the case where the particle size is relatively large and 2000 lumens is sufficient for the exposure of the video.

Another light source is the portable HID light with an output of high up to 7300 lumens. The flux can be adjusted at 7300, 2500 and 850 lumens respectively depending on the particle size and flow rate. The light is used to illuminate the target position of the test section that the camera is focusing on during the particle tracking test. The light is also working for the fine particle up to 200 μm during the particle settling test.

It is worth noting that for the traditional light in the Particle Image Velocimetry (PIV) or PTV system, the laser is usually employed due to the ability of emitting light with controllable pulse, and the light sheet of the laser beam acts like a very thin plane. However in the PTV system of this research, HID light is employed instead because the experiments using various light sources find out the HID light can offer a wider beam but still intensive enough to illuminate the whole field. Different from the image of PIV which only shows the particles appearing on a plane, the images of this research present all the particles on the cross section of the test section.

Figure 3.16 HID and LED light of the PTV.

Image analysis

The images saved on the camera are transferred to the computer for further analysis. Firstly some preliminary adjustments are performed on the raw images to modify the brightness and apply filters. As the size of the particles decreases or flow rate increases the quality images deteriorates and it is required to apply further rectification to improve the quality of images. Figure 3.17 shows an example of the image adjustment. It can be seen that the blurred particles become distinct and can be identified.

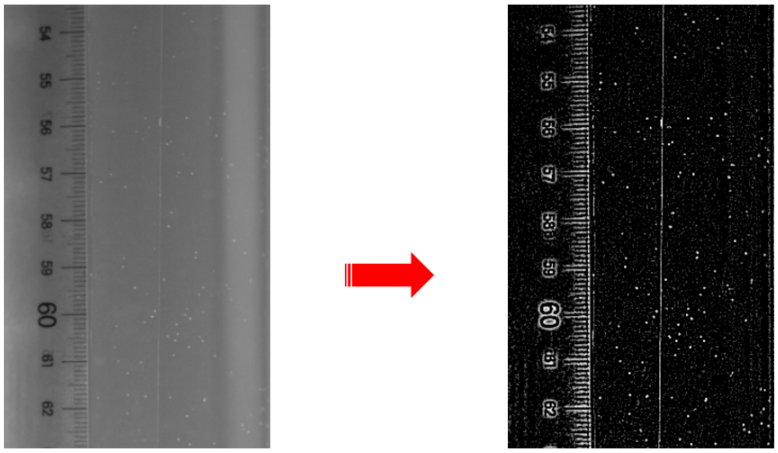

Figure 3.17 Comparison of raw image and improved image for a test of 0.2-0.3 mm particles at the flow rate of 1.5 l/s.

To calculate the particle velocity, it is required to calculate the distance travelled by particles between the different frames captured. This process is shown in Figure 3.18. The operation of the software timeline can illustrate the motion trajectory of each particle since the background

of the test section is kept stationary. Thus the particle displacement can be obtained by using the distance reference provided by the ruler attached on the pipe wall and the grids set in the software. The corresponding travelling time is the time interval of the selected images, which can be readily determined from the frame number divided by the frame rate. The PTV method does not require a synchronizer which is usually used to coordinate the light and camera, and the large number of the images captured can demonstrate every position of the particle at each interval, which can help to evaluate the velocity variation.

Using one high speed camera, the particles movement can be characterised in terms of movement along the streamline (Y-direction) and perpendicular to the streamline (X-direction). The particle velocity is mainly in Y-direction, and can be obtained by:

$$V(y) = \frac{Displacement\ Y}{Frame\ difference/Frame\ rate}$$

$$V(x) = \frac{Displacement\ X}{Frame\ difference/Frame\ rate} \qquad \text{(Equation 3.1)}$$

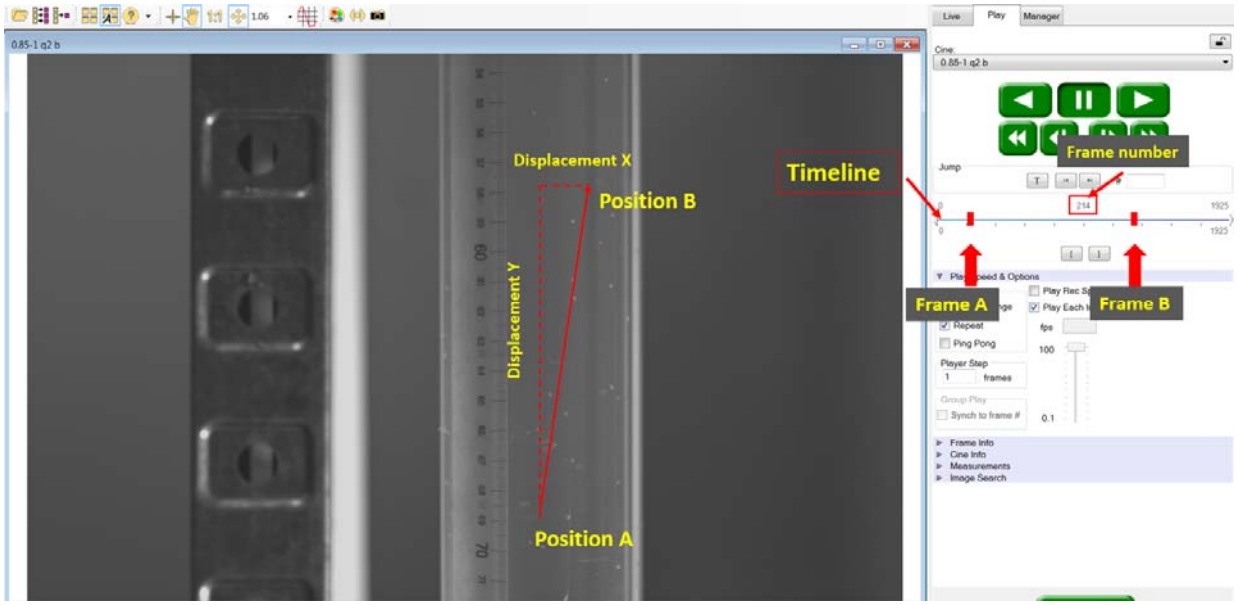

Figure 3.18 Determination of the particle transport distance and travelling time.

3.3. Test materials

In this section, the preparation of solid particles and fluids and also the description of the testing equipment used to measure fluid and solid properties are introduced.

3.3.1. Cuttings

The particles used in the experiment are supplied from two sources, which are the real drilled cuttings and graded solid particles (sands). The real cuttings were collected from the Brukunga mine site located close to Adelaide in South Australia. This site has been used for conducting drilling field experiments including the field tests of particle tracking.

Two types of cuttings are collected from the mine site produced from impregnated diamond and percussive water hammer drilling. Images of cuttings from each drilling technique is shown in Figure 3.19.

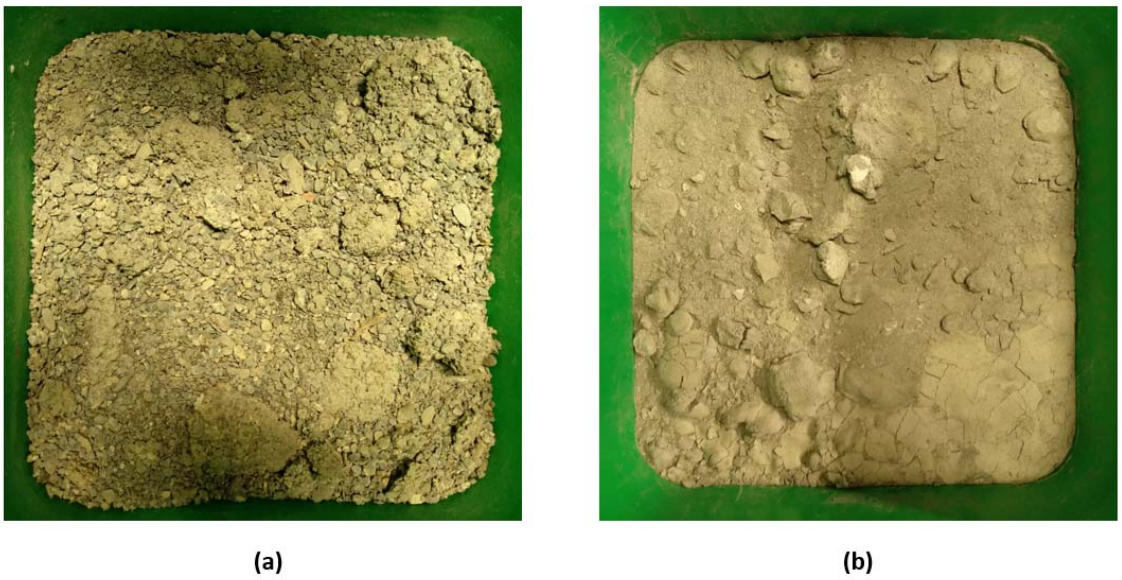

Figure 3.19 Real cuttings: (a) Percussive hammer cuttings, (b) Impregnated diamond bit cuttings.

The particles were collected from recovered drilling muds to minimise any changes in the size distribution and shape. The cuttings were dried for the experiments. Therefore, the particle size and sphericity of cuttings were measured under the wet condition. Then the cuttings were dried using oven, and the particle size of dried cuttings were measured. Figure 3.20 shows one example of the particle size distribution (PSD) of diamond bit cuttings and hammer bit cuttings.

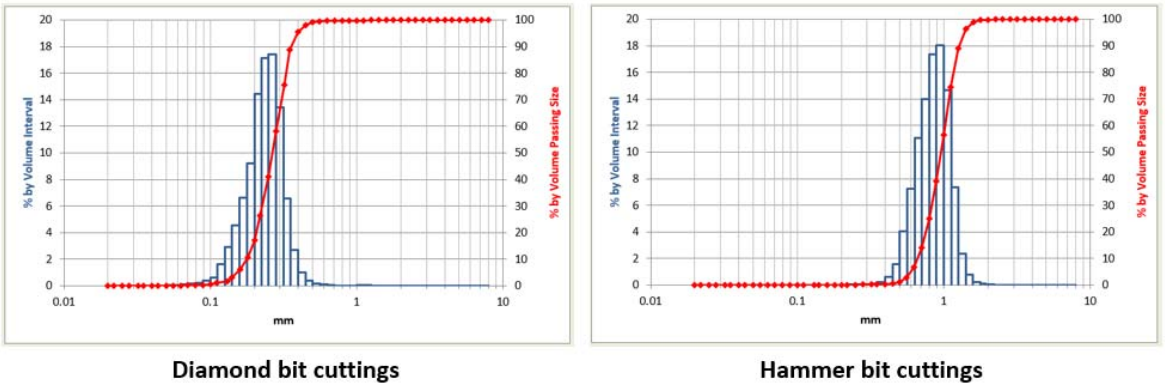

Figure 3.20 The particle size distribution of diamond bit cuttings and hammer bit cuttings.

The measurement found that the diamond bit cuttings are fine powders, and the PSD is narrowly focused below 500 μm. On the other hand, the PSD of hammer bit cuttings covers a wider range, and the maximum size usually reaches up to 2 cm.

The supply of real cuttings especially at specific size range was limited: several kilograms of cuttings are required to separate sufficient amount of larger particles. Therefore, industrial graded sands were used to provide repeatable and unlimited supply of solid particles. The selected industrial sands have the density similar to wide range of drill cuttings, has similar in shape, and also are available at different size fractions. As it will be explained in more details, the graded sands were further separated using sieving method to narrow the size distribution of cuttings for each test.

Particle shape

The particle shape is a significant property of the cuttings. In this research the shape of cuttings is characterised using the sphericity Ψ in accordance with previous research on cuttings behaviour in fluid.

The particle sphericity Ψ quantifies how the particle shape resembles a perfect sphere, and can be obtained from the ratio of the surface area of the equivalent sphere with the same volume of the particle over the surface area of the particle. The particle sphericity can be calculated from:

$$\psi = \frac{surface\ area\ of\ volume{-}equivalent\ sphere}{surface\ area\ of\ particle} = \frac{\pi^{\frac{1}{3}} \times (6V_p)^{\frac{2}{3}}}{A_p} \qquad \text{(Equation 3.2)}$$

where, V_p and A_p are particle volume and surface area.

The Haver Computerized Particle Analyser (CPA) is used to measure the cuttings sphericity, see Figure 3.21. The machine measures the sphericity using rapid image scanning of free falling particles and utilizing digital image processing to obtain the quantity, particle size and shape parameters such as minimum/maximum Feret, equivalent diameter, sphericity. In each run of the equipment, millions of particles can be counted and the average sphericity is provided as the representative particle shape factor.

Figure 3.22 demonstrates a series of image of the hammer bit cuttings tested by Haver CPA. It can be seen that the drill cuttings present various shapes. Figure 3.23 shows one example of the cuttings sphericity distribution. The measurement found most cuttings have a sphericity Ψ of 0.7 to 0.9, the same range as the previous study which asserts the sphericity of 0.8 for cuttings [58].

Figure 3.21 Haver Computerized Particle Analyser for particle shape measurement.

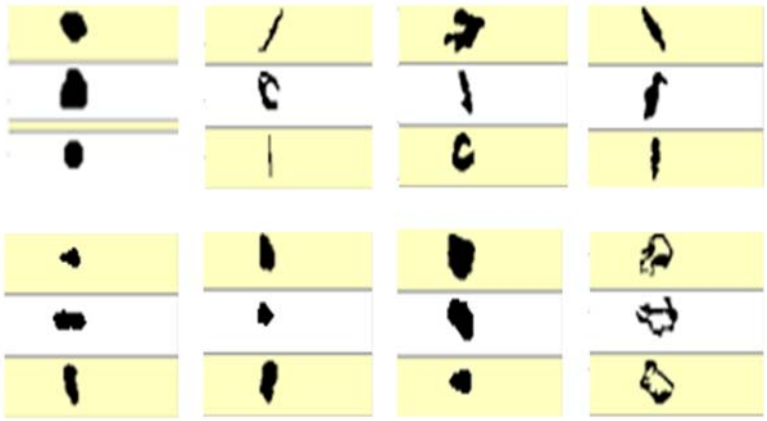

Figure 3.22 Haver Computerized Particle Analyser for particle shape measurement.

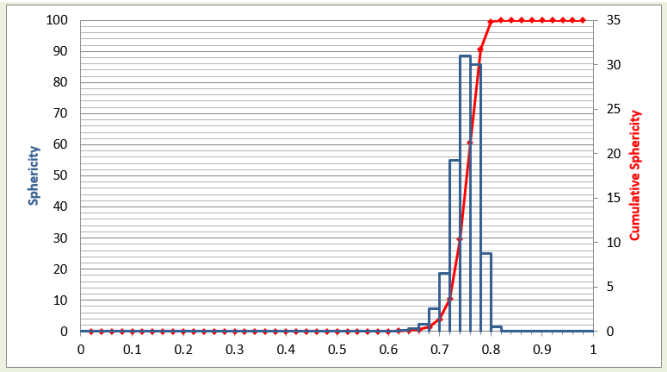

Figure 3.23 Cuttings sphericity distribution by Haver CPA.

Particle size

There is a series of particle size factors for the cuttings due to the irregular shapes, such as the equivalent diameter or the projected area diameter. In this research, the cuttings were separated and grouped using sieving to narrow the size distribution of cuttings. The cuttings were divided into 12 groups of 0.2-0.3 mm, 0.3-0.4 mm, 0.4-0.5 mm, 0.5-0.6 mm, 0.6-0.71 mm, 0.71-0.85 mm, 0.85-1 mm, 1-1.18 mm, 1.18-1.4 mm, 1.4-1.7 mm, 1.7-1.8 mm and 1.8-2 mm. Each groups was obtained by collecting the particles between two sieve sizes.

The sieves and the sieve shaker are shown in Figure 3.24. Samples of each group of cutting were obtained and measured using Haver CPA for 0-2mm particles and Malvern mastersizer for particle below 0.5mm. Figure 3.25 shows the Malvern mastersizer 3000.

Figure 3.24 Sieves and sieve shaker for particle separation.

Figure 3.25 Malvern Mastersizer 3000 for wet cuttings size measurement.

The Malvern Mastersizer 3000 is used to measure the wet cuttings size distribution. Previous laboratory experience indicates that the Mastersizer results are accurate for particle size below 500 μm, so it is only applicable for the fine cuttings. The cuttings with larger size is measured by the Haver CPA which can test particles up to 5mm.

Particle density

The absolute density of the cuttings are measured using the Density Bottle method based on the Archimedes' principle. The measurements were performed using distilled water. Demonstrated in Figure 3.26, first the mass of the empty bottle is measured (m_o), which is then filled with a given weight of dry samples. The weight of the container containing the dry sample is measured (m_1) and then filled with the fluid (water or oil) and the container weight is again recorded (m_2). The same procedure is repeated but without the cuttings, and the weight of the container filled with the fluid is recorded (m_3).

Thus the particle absolute density can be calculated by Equation 3.3.

$$\rho = \frac{m1-m0}{(m3-m0)-(m2-m1)} \qquad \text{(Equation 3.3)}$$

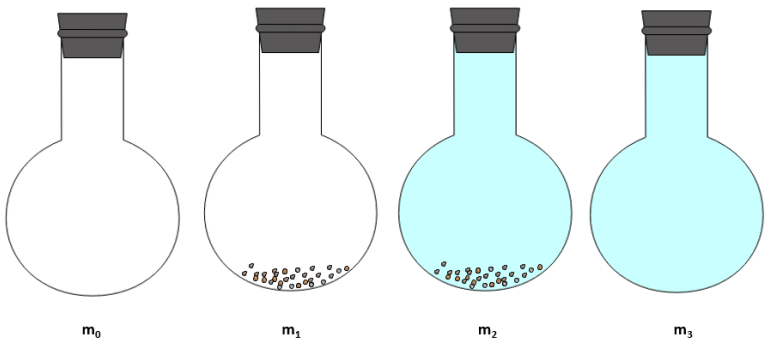

Figure 3.26 Density Bottle method for measuring particle absolute density.

3.3.2. Fluids

To better characterise the effect of fluid rheology, both Newtonian fluid and Non-Newtonian fluid were used in the cuttings transport experiments. Two types of Newtonian fluid were used including water and glycerine solution. The viscosity of Newtonian fluid was adjusted by the glycerine concentration.

The Non-Newtonian fluids were solutions of XCD polymer made from xanthan gum polymer mixed with water at different concentrations. The XCD polymer are provided by Australian Mud Company. Various concentrations of polymer solutions were tested from 0.01% to 0.2% in this research.

The measurement of the fluid rheology was conducted using two kinds of rheometer. A detailed rheology measurement was obtained using a HAAKE rheometer, see Figure 3.27. While detailed measurement of fluid rheology was conducted using HAAKE, a 12 speed OFITE viscometer was used to monitor the fluid rheology in the tanks during the cuttings transport experiments. The OFITE viscometer was made of R1B1 bob and rotor arrangement, which yields a 1.71 shear rate for each rpm of the machine.

Figure 3.27 OFITE 900 and HAAKE for fluid rheology measurement.

To ensure the fluid property uniformity, highly concentrated solution with polymer was prepared in 20 litres containers, which was then diluted with water in the storage tank using the agitator to reach the required rheology.

3.4. Results validation and error analysis

3.4.1. Calibration of the sensors

In this research, the experiments of measuring cuttings transport velocity have a high requirement for accuracy. This section introduces the calibration of the measurement instruments such as the flow meter and pressure sensors, and also repeatability of cuttings velocity measurement using the PTV image analysis.

The calibration of the flow meter and pressure sensors were performed regularly. The measurements of bias of sensors were performed before and after each experiment. The average of flow rate and pressure sensor measurements was taken into account as the bias of each sensor, which were used to calculate the actual magnitude of the data during the experiment.

Figure 3.28 illustrates the flow meter bias examination. First all the valves on flow meter are closed to make sure the fluid inside the system is stationary. Then the condition is kept for a long time until the signal is steady. Finally the flow meter bias is the measurement difference from 0. It can be seen the bias is 0.03 l/s.

Example of variation of flow rate during an experiment is shown in Figure 3.29. It can be seen that the flow rate over a long time is quite stable and the variation range is relatively small. For example, for the flow rate of 1 l/s, the mean of signal varies from 0.95 to 1.05, which is within 5% of the mean flow rate.

Figure 3.30 shows the same procedure for the pressure sensor bias measurement. It can be seen that the measurement difference of the two pressure sensor is almost zero

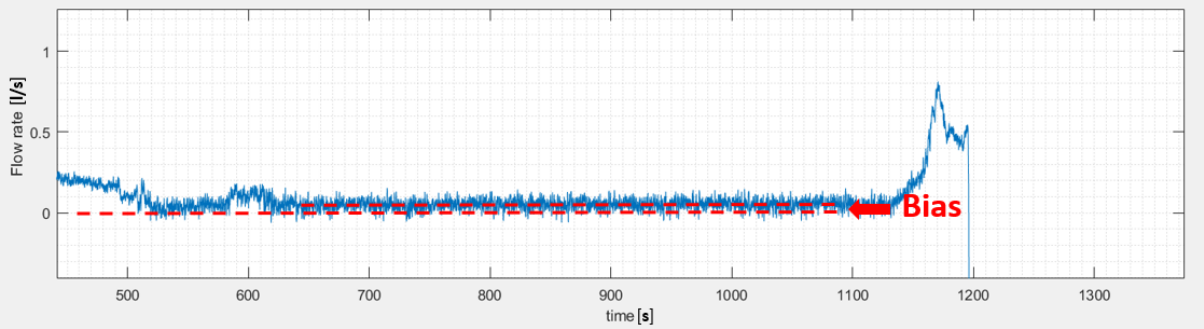

Figure 3.28 Flow meter bias examination.

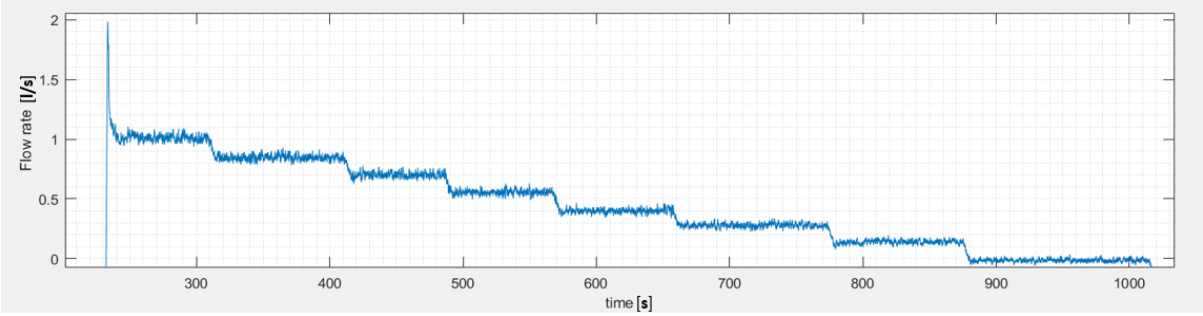

Figure 3.29 Fluctuation of various flow rate.

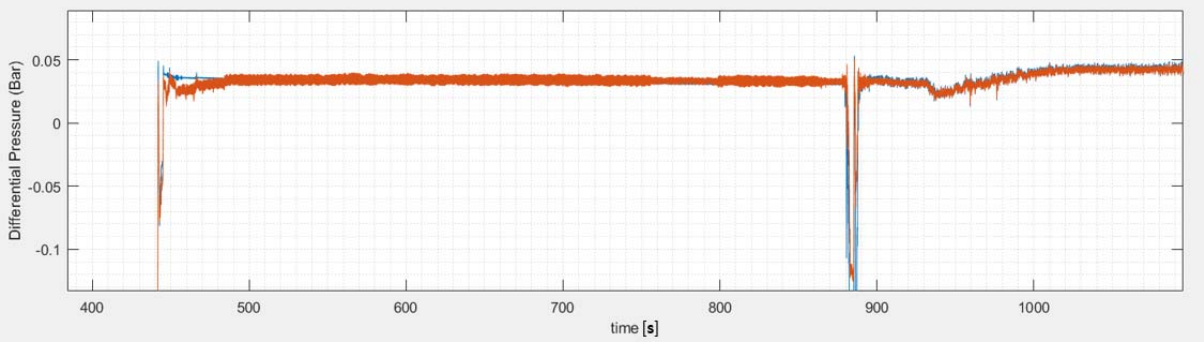

Figure 3.30 Pressure sensors bias examination.

3.4.2. Results verification for cuttings transport velocity

As the particle velocity is analysed using PTV method, the particle travel distance determination is critical for the accuracy of the final results. Except the ruler attached on the test section which demonstrates the length of the particle movement in the image analysis, the calibration must be performed as well.

The image calibration is conducted in the camera software by establishing a real size/image pixel relationship. As is presented in Figure 3.31, the gauge can be set to correlate the real size corresponding to each pixel for the image. The coordinates can be set in the calibration process, and based on the pixel unit conversion the particle transport distance is calibrated and demonstrated in the software. This distance will be prepared with the value shown by the ruler, which helps to evaluate the image deformation.

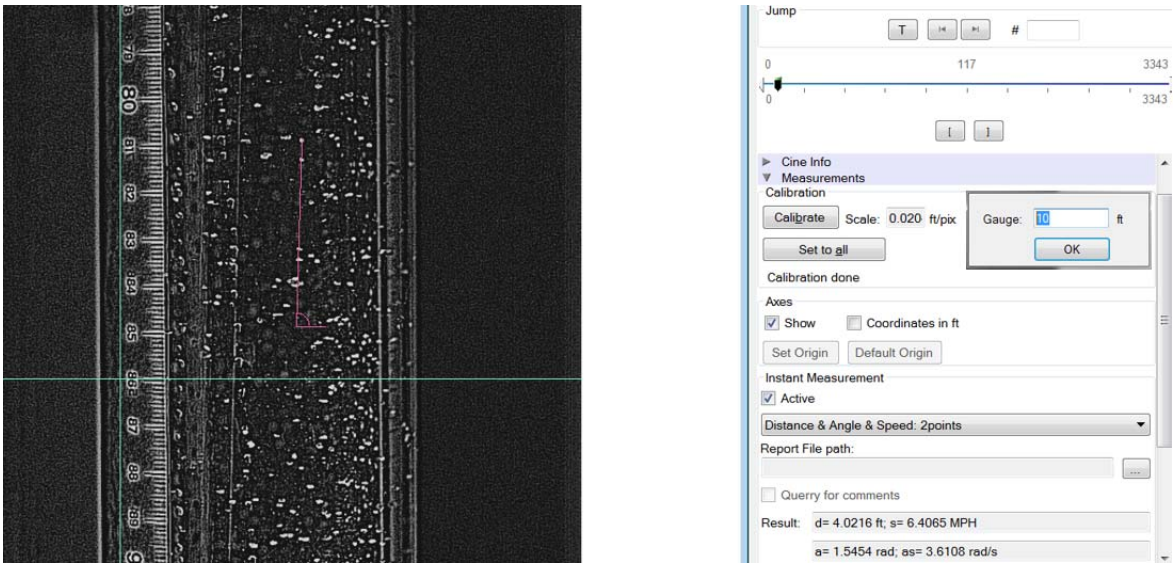

Figure 3.31 Image calibration in PTV.

In PTV method, several practices were adopted to ensure that the results are accurate and repeatable. In each test, the velocity of several particles was measured and averaged to provide an average particle velocity for that particle class of cuttings. Furthermore, each test was repeated two or three times, and in each repeat the camera position was moved along the test section to make sure the flow is fully developed and stable in each target areas.

Figure 3.32 presents the cuttings velocity of twenty particles measured in a settling experiment with 0.85-1 mm particles in water. The data analysis shows that the average of cuttings settling velocity is 0.123 m/s, while the variance is only 0.00011.

Figure 3.33 shows the cuttings velocity variation of 50 cuttings measured in a cutting transport experiment performed with 0.85-1mm particles in water. In this class of data, the average of cuttings velocity is 1.503 m/s with the variance of 0.00286, which is higher than the settling experiments.

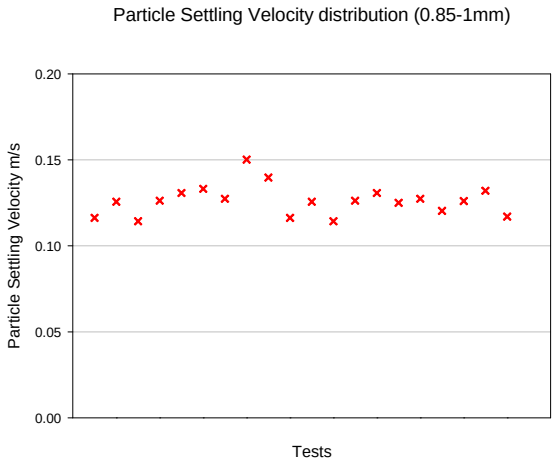

Figure 3.32 Distribution of 20 tests of single 0.85-1 mm particle settling in annulus with water.

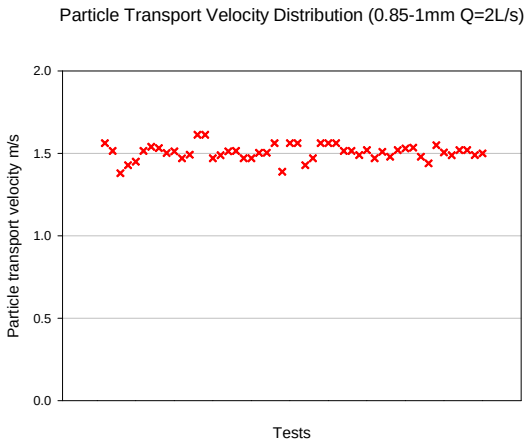

Figure 3.33 Distribution of 50 tests of cuttings transport velocity for 0.85-1 mm in water with flow rate of 2 l/s.

Chapter 4. Particle settling

4.1. Introduction

Before measuring the cuttings transport velocity in flowing fluids, the cuttings settling velocity in stationary media is obtained first in this chapter.

In this chapter, we present the results related to the influence of the cuttings size and fluid rheology on the settling velocity. The settling experiments were conducted in both annulus column and infinite media to study the wall effect in the narrow annulus wellbore. Furthermore, the settling behaviour of multiple particles, i.e. hindered settling, was performed on the flow loop to investigate the cuttings concentration on the cuttings settling velocity.

The experimental results of this study were compared with the settling velocity prediction of previous published correlations. Based on the settling velocity results, the relationship between the drag coefficient C_D and particle Reynolds number Re_P was derived and presented as the drag curve. This C_D-Re_P relationship is essential for the particle mechanics in annulus column, and also provides the foundation to study the fluid flowing effect on the particles which is introduced in Chapter 5.

4.2. Settling of single particle

The settling velocity of single particle was measured in a series of annulus columns and pipes to obtain the "standard drag curve" for the cuttings with sphericity Ψ of around 0.8. The results are analysed and compared with previous research, and the effect of particle size, fluid rheology and wall effect was analysed aiming at single particle.

4.2.1. Experimental methodology

Figure 4.1 presents the schematic diagram of the experimental setups for measuring the single particle settling velocity. The system is actually the application of the PTV on the independent settling column with height of 2 meters. The experiments were carried out on 45mm-60mm annulus, and also pipe with internal diameters of 80mm. A needle device was used to introduce the particle into the fluids with zero initial velocity.

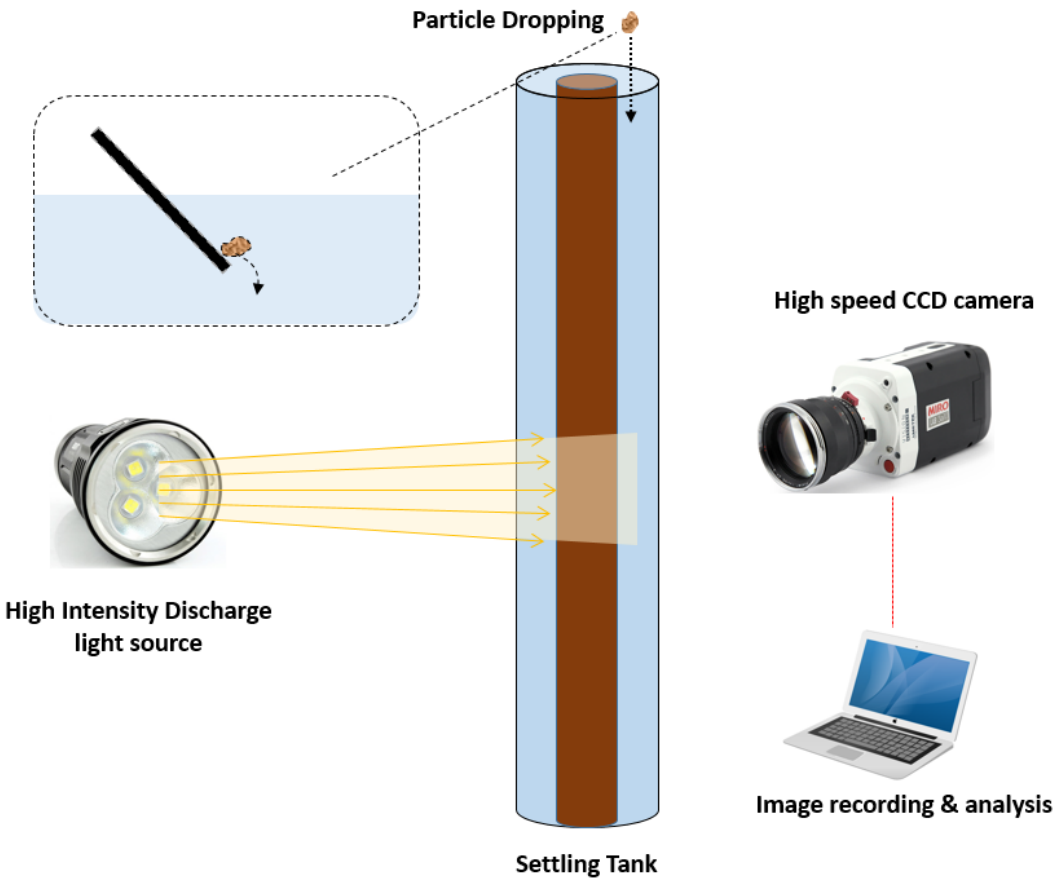

Figure 4.1 Schematic diagram of particle settling test.

The brief procedure of the experiment is below:

1. Setup the experiment and prepare particles and fluids.
2. Measure the rheology of the fluids.
3. Start PTV to record the single particle settling.
4. Drop the particle into the fluids and make sure the initial velocity is zero. Capture the video when the particle is steady (after travel distance of 1 meter).
5. Monitor the fluids temperature during the experiment, and in the middle take samples for rheology measurement.
6. Repeat the tests at least 10 times. Make sure the interval time between each test is at least 5 minutes.
7. Measure the fluids rheology in the end of the test.
8. PTV image analysis.

12 groups of cuttings were tested for the single particle settling. Table 4.1 shows the particle size range for each sieved group.

Table 4.1 Sieved size of the cuttings for single particle settling test.

Group	1	2	3	4	5	6	7	8	9	10	11	12
Sieve Size /mm	0.2-0.3	0.3-0.4	0.4-0.5	0.5-0.6	0.6-0.71	0.71-0.85	0.85-1	1-1.18	1.18-1.4	1.4-1.7	1.7-1.8	1.8-2

The test fluids include Newtonian fluids (water and glycerine solution) and Non-Newtonian fluids (XCD polymer solution). Six different concentrations were tested for the particle settling, and their rheology are given in Figure 4.2. The rheology data of the polymer solutions are characterised using Power Law model $\tau = K\gamma^n$, and the consistency index K and flow behaviour index n are listed in Table 4.2.

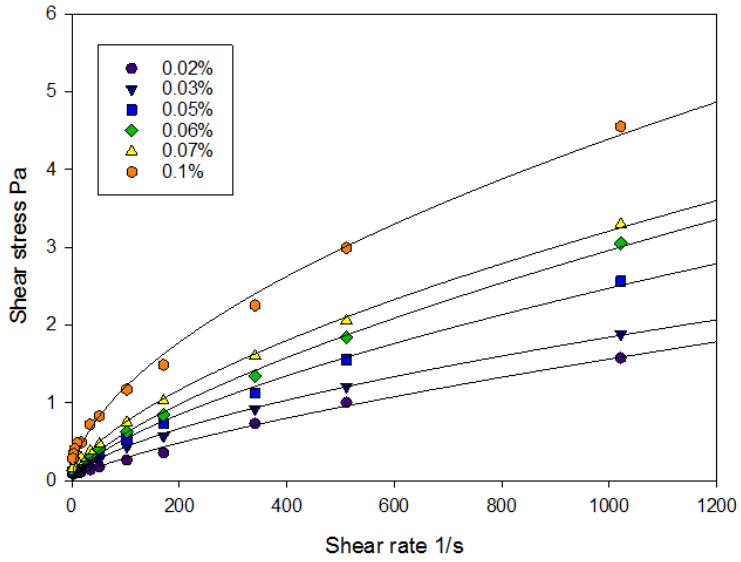

Figure 4.2 Rheology of various polymer solutions with concentration from 0.02% to 0.1%.

Table 4.2 Consistency index K and flow behaviour index n of test power law fluids.

Fluids	1	2	3	4	5	6
Polymer concentration	0.02%	0.03%	0.05%	0.06%	0.07%	0.1%
Consistency index K	0.0102	0.0235	0.0252	0.026	0.0413	0.0905
Exponent n	0.728	0.6311	0.6636	0.6856	0.63	0.562

4.2.2. Prediction of particle settling velocity

As mentioned in Chapter 2, most particle settling processes encountered in industrial application including drilled cuttings settling are within the intermediate regime where particle Reynolds number varies approximately from 1 to 1000, and the drag coefficient C_D cannot be obtained theoretically. Therefore various empirical correlations of C_D and Re_P have been proposed in the literature aiming at predicting the settling velocity of particles.

The settling experimental results obtained in this thesis are compared with the prediction of these correlations. Table 4.3 lists the correlations used in this research. These correlations are either the equations which have been proved to have a high accuracy, or those that are widely used for the drilled cuttings. For example, Equation 4.5 is part of the standard drag curve, Equation 4.2 is established based on the tests using real drilled cuttings, and Equation 4.4 is summarised from extensive data and considered the particle sphericity of 0.8.

Table 4.3 Correlations of Drag Coefficient CD and Reynolds Number Re.

Source	C_D-Re correlations	Note	Equation NO.
Michell [64]	$C_D = \frac{18.5}{Re^{0.6}}$	Unbounded volume, spherical particles, Re 0.2-500	(4.1)
Moore [65]	$C_D = \frac{22}{Re^{0.5}}$	Drill cuttings, Newtonian fluid, Re 10-100	(4.2)
Bourgoyne [98] *	$C_D = \frac{53.31}{Re^{0.908}}$ $C_D = \frac{55.47}{Re^{0.73}}$ $C_D = \frac{34.386}{Re^{0.51}}$ $C_D = \frac{14.288}{Re^{0.315}}$	Particle ψ=0.8	(4.3)
Chien [58]	$C_D = \frac{30}{Re}$+1.203	Particle ψ=0.8, Newtonian or Non-Newtonian fluid, Re 0.001-10000	(4.4)
Khan and Richardson [62]	$C_D = (2.25Re^{-0.31} + 0.36Re^{0.06})^{3.45}$	Re 0.01-3×10^5	(4.5)

* The equations were obtained from regression for Re 0.1-1, 1-10, 10-100, 100-500 respectively

To use these correlations to predict the cuttings settling velocity, an iterative code was written in Fortran language. Figure 4.3 presents the flow chart of this iterative calculation. First a small initial drag coefficient is assumed, which is used to calculate the settling velocity. The particle Reynolds number is then calculated, which is used to obtain a new drag coefficient based on the Reynolds number and using the correlation of drag coefficient. The drag coefficient and Reynolds number is considered if the discrepancy between the two drag coefficients is smaller than 0.0001, otherwise the iterations continue using a new drag coefficient, that is 0.0001 larger than the initial guess. It is worth mentioning that this iteration requires higher processing time than the case where the obtained drag coefficient would be used as the new drag confident. However, this method is used as it was found that the later method sometimes fails in converging to a unique answer.

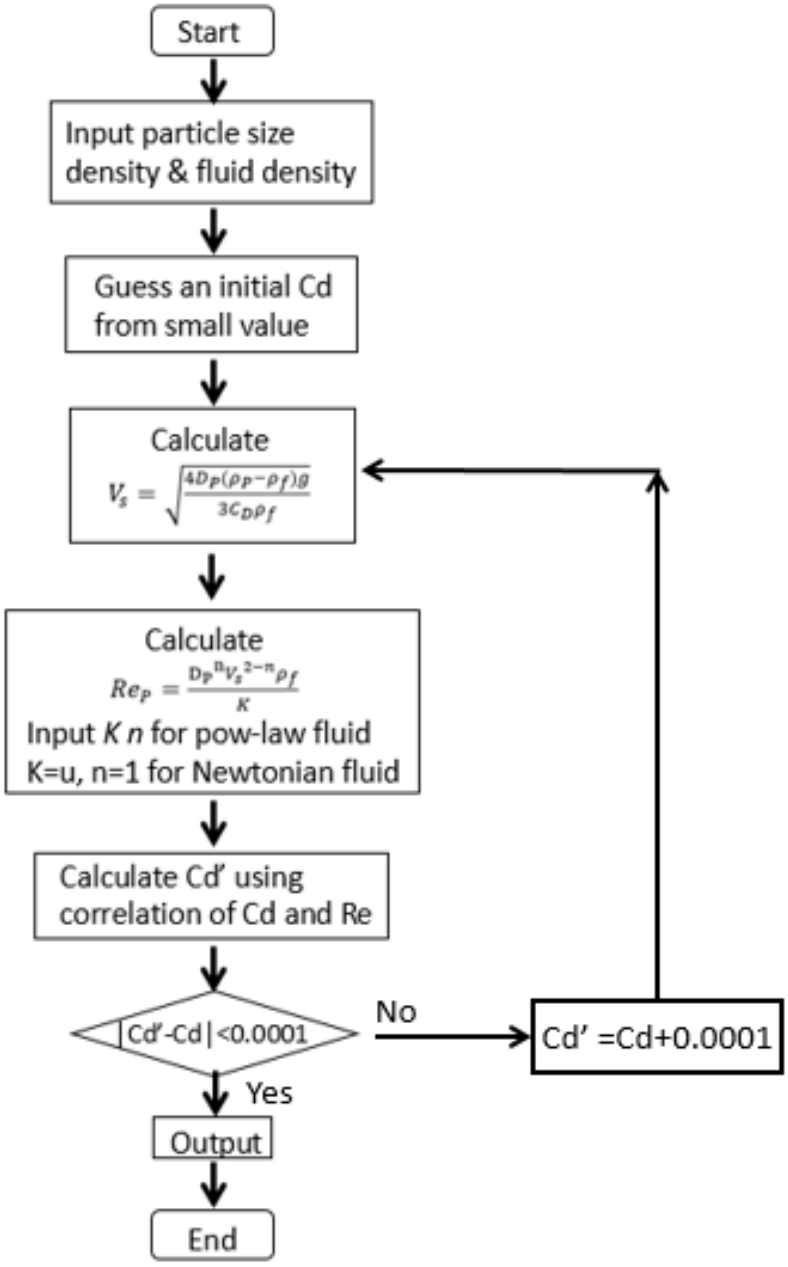

Figure 4.3 Flow chart of the iteration program for predicting single particle settling velocity.

4.2.3. Results and discussion

4.2.3.1. Determination of the cuttings size

One of the important parameters in correlating the particle Reynolds number and drag coefficient is the cuttings size. However it is difficult to determine the precise particle diameter, as the cuttings size covers a range. For example, in this research, the cuttings were prepared

using sieving method. Although a narrow range was obtained, the particles of 0.5mm collected were between the two sieves with apertures of 0.5 mm and 0.6mm.

The irregular shapes of the drill cuttings make it more difficult to identify the particle size, and particles with the same size but different shapes exhibit different velocities [99]. In this research, the cuttings have similar shape with a sphericity in the range of 0.7 to 0.9. Each velocity measurement was performed for at least ten repeats, and the average was considered as the representation of cuttings settling velocity. For example, the settling velocity in water of the particles between 1.8 mm and 2 mm varied from 0.182 m/s to 0.216 m/s with an average of 0.207 m/s.

Previous study has investigated the relationship of the sieve size and the particle size by measuring the settling velocity of natural sands using precise camera technique [99]. The equivalent circular diameter was proposed as the precise particle size:

$$D_{Eq} = 1.2489 D_{Sieve} - 0.1267 \quad \text{(Equation 4.6)}$$

This thesis adopts a simpler but effective method of determining the cuttings diameter for settling velocity. The particle diameter is calculated as the average size of the two sieves separating the sands. Table 4.4 shows the average size and the equivalent diameter for each group of cuttings used for the settling experiments.

Figure 4.4 shows the comparison of the two methods. It can be seen that for the cuttings with sieve size 0.5 mm-1.5 mm, the difference is tiny and can be neglected. But for cuttings size bigger than 1.7 mm, the results given by Equation 4.6 are even larger than the upper range of the cuttings. On the contrary, the equivalent diameter is smaller than the sieve size for the cuttings below 0.5 mm. Therefore in this research the average sieve size is used as the cuttings size.

Table 4.4 Determination of the average size and equivalent diameter based on the cuttings sieve size.

Sieve size mm	Actual size range mm	Average size mm	Equivalent circular diameter mm
0.2	0.2-0.3	0.25	0.123
0.3	0.3-0.4	0.35	0.248
0.4	0.4-0.5	0.45	0.373
0.5	0.5-0.6	0.55	0.498
0.6	0.6-0.71	0.65	0.623
0.71	0.71-0.85	0.78	0.760
0.85	0.85-1	0.92	0.935
1	1-1.18	1.09	1.122
1.18	1.18-1.4	1.29	1.347
1.4	1.4-1.7	1.55	1.623
1.7	1.7-1.8	1.75	1.996
1.8	1.8-2	1.9	2.121

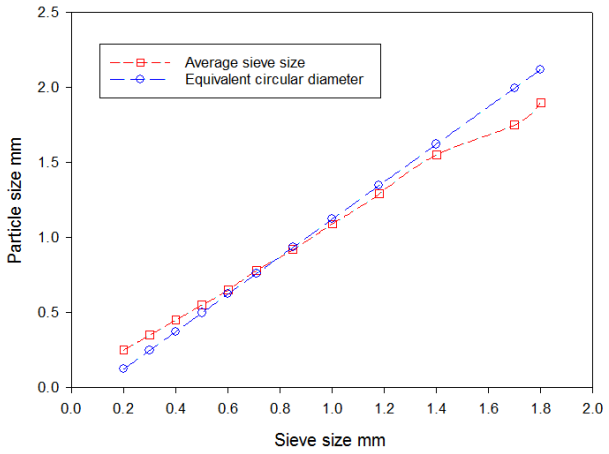

Figure 4.4 Determination of the particle size based on the cuttings sieve size.

4.2.3.2. Effect of fluid rheology

The cuttings settling velocity in Newtonian fluid of water and glycerine solution for annulus of 45-60 mm are shown in Figure 4.5, and the settling velocity in a series of power law fluids are presented in Figure 4.6.

It can be seen that the settling velocity increases with the particle size in both types of Newtonian and non-Newtonian fluids. However, the variation of the particle size is affected by the type of fluid. For Newtonian fluids, while the increase in viscosity (Glycerine solution compared to water) results in a decrease in settling velocity, the settling velocity tends to increase with the increase of the cuttings size with a similar rate, i.e. the water response seems

like the glycerine solution. These results can explain why in some published work a simplified linear correlation is considered for the variation of settling velocity with particle size [100].

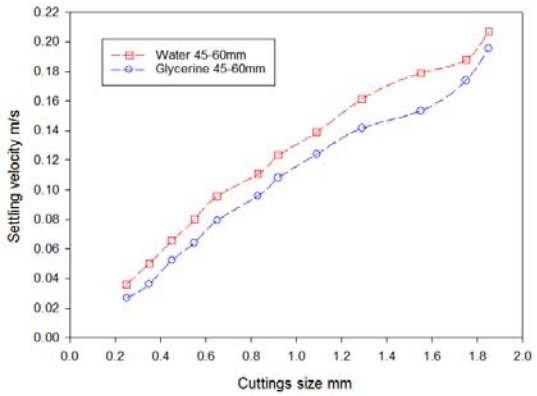

Figure 4.5 Cuttings settling velocity in water (1 cP) and Glycerine (1.5 cP) for annulus of 45-60 mm.

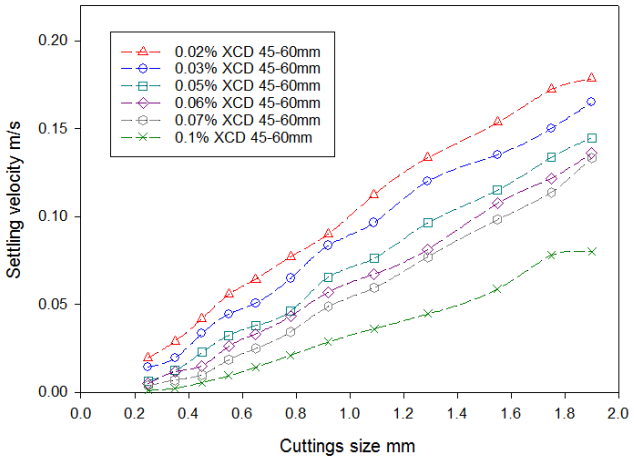

Figure 4.6 Cuttings settling velocity in various power law fluids for annulus of 45-60 mm.

In the case of non-Newtonian fluids, the results suggest that the rate of settling velocity increase with the particles is affected by fluid rheology. The particles velocity tends to increase with the size of the particles at smaller rate for more viscous fluids. In particular, this trend can be observed in the results obtained at concentrations from 0.07% to 0.1 % of XCD solutions.

Unlike Newtonian fluid, the viscosity of power law fluid is unable to be directly applied for the settling velocity. The results obtained from the tests are compared with the prediction of previous correlations. The cuttings settling velocity in annulus of 45-60mm with various polymer solutions are demonstrated in Figure 4.7-4.12.

The comparison shows that the correlations based on the drag coefficient C_D and particle Reynolds number Re_P have various predictions. The settling velocity derived from Equation 4.2 and 4.3 gives the lowest value for the cuttings size from 0 to 2 mm, and the results of Equation 4.1, 4.4 and 4.5 are relatively close. For 0.02% and 0.03% XCD solutions, the cuttings settling velocity is following Equation 4.1 and 4.5 only, although the prediction is based on the spherical particles. Due to the low viscosity, equation 4.4 gives lower settling results. But when the viscosity increases, the results of equation 4.4 approach to the prediction from equation 4.5 and can be used for the rough evaluation of the cuttings settling velocity. After the fluid viscosity is higher than 0.05% XCD, the settling velocity becomes smaller than the Equation 4.4 and 4.5 prediction, and for fluid with high viscosity, Equation 4.2 and 4.3 are closing the other correlations. For fluid with viscosity higher than 0.1% XCD solution, Equation 4.2 give acceptable results for certain size range.

Although the equations above used for the prediction of settling velocity have similar format, the results vary significantly according to the particle size and fluid viscosity. Generally, equation 4.4 is able to give relatively accurate settling velocity for cuttings size below 1mm regardless the fluid viscosity, and Equation 4.1 can be used for the cuttings size from 1mm to 2mm.

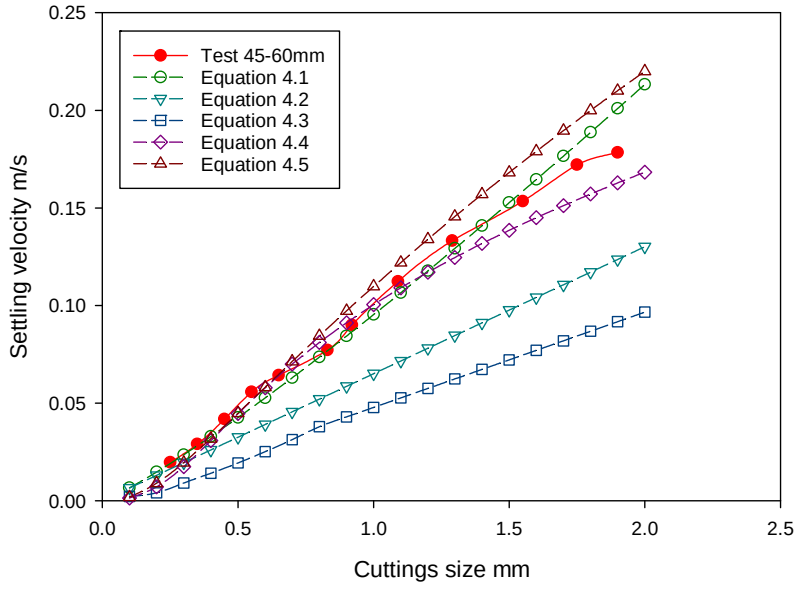

Figure 4.7 Comparison of test results with prediction for 45-60 mm annulus and 0.02% XCD fluid.

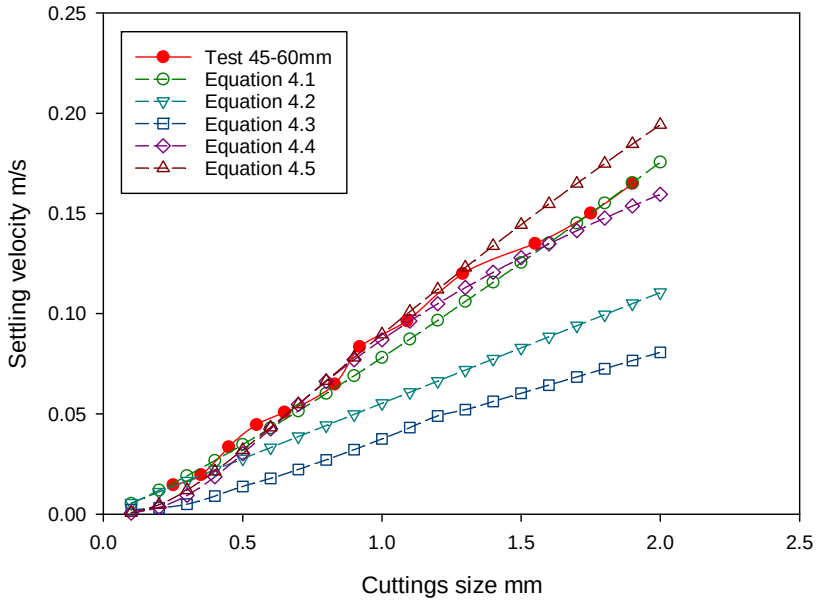

Figure 4.8 Comparison of test results with prediction for 45-60 mm annulus and 0.03% XCD fluid.

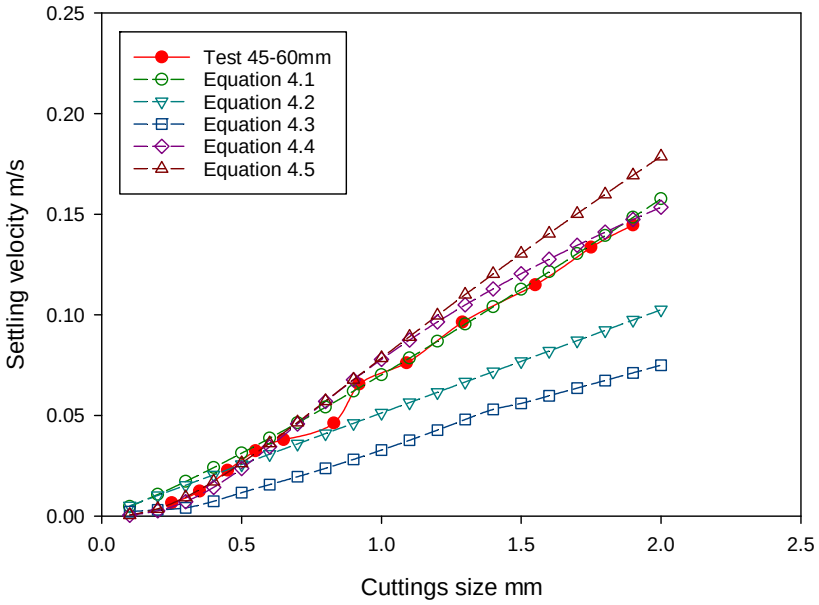

Figure 4.9 Comparison of test results with prediction for 45-60 mm annulus and 0.05% XCD fluid.

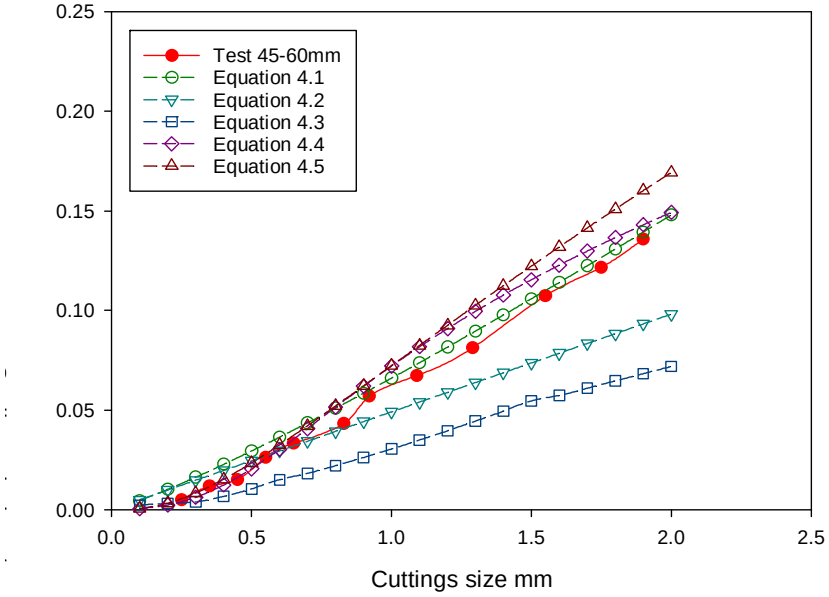

Figure 4.10 Comparison of test results with prediction for 45-60 mm annulus and 0.06% XCD fluid.

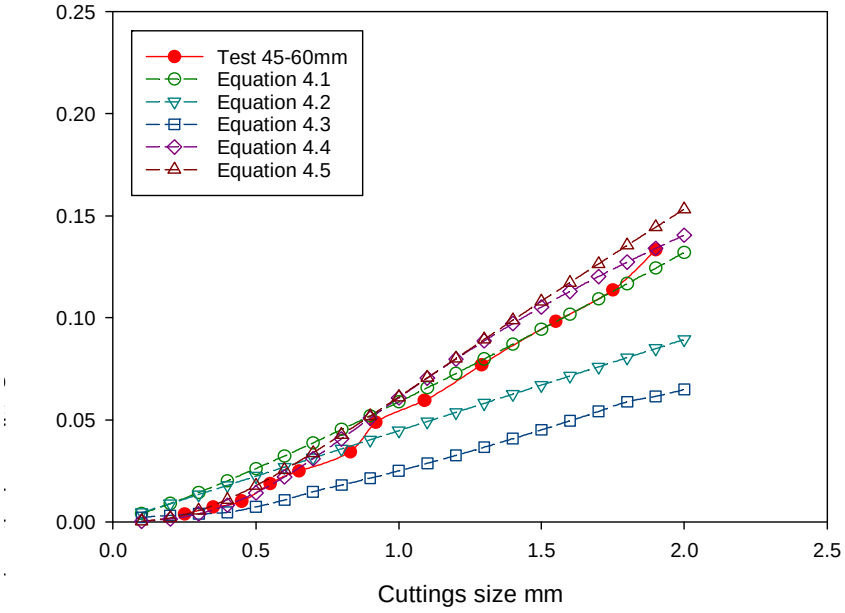

Figure 4.11 Comparison of test results with prediction for 45-60 mm annulus and 0.07% XCD fluid.

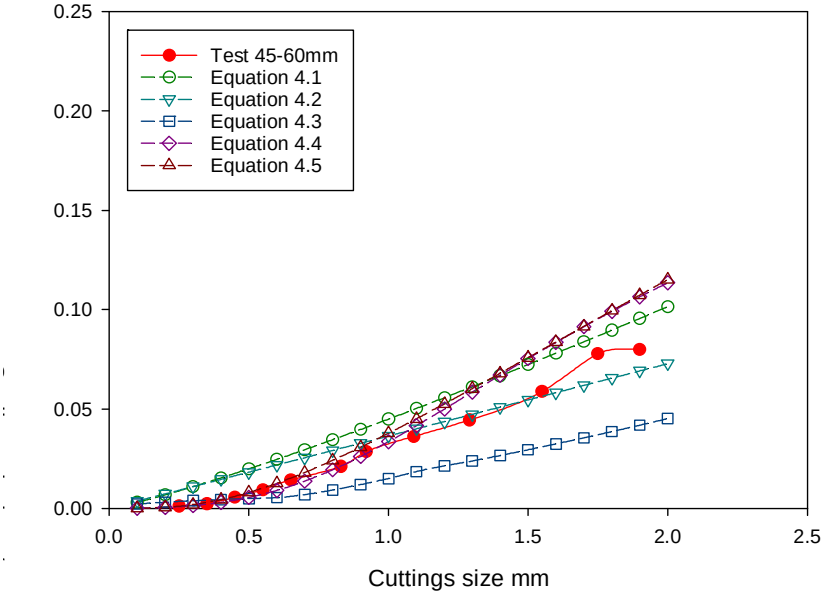

Figure 4.12 Comparison of test results with prediction for 45-60 mm annulus and 0.1% XCD fluid.

The critical component for investigating the effect of power law fluid on the settling velocity is to determine the viscosity for each specific settling particle. But unlike the Newtonian fluid for which the viscosity is independent of shear rate, the relationship of the shear stress and shear rate of Non-Newtonian fluid is unable to be applied directly for the settling particles. To better illustrate the viscosity of the surrounding media where the particle is settling, the settling shear rate is presented in Figure 4.13 for the cuttings settling in water and various polymer solutions. In this research the settling shear rate is considered as the ratio of settling velocity to particle size, i.e. V_s/D_P.

The settling shear rate change with particle size is different for Newtonian fluid and power law fluid. As the particle size increases, the settling shear rate in water drops from around140 to 100 1/s. But for polymer solutions the shear rate increases with particle size. The variations illustrate how the fluid rheology affects the particle settling. Previous study on the cuttings settling velocity has provided the settling shear rate range which is around 120 1/s for water and 20-50 1/s for drilling fluids [58], which covers the settling in water. But this research provides a wider range for different power law drilling fluids. The impact of fluid rheology on the particle for small size is greater than bigger particles, and the variation range is also larger for more viscous power law fluids.

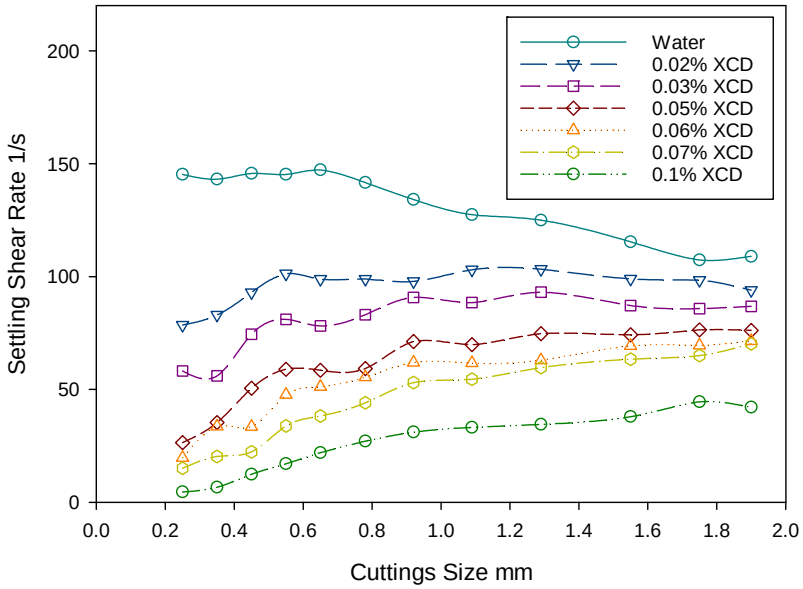

Figure 4.13 The settling shear rate variation with particle size for various fluids.

The settling shear rate can be used to estimate the fluid viscosity at the interface of fluid and particle. Based on the settling shear rate shown in Figure 4.13, the shear stress and viscosity are shown in Figure 4.14.

The results of polymer solutions at higher concentration show that the viscosity decrease with the increase in particle size. This is related to the shear thinning behaviour of drilling fluids, where the viscosity decreases with shear rate. This variation is more noticeable for particles smaller than 0.5 mm, and the viscosity tends to be relatively constant for particles bigger than 0.8 mm. At lower concentrations, the viscosity tends to be constant and not less affected by the size of cuttings or shear rate. This trend can be explained by the fact that the polymer solutions at low concentrations behave similar to a Newtonian fluid, where the viscosity is not affected by shear rate.

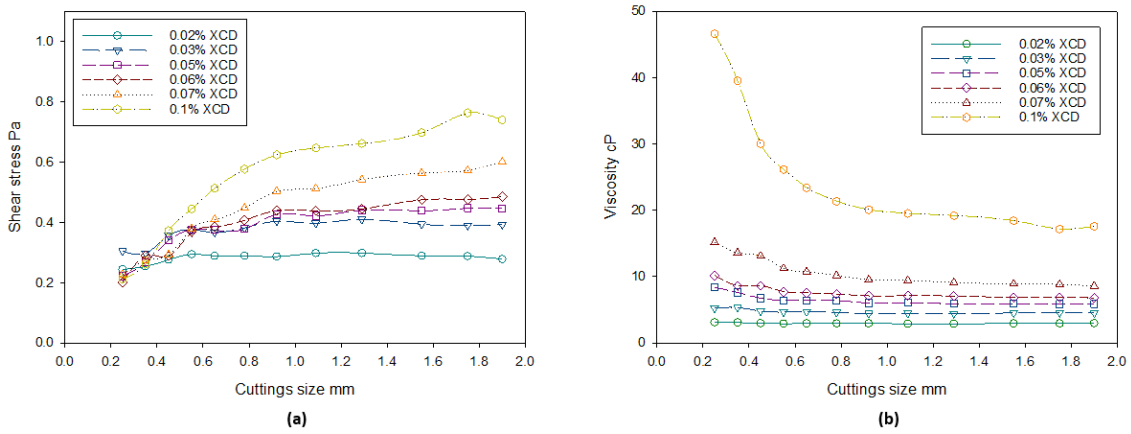

Figure 4.14 Shear stress and viscosity according to the settling shear rate for various fluids.

4.2.3.3. Wall effect of annulus

One of the factors that can impact on the settling velocity of particles is the geometry of the media. The closer the particles are to the restraining solid boundary, particles tend to settle at smaller rate. This effect can be studied by comparing the settling velocity of particles in the particular geometry with the unbounded conditions, where the diameter of the pipe is significantly larger comparing to particle size.

The wall effect of 45-60 mm annulus is characterised using the wall factor. The wall factor is defined as the ratio of particle settling velocity in a bounded conduit to the settling velocity in unbounded media. The cuttings settling velocity in the 80 mm pipe is regarded as the settling velocity in unbounded media in this research, as the maximum diameter ratio for this case is 2 mm/79 mm, which is only 0.025.

Figure 4.15 shows the wall factor variation with cuttings size and the ratio of particle size to annulus hydraulic diameter for various fluids. The hydraulic diameter of the annulus is defined as the difference between the outer and inner diameter of the annulus. The results show that the wall factor is a function of particle size and hydraulic ratio. For small particles corresponding to small hydraulic ratios, the settling velocity is almost the same as the unbounded condition, and the wall factor is almost one. All the fluids tend to exhibit the same response, and the fluid rheology shows a minimum impact on the wall factor for small particles particularly those in the range of 0.2-0.3 mm and 0.3 to 0.4 mm (equivalent to average size of 0.25 and 0.35 mm in the graph).

By increasing the particle size, the effect of fluid rheology on the wall effect becomes more dominant. It can be seen that the wall factor decreases with the increase of viscosity, illustrating that the wall effect is greater for more viscous fluids. To better demonstrate the wall effect with different fluids, the wall factor of three size groups of cuttings are shown in Figure 4.16. When the particles size is relatively small, the wall effect with various fluids viscosity almost maintains the same tendency. However, for larger cuttings size the wall effect becomes more sensitive to rheology and decreases dramatically with the increase of the polymer concentration.

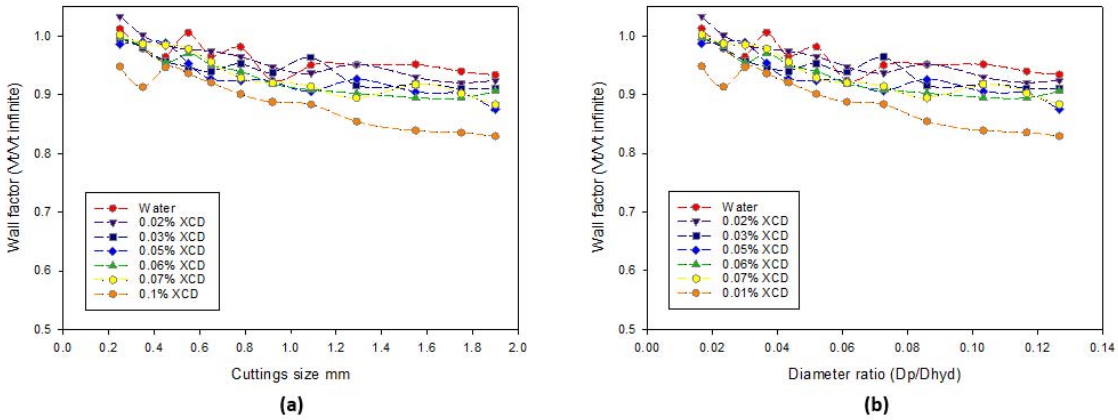

Figure 4.15 Wall factor for various fluids with (a) cuttings size, (b) diameter ratio of cuttings size to hydraulic diameter of annulus.

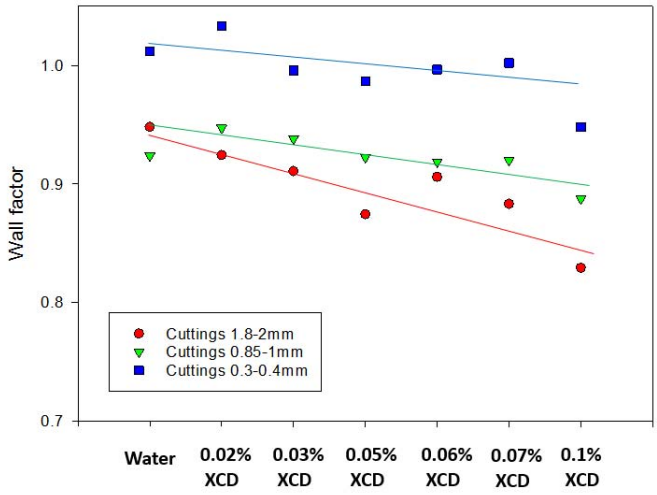

Figure 4.16 Wall factor variation with fluids for the cutting of size 0.3-0.4 mm, 0.85-1 mm and 1.8-2 mm.

It is worth mentioning that the wall effect of annulus geometry has been rarely studied, and it is still unclear how to select proper characteristic size for determining the diameter ratio for annular column. Therefore, both hydraulic diameter and the gap width of the annulus are used

for the diameter ratio calculation and are shown in Figure 4.17 with the wall factor. The previous correlation of the wall effect for particle settling in Non-Newtonian fluids is seen below as Equations 4.7 and 4.8 [55] and Equation 4.9 [57], and is plotted in Figure 4.17 as well. The comparison demonstrates that for the determination of the annulus geometry wall effect, the hydraulic diameter should be used for the diameter ratio instead of gap width.

$$f = 1 - 1.52\frac{D_P}{D_{Column}} \quad \text{(Equation 4.7)}$$

$$f = 1 - 1.28\frac{D_P}{D_{Column}} \quad \text{(Equation 4.8)}$$

$$f = 1 - 1.25\frac{D_P}{D_{Column}} \quad \text{(Equation 4.9)}$$

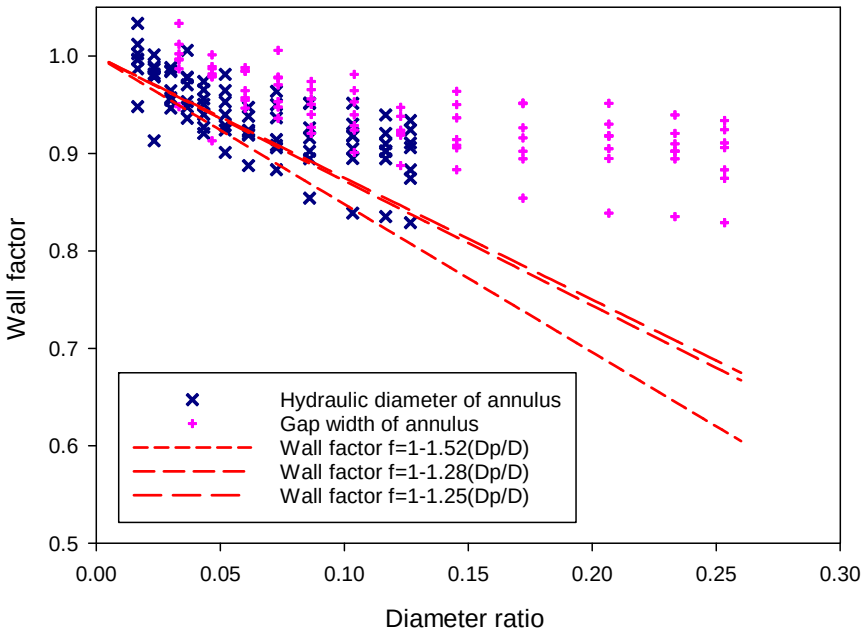

Figure 4.17 Determination of diameter ratio for annulus wall effect based on hydraulic diameter and gap width.

4.2.3.4. Drag coefficient of particle settling

Based on the settling velocity results in various types of fluids for 45-60 mm annulus, the cuttings drag coefficients were obtained using the equations introduced in Chapter 2. Figure 4.18 shows the relationship of the drag coefficient and the particle Reynolds number, which is compared with the estimation of drag coefficient using previously published correlations.

The results show that the drag coefficients calculated from the settling tests in different fluids follow the same pattern. With the increase of viscosity, the particle Reynolds number has changed from around 400 for the settling experiments carried out using water to less than 100 and only 30 for polymer tests, which means the settling particles have been approaching towards laminar flow typical intermediate regime. In addition, the range of the Reynolds number also reduces for power law fluids. From a practical perspective, if the cuttings are around the same size, the drag coefficient are closer for drilling fluid than thin muds, and the cuttings movement pattern are more likely to be the same.

As shown in Figure 4.18, the previous published correlations is unable to be used to predict the drag coefficient especially at moderate and high values of Reynolds number. For Reynolds number above 100, none of the previous correlation provide accurate drag coefficients. But this range is beyond the regime of the cuttings settling for drilling. For the intermediate range of Reynolds number from 0.1 to 100, Equations 4.2 and 4.3 overestimate the drag coefficient and therefore underestimates the settling velocity. Equation 4.1, 4.4 and 4.5 provide relatively an acceptable estimation of the darg in the Reynolds number range of 50 to 100. When the Reynolds number is below 0.1, the settling particles have approached laminar regime, and the settling velocity can be obtained readily using Stokes' law. Although the correlations were developed to estimate the drag coefficient in the intermediate regime, the data suggest that the correlations give acceptable prediction in the laminar regime.

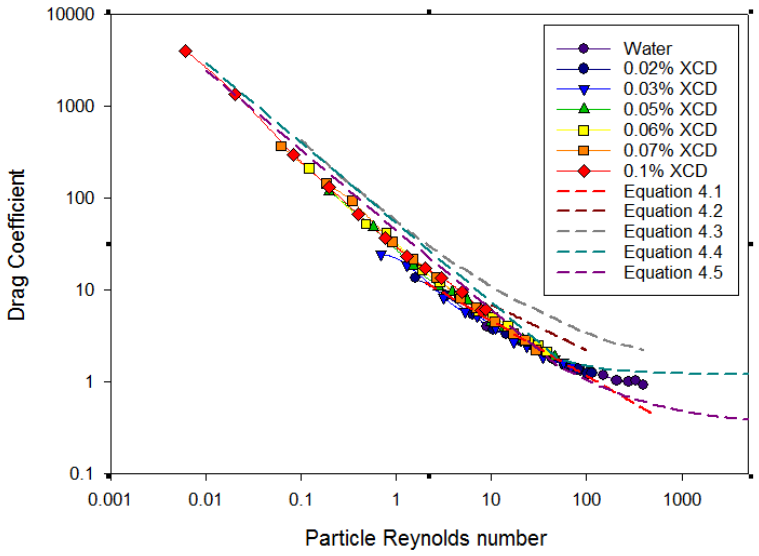

Figure 4.18 Comparison of previous correlations and the drag coefficient based on the settling velocity in various fluids for 45-60 mm annulus.

4.3. Hindered settling/Settling of concentrated particles

In addition to fluid and conduit geometry, the concentration of particles also has a significant impact on the cuttings settling. On one hand, the impact of solid concentration can be explained by the collision between the particles. In addition, when multiple particles are settling, the total volume of the displaced fluid moving upward is much higher than the volume of single particle, which results in hindering the particles settling compared with single particle settling. Therefore the settling of concentrated particles are called “hindered settling”.

To study the cuttings concentration effect, the hindered settling experiments are performed on the flow loop annulus test section instead of the settling conduit.

4.3.1. Experimental methodology

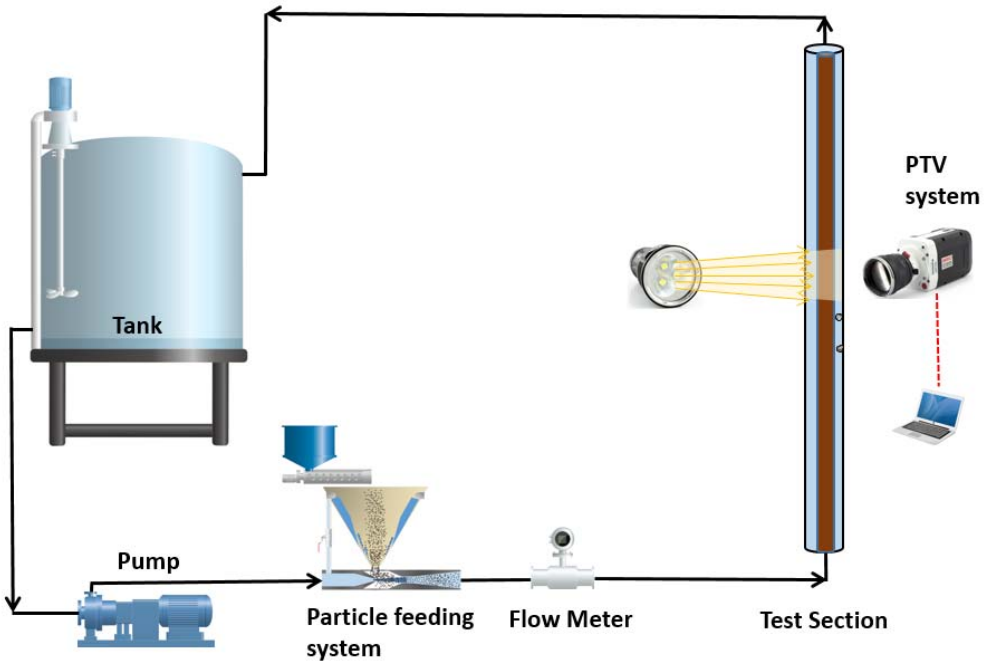

Figure 4.19 Schematic diagram of the hindered settling experimental setup.

A special test procedure was developed to study the hindered settling of solid particles using the flow. Figure 4.19 demonstrates the schematic setup of the hindered settling experiment. These experiments were conducted after the measurement of the cuttings transport velocity, which is introduced in Chapter 5.

Before the test, the desired fluid was prepared in the storage tank and pumped into the flow loop for stable circulation, and the rheology was measured. The fluids rheology for the hindered settling experiments was the same as single particle test, see Table 4.2. The cuttings were then added into the flow using the volumetric feeder and the eductor.

When the flow rate of the solid fluid mixture is stable, the volumetric feeding rate and the flow rate are recorded, so the cuttings volumetric concentration is:

$$C_P = \frac{M}{Q\rho_P} \qquad \text{(Equation 4.10)}$$

where M is the weight of the mass feeding rate into the flow loop per minute, Q is the flow rate of the slurry mixture per minute, and ρ_P is the particle density.

Then, the high speed camera was positioned at the lower part of the vertical annulus test section, and the pump was turned off and the valves besides the test section are closed to start the hindered cuttings settling in the annulus. The 4 meter test section is long enough for the particles to reach the terminal velocity. The images of the hindered settling is recorded by camera and analysed using PTV.

It is worth pointing out that the developed procedure of flow circulation of cuttings and the settling after pump shut off simulates the real condition of the cuttings settling in drilling operation in the field. In the previous published work, the hindered settling velocity experiments were performed by simply adding the cuttings from the top of circular conduits similar to the single particle settling test, which can result in aggregation of cuttings, and therefore larger settling velocity comparing to the single particle velocity [101, 102]. In these experiments as the particles tend to form clusters/aggregates potentially due to the charged particle surfaces [103], the results exhibited a higher settling velocity. Therefore, it is imperative to obtain a fully developed flow of the solid/liquid mixture to ensure that the particles are fully dispersed throughout the whole fluid before conducting the settling test.

The developed procedure was compared with the traditional method of conducting settling velocity. Figure 4.20 shows the advantage of using flow loop by comparing the hindered settling in 0.1% XCD solution using different experiment procedures. Figure 4.20 (a) demonstrates the hindered settling after fully developed flow, and it can be seen that the particles are dispersed homogeneously throughout the annulus space, while Figure 4.20 (b)

shows the settling phenomenon of directly putting particles into the fluids, which forms as particle streams.

Figure 4.21 presents the comparison of hindered settling for 0.85-1 mm size particles. It can be seen with the increase of the particle size, the particles flocculation varies from streams to clusters, and the measurement found the stream settling velocity of 0.3-0.4 mm particles was much larger than that of the clusters for 0.85-1 mm particles.

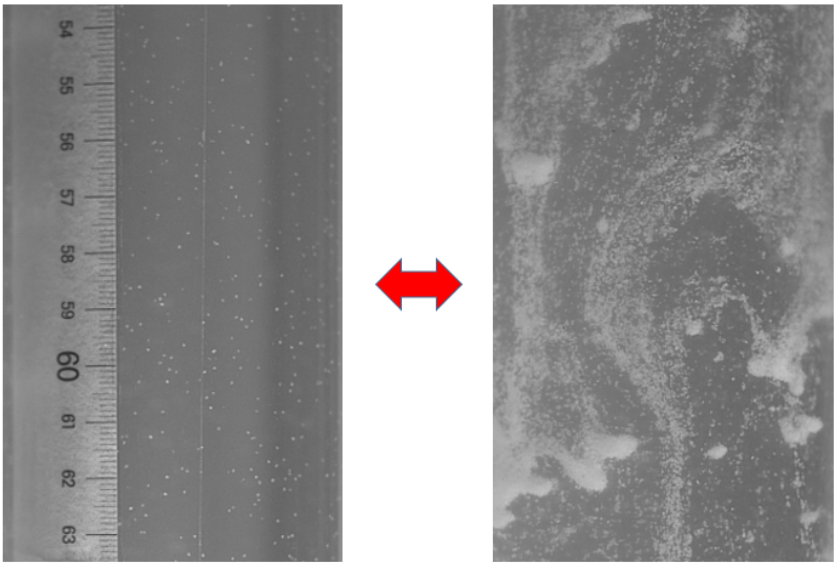

Figure 4.20 Comparison of hindered settling tests for 0.3-0.4 mm size particles, (a) fully dispersed particles on flow loop, (b) particle aggregation in conventional settling test.

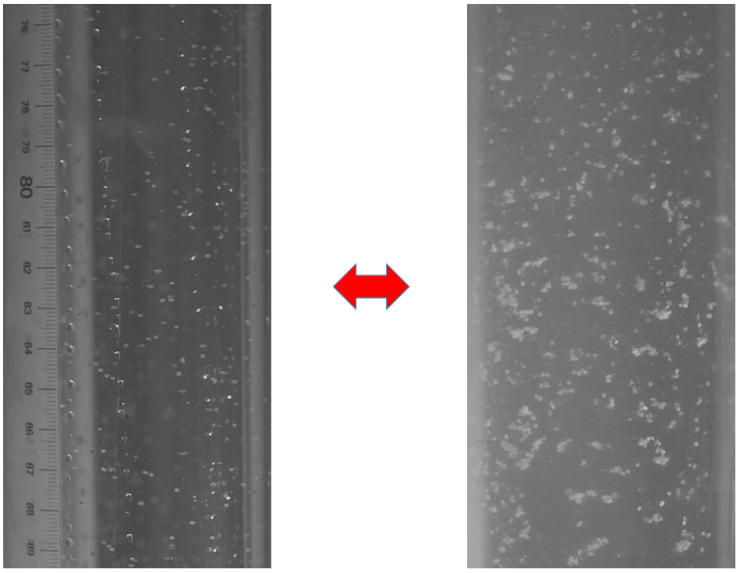

Figure 4.21 Comparison of hindered settling tests for 0.85-1 mm size particles, (a) fully dispersed particles on flow loop, (b) particle flocculation in a conventional particle settling test.

4.3.2. Effect of the cuttings volume concentration on the settling velocity

The cuttings hindered settling velocities in annulus for various fluids are presented in Figure 2.22-2.28. It can be seen that with the increase of the particles volume concentration, the cuttings settling velocity decreases significantly. The impact of the cuttings concentration is tremendous, but not proportional with the volumetric percentage, as the settling velocity decrease affected by the concentration of 5% is much larger than that of 1% and 3%. The hindered settling variation with the cuttings concentration follows almost the same pattern for various fluids, although the fluids viscosity is very different.

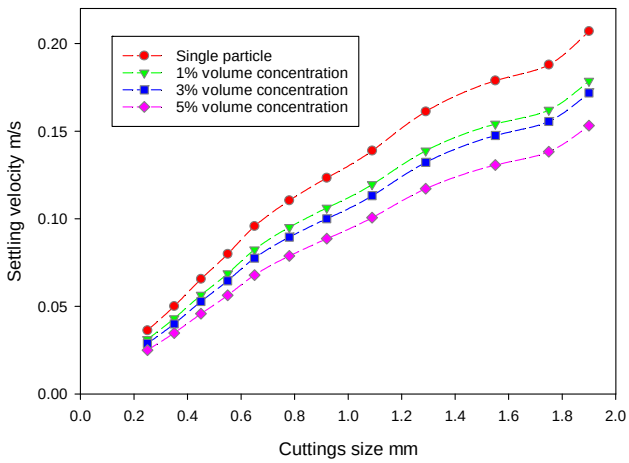

Figure 4.22 Cuttings hindered settling velocity in annulus for water.

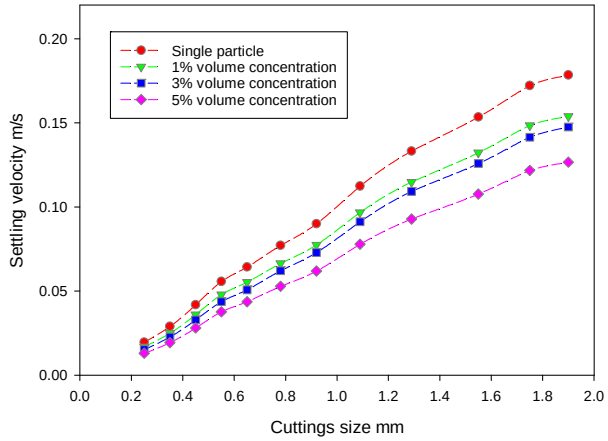

Figure 4.23 Cuttings hindered settling velocity in annulus for 0.02% XCD solution.

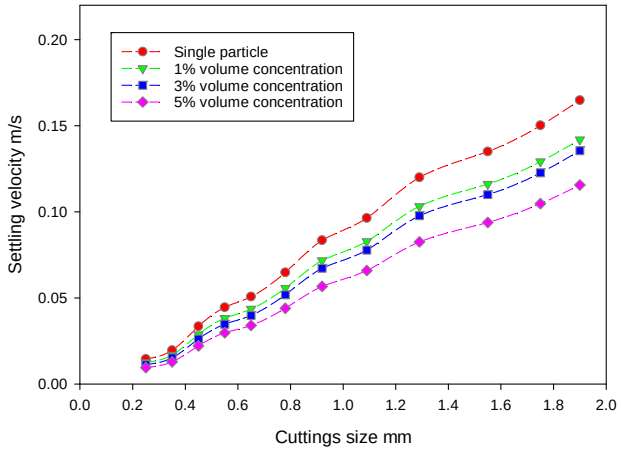

Figure 4.24 Cuttings hindered settling velocity in annulus for 0.03% XCD solution.

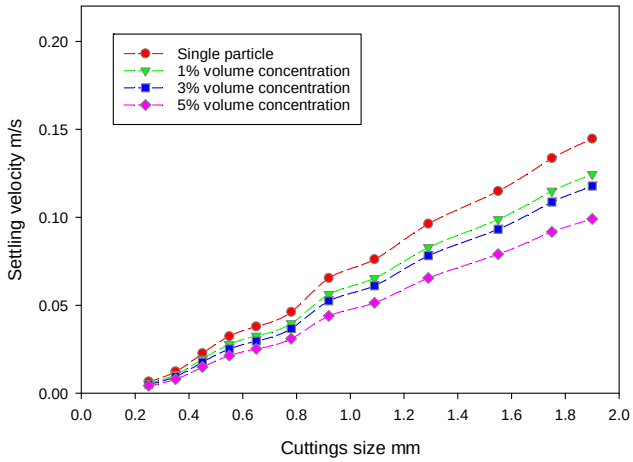

Figure 4.25 Cuttings hindered settling velocity in annulus for 0.05% XCD solution.

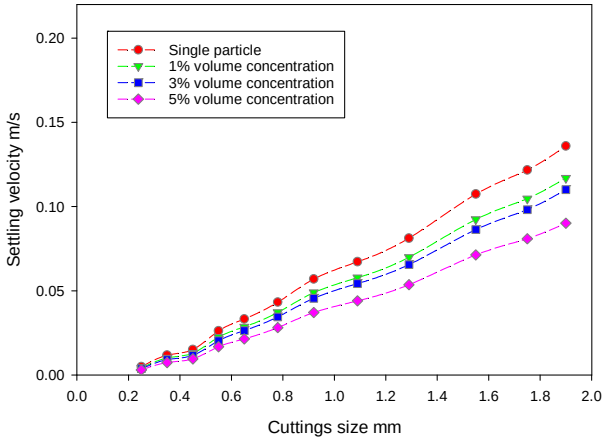

Figure 4.26 Cuttings hindered settling velocity in annulus for 0.06% XCD solution.

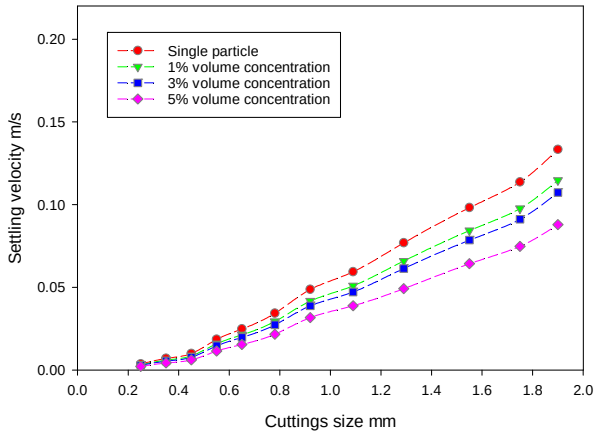

Figure 4.27 Cuttings hindered settling velocity in annulus for 0.07% XCD solution.

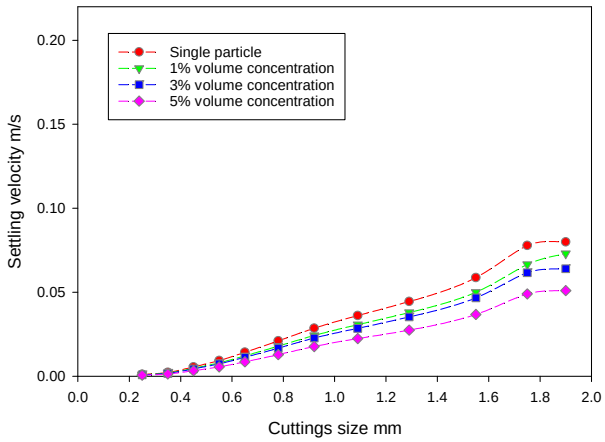

Figure 4.28 Cuttings hindered settling velocity in annulus for 0.1% XCD solution.

To better illustrate the cuttings concentration effect on the hindered settling with the variation of fluids viscosity and particle size, the ratio of hindered settling velocity to single particle settling velocity is compared for different sized particles. Figure 2.29 shows the ratio at different concentration for 0.02% and 0.1% XCD solution.

It can be seen that when the cuttings concentration is 1%, the ratio is almost constant and not affected by the particle size or fluids viscosity, which means the reduction of the settling velocity is linear. But as the cuttings concentration increases, the settling velocity become to be affected by the concentration impact but only for the large size particle, while the small size particle the ratio is the same, see the green curve for 3% concentration in Figure 2.29. And for the concentration of 5%, the impact of the fluids viscosity becomes dominant, and the decrease of the hindered settling is more significant in 0.1% XCD solution than that in 0.02% XCD solution.

Figure 2.30 shows the impact of the fluids viscosity on the settling for the same cuttings concentration. It's noted that with the increase of fluid viscosity, the ratio begins to rise slightly as the particle size increases, which suggests the small size particles have a larger impact. The influences of both particle size and fluid viscosity on the hindered settling start to show up with the cuttings concentration increase.

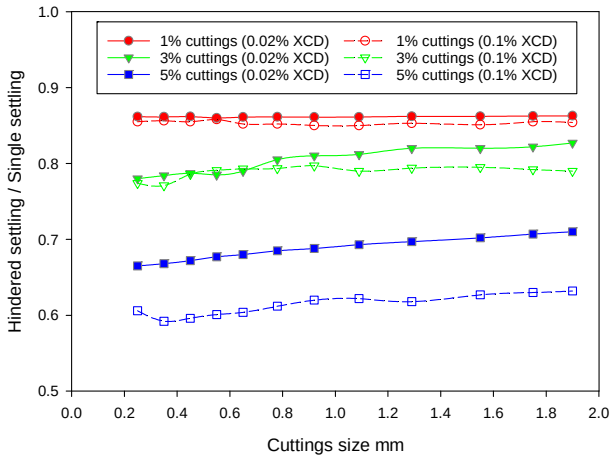

Figure 4.29 Hindered settling effected by the cuttings concentration for 0.02% XCD solution and 0.1% XCD solution.

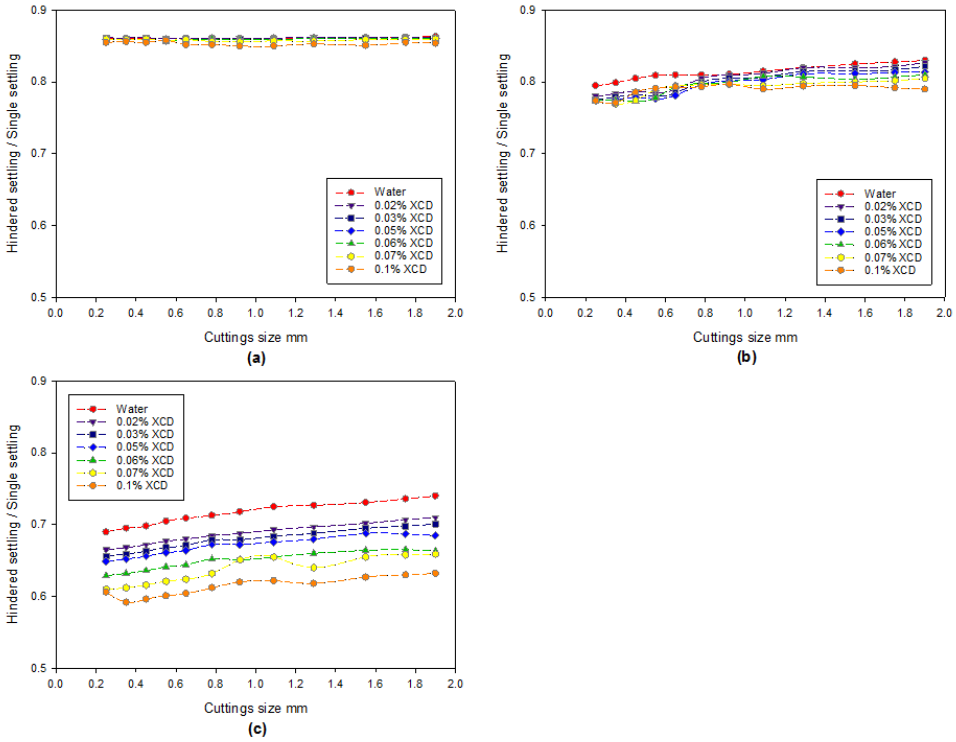

Figure 4.30 Hindered settling effected by fluid viscosity for various cuttings volume concentration, (a) cuttings volume fraction of 1%, (b) cuttings volume fraction of 3%, (c) cuttings volume fraction of 5%.

4.4. Summary

This chapter presented the cuttings settling velocity of both single particle and at various concentrations. The effect of particle size, fluid rheology and wall effect was studied. The power law fluid rheology impact was explained using the settling shear rate and the corresponding shear stress. The wall effect was analysed for the cuttings, and it was found that it is accurate to use hydraulic diameter of annulus instead of the gap width for the wall factor. The hindered settling of the cuttings in annulus was investigated. The results showed that the cuttings concentrations impact for various fluid rheology was different.

Chapter 5. Cuttings transport velocity

5.1. Introduction

This chapter summarises the measurement results of the cuttings transport velocity in the annulus using Particle Tracking Velocimetry setup on the flow loop.

Before the presenting the cuttings transport velocity, the rheology measurement of the cuttings and polymer solutions mixtures was introduced. The maximum cuttings concentration that polymer solutions can support was determined using the particle volume fraction. Then the suspensions viscosity was measured for different particle sizes and volume fractions (cuttings concentration) using a series of base polymer solutions.

The cuttings transport experiments were conducted on the flow loop, and the high speed camera was used to obtain the cuttings transport velocity. Various fluids and cuttings were tested to study the effect of fluids rheology, particle size and concentration on the cuttings transport velocity. The slip velocity obtained in this chapter is compared with the settling velocity derived in chapter 4 to study the flowing fluid impact on the particle mechanics.

In addition to the experimental work, the simulation results were presented to explain some phenomena observed in the experimental results. It was found that the cuttings transport velocity in some cases was higher than the fluid superficial velocity or the average velocity. This phenomenon was repeatedly noticed in the experiments, and is explained using the fluid velocity distribution in the annulus. The simulations of the fluid velocity on the cross section were performed using ANSYS Fluent for the turbulent regime in the annulus, and the results of the fluid velocity were compared with the experimental results of the cuttings velocity.

5.2. Rheology of the suspensions

The cuttings concentration has a significant influence on the cuttings velocity. For example, cuttings settling is hindered due to the interaction between the particles, and the cuttings transport velocity is decreased dramatically by the cuttings concentration, which is presented in this chapter. However, the previous study of the cuttings velocity only considered the viscosity of the base fluid, like the drag coefficient evaluation for the cuttings transport. The viscosity of the fluids and cuttings mixture is usually ignored, and the cuttings property effect on the rheology is neglected, especially for the high concentrated cuttings transport. Therefore

in this thesis, the viscosity change affected by the cuttings concentration and size is investigated to study the mixture viscosity effect on the cuttings transport velocity.

The cuttings and drilling fluid can form two different types of mixtures, suspensions and slurry. A suspension refers to the mixture of the solid particles (cuttings) and the dispersion medium (polymer solutions). The particles contained in the suspensions settle down at an extremely slow rate, so the suspensions can be stable for quite a long time. In previous study especially for simulations on the cuttings transport, it was assumed that there is no slip between the cuttings and the fluids [45].

On the other hand, when the cuttings concentration is higher, the drilling fluids and the cuttings form slurry, which requires a minimum flow rate to avoid the cuttings settling down during the transport, and most research on the particle slip velocity has been focused on this condition. Therefore to evaluate the property of the fluids and cuttings property and the cuttings slip velocity, it is essential to determine the maximum cuttings concentration and the cuttings size which the fluids are able to suspend.

5.2.1. Test procedure

The property and the preparation method of the cuttings and polymers materials have been introduced in Chapter 3. In this test, 12 groups of cuttings have been used including 0.2-0.3 mm, 0.3-0.4 mm, 0.4-0.5 mm, 0.5-0.6 mm, 0.6-0.71 mm, 0.71-0.85 mm, 0.85-1 mm, 1-1.18 mm, 1.18-1.4 mm, 1.4-1.7 mm, 1.7-1.8 mm and 1.8-2 mm. The experiments are performed using 6 solutions made up from different concentrations of XCD polymer as the base fluids. The rheology of the base polymer fluids is shown in Figure 5.1. The consistency index *K* and flow behaviour index *n* of the power law model $\tau = K\gamma^n$ are listed in Table 4.2.

There were 7 different cuttings volume concentrations used, including 1%, 2%, 3%, 4%, 5%, 8% and 10%. The concentrations were selected on the basis that the concentration in the cuttings transport is below 5%. The weight of the cuttings W_c added into the base fluids were prepared using the equation below.

$$W_c = V \times C_P \times \rho_P \qquad \text{(Equation 5.1)}$$

where V is the fluids volume, C_P is the cuttings concentration, and ρ_P is the absolute density of the cuttings.

Rigorous procedures were implemented to ensure that the cuttings in the suspension were stable during the measurement of fluids rheology. 10 litres of XCD polymer solutions are prepared for each test fluid using a mixer to ensure the viscosity consistency.

The weighed dry cuttings were added into 400ml fluid, and mixed for 30 seconds. When the cuttings particles were fully dispersed, the mixture was left for 5 min for observation. If particle settling down was not observed, the suspension would be used for the rheology measurement, and the polymer solutions would be tested at higher cuttings concentration.

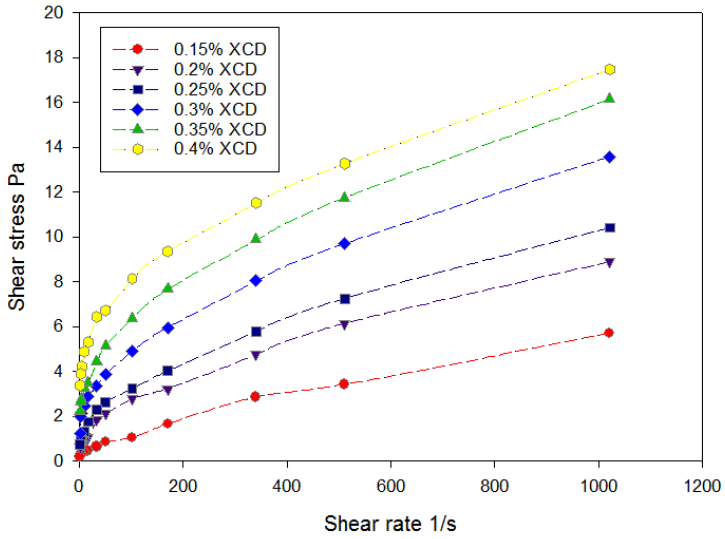

Figure 5.1 Rheology of various base solutions with different XCD polymer concentration.

Table 5.1 Consistency index *K* and flow behaviour index *n* of various polymer solutions shown in Figure 5.1.

Polymer concentration	0.15%	0.2%	0.25%	0.3%	0.35%	0.4%
Consistency index K	0.0602	0.2771	0.3994	0.8517	1.2864	2.3764
Exponent n	0.6554	0.4973	0.4666	0.3934	0.3582	0.2792

If the suspension of the cuttings is stable, the rheology is measured using HAAKE and Ofite rheometer. Previous research has measured the suspension viscosity using similar concentric cylinder rheometer [104, 105], but in this research the cuttings density is much larger than previous work. The drill cuttings are more likely to settle down to form slurry, which cannot

be tested by rheometer. Therefore in the rheology measurements, the samples of the suspensions are agitated again after the viscosity reading at each shear rate.

It is worth mentioning that for the small shear rate, the suspensions are more stable than the higher shear rate, but the dial reading of the viscosity at the small shear rate has a wider range of fluctuation and sometimes is unable to provide acceptable results, while the viscosity at high shear rate is quite stable even when the particles are more likely to settle.

5.2.2. Maximum volume fraction of the cuttings suspensions

Tables 5.2 to 5.7 list the maximum volume fraction of the cuttings that can be suspended by the solution of various XCD polymer concentration. The symbol "×" in the tables means for certain particle size and concentration, the polymer solution is thick to support the particles.

It can be seen that the maximum concentration is affected by both the particle size and the polymer concentration (base fluid rheology). With the increase of the base fluids viscosity, the maximum particle size that the solutions can suspend increases proportionally with the polymer concentration. For example, for the 1% cuttings concentration, when the polymer concentration increases by 0.05%, the particle size that can be suspended increases around 0.1 mm.

As the maximum particle size and concentration have been determined for the suspensions of the cuttings and fluid, based on earlier discussion, it was believed that the cuttings have the same velocity as the fluid velocity when the cuttings size and concentration are below the critical conditions. However, the experiments results showed that the cuttings transport velocity was different from the fluid velocity, which was presented later in this thesis.

Table 5.2 Volume fraction of the cuttings suspended in 0.15% XCD polymer solution.

Size	Sand volume fraction						
(mm)	1%	2%	3%	4%	5%	8%	10%
0.2-0.3	×	×	×	×	×		
0.3-0.4	×	×					

Table 5.3 Volume fraction of the cuttings suspended in 0.2% XCD polymer solution.

Size	Sand volume fraction						
(mm)	1%	2%	3%	4%	5%	8%	10%
0.2-0.3	×	×	×	×	×	×	×
0.3-0.4	×	×	×	×	×	×	×
0.4-0.5	×	×	×				

Table 5.4 Volume fraction of the cuttings suspended in 0.25% XCD polymer solution.

Size (mm)	Sand volume fraction						
	1%	2%	3%	4%	5%	8%	10%
0.2-0.3	×	×	×	×	×	×	×
0.3-0.4	×	×	×	×	×	×	×
0.4-0.5	×	×	×	×	×	×	
0.5-0.6	×	×	×	×			
0.6-0.71	×	×					

Table 5.5 Volume fraction of the cuttings suspended in 0.3% XCD polymer solution.

Size (mm)	Sand volume fraction						
	1%	2%	3%	4%	5%	8%	10%
0.2-0.3	×	×	×	×	×	×	×
0.3-0.4	×	×	×	×	×	×	×
0.4-0.5	×	×	×	×	×	×	×
0.5-0.6	×	×	×	×	×	×	
0.6-0.71	×	×	×	×			
0.71-0.85	×						

Table 5.6 Volume fraction of the cuttings suspended in 0.35% XCD polymer solution.

Size (mm)	Sand volume fraction						
	1%	2%	3%	4%	5%	8%	10%
0.2-0.3	×	×	×	×	×	×	×
0.3-0.4	×	×	×	×	×	×	×
0.4-0.5	×	×	×	×	×	×	×
0.5-0.6	×	×	×	×	×	×	×
0.6-0.71	×	×	×	×	×		
0.71-0.85	×	×	×				
0.85-1	×	×					

Table 5.7 Volume fraction of the cuttings suspended in 0.4% XCD polymer solution.

Size (mm)	Sand volume fraction						
	1%	2%	3%	4%	5%	8%	10%
0.2-0.3	×	×	×	×	×	×	×
0.3-0.4	×	×	×	×	×	×	×
0.4-0.5	×	×	×	×	×	×	×
0.5-0.6	×	×	×	×	×	×	×
0.6-0.71	×	×	×	×	×	×	
0.71-0.85	×	×	×	×	×		
0.85-1	×	×	×				
1-1.18	×						

5.2.3. Effect of the cuttings size and concentration on the slurry viscosity

Figures 5.2 to 5.7 present the suspensions viscosity variation as various shear rates affected by the particle size and volume concentration. All the results of the cuttings effect on the fluid rheology are listed in Appendix.

It can be seen that the suspensions show the same shear thinning behaviour as the base fluids after added solid particles. For the fluids with relatively high concentrations (0.35% and 0.4% XCD base fluids), the viscosity at low shear rate is unstable for particles above 0.71 mm even at low concentration of 1%.

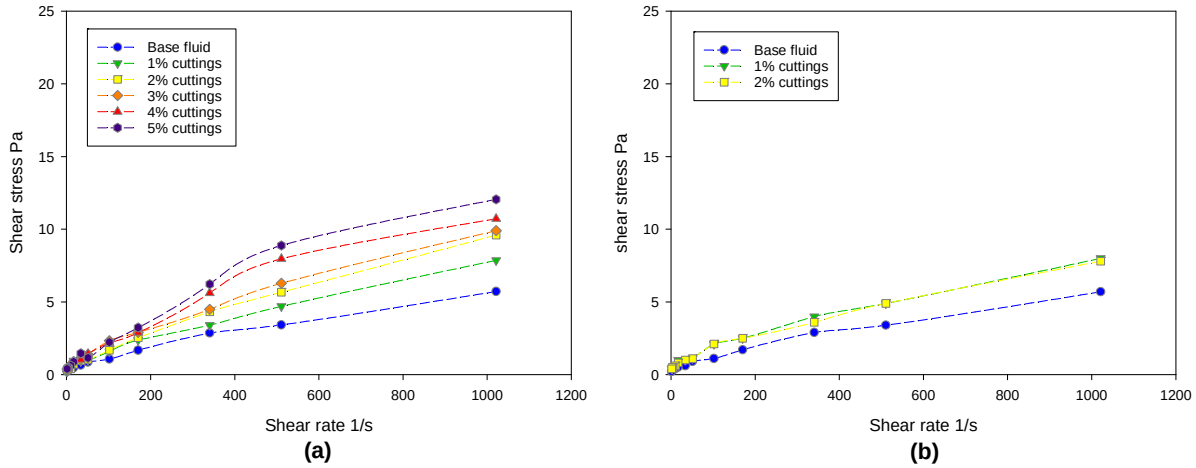

Figure 5.2 Rheology change of the suspensions for 0.15% XCD polymer solution at different cuttings volume fraction, (a) 0.2-0.3 mm, (b) 0.3-0.4 mm.

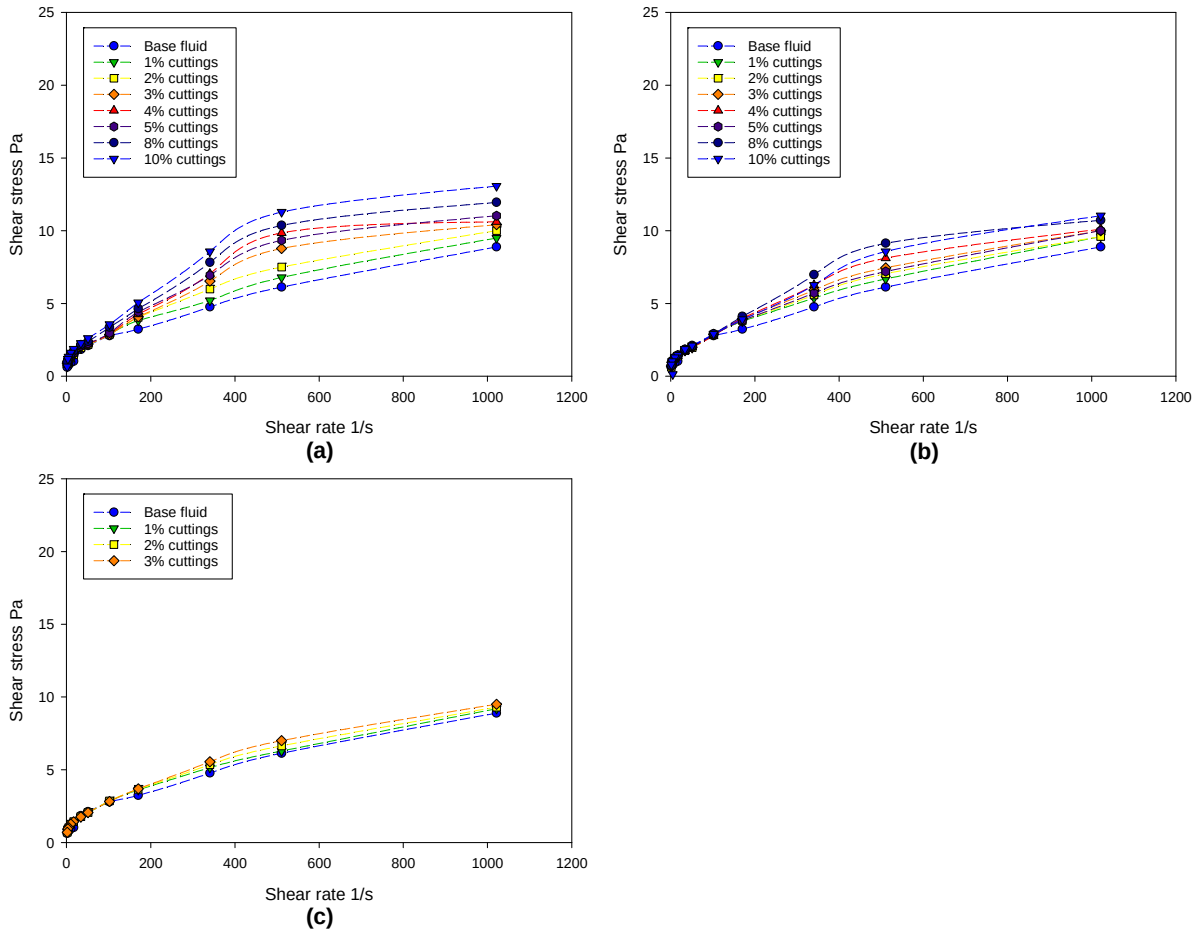

Figure 5.3 Rheology change of the suspensions for 0.2% XCD polymer solution at different cuttings volume fraction, (a) 0.2-0.3 mm, (b) 0.3-0.4 mm, (c) 0.4-0.5 mm.

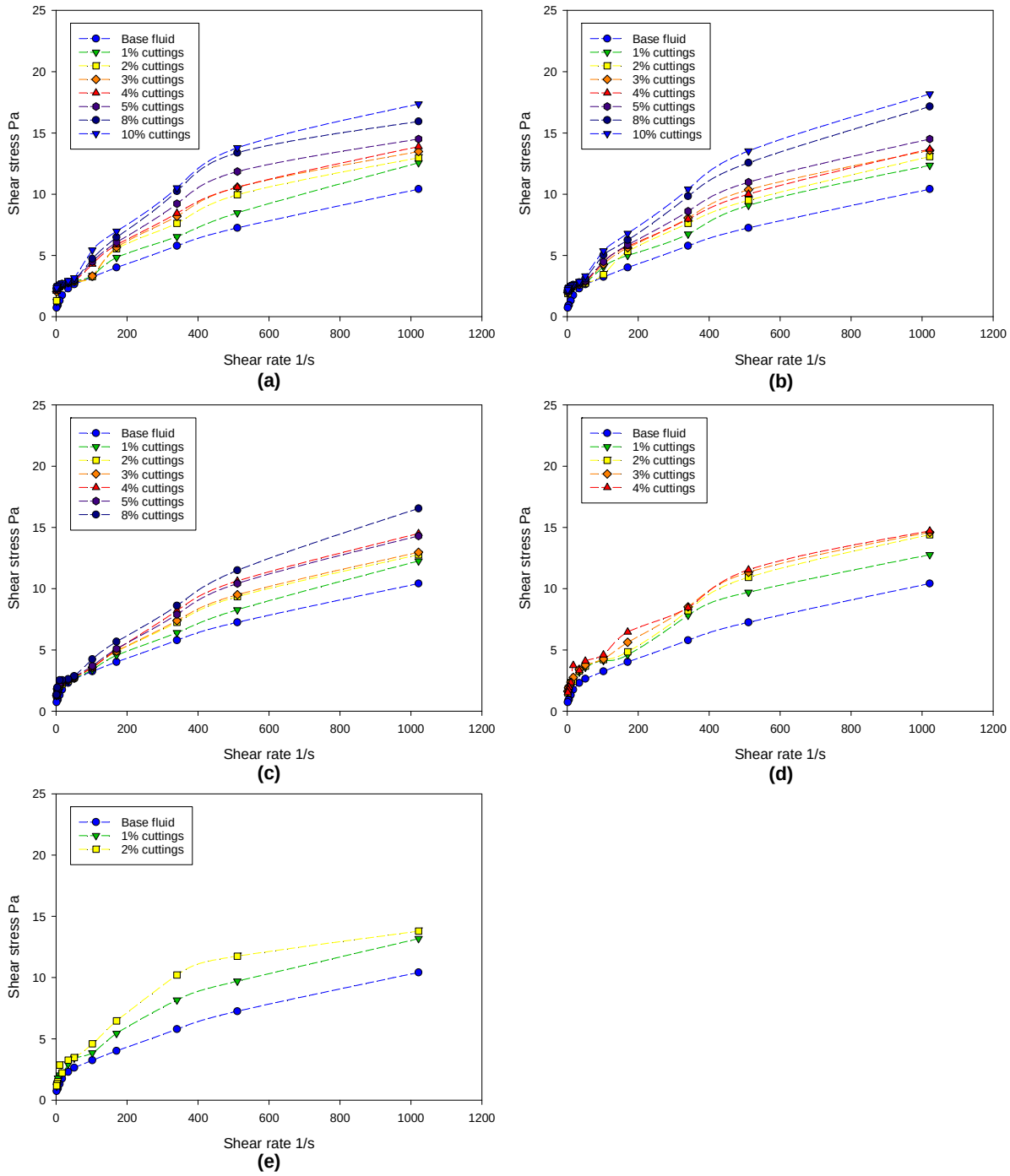

Figure 5.4 Rheology change of the suspensions for 0.25% XCD polymer solution at different cuttings volume fraction, (a) 0.2-0.3 mm, (b) 0.3-0.4 mm, (c) 0.4-0.5 mm, (d) 0.5-0.6 mm, (e) 0.6-0.71 mm.

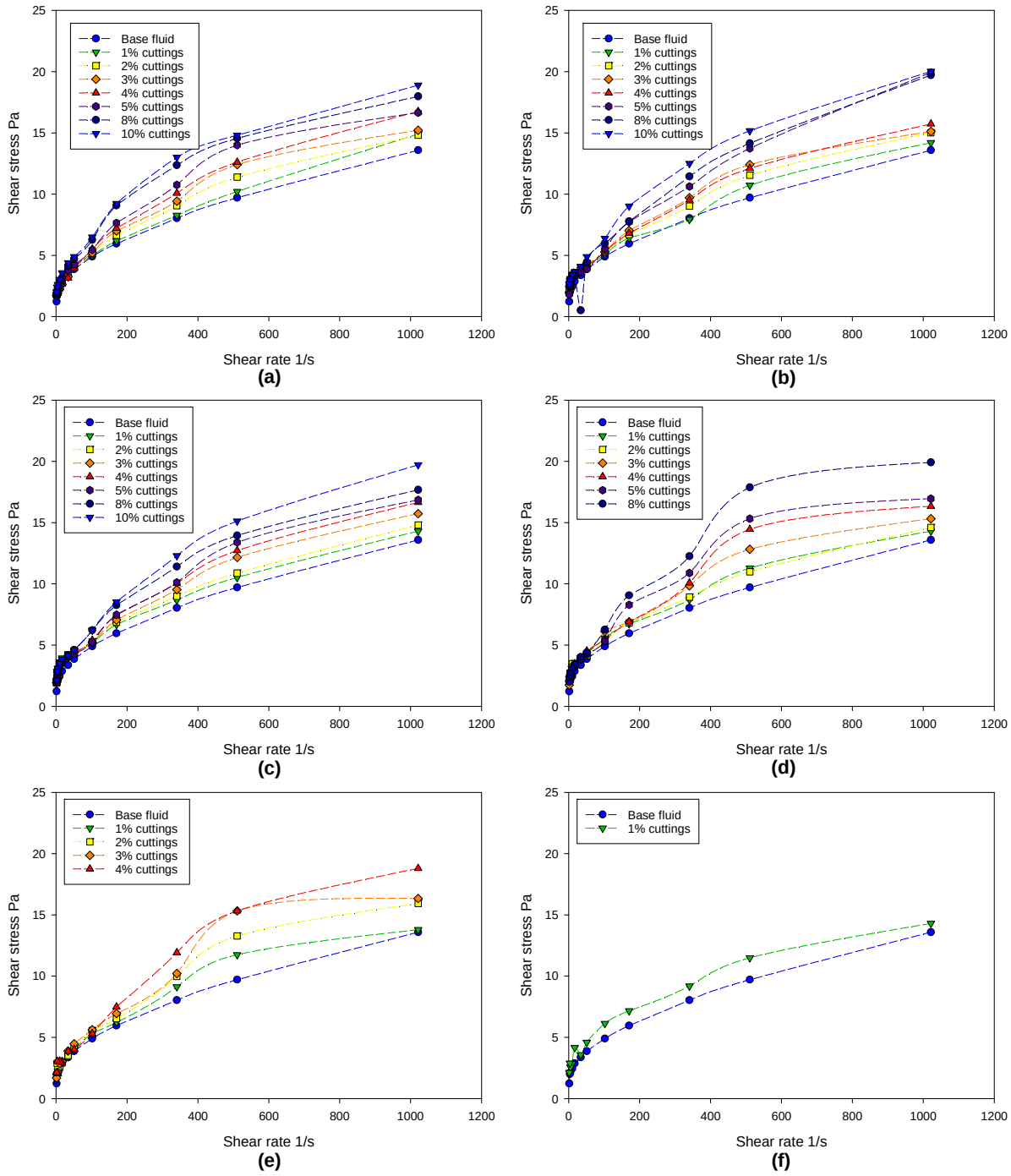

Figure 5.5 Rheology change of the suspensions for 0.3% XCD polymer solution at different cuttings volume fraction, (a) 0.2-0.3 mm, (b) 0.3-0.4 mm, (c) 0.4-0.5 mm, (d) 0.5-0.6 mm, (e) 0.6-0.71 mm, (f) 0.71-0.85 mm.

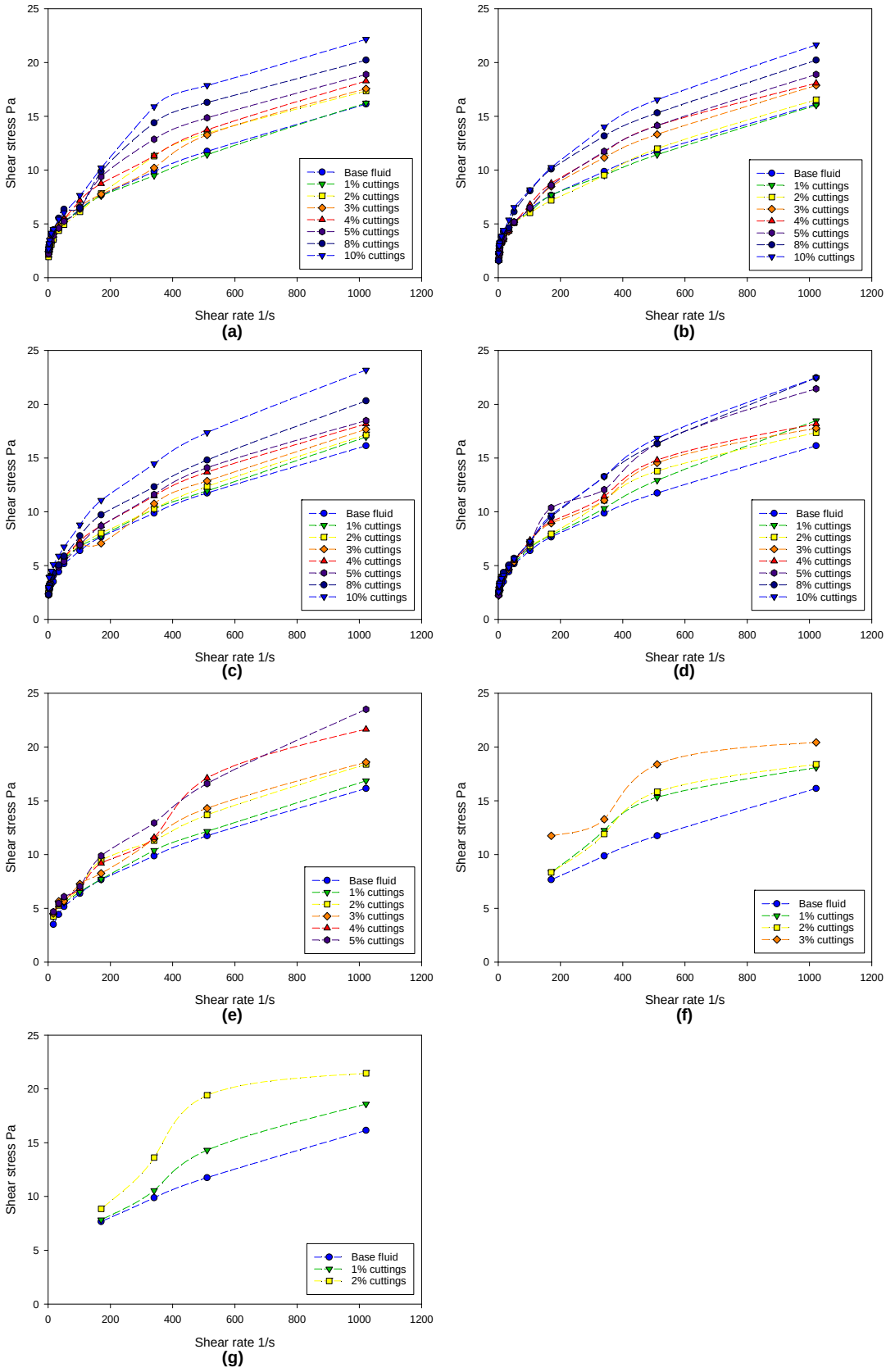

Figure 5.6 Rheology change of the suspensions for 0.35% XCD polymer solution at different cuttings volume fraction, (a) 0.2-0.3 mm, (b) 0.3-0.4 mm, (c) 0.4-0.5 mm, (d) 0.5-0.6 mm, (e) 0.6-0.71 mm, (f) 0.71-0.85 mm, (g) 0.85-1 mm.

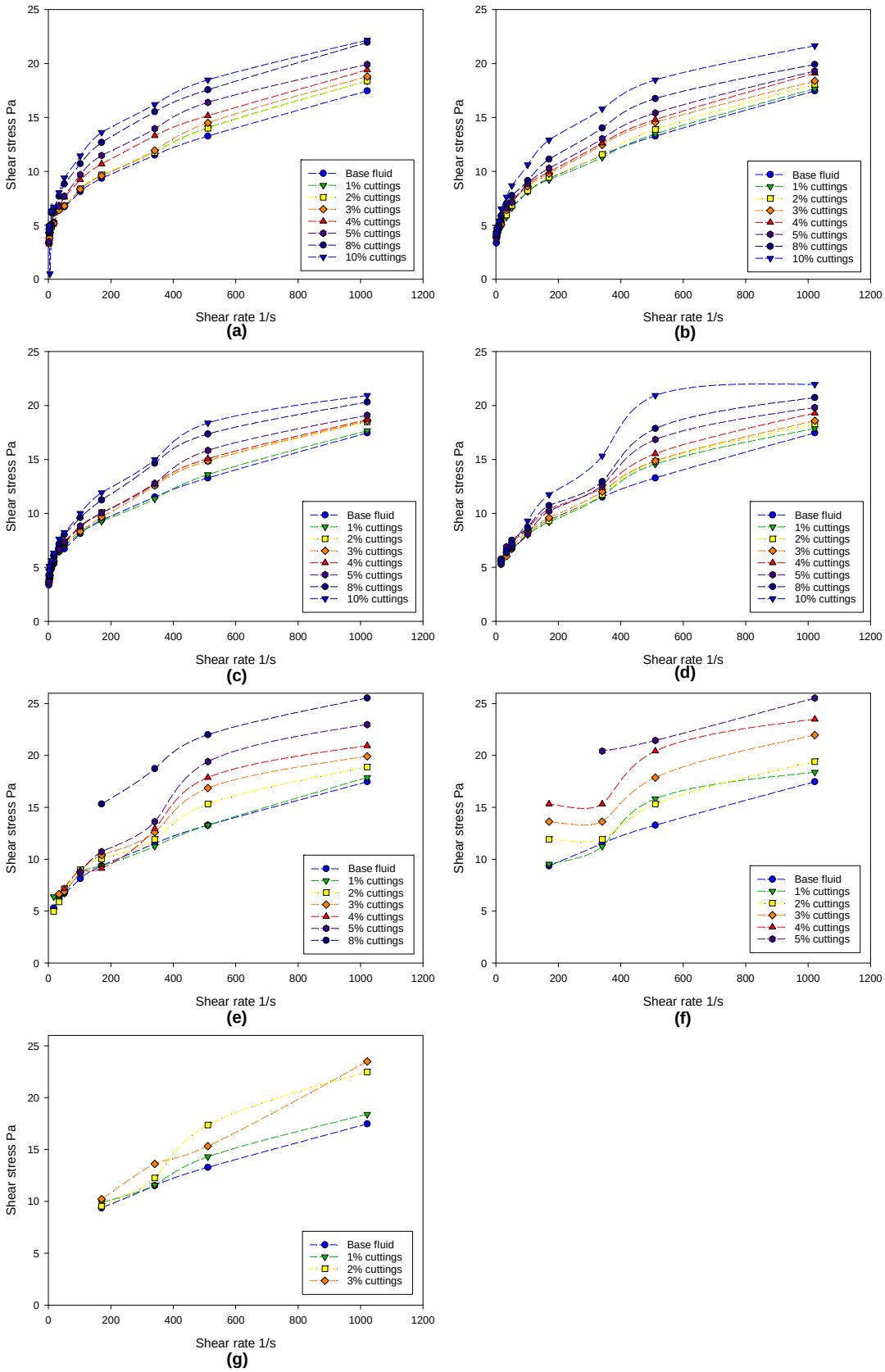

Figure 5.7 Rheology change of the suspensions for 0.4% XCD polymer solution at different cuttings volume fraction, (a) 0.2-0.3 mm, (b) 0.3-0.4 mm, (c) 0.4-0.5 mm, (d) 0.5-0.6 mm, (e) 0.6-0.71 mm, (f) 0.71-0.85 mm, (g) 0.85-1 mm.

With the increase of the cuttings volume concentration, the suspension viscosity increases over the tested shear rate range up to 1021 1/s. The results show that the variation of viscosity with the cuttings concentrations is also affected by the particle size and the base fluids. The smaller sized particles have a more significant effect on the suspensions rheology. For example, the increase of viscosity affected by 0.2-0.3mm particles is greater than the other larger size classes. To indicate the particle size effect on suspension rheology, the relative viscosity is used which is defined as the ratio of the suspension viscosity over the base fluids [106].

Figure 5.8 shows an example of the relative viscosity as a function of the shear rate above 150 1/s for 0.2% XCD fluids. It can be seen that the change varies with the shear rates. The viscosity increases with the shear rate below 510 1/s, but then drops rapidly at 1021 1/s. It is worth mentioning that the results were obtained based on more than five tests, and it is confirmed that depending on the cuttings property and fluid rheology, the suspensions relative viscosity can increase and then decrease with the increase of the shear rate.

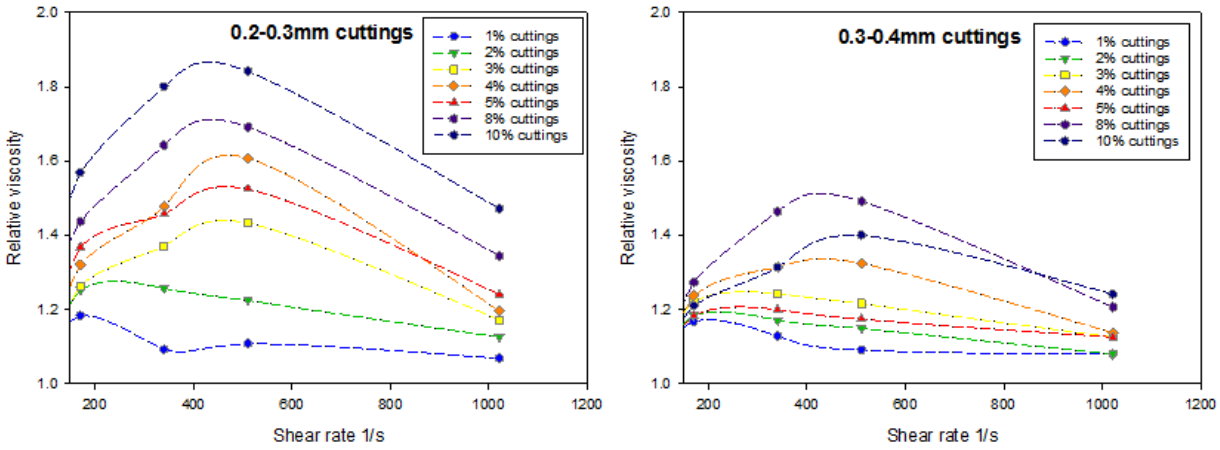

Figure 5.8 Relative viscosity with shear rate for 0.2% XCD polymer solution.

However, this trend declines when the polymer solutions rheology increases and the cuttings concentration decreases. For example, for the 0.3-0.4 mm cuttings in 0.2% XCD polymer solutions, when the cuttings concentration drops to below 3%, the relative viscosity decreases over the tested shear rate range.

To show the relative viscosity variation trend for more viscous solutions, the relative viscosity variation with shear rate for various solutions of XCD polymer is presented in Figure 5.9. A prominent phenomenon is that the trend of first increase and then decrease becomes to be decreasing almost over the tested shear rate range. Figure 5.9 shows the impact of the XCD

polymer concentration (base fluid rheology) for 0.2-0.3 mm cuttings. It can be seen that with the increase of the base fluid viscosity, the relative viscosity decreases for cuttings concentration below 10%. This means the particle effect on the fluid rheology declines when the fluid viscosity increases.

As the viscosity increases, the suspensions with the cuttings are more likely to be stable, but the effect of the fine particles is limited to fluids with higher polymer concentration. Although, the base fluid is power law fluid, the suspensions relative viscosity for higher polymer concentration (>0.3% XCD) is quite constant. Similar phenomenon has been reported in previous work on Newtonian fluids [95].

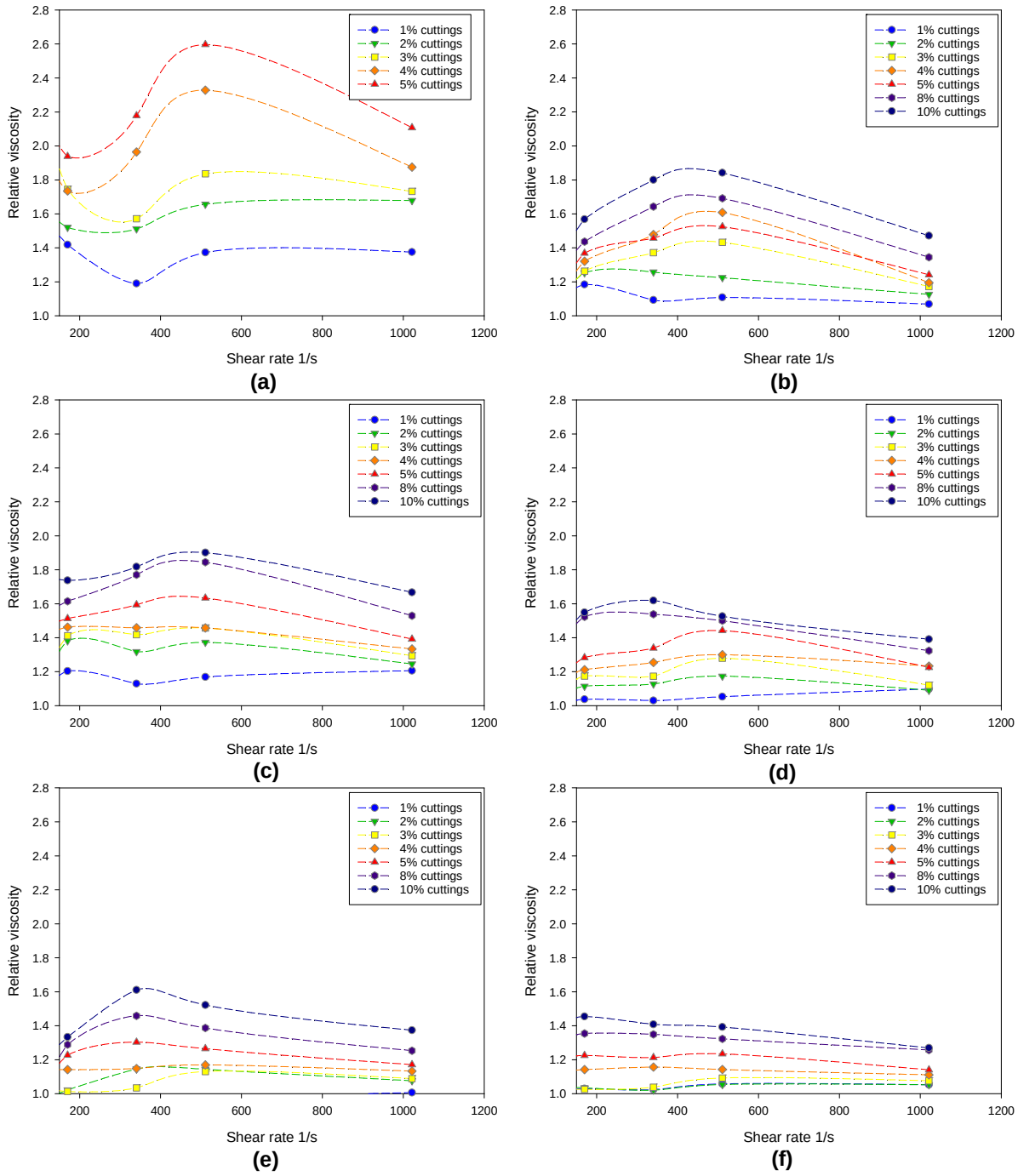

Figure 5.9 Effect of the base fluid on suspensions viscosity for cuttings of 0.2-0.3 mm, (a) 0.15 XCD, (b) 0.2% XCD, (c) 0.25% XCD, (d) 0.3% XCD, (e) 0.35% XCD, (f) 0.4% XCD.

5.3. Cuttings transport velocity

5.3.1. Research methodology

In this section, the measurement results of the cuttings transport velocity using PTV method during the cuttings transportation is presented. The impacts of the fluid rheology, cuttings property and concentration on the particle velocity in the flowing fluid are investigated. The results obtained are analysed and compared with the cuttings settling velocity which is presented in previous chapter.

The measurement of the cuttings transport velocity in annulus is briefly introduced in this section. Figure 5.10 shows the experimental setup which has been used for the cuttings hindered settling tests. The stable cuttings transport is established first on the flow loop. Then the high speed camera is turned on to capture the images of the cuttings movement.

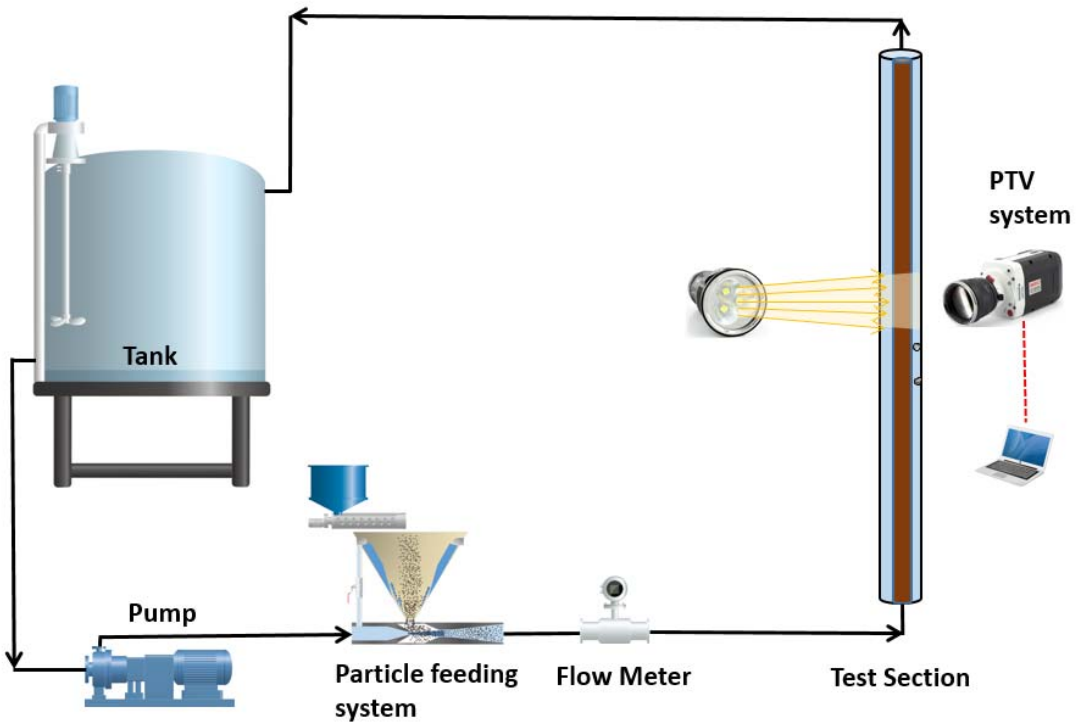

Figure 5.10 Schematic diagram of the hindered settling experimental setups.

The cuttings are introduced into the drilling fluid using the feeder and eductor. After the adjustment of the flow rate and solid particle feeding rate, the cuttings volumetric concentration C_P can be calculated by $C_P = \frac{M}{Q\rho_P}$,

where M is the mass feeding rate of the cuttings, Q is the flow rate of the slurry mixture measured by the flow meter, and ρ_P is the particle absolute density.

The experiments were performed for both single particle of the cuttings and the cuttings transport at the concentration of 1% and 3% (volume fraction). The polymer solutions used for the cuttings transport cover a wider range than the fluids used for the cuttings settling tests. The rheology of the polymer solutions is characterised by power law models, and the model indexes are summarised in Table 5.8.

Table 5.8 Consistency index K and flow behaviour index n of the fluids for cuttings transport.

Fluids	1	2	3	4	5
Polymer concentration	0.02%	0.05%	0.1%	0.15%	0.2%
Consistency index K	0.0102	0.0252	0.0905	0.0602	0.2771
Exponent n	0.728	0.6636	0.562	0.6554	0.4973

In addition to the experimental measurement of the cuttings transport velocity, it is essential to obtain the fluid velocity distribution on the annulus cross section, as the experimental results showed that the cuttings velocity in some cases is larger than the fluid average velocity. By comparing the fluid velocity distribution and the cuttings velocity, the study found that the cuttings transport is in the centre of the flow field.

The simulation was conducted using CFD software ANSYS Fluent by solving the incompressible Navier-Stokes equations using finite volume method. The annulus model was built and set for meshing, see Figure 5.18. The shear stress transport k-w model was used as the turbulent model for the vertical wellbore. The roughness of the annulus was set 0.01mm for acrylic wall. The flow rate, wellbore size and fluids rheology was set the same as the experiments. Figure 5.19-5.21 shows the fluid velocity distribution on the annulus section. As the annulus geometry is symmetric along the inside pipe, the figures only present half of the fluid velocity.

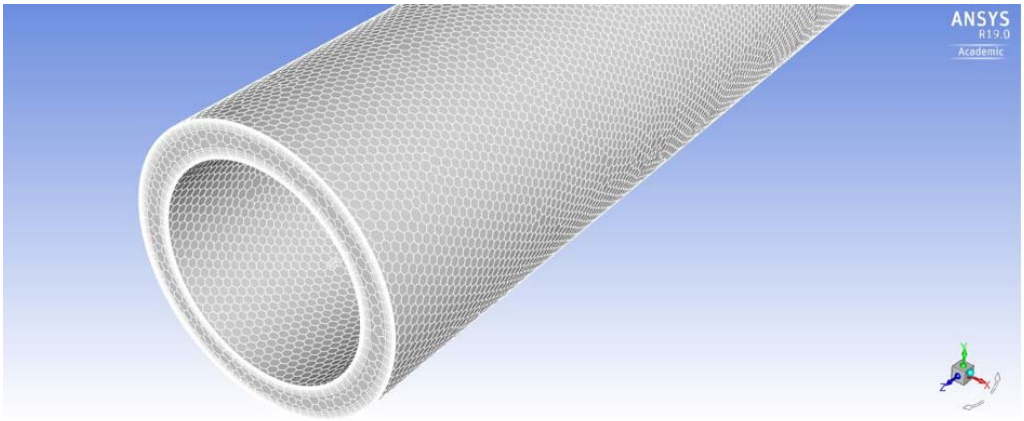

Figure 5.11 Annulus model in ANSYS Fluent.

5.3.2. Results and discussion

5.3.2.1. Cuttings transport velocity distribution

It was found during the PTV measurements that the cuttings transport velocity varied slightly in a range even when the experimental condition was constant. To obtain the precise results of the cuttings transport velocity, it is essential to repeat the experiments several times to obtain an average cuttings velocity from a large quantity of data for the given test condition. For the single particle velocity, more than 100 particles have been analysed for each test condition, and for the cuttings transport at 1% and 3% concentration, 3 videos were recorded each containing more than 50 particles.

The cuttings transport velocity of each particle was obtained, and the percentage distribution of the cuttings velocities was developed for each test condition. It is worth mentioning that due to the limitation of the PTV method and the light source, the percentage distribution in this research is not directly related to the particles location in the cross section of the annulus. However, based on the cuttings velocity combined with the fluid velocity distribution, this research found that most particles in the cuttings transport are travelling in the centre of the flow field.

Figures 5.12-5.14 show the cuttings velocity percentage for various flow rates at the volume concentration of 1% for water, 0.1% XCD and 0.2% XCD respectively. The percentage is defined as the ratio of the particles that have certain transport velocity to the total number of the particles that have been analysed in the PTV. It can be seen that with the increase of the fluids viscosity, the percentage of the maximum fluid velocity decreases and the distribution

becomes more even, meaning that the cuttings velocity covers a wider range. The cuttings size has a similar effect. When the cuttings size increases from 0.2-0.3 mm to 1.8-2 mm, the distribution becomes even as well. The percentage for the higher cuttings velocity decreases but varies in a wider range of the velocity.

Figures 5.15-5.17 show the cuttings velocity percentage with the cuttings size of 0.2-0.3mm, 0.71-0.85mm and 1.8-2mm at the volume concentration of 1% for water, 0.1% XCD and 0.2% XCD respectively. It can be seen that the cuttings velocity increases with the flow rates, but the difference of the velocity for the same particle size increases as well. The flow rate impact on the smaller sized particles is more significant. In addition, the percentage of the maximum cuttings velocity decreases with the increase of the flow rate.

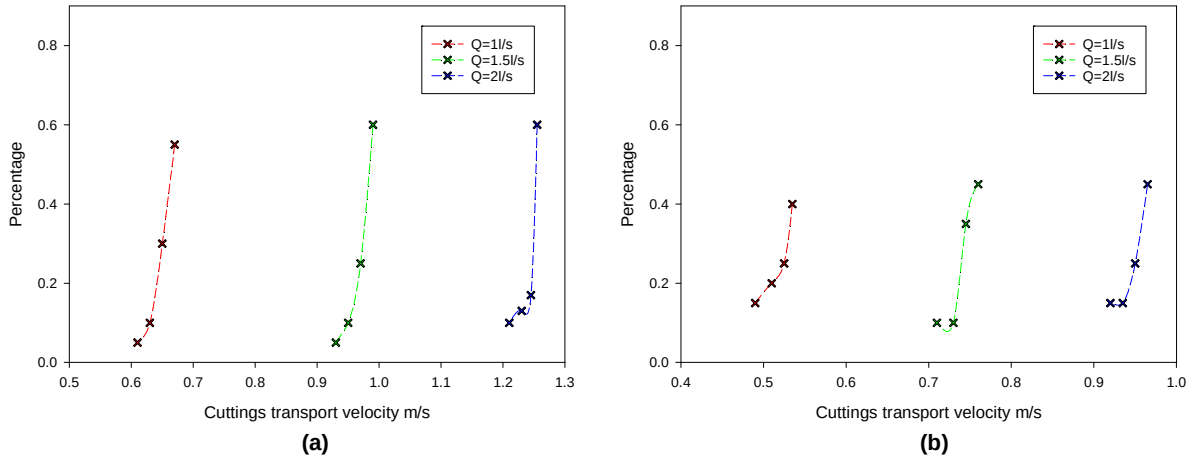

Figure 5.12 Cuttings transport velocity percentage distribution for water at various flow rates with 1% cuttings concentration, (a) 0.2-0.3 mm, (b) 1.8-2 mm.

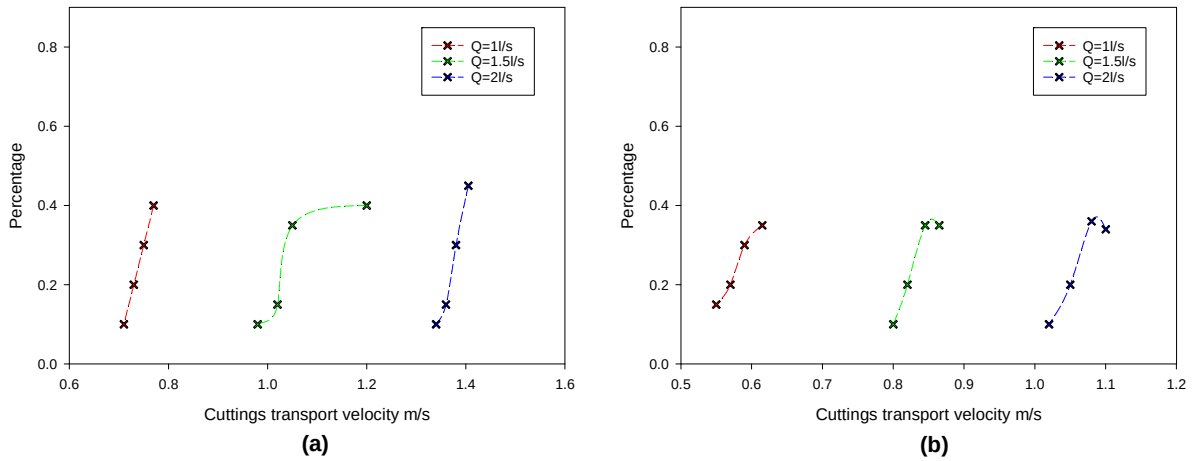

Figure 5.13 Cuttings transport velocity percentage distribution for 0.1% XCD solutions at various flow rates with 1% cuttings concentration, (a) 0.2-0.3 mm, (b) 1.8-2 mm.

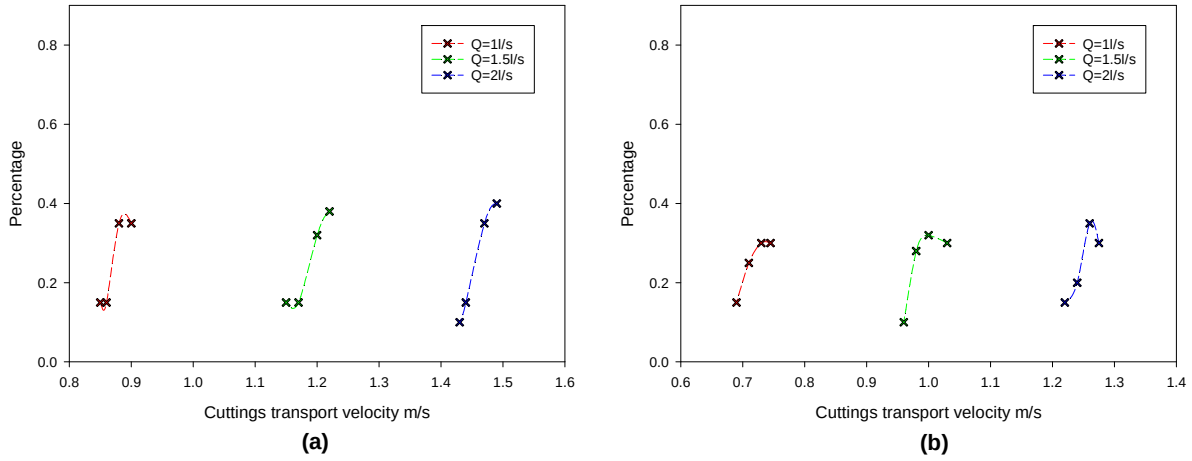

Figure 5.14 Cuttings transport velocity percentage distribution for 0.2% XCD solutions at various flow rates with 1% cuttings concentration, (a) 0.2-0.3 mm, (b) 1.8-2 mm.

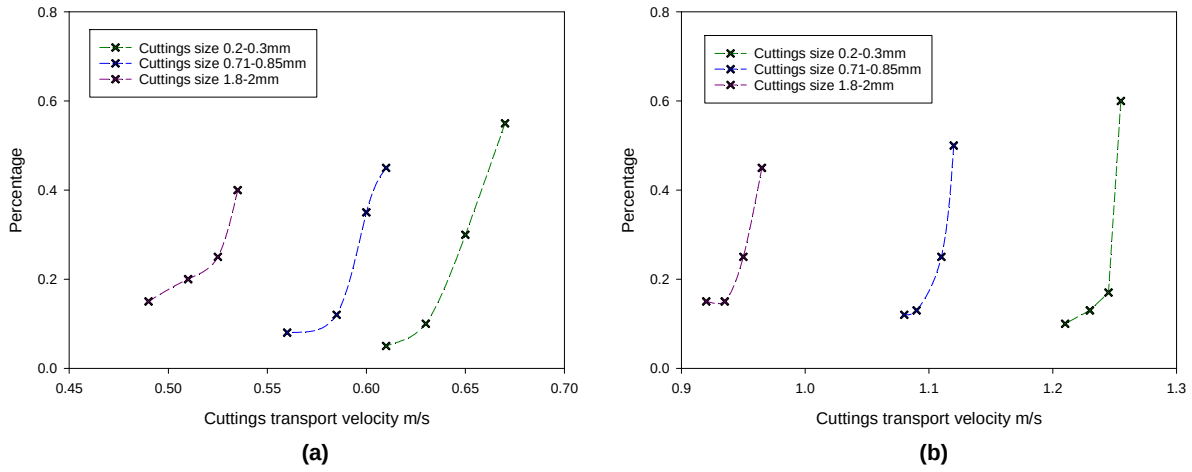

Figure 5.15 Cuttings transport velocity percentage distribution for water with various cuttings size and 1% cuttings concentration, (a) flow rate of 1 l/s, (b) flow rate of 2 l/s.

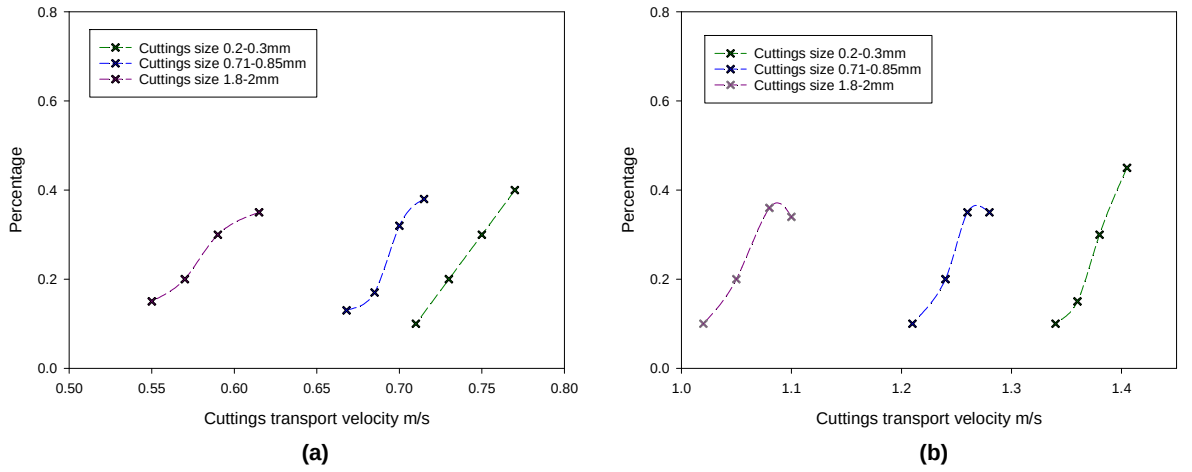

Figure 5.16 Cuttings transport velocity percentage distribution for 0.1% XCD solutions with various cuttings size and 1% cuttings concentration, (a) flow rate of 1 l/s, (b) flow rate of 2 l/s.

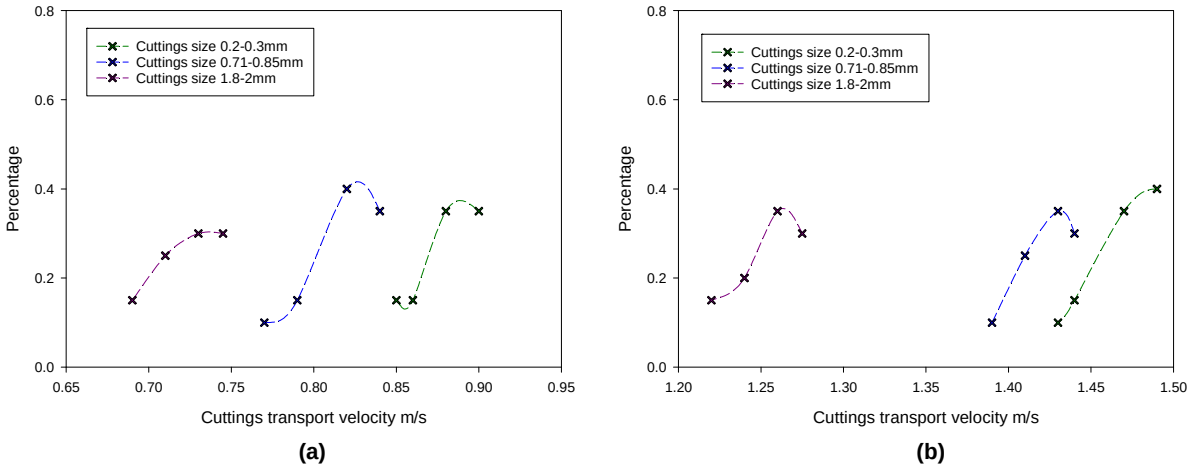

Figure 5.17 Cuttings transport velocity percentage distribution for 0.2% XCD solutions with various cuttings size and 1% cuttings concentration, (a) flow rate of 1 l/s, (b) flow rate of 2 l/s.

The cuttings transport velocity was obtained based on the average of the velocity distribution. When explaining the experimental data within the text, the cuttings velocity is used instead of the average cuttings velocity.

The experimental results showed that the cuttings transport velocity in some cases is higher than the fluid average velocity. For example, shown in Figure 5.17, the cuttings velocity for particles below 0.85 mm is larger than the fluid average velocity $V_{f\ ave}$ of 0.808 m/s for the flow rate of 1 l/s. The experiments also found that the cuttings velocity is higher when the cuttings concentration decreases and the fluid rheology increases. For example, Figure 5.18 shows the cuttings velocity of single particle in 0.2% XCD polymer solutions. It can be seen that compared with the average fluid velocity of 0.808 m/s, 1.213 m/s and 1.617 m/s for the flow rates of 1 l/s, 1.5 l/s and 2 l/s respectively, the particle velocity without the cuttings concentration effect is much higher than the fluid average velocity.

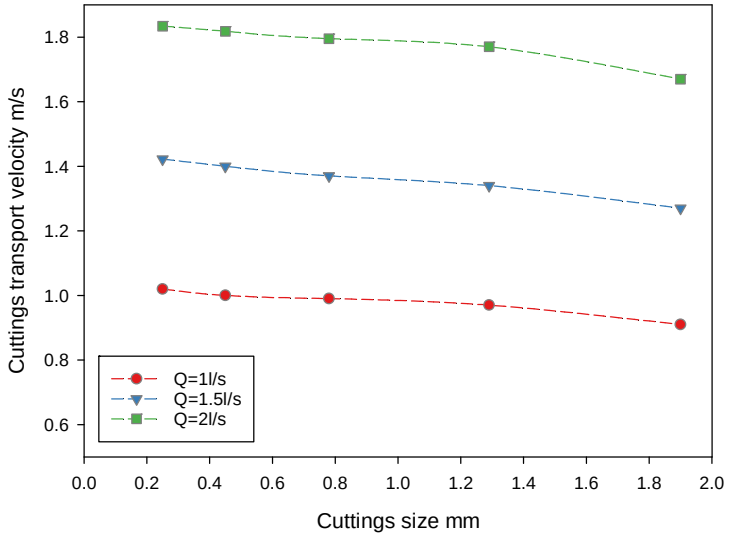

Figure 5.18 Cuttings transport velocity of single particle at various flow rates in 0.2% XCD polymer solutions.

To explain the reason why the cuttings transport velocity is larger than the fluid average or superficial velocity, fluid velocity distribution on the annulus cross section obtained from the simulation is compared with the experimental results of the cuttings transport velocity. Figures 5.19-5.21 shows the fluid velocity distribution on the annulus section. As the annulus geometry is symmetric along the inside pipe, the figures only present half of the fluid velocity.

The fluid distribution shows that in the middle of the flow, the fluid velocity is almost constant, but in the areas close to the walls, the fluid velocity is much smaller due to the boundary effect. The shear rate reaches the minimum in the centre, where the fluid velocity remains almost constant, similar to the flow pattern that the fluid in the centre travels like a plug as a rigid part [107, 108]. The fluid local velocity in the centre is much larger than the average fluid velocity. With the increase of the power law fluids viscosity, the fluid local velocity increases, while the area of the maximum fluid velocity decreases. At higher flow rate, the discrepancy of the velocity distribution for different fluids decreases due to higher turbulence.

Based on the fluid velocity distribution, the areas for each velocity is obtained and the percentage of the area to the annulus area is presented with different local velocity, see Figure 5.19-5.21.

Based on the experimental results of the cuttings velocity and the fluid velocity distribution from the numerical simulation, it can be inferred that the cuttings transport is in the centre of

the flow field where the shear rate of the fluid is minimum. The fluid velocity close to the annulus boundary is much smaller than the cuttings velocity which is obtained from the experimental measurement, and although the cuttings velocity varies in a range, the velocity is much larger than the fluid velocity presented by the simulation.

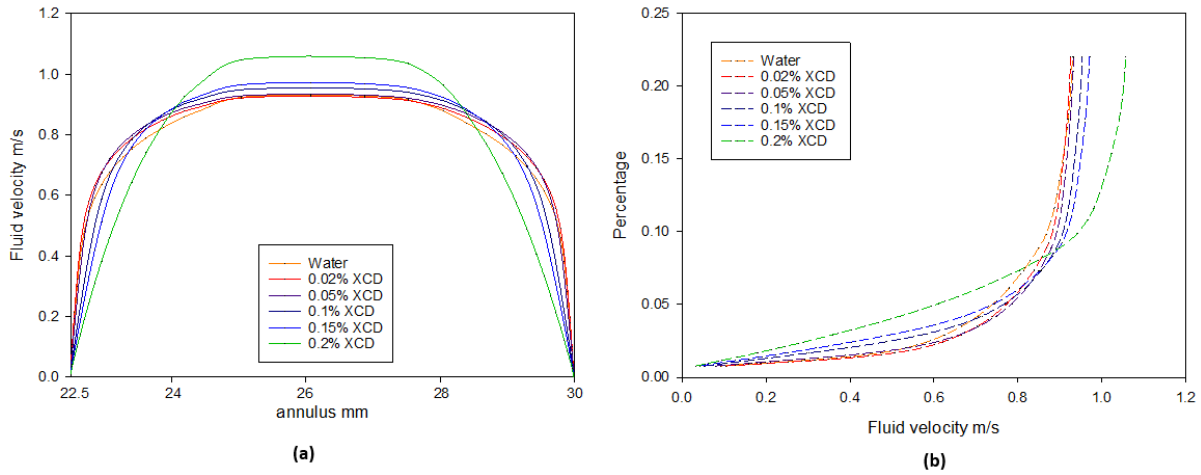

Figure 5.19 Fluid velocity distribution on the cross section and flowing area percentage with different fluid velocity for various fluids at flow rate of Q=1 l/s (fluid average velocity $\boldsymbol{V_{f\,ave}}$ = 0.808 m/s), (a) fluid distribution, (b) flowing area percentage.

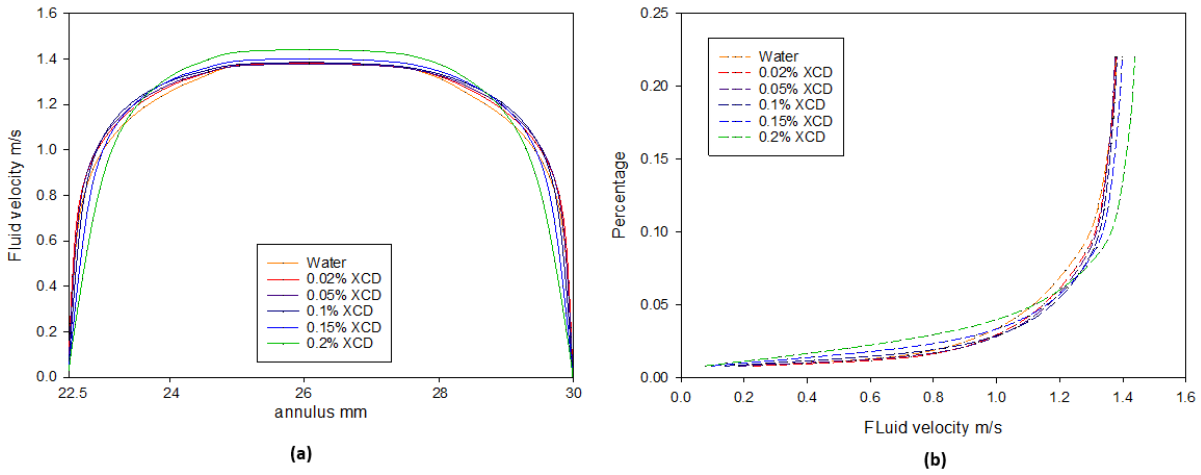

Figure 5.20 Fluid velocity distribution on the cross section and flowing area percentage with different fluid velocity for various fluids at flow rate of Q=1.5 l/s (fluid average velocity $\boldsymbol{V_{f\,ave}}$ =1.213 m/s), (a) fluid distribution, (b) flowing area percentage.

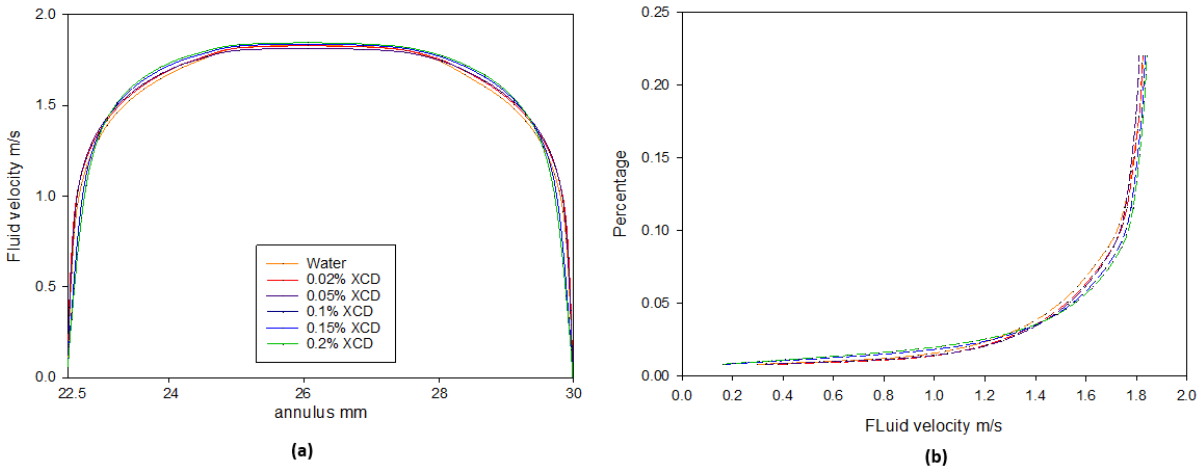

Figure 5.21 Fluid velocity distribution on the cross section and flowing area percentage with different fluid velocity for various fluids at flow rate of Q=2 l/s (fluid average velocity $\boldsymbol{V_{f\,ave}}$ =1.617 m/s), (a) fluid distribution, (b) flowing area percentage.

5.3.2.2. Cuttings transport velocity of single particle

Figure 5.22 shows the cuttings transport velocity of single particle in the annulus at different flow rates for various fluids. As shown in the graph, the cutting transport velocity decreases with the cuttings size. Although the fluids rheology is quite different, the trend of the velocity variation with the cuttings size is very similar. For example, for water at the flow rate of 2 l/s, the cuttings velocity decreases from 1.7 m/s to 1.55 m/s when the cuttings size increases from 0.2-0.3 mm to 1.8-2 mm, and similarly for 0.1% XCD polymer solutions, the cuttings velocity decreases from 1.8 m/s to 1.65 m/s for the same cuttings size variation.

However the flow rate has a more significant impact, and the cuttings velocity variation by increasing flow rate is more noticeable. At higher flow rates, the variation of the cuttings velocity with the cuttings size is larger. For example, the cuttings velocity at the flow rate of 1 l/s is relatively constant for all the various fluids. But when the flow rate reaches 2 l/s, the cuttings velocity for smaller particle size is larger than the velocity of bigger particles.

The fluids viscosity effect on the cuttings velocity is shown in Figure 5.23. In the graph the effect of the fluids rheology is shown using the velocity ratio which is defined as the particle velocity in XCD polymer solutions to the particle velocity in water. It can be seen that the cuttings velocity is approximately linear with the cuttings size at each flow rate. For example, the cuttings velocity decrease with the cuttings size increase is all around 0.15 m/s for the fluids of various polymer concentration at the flow rate of 1.5 l/s.

The graph of the velocity ratio shows a clear trend of the flow rate and fluids rheology impact. It can be seen that the velocity ratio decreases generally as the flow rate increases, especially for the more viscous fluids. For example, for the 0.2-0.3 mm particles in the 0.2% XCD solutions, the velocity ratio decreases from around 1.2 to 1.08 when the flow rate increases from 1 l/s to 2 l/s. The other fluids follow the same trend. However, this trend declines as the fluids viscosity decreases. For example, the velocity ratios decreases only from 1.02 to 1.01 for the same flow rate change in the 0.02% XCD polymer solutions.

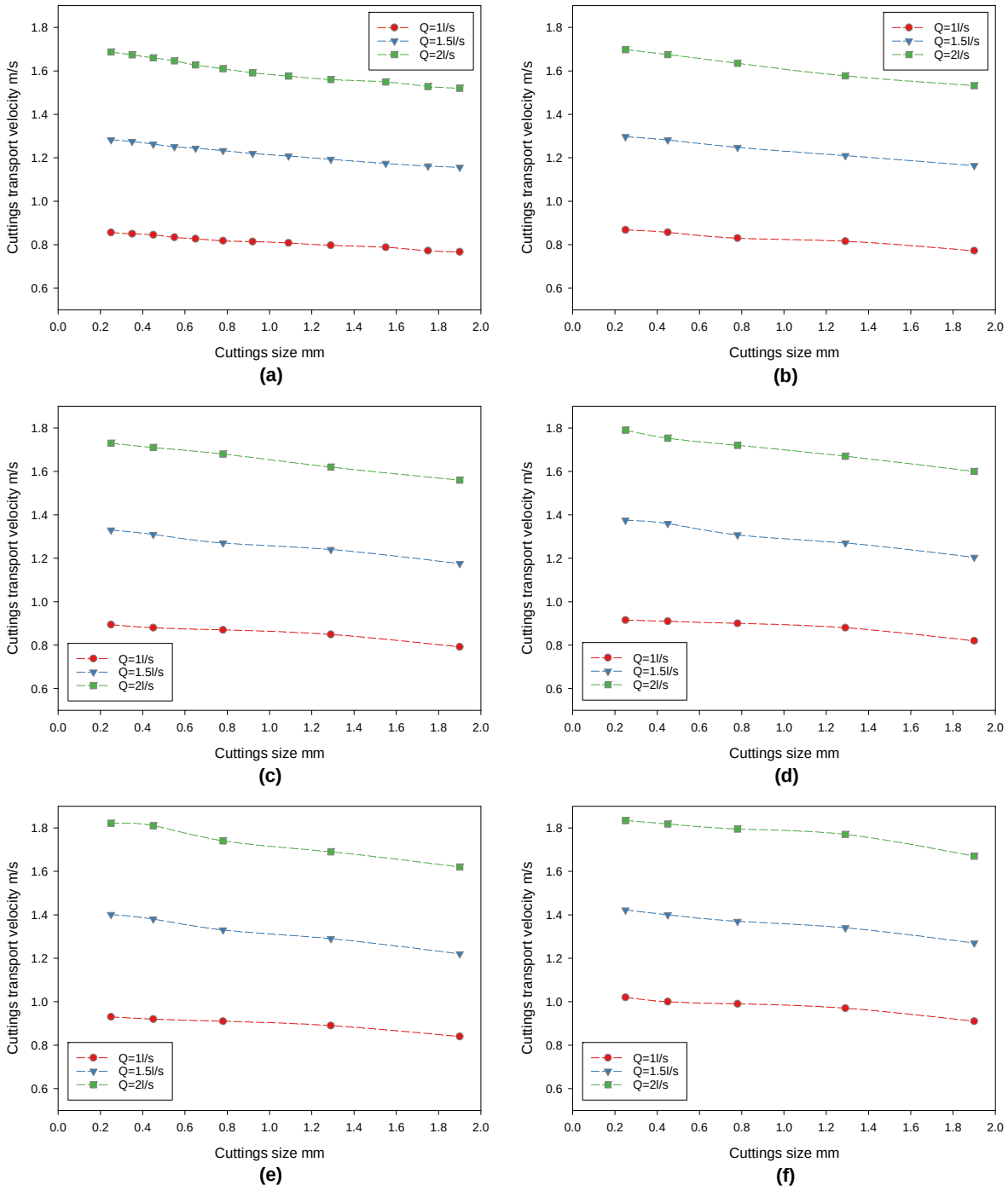

Figure 5.22 Cuttings transport velocity of single particle in annulus at flow rates of 1 l/s ($\boldsymbol{V_{f\,ave} = 0.808\ m/s}$), 1.5 l/s ($\boldsymbol{V_{f\,ave} = 1.213\ m/s}$) and 2 l/s ($\boldsymbol{V_{f\,ave} = 1.617\ m/s}$) for various fluids: (a) water, (b) 0.02% XCD, (c) 0.05% XCD, (d) 0.1% XCD, (e) 0.15% XCD, (f) 0.2% XCD.

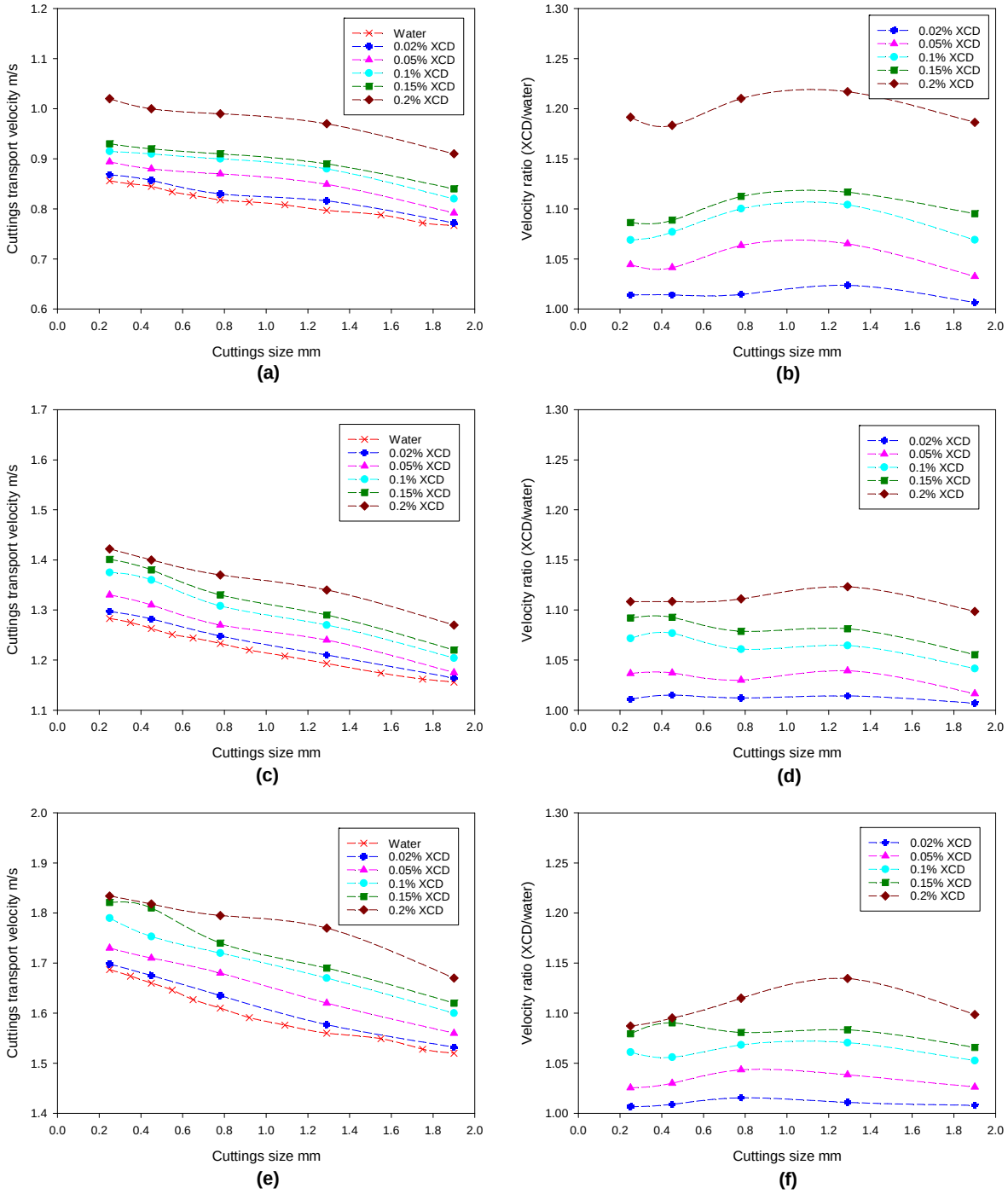

Figure 5.23 Effect of fluids viscosity on the cuttings transport velocity of single particle at various flow rates, (a) (b) Q=1 l/s ($\boldsymbol{V_{f\,ave} = 0.808\ m/s}$), (c) (d) Q=1.5 l/s ($\boldsymbol{V_{f\,ave} = 1.213\ m/s}$), (e) (f) Q=2 l/s ($\boldsymbol{V_{f\,ave} = 1.617\ m/s}$).

In conclusion, the cuttings transport velocity is influenced by both fluids viscosity and flow rate. It is evident that the cuttings velocity can be larger than the fluids average velocity due to

the fluid velocity distribution. The cuttings slip velocity is shown in Figure 5.24 using the fluid average velocity along with the single particle settling velocity. The slip velocity change for flow rate of 1l/s is relatively constant as the fluids viscosity increases. However, for higher flow rates, the slip velocity for smaller sized particles rises dramatically, while for the 2mm particle the variation is little. But the change of the cuttings slip velocity is not proportional with the particle size, which means no matter which fluid velocity is used for calculating the slip velocity, it is not accurate to use the settling velocity for the slip velocity, as the settling velocities overestimates the slip velocity and therefore overestimates the minimum transportation velocity. From the practical perspective of the cuttings transport and hole cleaning, it is critical to determine the cuttings transport velocity based on the maximum fluid velocity in the centre of the cross section.

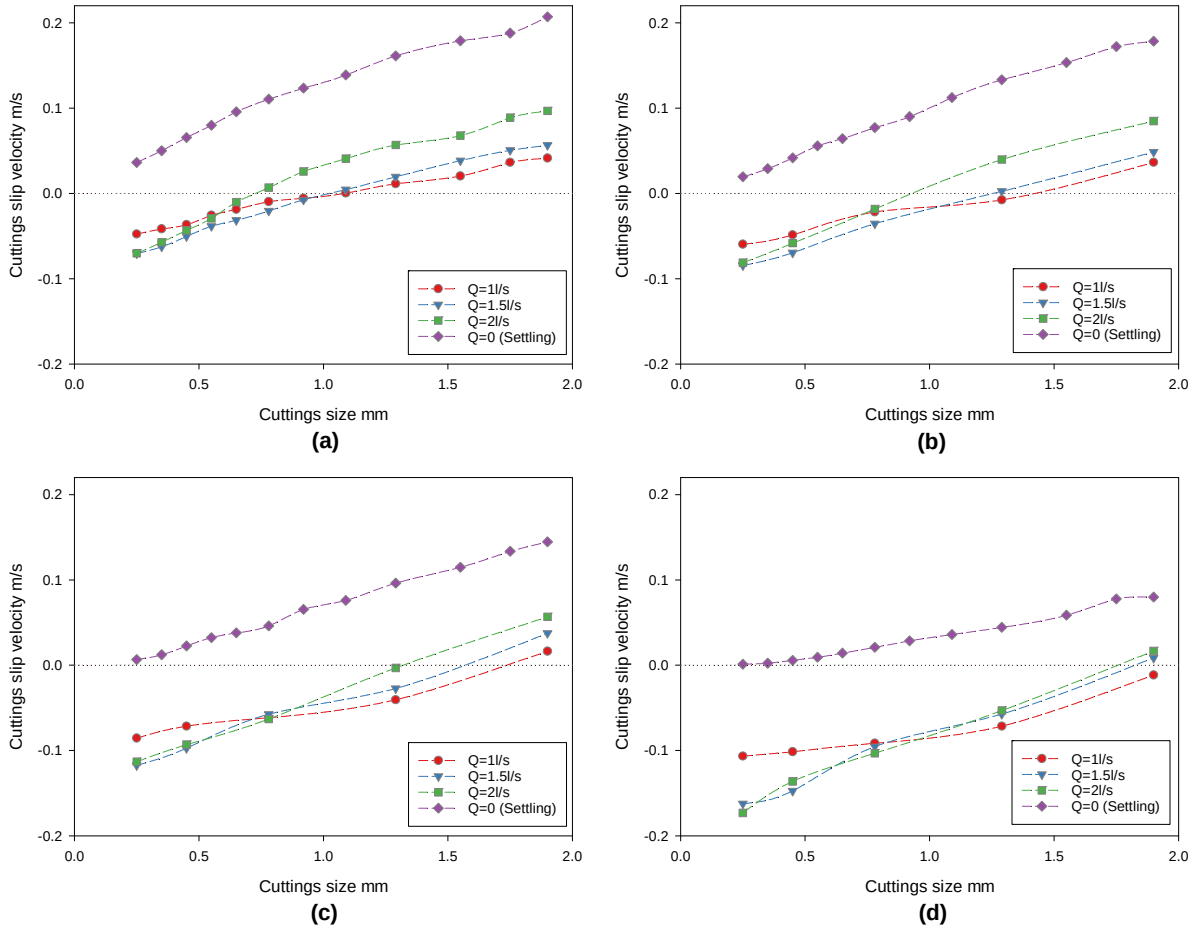

Figure 5.24 Cuttings slip velocity of single particle in annulus at flow rate of 1l/s ($\boldsymbol{V_{f\,ave} = 0.808\ m/s}$), 1.5l/s ($\boldsymbol{V_{f\,ave} = 1.213\ m/s}$), and 2l/s ($\boldsymbol{V_{f\,ave} = 1.617\ m/s}$) for various fluids, (a) water, (b) 0.02% XCD, (c) 0.05% XCD, (d) 0.1% XCD.

5.3.2.3. Effect of cuttings concentration

The cuttings transport velocities at the volume concentration of 1% and 3% are presented in Figure 5.25. The results are compared with the velocity of single particle to show the cuttings concentration impact.

It can be seen that the cuttings concentration impact on the cuttings velocity is significant compared with the cuttings velocity of single particle. For example, for the 0.2-0.3 mm particles in the 0.1% XCD solutions at 1.5 l/s flow rate, the cuttings transport velocity decreases from 1.8 m/s to 1.4 m/s when the cuttings concentration increases from single particle to 1%. However the impact of concentration becomes less significant with the further increase of the cuttings concentration, i.e. the cuttings velocity decreases at a much smaller rate. For example, for the 0.2-0.3 mm particles, the cuttings velocity decreases only from 1.4 m/s to 1.3 m/s when the cuttings concentration increases from 1% to 3%. This means that the particles interaction is severe when the cuttings transport start to be concentrated from single particle, but the impact of the concentration on the particles collision is less significant when the concentration increases further.

Similar to the single particle, the cuttings velocity decreases with the increase of cuttings size, and the flow rate has a significant effect on the reduction of the cuttings velocity at different concentrations. The cuttings velocity decrease is more prominent at high flow rate. For example, for 0.2-0.3 mm particles in water, when the cuttings concentration increases to 1%, the cuttings velocity decreases from 1.7 m/s to 1.2 m/s at the flow rate of 2 l/s, while it only decreases from 0.9 m/s to 0.6 m/s at flow rate of 1 l/s.

Furthermore, the cuttings concentration impact becomes less noticeable when the fluids viscosity increases, and the flow rate effect on the cuttings velocity reduction declines as well compared with water. For example, for the 0.2-0.3 mm particles at the flow rate of 2 l/s, when the cuttings concentration increases from single particle to 1%, the cuttings velocity decreases from 1.7 m/s to 1.2 m/s in water, while it decreases only from 1.7 m/s to 1.5 m/s in the 0.2% XCD solutions. This trend suggests that the decrease of the cuttings velocity due to the cuttings concentration impact can be compensated by the fluid rheology. From a practical perspective, to increase the cuttings recovery rate in the drilling process, it is critical to increase the fluid rheology to reduce the cuttings concentration impact.

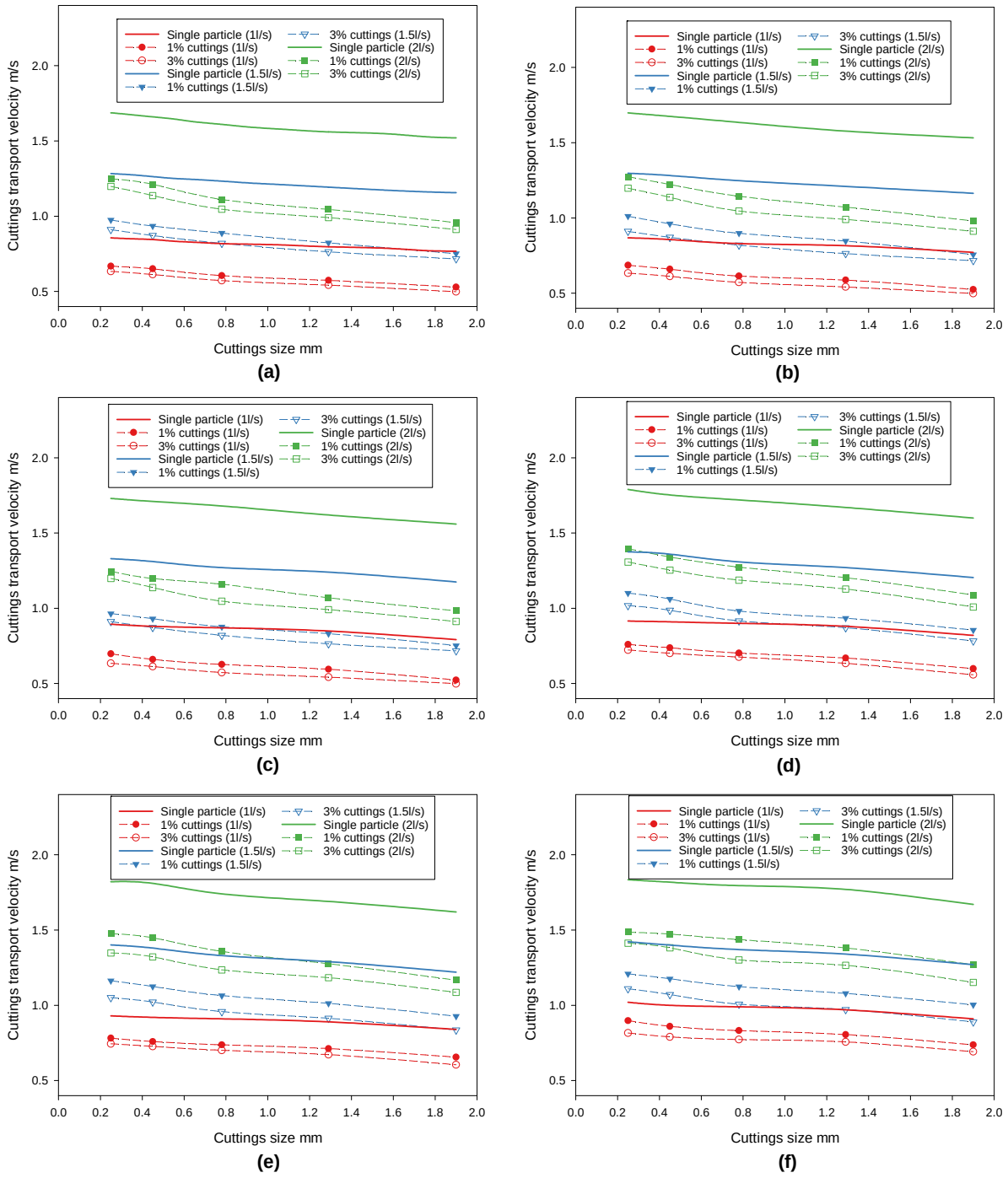

Figure 5.25 Cuttings transport velocity at the volume concentration of 1% and 3% for various fluids, (a) water, (b) 0.02% XCD, (c) 0.05% XCD, (d) 0.1% XCD, (e) 0.15% XCD, (f) 0.2% XCD.

Figure 5.26 presents another graph to illustrate the fluids viscosity influence on the cuttings velocity for the same flow rate and cuttings concentration. It can be seen that the cuttings velocity increase becomes more prominent as the fluids viscosity increases for both cuttings concentration of 1% and 3%.

To better show the extent of cuttings velocity variation, the velocity ratio of the concentrated cuttings transport velocity to the single particle velocity is presented in Figure 5.27. It can be seen that compared with the fluids effect on the cuttings velocity which is subtle in Figure 5.26, the fluids viscosity impact is evident using the velocity ratio, as the absolute value change is relatively small. For example, for the 0.2-0.3 mm particles at the cuttings concentration of 1%, the velocity ratio decreases from 0.88 to 0.85 and then drop to 0.8 when the flow rate increases from 1 l/s to 1.5 l/s and 2 l/s. But for the same case at the concentration of 3%, the velocity ratio varies from 0.8 to 0.78 and 0.77. It can be seen that the velocity ratio is a better illustration method to explain the impact of the fluid viscosity and the cuttings concentration.

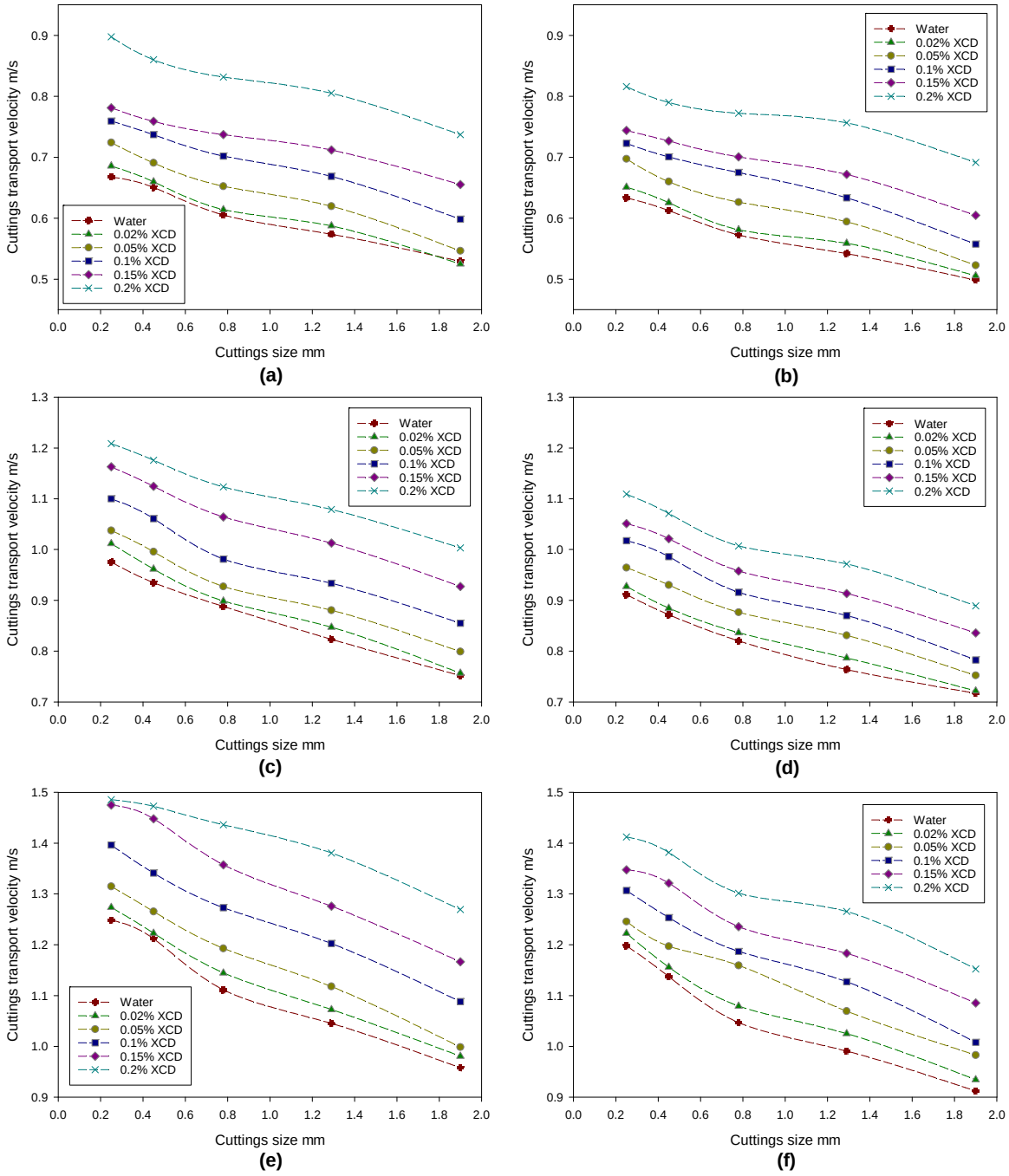

Figure 5.26 Effect of fluids viscosity on the cuttings transport velocity at different cuttings volume concentration, (a) Q=1 l/s for 1% cuttings, (b) Q=1 l/s for 3% cuttings, (c) Q=1.5 l/s for 1% cuttings, (d) Q=1.5 l/s for 3% cuttings, (e) Q=2 l/s for 1% cuttings, (f) Q=2 l/s for 3% cuttings.

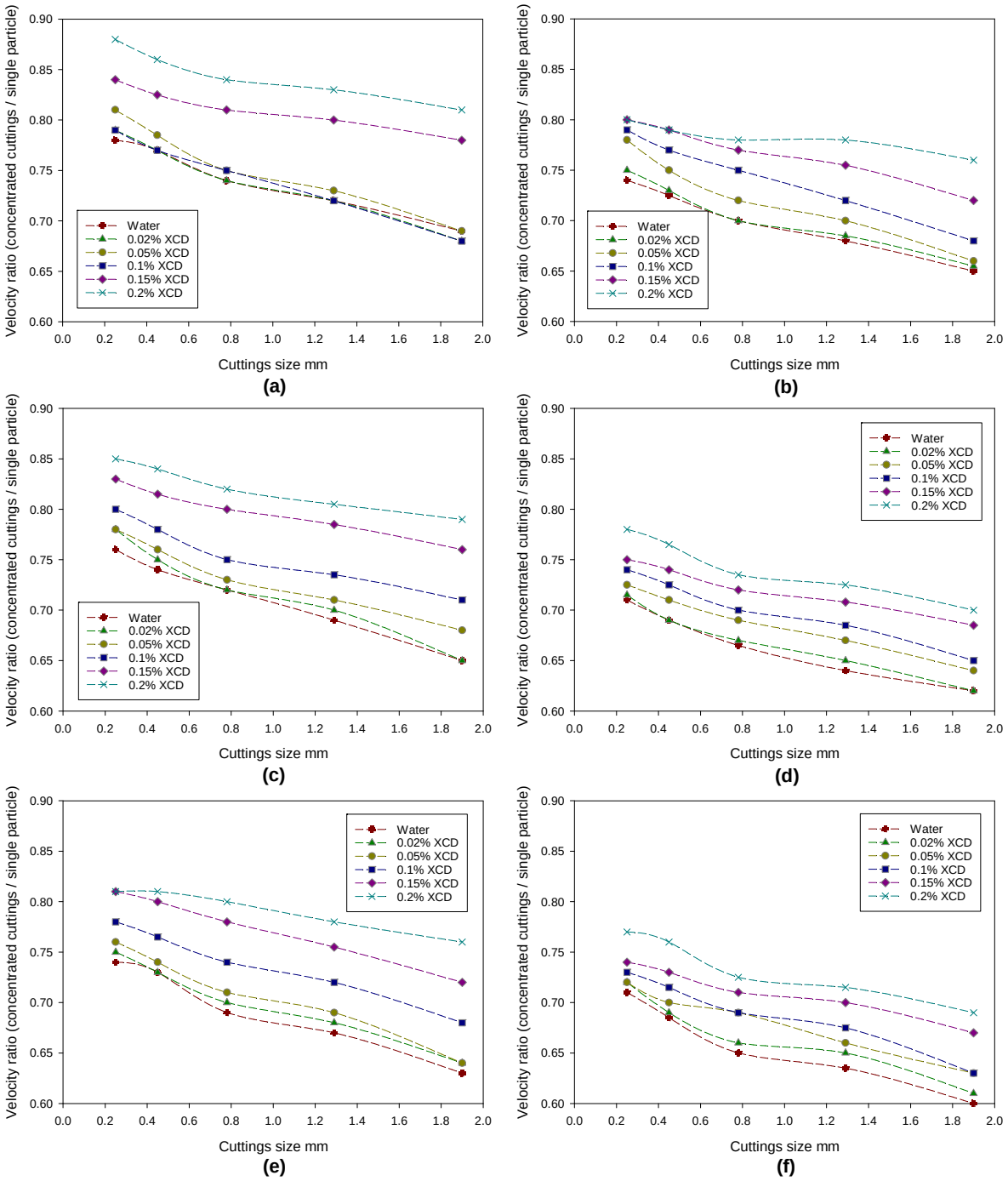

Figure 5.27 Effect of fluids viscosity on the cuttings transport velocity ratio at different cuttings volume concentration, (a) Q=1 l/s for 1% cuttings, (b) Q=1 l/s for 3% cuttings, (c) Q=1.5 l/s for 1% cuttings, (d) Q=1.5 l/s for 3% cuttings, (e) Q=2 l/s for 1% cuttings, (f) Q=2 l/s for 3% cuttings.

Similar to the fluids viscosity effect, the velocity ratio is shown in Figure 5.28 to show the flow rate effect on the cuttings velocity. It can be seen that the variation of velocity ratio is almost proportional to the increase of flow rate at the cuttings concentration of 1%. However, the velocity ratios at the concentration of 3% for various flow rate of 1.5l/s and 2l/s are quite similar,

and the ratio at 1 l/s is much higher than high flow rates. Although both fluids viscosity and flow rate have a significant effect on the cuttings velocity ratio, the impact of the cuttings concentration is the most prominent on the cuttings transport velocity.

5.4. Summary

This chapter presented the experimental results of the cuttings transport velocity using PTV method. The cuttings velocity was obtained based on the velocity distribution from a large quantity of data, and the effects of fluid rheology, flow rate, cuttings size and concentration on the cuttings velocity were investigated. The experiments found that the cuttings velocity variation with the cuttings size follows the same trend for various fluids rheology. The impact of the cuttings concentration on the cuttings velocity is significant. The cuttings slip velocity in the cuttings transport process was compared with the cuttings settling velocity from Chapter 4, and it was found that the effect of the flow rate and cuttings concentration is different. It is also found that the cuttings transport velocity can be large than the fluid average velocity especially for fluids of high viscosity and at low concentrations. Through the comparison of the experimental results and the fluid velocity distribution from numerical simulations, it is inferred that the cuttings transport is in the centre of the flow field.

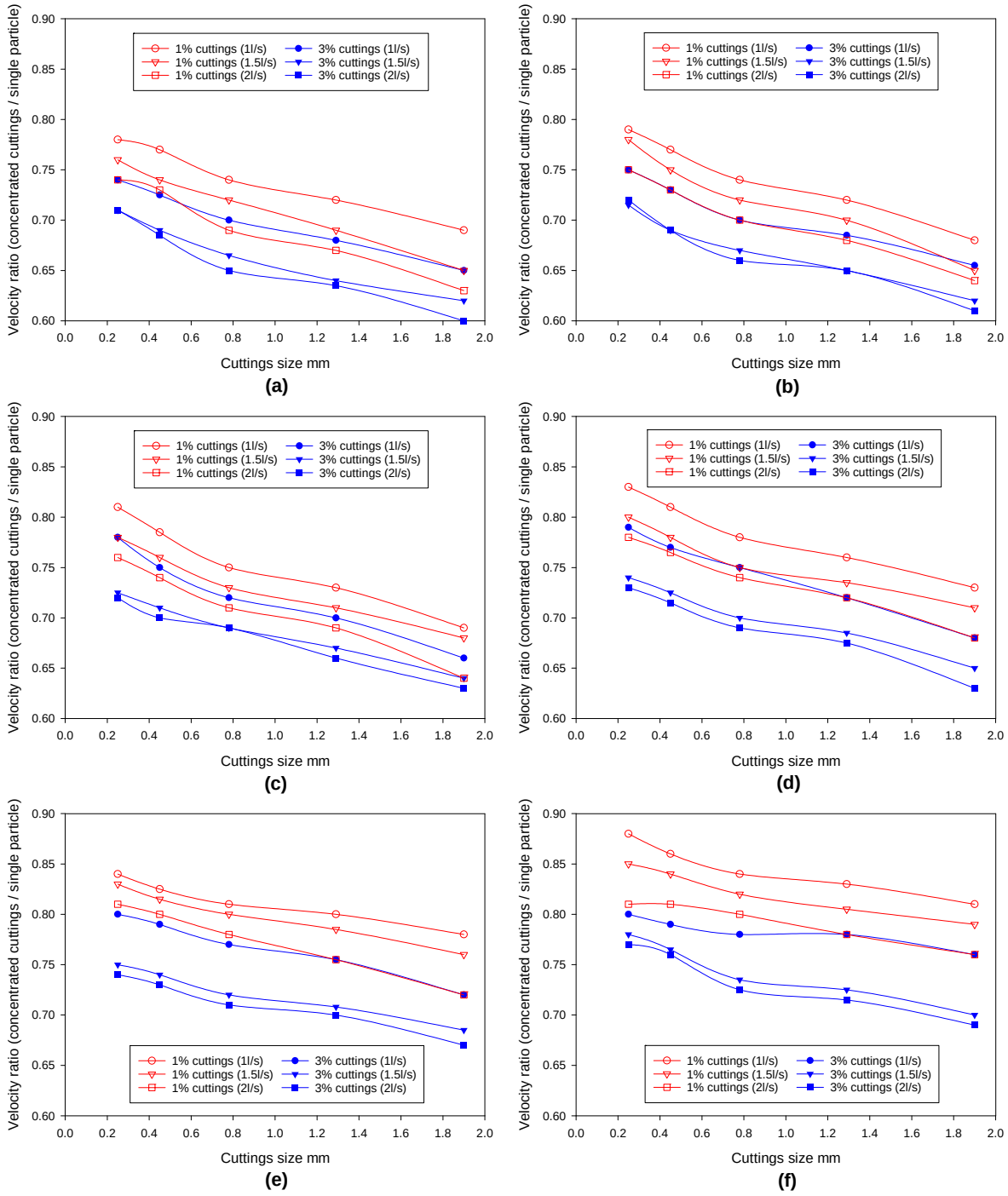

Figure 5.28 Effect of flow rate and cutting concentration on the cuttings transport velocity ratio for various fluids, (a) water, (b) 0.02% XCD, (c) 0.05% XCD, (d) 0.1% XCD, (e) 0.15% XCD, (f) 0.2% XCD.

Chapter 6. Field test

6.1. Introduction

In previous chapters, the cuttings transport velocity has been investigated using the PTV method on the flow loop in lab. Several approaches have been used to ensure that the high speed camera is able to obtain the most precise measurement of the particle velocity, and the solid liquid flow is under control by the adjustment of the flow loop to make sure that the particles have reached the stable velocity. However the PTV method is limited, as the test section length of the flow field that the camera is focusing on is only around 20cm. To verify the experimental results and investigate the cuttings transport under field drilling conditions, the particle tracking field tests were carried out in the field using the drilling rig.

In the field experiments, the influence of fluid viscosity and the cuttings size and density on the particle tracking were investigated. Furthermore, additional parameters were studied which were not possible to investigate using the flow loop experiments. Examples of these parameters is drill string rotation effect on the cuttings transport velocity, which is the main difference between the coiled tubing and conventional drilling. While cuttings transport velocity was measured in the last chapters to predict the impact on the lag time of cuttings, the lag time was measured directly in the field tests. Furthermore, the cuttings weight distribution over the arrival time is investigated in this chapter. The mixture sample of multiple sized cuttings were used in the field test to study the cuttings smearing.

The field tests were conducted at the Brukunga mine site located near Adelaide, South Australia. The site is a pyrite mine, and has been used as a research drilling site in the DET CRC. Figure 6.1 shows the Brukunga mine site.

Figure 6.1 Location of Brukunga mine site for field tests [109].

6.2. Research methodology

Figure 6.2 shows the Boart Longyear drilling rig used for the field tests. The drill string is composed by three drill rods and driven by the top drive rotation if needed. The rod is 3 meter and the outside diameter is 45mm, seen in Figure 6.3. The rig can control the rate of the penetration and circulation flow rate. All the rods were marked so the exact location of the drill bit is known by reading the rod number on the surface.

Figure 6.2 Drilling rig for the field tests.

Figure 6.3 Drill rods with outer diameter of 45 mm.

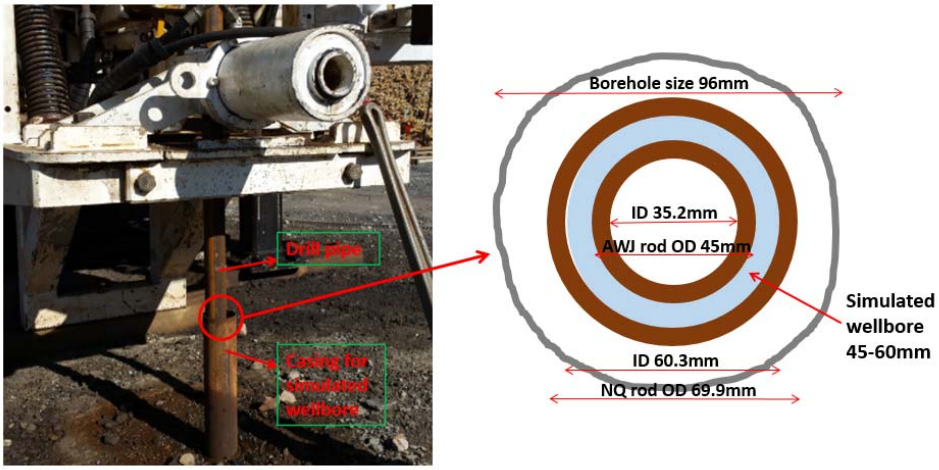

Figure 6.4 Wellbore and drill pipe: ID of NQ rod is 60 mm, OD diameter of AWJ rod is 45 mm.

To track the cuttings lag time in the wellbore, the depths of the cuttings is required to be known. So in this field test, the cuttings were prepared first and placed at a certain location in a predrilled borehole. The borehole depth is 130m, and a series of NQ pipe with ID 60mm was placed in the wellbore to simulate the coiled tubing drilling borehole where the inside diameter is 60 mm. Figure 6.4 shows the simulated wellbore and drill pipe for the field test.

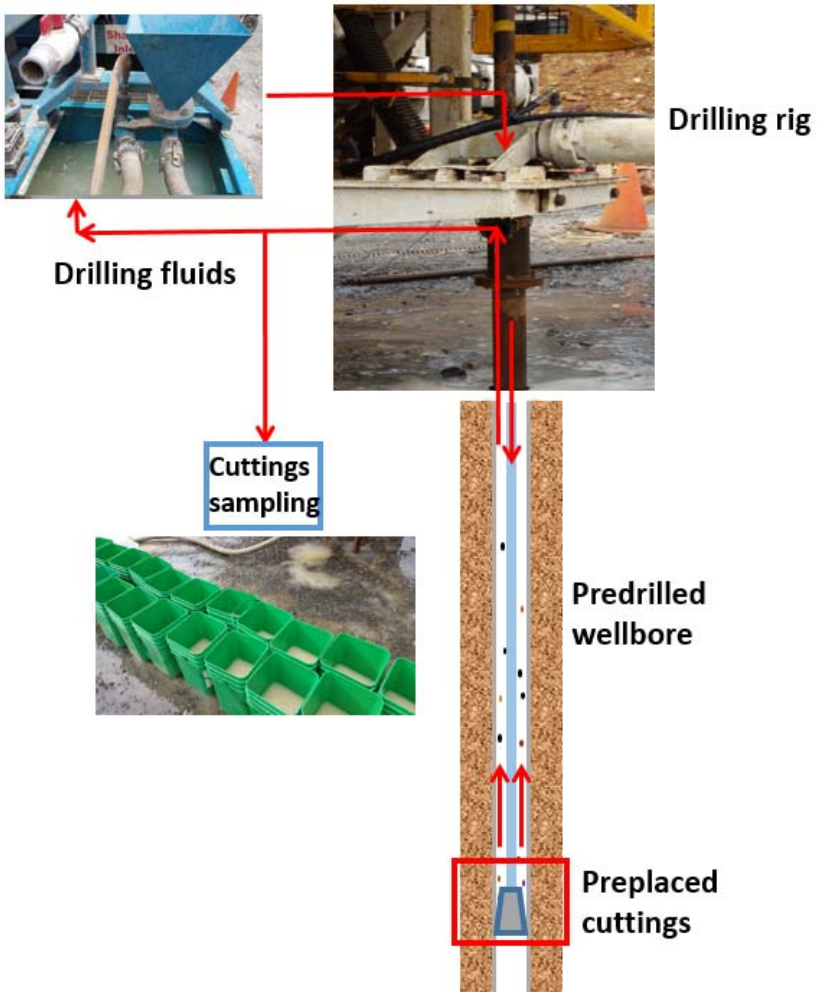

Figure 6.5 Setup of the field test.

The setup of the field test is presented in Figure 6.5. The drilling fluids were prepared using the mixing tanks of one of AMC (Australia Mud Company) Solid removal units (SRU), see Figure 6.6. After placement of the cuttings in the annulus, the drilling fluid was circulated carrying the cuttings to the surface, where a sampling hose was set at the bypass to collect the cuttings and the return fluid. The cuttings were collected at 5s time intervals in different buckets. The cuttings in each bucket were then collected using a filtration method and were sent to lab

for particle distribution analysis. The cuttings were wet sieved first, and dried in oven to measure the weight of each single sized particles.

Figure 6.7 shows the cuttings collection during the field test, and Figure 6.8 shows an example of the analysed cuttings in the lab.

Figure 6.6 Solid removal unit (SRU) for drilling fluids circulation.

Figure 6.7 Cuttings collection in field test.

Figure 6.8 Cuttings analysis from sieving and drying.

Two different methods were used to place the cuttings in the annulus. Figure 6.9 shows the first method of placing the cuttings. In this method, first the borehole was circulated with the test fluid. The cuttings were added to the inside of the drill string (with no bit at the end), see Figure 6.10, and sufficient time was allocated for settlement of particles at the bottom of the drill string. The time was estimated based on the settling velocity measurements from chapter 4. The drill string was off bottom at 5-10 cm to allow settlement of particles at the bottom of the borehole. Similar test protocol was implemented in the lab using the flow to ensure about the settlement of particles.

Single sized cuttings were used to obtain the cuttings transport velocity in real drilling operations, and the mixture of multiple sized cuttings were to investigate the cuttings smearing phenomenon. The size distribution of the mixture was prepared based on the hammer bit cuttings. The cuttings samples were tested which covered a wide range of particle sizes. Furthermore, some experiments were conducted using metal particles to study the effect of cuttings density on the cuttings transport.

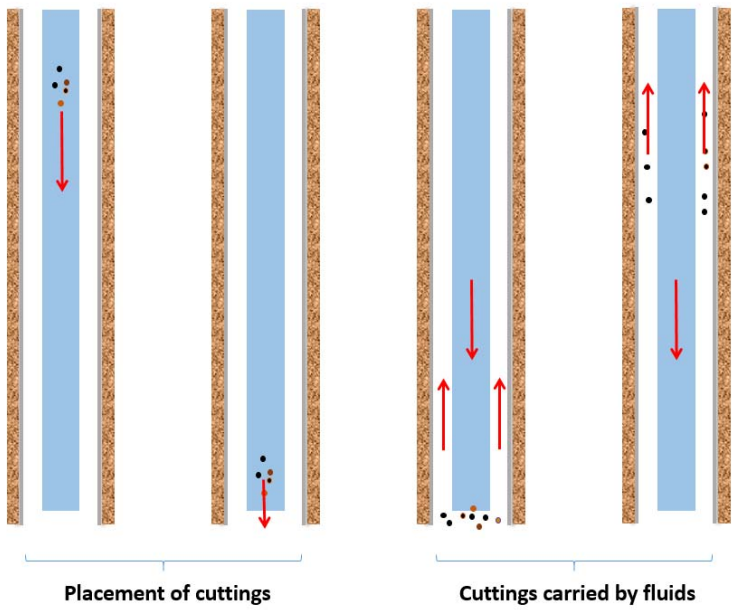

Figure 6.9 Placement of the cuttings and field test design.

Figure 6.10 Disconnection of drill pipe to drop prepared cuttings.

In the second method of the cuttings placement, NQ rods were loaded with cuttings with various sizes which were separated by wood disks. The loaded rods were placed at the bottom of the borehole at the depth of 130m. Figure 6.11 demonstrates the arrangements of cutting compartments in the loaded rods. Various types of cuttings were placed sequentially. The length of each layer of the cuttings is 0.5 m with a 30 cm cement section as a separator. Drillable membranes made from wood were placed on the top and the bottom of each compartment.

In each experiment, a hammer bit was used to penetrate into each cutting compartment flushing the cuttings to the surface. After flushing the particular compartment of cuttings and collecting the cuttings at the surface, the experiments in other compartment were continued.

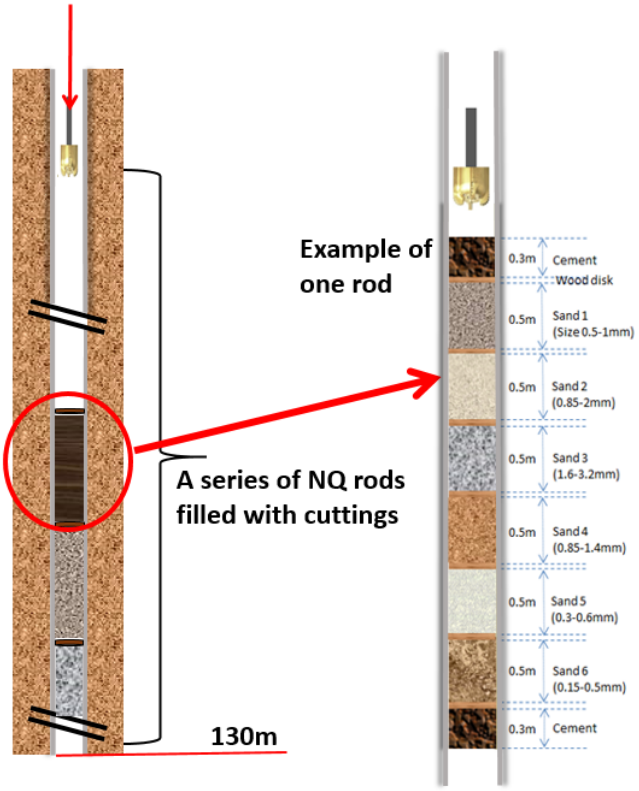

Figure 6.11 Placements of the NQ rods filled with cuttings.

According to the arrival time of each sized cuttings, the cuttings residence time can be presented in Figure 6.12, which shows the results of the field test with water with flow rate of 230 l/min.

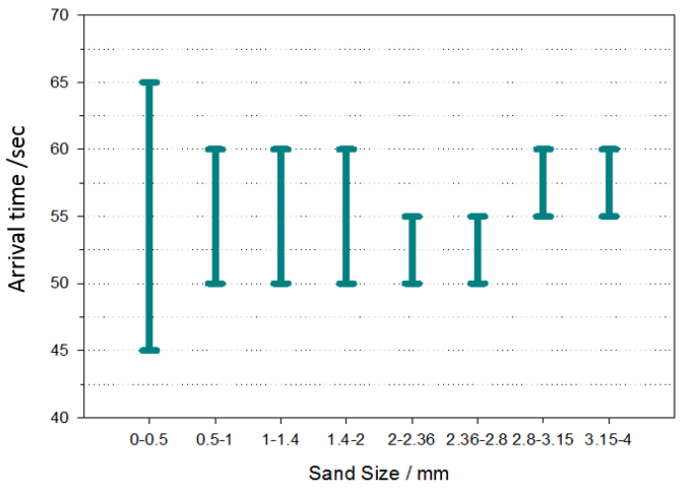

Figure 6.12 Cuttings arrival time distribution of a water test with flow rate of 230 l/min.

The cutting weight over its arrival time was measured. Table 6.1 shows the cuttings weight of each sized particle over the sampling time. The percentages of each sized cuttings over total arrival time are listed in Table 6.2.

Table 6.1 Cuttings weight of each sized particle over arrival time.

	Size mm							
Bucket	<0.5	0.5-1	1-1.4	1.4-2	2-2.36	2.36-2.8	2.8-3.15	3.15-4
B5	2.7	-	-	-	-	-	-	-
B6	8.5	2.2	2.2	1.1	0.6	0.6	-	-
B7	18.1	11.4	4.4	7.2	3.3	2.5	1.7	1
B8	4.4	6.9	1.7	2.9	0.8	0.7	2.4	1.2
B9	-	-	-	-	-	-	-	-
Total	32.8	23.2	9	11.7	5	4.8	5.7	2.8

Table 6.2 Cuttings weight percentage distribution on arrival time.

	Size mm							
Time s	<0.5	0.5-1	1-1.4	1.4-2	2-2.36	2.36-2.8	2.8-3.15	3.15-4
45-50	8.1%							
50-55	25.2%	9.4%	25.1%	9.6%	13.2%	12.8%		
55-60	53.5%	49.3%	48.4%	61.7%	66.7%	53.1%	29.7%	35.3%
60-65	13.2%	29.8%	19.6%	25.3%	16.1%	13.7 %	41.4 %	43.7%

Figure 6.13 shows an example of the analysis of the cuttings weight distribution on the arrival time. The bars in Figure 6.12a clearly shows the cuttings weight variation, but to compare the results of various sized cuttings, the red curve passing the median of each bar is used to simplify the demonstration.

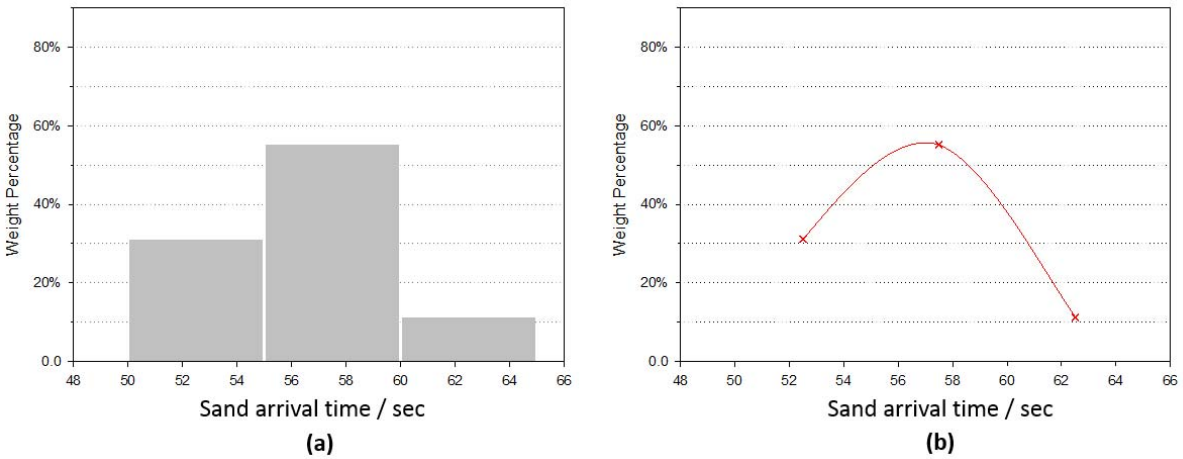

Figure 6.13 Cuttings weight distribution on arrival time: (a) bar chart, (b) curve graph.

6.3. Results and discussion

6.3.1. Cuttings transport velocity

The cuttings transport velocity of monodispersed particles was obtained first. The arrival times of the cuttings were measured while circulating with water and also 0.2% XCD polymer solution, see Figure 6.14. It can be seen that for water the difference of the cuttings arrival time decreases with the increase of the flow rate. The data suggests that the level of smearing can be minimised drastically by increasing the viscosity of the drilling fluid. Figure 6.14b shows that the arrival time of particles transported by 0.2% XCD solution exhibit small time discrepancy particle size, and the arrival time is almost the same when the cuttings size is below 2.8 mm.

It is worth mentioning due to the precision of the field test, for the cuttings transport using 0.2% XCD solutions it is unable to distinguish the difference of the cuttings arrival time, however, the flow rate impact on the cuttings velocity in water can be still demonstrated explicitly using the arrival time.

The cuttings transport velocity is obtained for various particle size according to the arrival time, see Figure 6.15. The irregular part for the flow rate of 180 l/min in cuttings arrival time is amplified for the cuttings velocity, but it still can be seen that for water the impact of high flow rate on the cuttings velocity is larger than for the low flow rate. For 0.2% XCD solutions, the cuttings velocity is much higher and the same as water, the flow rate impact on the small sized cuttings are larger than the low flow rate.

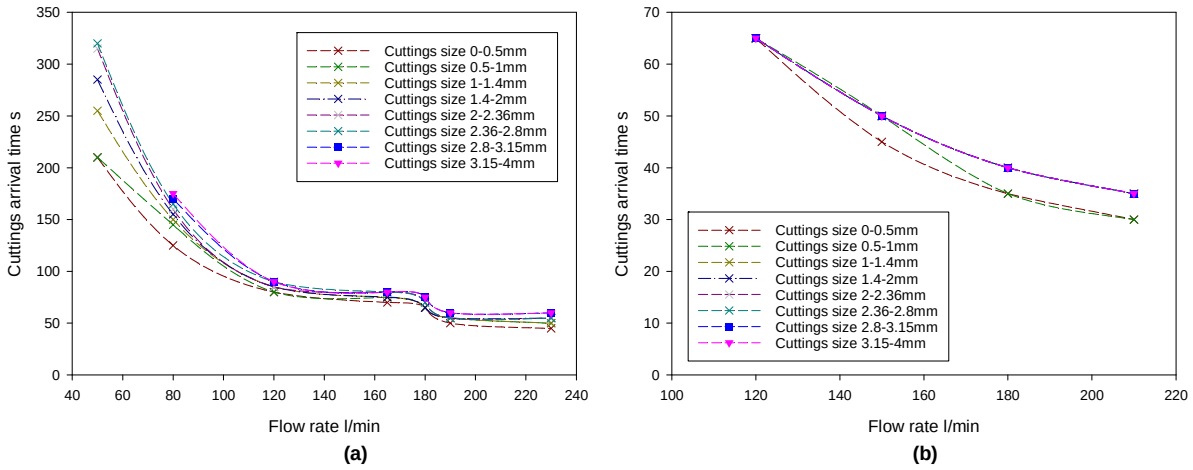

Figure 6.14 Cuttings arrival time for different particle sizes at various flow rate, (a) water, (b) 0.2% XCD solutions.

The cuttings transport velocity obtained from the field test were compared with the experimental measurements presented in Chapter 5, see Figure 6.16. As the cuttings size range is wider in the field results, the closest average size was selected for the comparison. It can be seen that the obtained cuttings transport velocity is restricted between the cuttings velocity of single particle and 1% concentration of cutting. With the increase of the flow rate, the field tests result approaches the single particle velocity. The analysis based on the cuttings collected from a series of buckets shows that the cuttings concentration is always smaller than 0.2%, and the concentration decreases with the flow rate increase due to the dispersing effect.

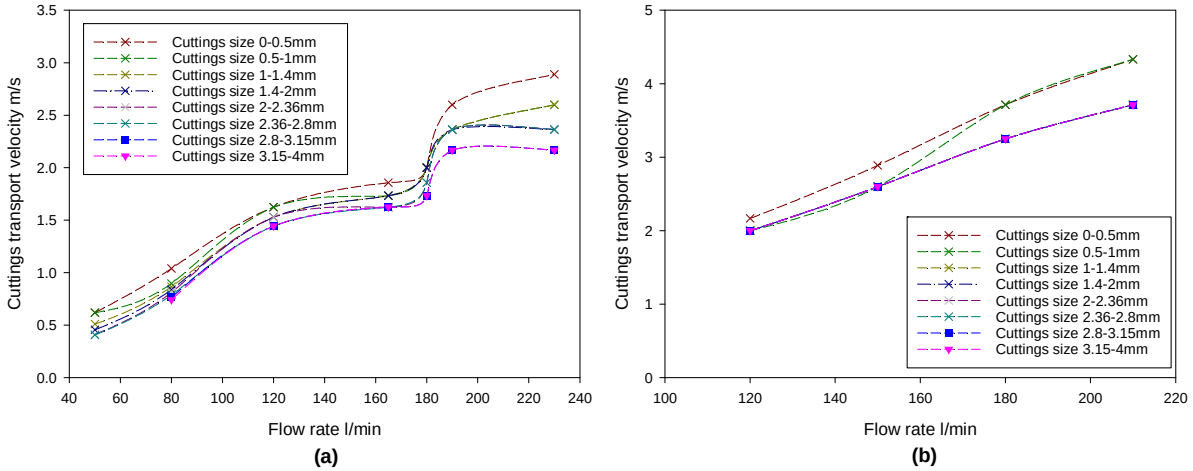

Figure 6.15 Cuttings transport velocity for different particle sizes at various flow rate, (a) water, (b) 0.2% XCD solutions.

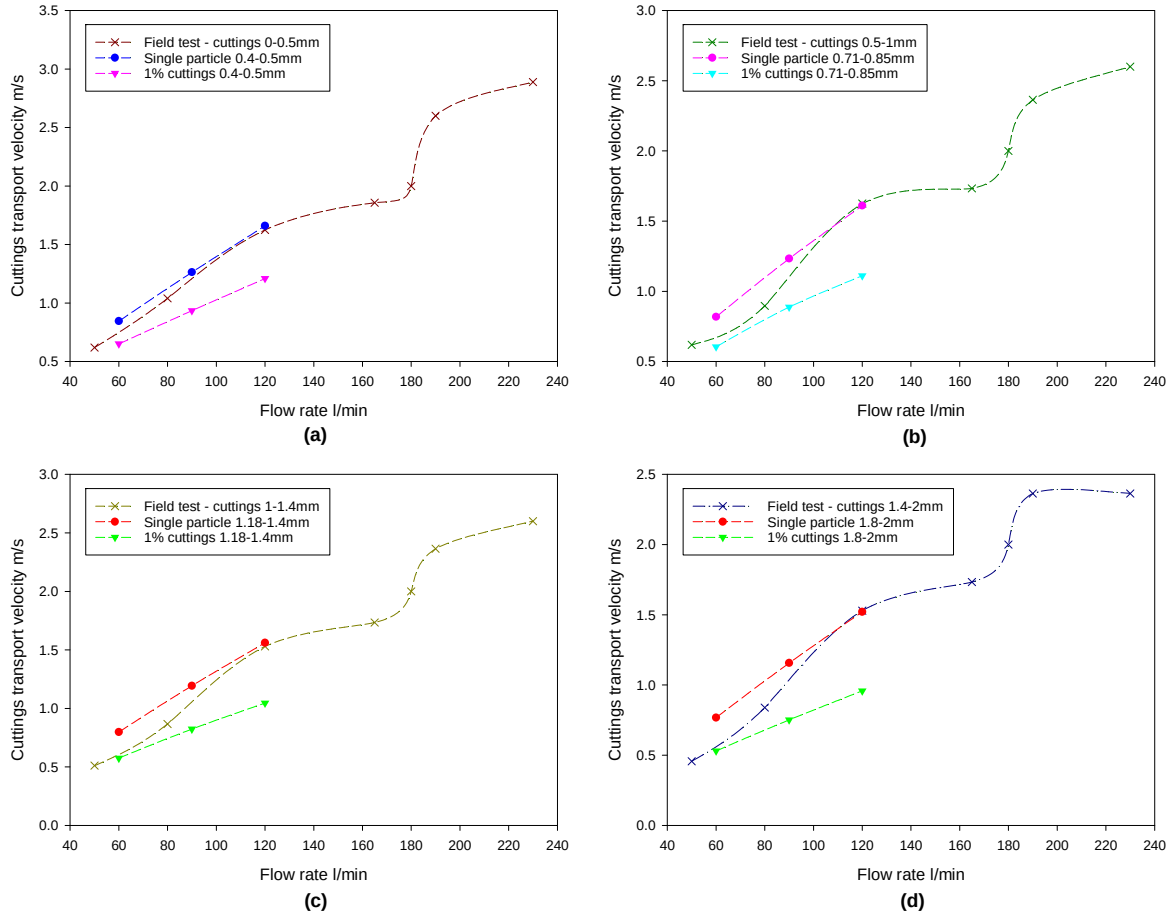

Figure 6.16 Comparison of field test results and experimental measurement for the cuttings transport velocity in water, (a) cuttings size 0-0.5 mm, (b) cuttings size 0.5-1 mm, (c) cuttings size 1-1.4 mm, (d) cuttings size 1.4-2 mm.

The particle density impact on the cuttings arrival time is investigated by comparing the arrival time of steel and sand particles. Figure 6.17 shows the cuttings arrival time distribution (includes the arrival time and end time) of cuttings and metal particles. The distribution shows that for almost all flow rates the steel particles are spread over interval. For the flow rate of 80 l/min, the arrival time is delayed with the increase of the particle density and size, however when the flow rate increases the arrival time is almost the same. The mineral cuttings distribution is wider than the sand cuttings even for the same arrival time, i.e. the flow rate rise is able to increase the cuttings arrival time, but the cuttings lag is more severe for the cuttings with bigger particle density.

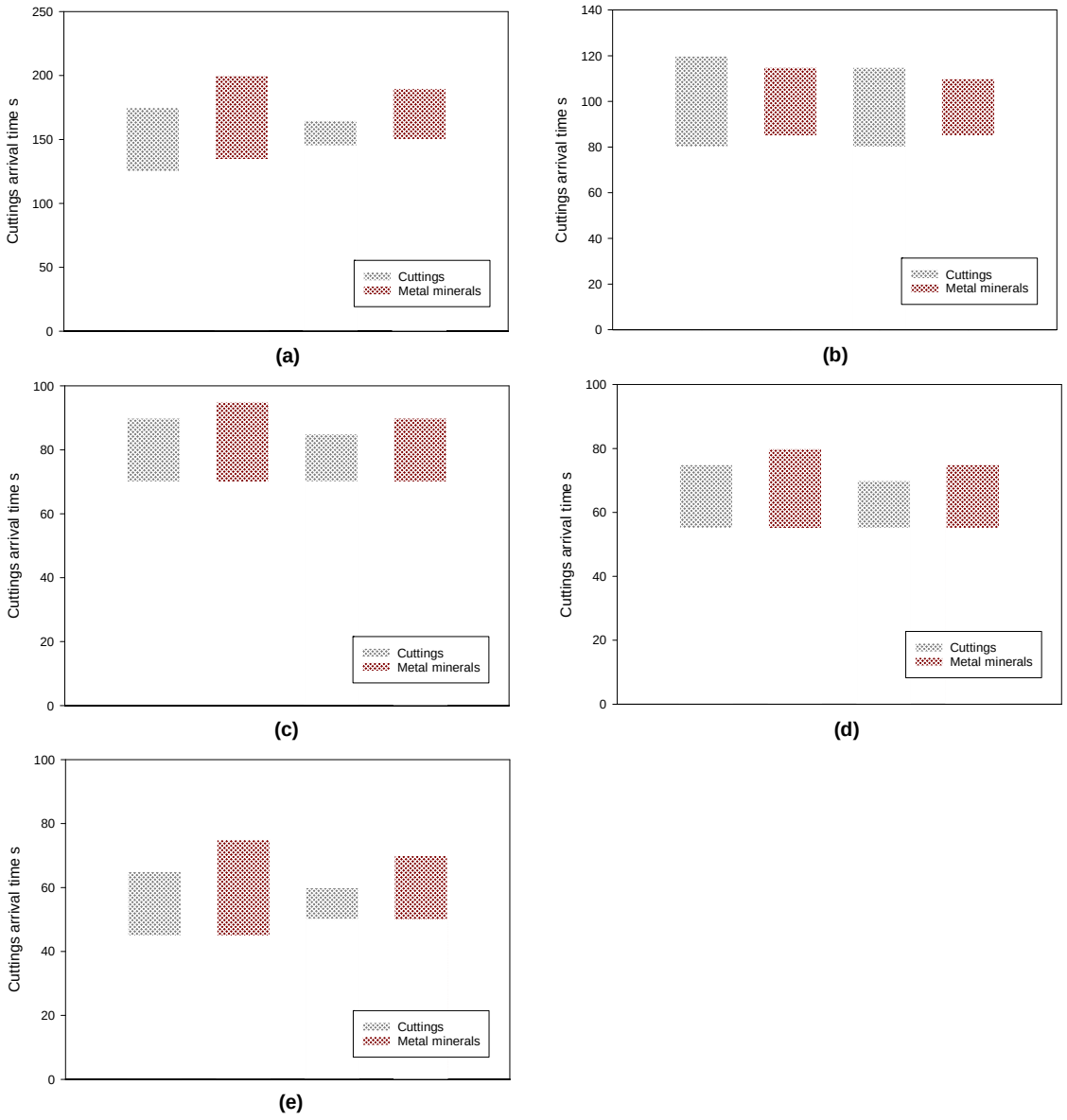

Figure 6.17 Effect of the particle density on the cuttings arrival time distribution for various flow rates of water, (a) 80 l/min, (b) 120 l/min, (c) 160 l/min, (d) 200 l/min, (e) 230 l/min.

6.3.2. Cuttings arrival time distribution

The cuttings transport time and velocity for each size of particles are presented above, but in real drilling the cuttings usually cover a wider range, and most important of all, the cuttings from the same depths can arrive to the surface with different time, which appears as the cuttings arrival time and the cuttings lag distribution.

The cuttings arrival time and the cuttings weight percentage distribution over time are presented in Figures 6.18 to 6.21 for water at various flow rates. It can be seen the cuttings lag

of 0-0.5 mm particles is the most widespread. With the flow rate increase, the difference of the cuttings arrival time becomes smaller, but compared to the arrival time of single sized cuttings from earlier section, the cuttings are delayed due to the cuttings concentration. The cuttings of similar size usually have the roughly same arrival time, for example for the particles of 0-2 mm at the flow rate of 180 l/min, but the arrival time distribution has a huge difference in terms of the cuttings lag, which is unable to be shown simply using the cuttings arrival time or velocity.

The cuttings weight distribution covers a wide range from 140 seconds to 190 seconds for flow rate of 80 l/min, but with the flow rate increase the distribution gets concentrated and finally becomes the same for the max flow rate of 230 l/min.

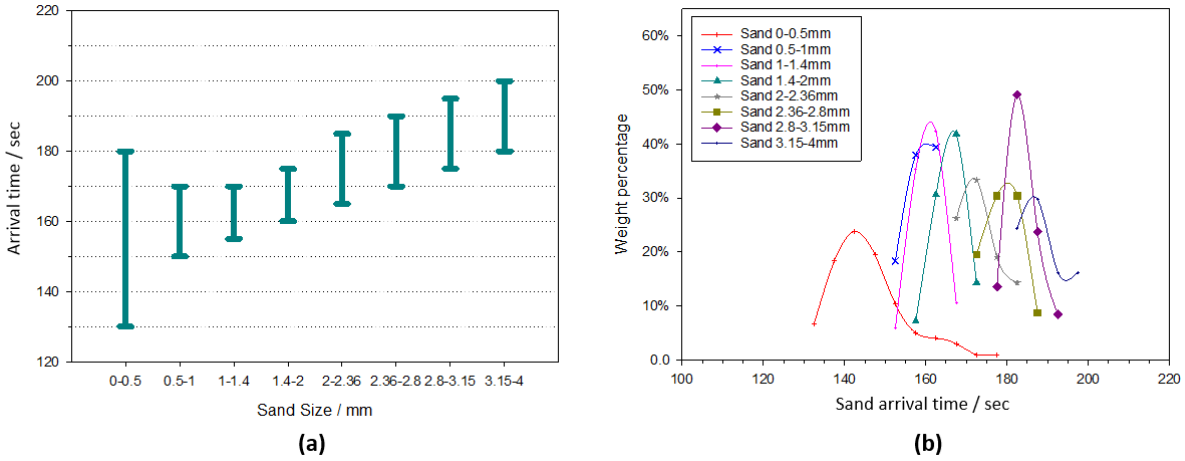

Figure 6.18 Cuttings arrival time and weight distribution over time for water at the flow rate of 80 l/min, (a) cuttings arrival time, (b) weight percentage distribution.

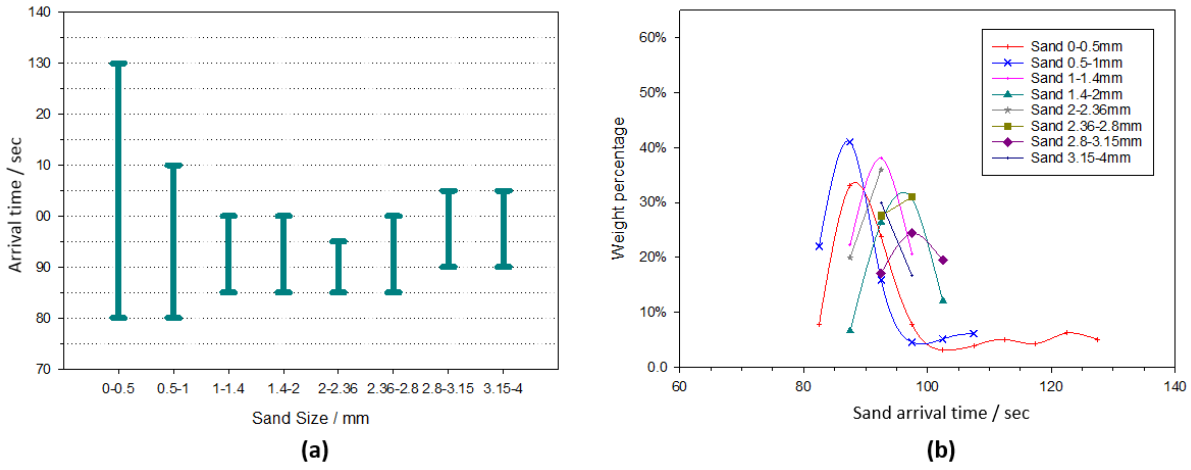

Figure 6.19 Cuttings arrival time and weight distribution over time for water at the flow rate of 120 l/min, (a) cuttings arrival time, (b) weight percentage distribution.

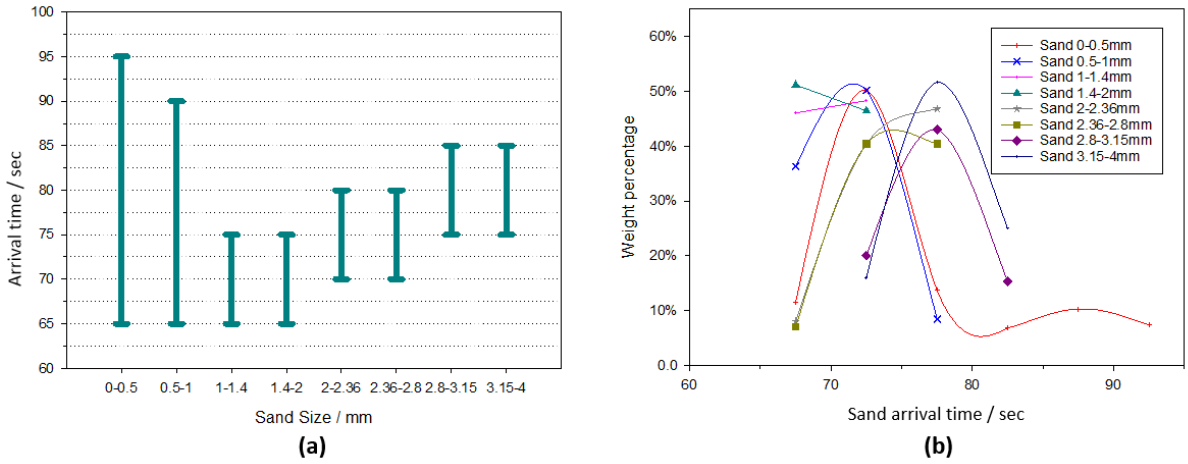

Figure 6.20 Cuttings arrival time and weight distribution over time for water at the flow rate of 180 l/min, (a) cuttings arrival time, (b) weight percentage distribution.

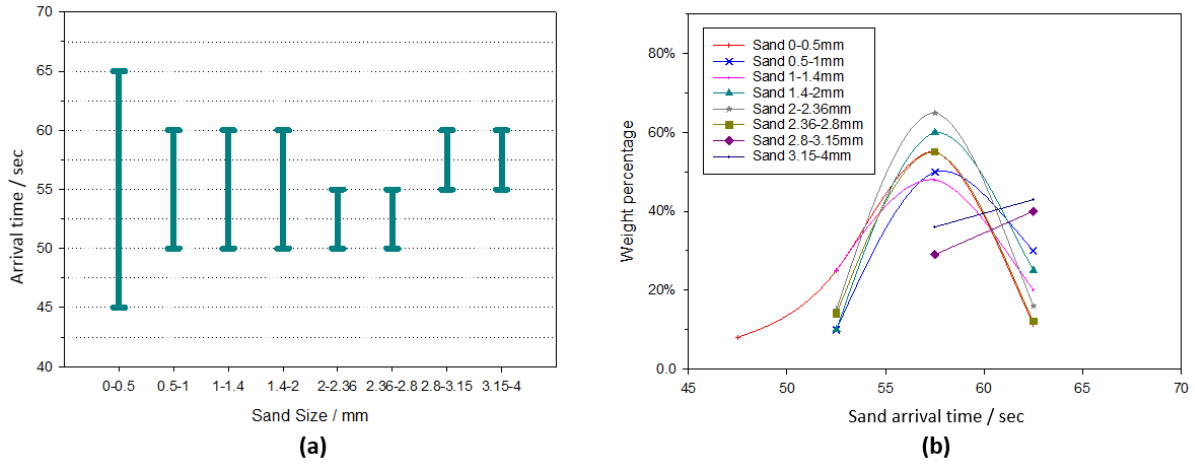

Figure 6.21 Cuttings arrival time and weight distribution over time for water at the flow rate of 230 l/min, (a) cuttings arrival time, (b) weight percentage distribution.

Similarly the cuttings arrival time and weight distribution are shown for the 0.2% XCD drilling fluids with various flow rates in Figure 6.22-6.25. Compared with the results of water, the cuttings time distribution becomes narrowed down significantly, but the flow rate impact for polymer drilling fluids on the concentration of the cuttings lag is not as great as water. For the same flow rate as water, due to the greater carrying capacity of polymer fluids, the cuttings also likely to arrive to the surface at the same time with less cuttings lag or smearing.

For polymer drilling fluids, the cuttings weight distribution for particles of 0-1 mm has similar pattern as water, and the cuttings lag is improved because of the better carrying capacity of polymers.

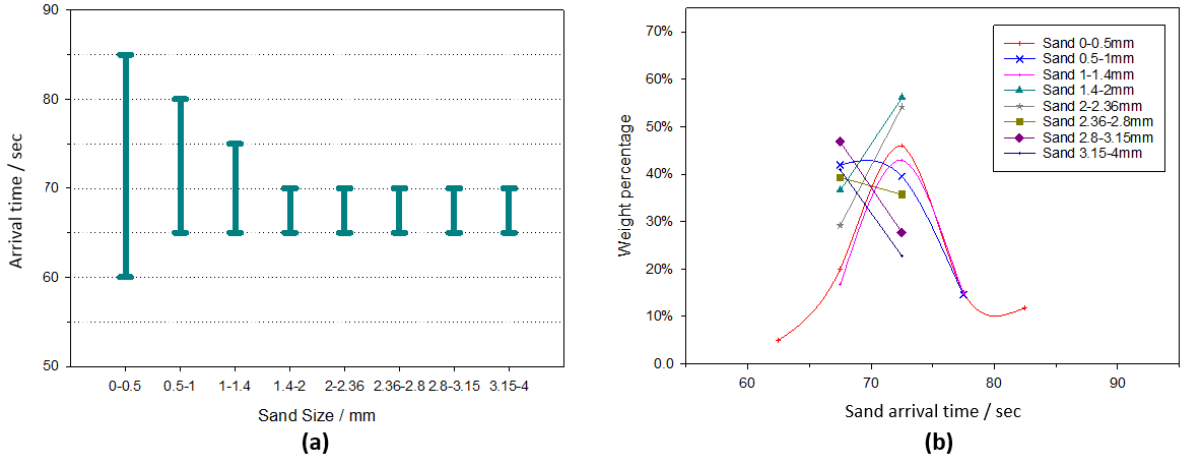

Figure 6.22 Cuttings arrival time and weight distribution over time for 0.2% XCD drilling fluids at the flow rate of 120 l/min, (a) cuttings arrival time, (b) weight percentage distribution.

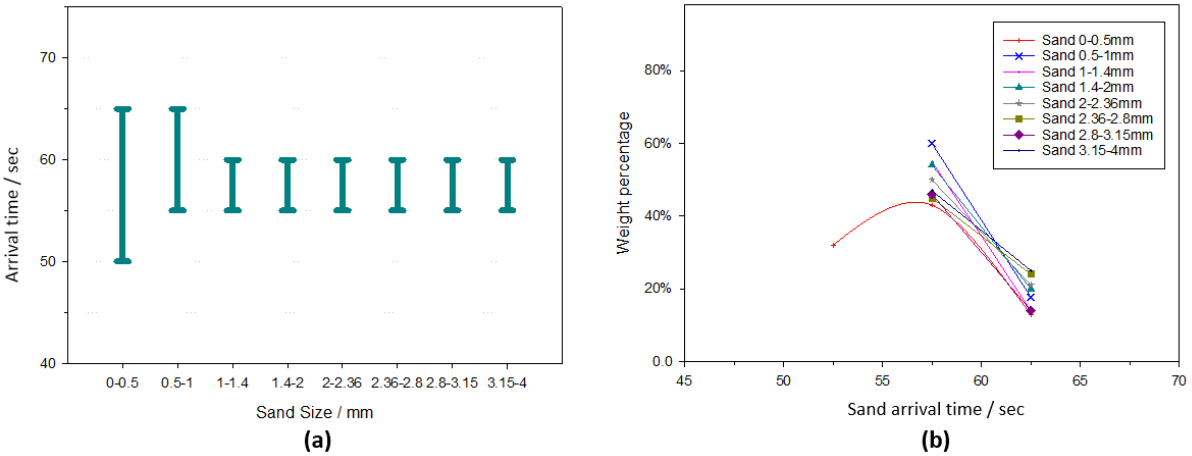

Figure 6.23 Cuttings arrival time and weight distribution over time for 0.2% XCD drilling fluids at the flow rate of 150 l/min, (a) cuttings arrival time, (b) weight percentage distribution.

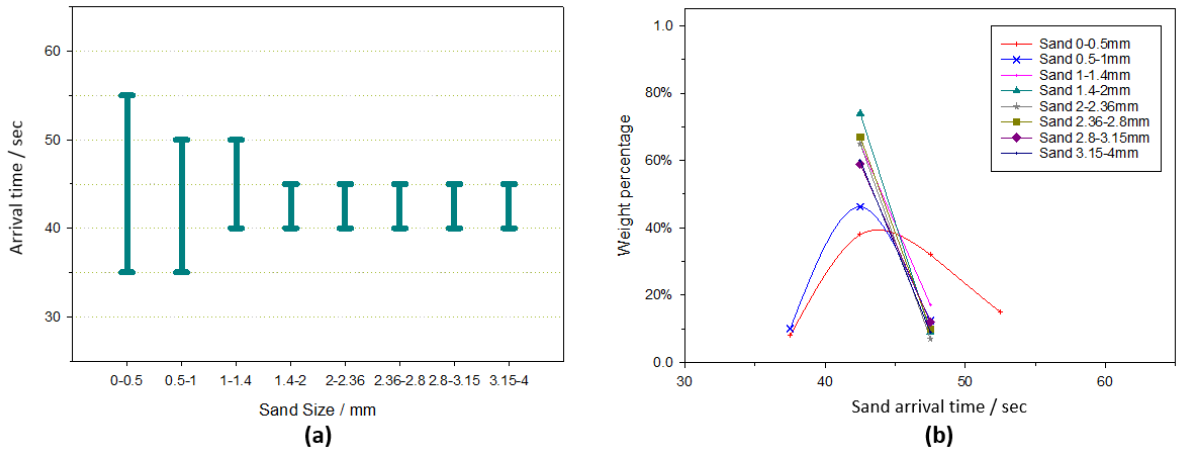

Figure 6.24 Cuttings arrival time and weight distribution over time for 0.2% XCD drilling fluids at the flow rate of 180 l/min, (a) cuttings arrival time, (b) weight percentage distribution.

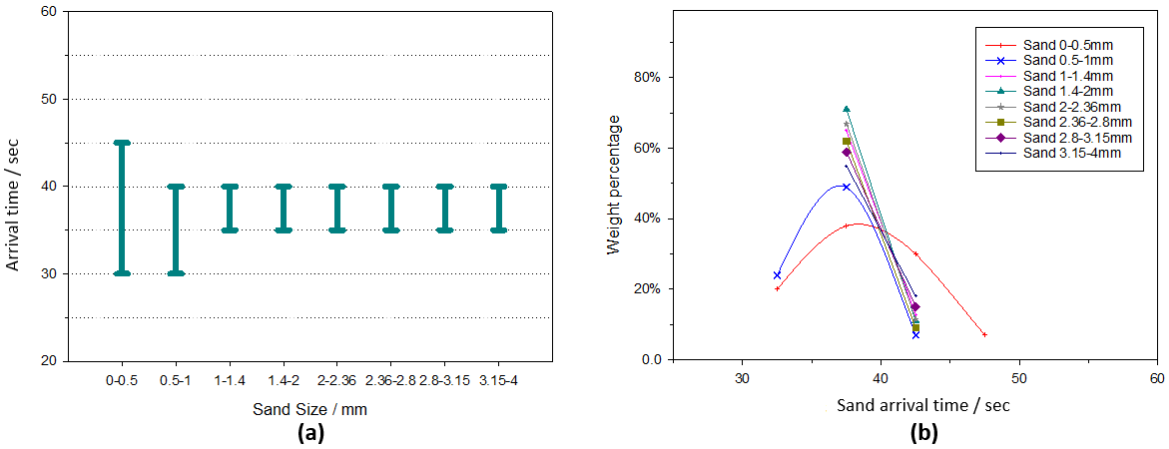

Figure 6.25 Cuttings arrival time and weight distribution over time for 0.2% XCD drilling fluids at the flow rate of 210 l/min, (a) cuttings arrival time, (b) weight percentage distribution.

6.3.3. Effect of drill string rotation

Due to the flow loop limitation, the drill string rotation effect on the cuttings transport was studied in the field. The cuttings weight distribution for water with various drill string RPM is shown in Figure 6.26. It can be seen that the drill string rotation increases the drilling fluid carrying capacity by increasing the cuttings recovery concentration in terms of earlier arrival time and reducing the cuttings lag.

Figure 6.26 shows that when the cuttings size is below 0.5mm, the cuttings recovered concentration in the earliest arrival time doesn't change much, but in later arrival time increases significantly. As the cuttings size increases to 1mm, the cuttings recovery moved to the earliest

arrival time. But when the cuttings size increases further, the cuttings concentration for the first arrival time decreases, and increases in later arrival time with the drill string rotation.

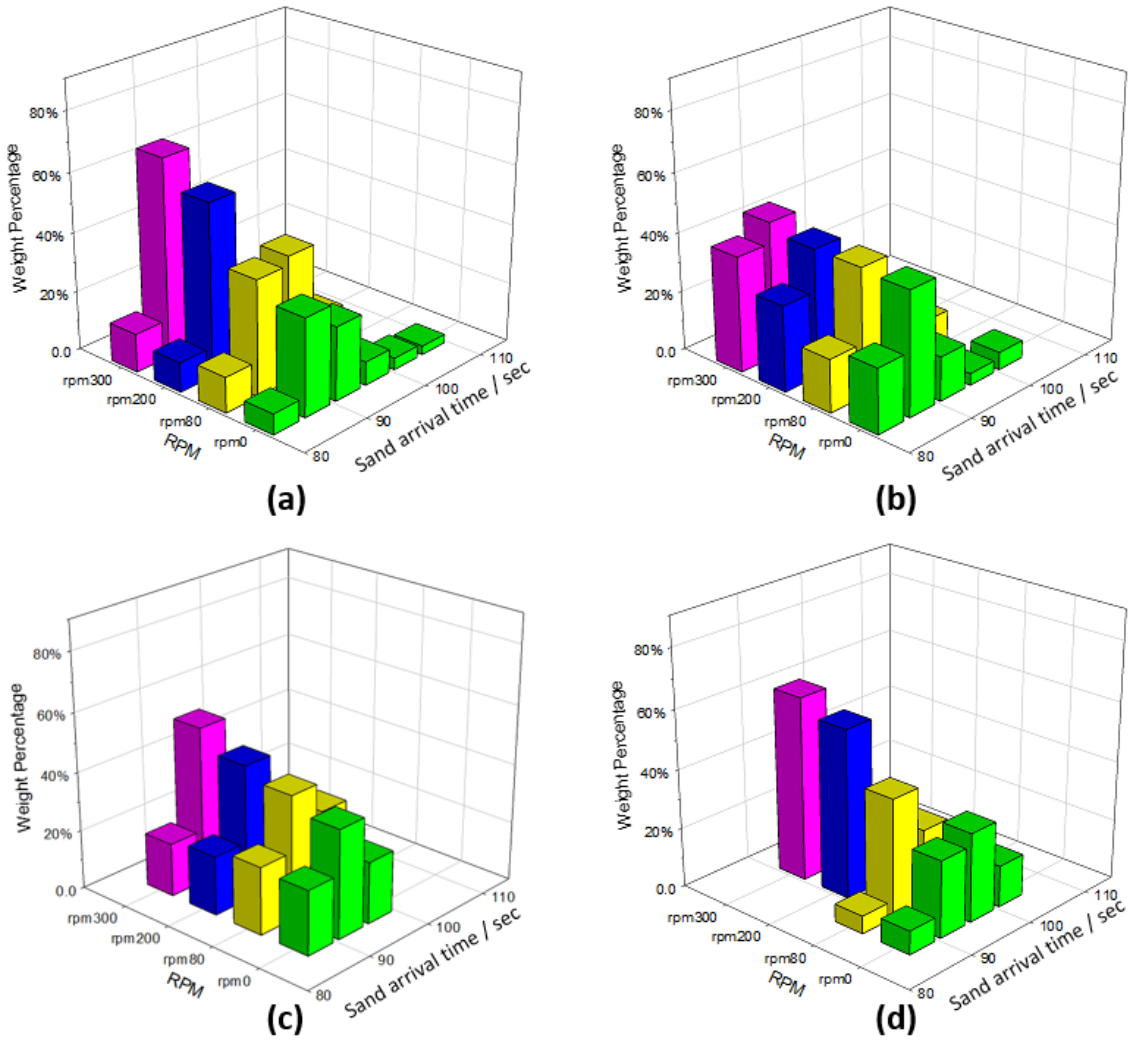

Figure 6.26 Effect of drill string rotation on the cuttings arrival time and weight distribution for tests using water at flow rate of 120 l/min with various RPM: (a) cuttings size 0-0.5 mm, (b) cuttings size 0.5-0.1 mm, (c) cuttings size 1-1.4 mm, (d) cuttings size 1.4-2 mm.

6.4. Cuttings transport through coiled tube

Reverse circulation is one of the drilling techniques used to increase the bottomhole pressure, and to minimise the effect of lost circulation and loss of the transported cuttings. In the reverse circulation, the drilling fluid is pumped into the annulus carrying the cuttings inside drill strings, see Figure 6.27.

As the sampling of cuttings has a paramount importance in the RoXplorer drilling, there is a possibility to use reverse circulation in the coiled tube drilling. In this context, the cuttings are

required to be circulated in the coil and, and therefore, it is essential to investigate the cuttings transport in the coiled tube besides in the vertical annulus. As shown in this section, the cuttings transport is totally different due to the centrifugal force induced by the curved pipe.

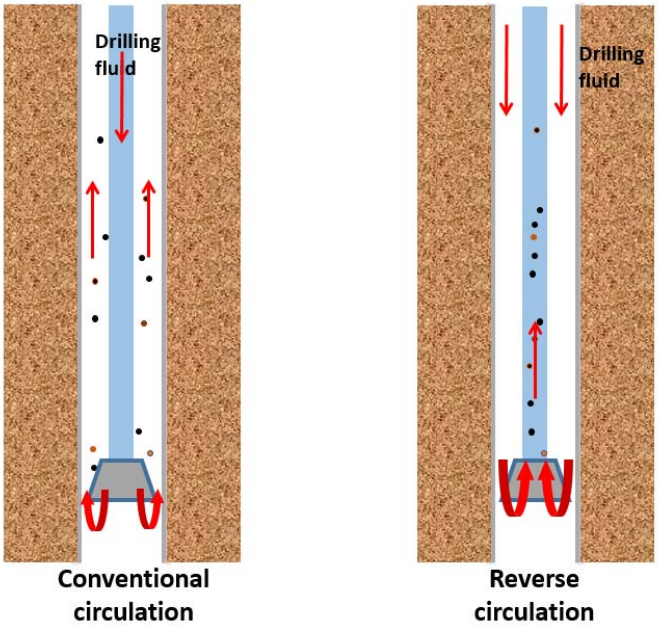

Figure 6.27 Comparison of conventional circulation and reverse circulation.

6.4.1. Research methodology

Figure 6.28 shows the experimental setup for the measurement of the cuttings transport velocity through coiled tube. The coiled tube is connected to the flow loop with a total length of 85 m.

The cuttings are introduced into the circulation before the coiled tube, and collected after the test section using buckets. As the test pipe is transparent, the cuttings can be observed visually so the accuracy of the transport time is improved than the field test using drilling rig at 5 second intervals.

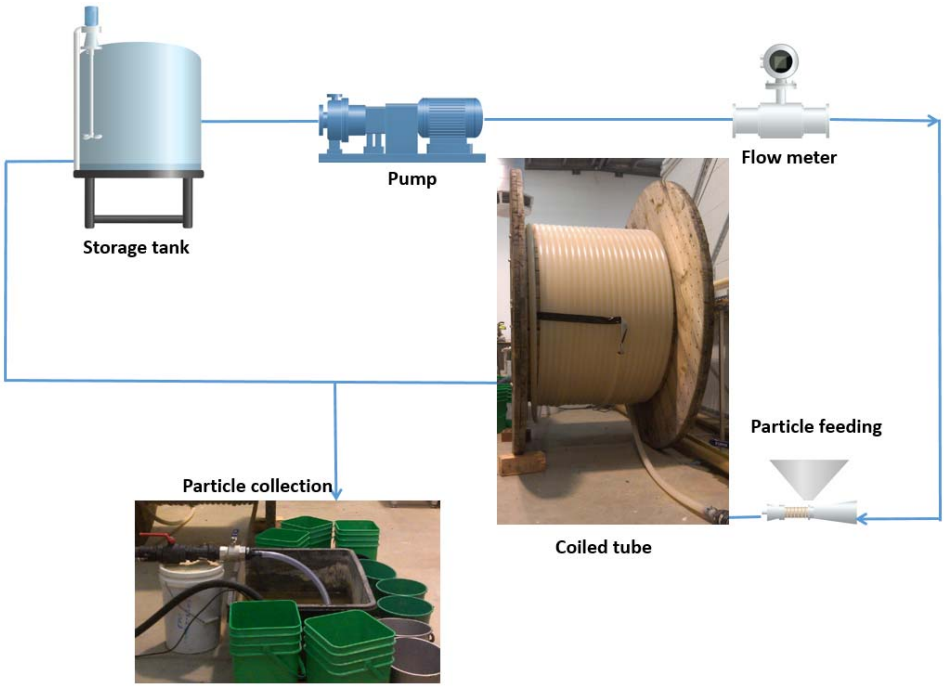

Figure 6.28 Schematic experimental setup for the cutting transport through coiled tube.

6.4.2. Results and discussion

Similar to the field test, the cuttings transport time through the test section is shown in Figure 6.29. For each size of sand, the first and last arrival of cuttings is shown at different average fluid velocity.

For a given size of the cuttings, the cuttings transport velocity increases with the increase of fluid velocity, and the spread of cuttings decreases with the increase of the flow rate. For example, in Figure 6.29a for the cuttings of size 0-0.5 mm the cuttings arrival time changes from 120 s to 65 s when the average fluid velocity increases from 1 m/s to 1.5 m/s, and correspondingly the cuttings distribution decreases from 30s to 15 s. With the increase of the cuttings size, for fluid velocity of 1m/s, the cuttings transport time decreases significantly from 120 s for 0.106-0.425 mm cuttings to 95 s for 2.8-3.15 mm cuttings, meaning that the transportation velocity increases with the size of the cuttings in the coiled tube. At higher fluid velocity of 2.5 m/s, for the same group of cuttings the arrival time decreases from 40 seconds to only 35 seconds, and lag time also decreases due to the high flow rate.

According to the arrival time, the cuttings velocity is obtained for the transportation through the coiled tube, see Figure 6.30. The results from Chapter 5 for both single particle and 1%

cuttings in vertical annulus were compared with the results of coiled tube for water at the flow rate of 90 l/min and 120 l/min.

It is surprisingly found that with the cuttings size increase, the cuttings velocity increases as well, which suggests that the particle size impact on the cuttings transport in the coiled tube is opposite to that in straight annulus, in which the cuttings velocity decreases with particle size increase. For example, for the 1% cuttings transport at the flow rate of 90 l/min in vertical annulus the cuttings transport velocity decreases from 0.98m/s to 0.76 m/s when the particle size increases from 0.2-0.3 mm to 1.8-2 mm, while the transport velocity in the coiled tube increases from 0.85 m/s to 0.96 m/s. Since all the parameters except the pipe geometry are the same as straight pipe, it can be suggested that the centrifugal force caused by the curved pipe is the most possible reason.

From a practical perspective, it is possible to determine certain cuttings size depending on the flow rate which can ensure the transport velocity is the same for coiled tube and straight pipe, which then does not require the consideration of the curved pipe influence.

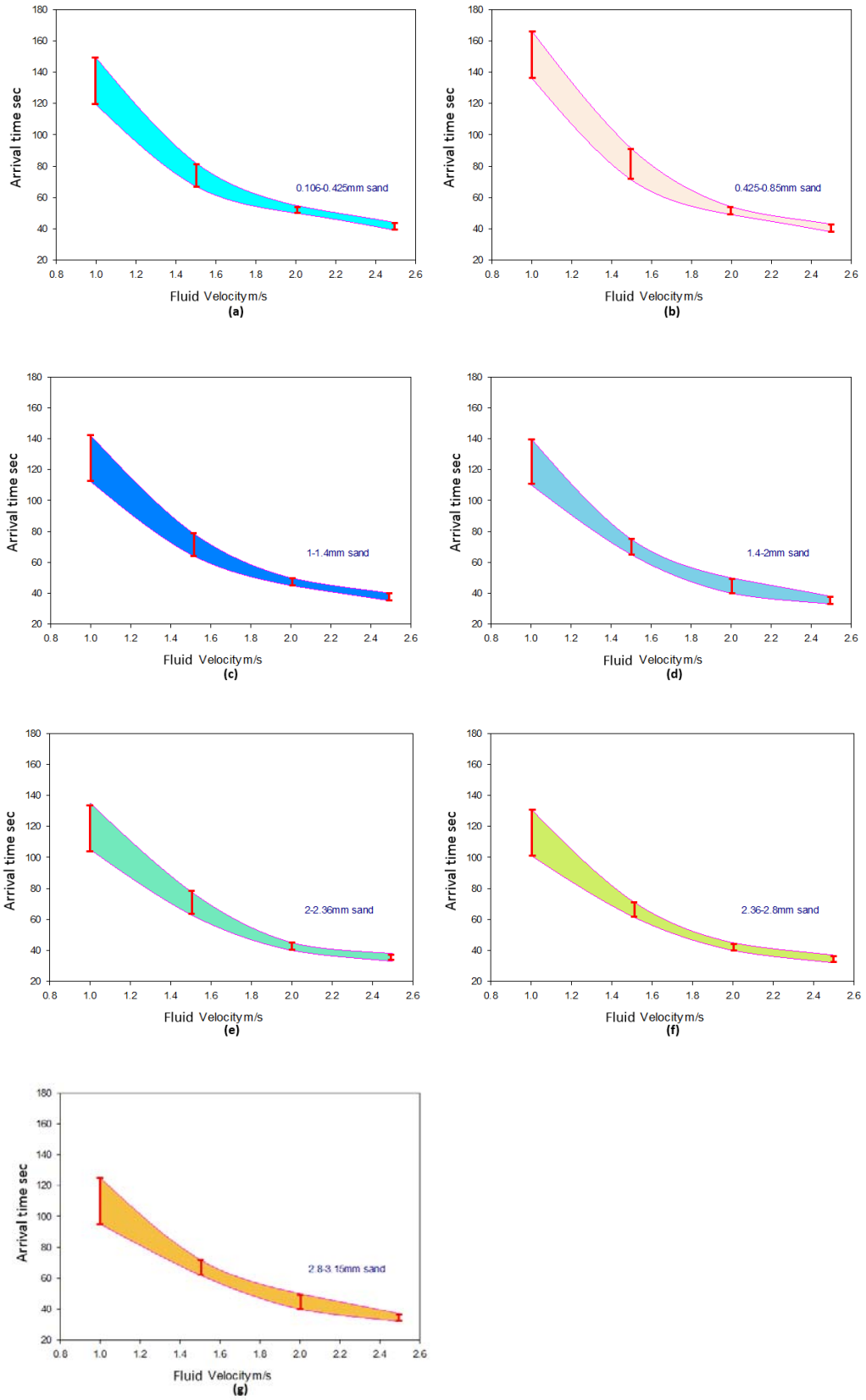

Figure 6.29 Cuttings arrival time distribution through coiled tube in water at various flow rates for different cuttings size.

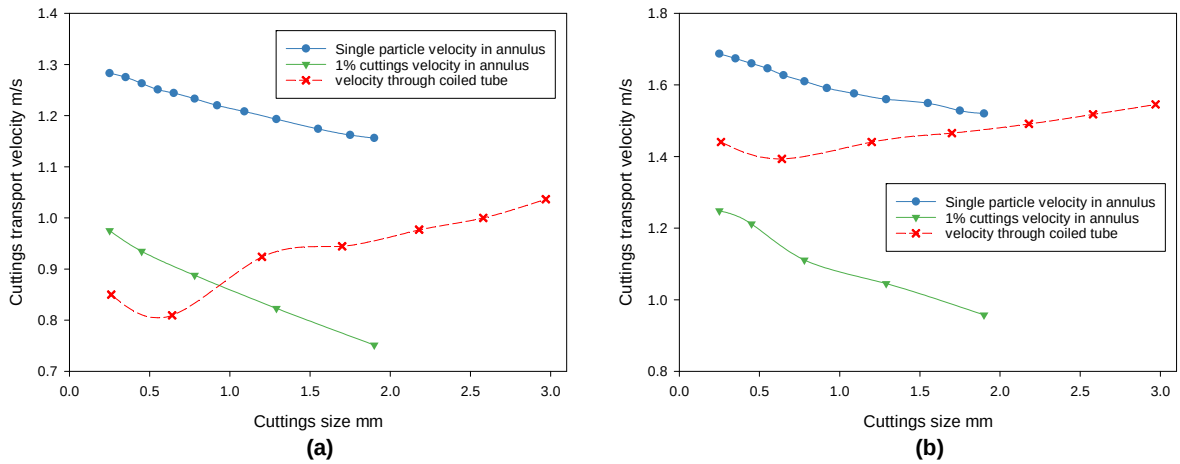

Figure 6.30 Comparison of cuttings transport velocity in vertical annulus and coiled tube for water, (a) flow rate of 90l/min, (b) flow rate of 120l/min.

6.5. Summary

This chapter investigated the cuttings transport velocity using field test. In addition to the cuttings size and fluid rheology effect, more parameters have been studied in the field test which are not possible for the flow loop test, including the drill pipe rotation and the cuttings lag. For the cuttings lag, the cuttings arrival time and the corresponding weight distribution were measured, and the effect of the cuttings size, density, fluid rheology and flow rate on the cuttings lag were analysed. The cuttings transport velocity obtained from the field test was compared with the measurement results of flow loop test, and it was found that the cuttings concentration has a great impact. Furthermore, this chapter also investigated the cuttings transport in the coiled tube in terms of reverse circulation. Through the cuttings lag and transport velocity test, it was found that the cuttings size effect on the cuttings velocity is opposite to the straight pipe, which shows that the cuttings transport velocity increases with the cuttings size increase.

Chapter 7. Conclusions

7.1. Contributions

This thesis has presented an experimental study of the cuttings transport velocity in micro borehole of coiled tubing drilling. In this study, a systematic methodology was implemented to measure the cuttings settling and transport velocity using particle tracking velocimetry (PTV). A series of measurements were performed to obtain the cuttings velocity under various conditions of fluid (rheology and flow rate), cutting (size and concentration) and borehole geometry (straight annulus, straight pipe and curved pipe). The experimental results of PTV measurements were compared with the cuttings settling velocity and the results of field tests.

The main contributions are presented based on the results from the cutting settling velocity of single particle, cuttings settling at various concentrations, and the cuttings transport velocity in an upward flow for vertical annulus.

The conclusion of single particle settling can be summarised as below:

- The settling velocity of single particles increases with the size of cuttings, and the rate of increase follows relatively a linear trend, see Figure 7.1.
- The fluid viscosity decreases the rate of increase of cuttings velocity with cuttings size. As a result, the magnitude of reduction of cuttings velocity is more significant for larger size cuttings, see Figure 7.1.

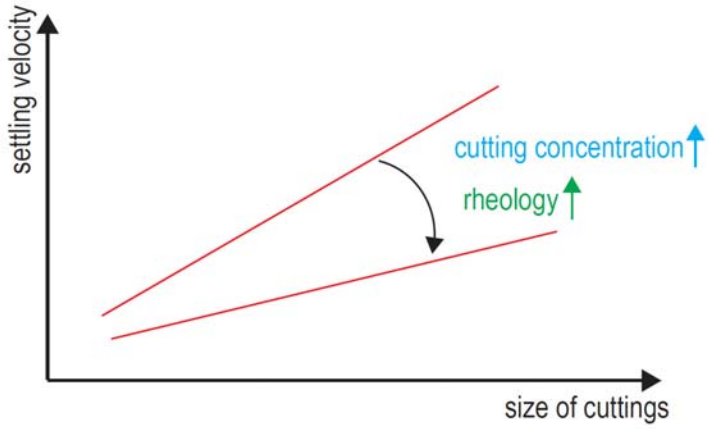

Figure 7.1 Conceptual parametric analysis of cuttings settling velocity.

- The effect of the fluid rheology on the cuttings settling velocity can be explained by the settling shear rate (the ratio of cuttings settling velocity to the particle size). The

variation of settling shear rate is affected by the fluid type: Newtonian and power law fluids. The settling shear rate decreases with the cuttings size for Newtonian fluid (water), while the settling shear rate increases with the cuttings size for power law fluids, and is relatively stable for larger particles, see Figure 7.2.

- Based on the fluid rheology, the shear stress corresponding to the settling shear rate is obtained for various cuttings size and fluid rheology. The shear stress is relatively constant for small sized cuttings, and increases with the cuttings size, see Figure 7.2.

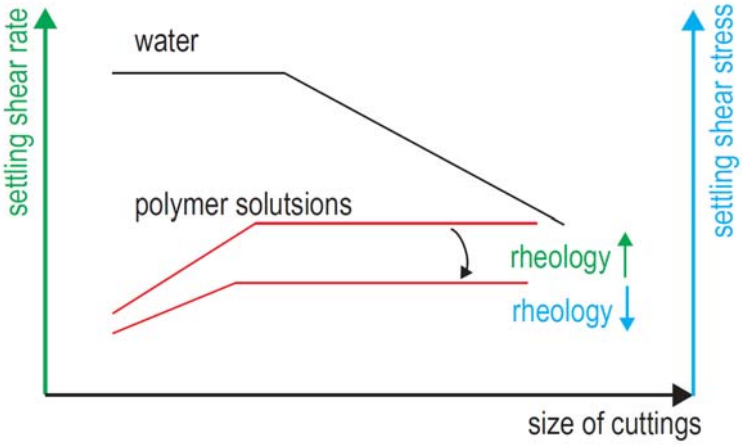

Figure 7.2 Conceptual variation of settling shear rate and shear stress with cuttings size and fluid rheology for water and polymer solutions.

- The effect of annulus wall on cuttings settling velocity can be quantified using the wall factor. The wall effect becomes significant for larger particles and more viscous fluid, see Figure 7.3.
- The wall factor obtained from the annulus settling experiments were compared with previous correlations of the wall effect. The results indicated a more accurate prediction of the annulus wall effect, where hydraulic diameter was used instead of gap width of annulus.

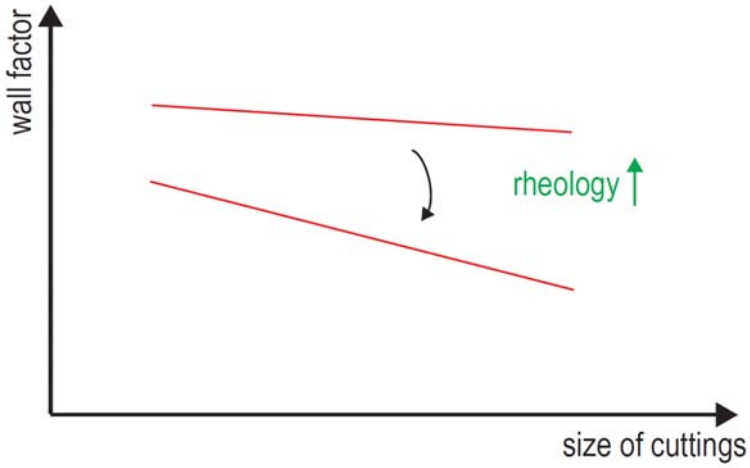

Figure 7.3 Conceptual variation of wall factor with cuttings size and fluid rheology.

- The cuttings settling for different particle sizes in various fluids in the annulus is summarised into the same correlation of the particle Reynolds number and drag coefficient, which is used as the standard drag curve for the given sized borehole of the coiled tubing drilling. The results follow the general trends predicted by previous correlations. However, there is no correlation that can provide accurate estimation of the drag coefficient covering the full range of particle Reynolds number.

The main conclusions of the impact of cuttings concentrations on the cuttings settling are summarised:

- A unique experimental procedure developed to quantify the effect of cuttings concentration on settling velocity of cuttings. Using this test method, the cuttings were fully dispersed in the suspending fluid before the start of the experiment, and therefore, any possibility of errors associated with particle aggregation was minimised.
- For the cuttings settling at various concentrations (hindered settling), the settling velocity decreases as the cuttings concentration increases. This effect is more significant when the cuttings size is larger for various fluids. The wall effect becomes significant with the increase of fluid rheology. However, this effect is noticeable only at higher cuttings concentrations. The cutting concentration has a similar but more significant role in decreasing the hindered settling velocity, see Figure 7.4.

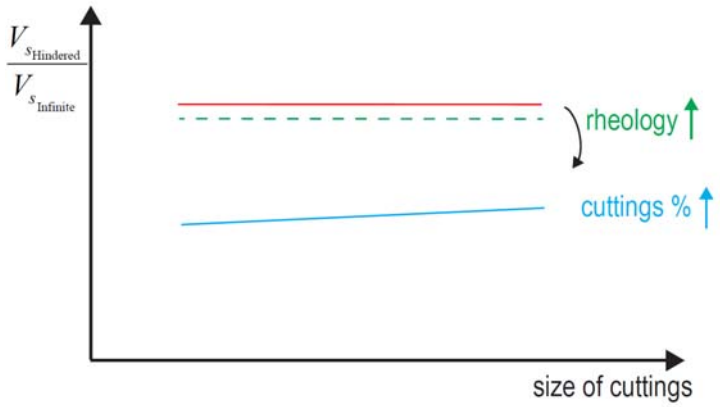

Figure 7.4 Conceptual variation of ratio of hindered settling velocity over the infinite settling velocity.

The main conclusions of the experimental study on the cuttings transport velocity in annulus are presented:

- The large quantity of the data of the cuttings transport velocity showed that the cuttings transport velocity has a distribution. The variation of the cuttings transport decreases for less viscous fluid, and also decreases at higher flow rates.
- The cuttings transport velocity can be higher than the fluid average velocity, which is contrary to perhaps the general perception that the cuttings velocity is always slower than the fluid velocity. This trend was explained using the fluid velocity distribution analysis carried out using numerical simulations. The increase of flow rate or rheology results in higher fluid velocity in the centre for the cuttings transport where the shear rate is minimum.
- It is inaccurate to predict the cuttings transport velocity based on the cuttings slip velocity from cuttings settling. The experimental results showed that not only the predictions are inaccurate, the settling velocity experiments cannot be used for parametric analysis to qualitatively characterise the effect of the cuttings transport parameters. Below points are the summary of our findings in this comparison:
    - The cuttings transport velocity decreases with the increase of the cuttings size, i.e. the cuttings transport slip velocity increases as the cuttings size increases, see Figure 7.5. The increase of both flow rate and fluid rheology results in increase of the cuttings transport velocity and decrease of the slip velocity, see Figure 7.6.

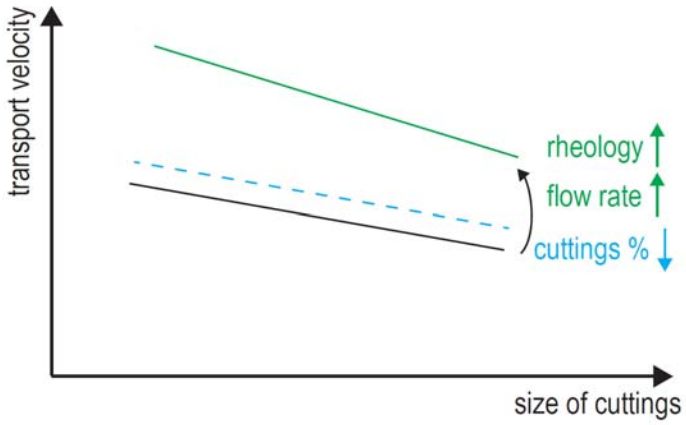

Figure 7.5 Conceptual variation of cuttings transport velocity with cuttings size, concentration, rheology and flow rate.

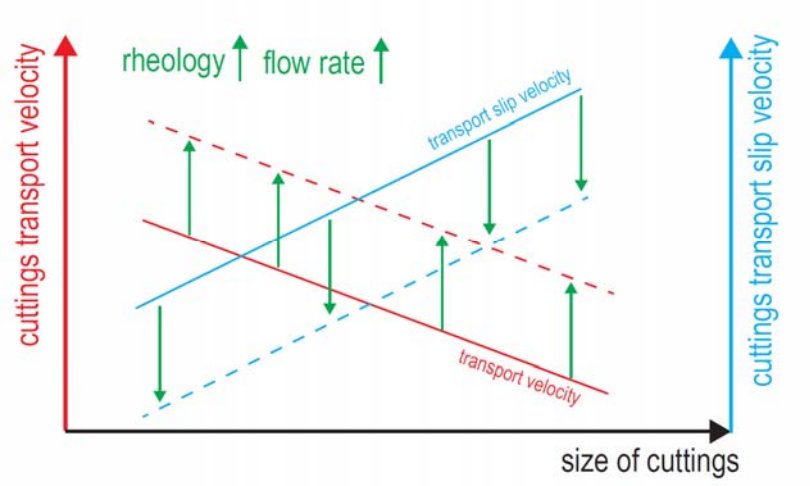

Figure 7.6 Conceptual variation of cuttings transport and slip velocity with cutting size, rheology and flow rate.

- The effect of fluid rheology on the cuttings transport velocity and settling velocity are not in agreement. The effect of fluids rheology on the settling velocity for large size cuttings is more significant than the small size cuttings. However, the variation of the cuttings transport velocity is almost proportional with the cuttings size for various fluids at different concentrations, see Figure 7.6.
- Contrary to the previous assumption that the cuttings slip velocity is not affected by fluid velocity, the transportation cuttings slip velocity shows that the transportation slip velocity is function of flow rate; the slip velocity becomes larger as the flow rate increases.

- The effect of cuttings concentration is distinct on the cuttings transport and settling velocity. The cuttings transport velocity decreases as the concentration increases, showing that the cuttings transportation slip velocity increases, which is contrary to the previous assumption based on the hindered settling that the slip velocity decreases with the increase of the cuttings concentration, see Figure 7.7.

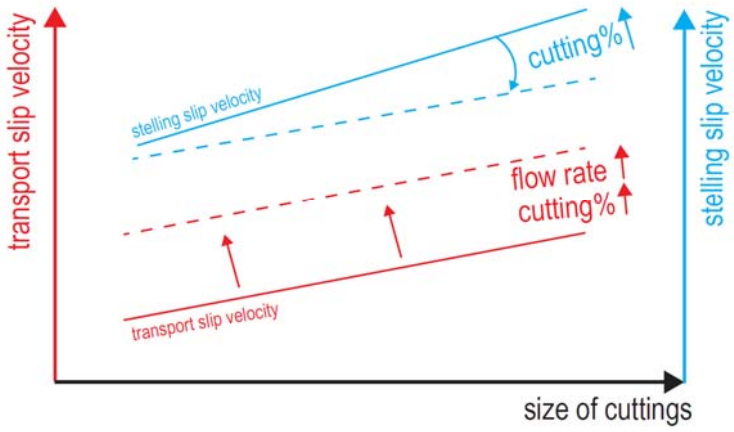

Figure 7.7 Conceptual variation of the cuttings slip velocity from cuttings transport and settling with cuttings size, flow rate and cutting concentration.

- The results of particle transportation in curved path shows that the cutting transportation has a unique pattern which is opposite to the transportation of cutting in straight annulus. Unlike transportation in straight annulus, larger particles have higher transport velocity with less variation in curved pipe (coiled tube) due to the centrifugal force.

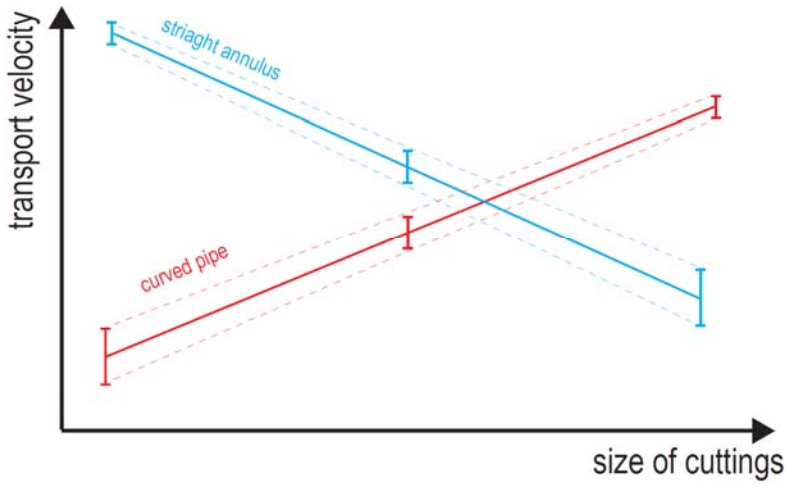

Figure 7.8 Conceptual variation of cuttings transport velocity in straight annulus and curved pipe.

7.2. Future work

- In this research, it was not possible to determine the locations of cuttings in the annulus due to the limitation of the PTV method. In future research, it is recommend to use other systems such as particle imaging velocimetry to locate the cuttings position with respect to axis of annulus to better understand the link between local velocity profile and cuttings transport velocity, and to develop correlations of particle Reynolds number and drag coefficient for the cuttings transport in the annulus.
- This research quantified the cuttings transport velocity for various cuttings and fluids properties. From a practical perspective, it is critical to develop an algorithm based on the cuttings transport velocity combined with the cuttings distribution and lag time for the depth matching of cuttings during drilling.
- Further research is required to study the effect of more parameters on the cuttings transport velocity such as drill pipe rotation and eccentricity. It is imperative to compare these effects on various cuttings transport conditions, for example in different pipe geometry or for some critical cases like cuttings suspended by minimum flow rate.
- This thesis investigated a little about the cuttings transport velocity in the coiled tube, and found that the cuttings size impact is opposite to the straight pipe due to centrifugal force. More experiments are required to study the solid liquid flow in the curved pipe for a better understanding of the reverse circulation application for the coiled tubing drilling.

References

1. Schodde, R. and P. Guj, *WHERE ARE AUSTRALIA'S MINES OF TOMORROW?* 2012, Centre for Exploration Targeting, University of Western Australia, September.
2. Schodde, R. *The declining discovery rate—What is the real story*. in *Presentation to the AMIRA International's Exploration Managers Conference, Yarra Valley, Victoria*. 2010.
3. *DET CRC*. Available from: http://detcrc.com.au/programs/program-1/project-1-1/.
4. Li, J. and S. Walker, *Sensitivity analysis of hole cleaning parameters in directional wells.* SPE Journal, 2001. **6**(04): p. 356-363.
5. Nguyen, D. and S. Rahman. *A three-layer hydraulic program for effective cuttings transport and hole cleaning in highly deviated and horizontal wells*. in *SPE/IADC Asia Pacific Drilling Technology*. 1996. Society of Petroleum Engineers.
6. Sifferman, T. and T. Becker, *Hole cleaning in full-scale inclined wellbores.* SPE Drilling Engineering, 1992. **7**(02): p. 115-120.
7. Pilehvari, A.A., J. Azar, and S.A. Shirazi, *State-of-the-art cuttings transport in horizontal wellbores.* SPE drilling & completion, 1999. **14**(03): p. 196-200.
8. Chien, S.-F. *Annular velocity for rotary drilling operations*. in *International Journal of Rock Mechanics and Mining Sciences & Geomechanics Abstracts*. 1972. Elsevier.
9. Sifferman, T.R., et al., *Drill cutting transport in full scale vertical annuli.* Journal of Petroleum Technology, 1974. **26**(11): p. 1,295-1,302.
10. Pigott, R. *Mud flow in drilling*. in *Drilling and production practice*. 1941. American Petroleum Institute.
11. Sifferman, T.R., *The Carrying Capacity of Drilling Fluids.* Energy Sources, 1983. **7**(1): p. 43-50.
12. Williams Jr, C. and G. Bruce, *Carrying capacity of drilling muds.* Journal of Petroleum Technology, 1951. **3**(04): p. 111-120.
13. Walker, R. and T. Mayes, *Design of muds for carrying capacity.* Journal of Petroleum Technology, 1975. **27**(07): p. 893-900.
14. Sample, K.J. and A.T. Bourgoyne Jr. *Development of Improved Laboratory and Field Procedures for Determining the Carrying Capacity of Drilling Fluids*. in *SPE Annual Fall Technical Conference and Exhibition*. 1978. Society of Petroleum Engineers.
15. Becker, T.E., *Correlations for drill cuttings transport in directional well drilling*. 1987, Tulsa Univ., OK (USA).
16. Duan, M., *Study of cuttings transport using foam with drill pipe rotation under simulated downhole conditions.* 2005.
17. Zhou, L., *Cuttings transport with aerated mud in horizontal annulus under elevated pressure and temperature conditions.* 2003.
18. Ozbayoglu, E.M., et al. *Cuttings transport with foam in horizontal & highly-inclined wellbores*. in *SPE/IADC Drilling Conference*. 2003. Society of Petroleum Engineers.
19. Chen, Z., *Cuttings transport with foam in horizontal concentric annulus under elevated pressure and temperature conditions.* 2006.
20. Iyoho, A.W., *DRILLED-CUTTINGS TRANSPORT BY NON-NEWTONIAN DRILLING FLUIDS THROUGH INCLINED, ECCENTRIC ANNULI.* 1981.
21. Cho, H., *Development of a three-segment hydraulic model for cuttings transport in horizontal and deviated wells*. 2001.
22. Campos, W., *Mechanistic modeling of cuttings transport in directional wells.* 1996.
23. Li, Y., *Numerical modeling of cuttings transport with foam in vertical and horizontal wells*. 2005.
24. Ford, J., et al. *Experimental investigation of drilled cuttings transport in inclined boreholes*. in *SPE Annual Technical Conference and Exhibition*. 1990. Society of

Petroleum Engineers.
25. Kelessidis, V. and G. Bandelis, *Flow Patterns and Minimum Suspension Velocity for Efficient Cuttings Transport in Horizontal and Deviated Wells in Coiled-Tubing Drilling.* SPE Drilling & Completion, 2004. **19**(04): p. 213-227.
26. Kamyab, M. and V. Rasouli, *Experimental and numerical simulation of cuttings transportation in coiled tubing drilling.* Journal of Natural Gas Science and Engineering, 2016. **29**: p. 284-302.
27. Hatala, R., M. Olanson, and P. Davis, *Canadian Coiled Tubing Horizontal Drilling: Technology And Applications*. Journal of Canadian Petroleum Technology, 1995. **34**(06).
28. Cox, R., J. Li, and G. Lupick, *Horizontal underbalanced drilling of gas wells with coiled tubing.* SPE drilling & completion, 1999. **14**(01): p. 3-10.
29. Graham, R., et al., *Horizontal Re-entry Drilling With Coiled Tubing: A Viable Technology.* Journal of Canadian Petroleum Technology, 1999. **38**(10).
30. Enilari, M., S. Osisanya, and K. Ayeni, *Development and Evaluation of Various Drilling Fluids for Slim Hole Wells.* Journal of Canadian Petroleum Technology, 2009. **48**(6): p. 30-32.
31. Fu, J., et al., *Characteristics of helical flow in slim holes and calculation of hydraulics for ultra-deep wells.* Petroleum Science, 2010. **7**(2): p. 226-231.
32. McDonald, S., F. Felderhoff, and K. Fisher, *Practical Drilling Technology New bits, motors improve economics of slim hole horizontal wells.* Oil & Gas Journal, 1996. **94**(11).
33. McCarty, T.M., M.J. Stanley, and L.L. Gantt. *Coiled tubing drilling: Continued performance improvement in Alaska*. in *SPE/IADC drilling conference*. 2001. Society of Petroleum Engineers.
34. Milligan, M., M. Andreychuk, and W. Lunan, *Coiled-Tubing Drilling of Horizontal Sidetrack in House Mountain Field, Alberta.* SPE Drilling & Completion, 2000. **15**(02): p. 92-96.
35. Kara, D., et al. *Dynamically overbalanced coiled tubing drilling on the north slope of Alaska*. in *SPE/ICoTA Coiled Tubing Roundtable*. 1999. Society of Petroleum Engineers.
36. Ramos Jr, A., et al., *Horizontal slim-hole drilling with coiled tubing: an operator's experience.* Journal of Petroleum Technology, 1992. **44**(10): p. 1,119-1,125.
37. McGregor, B., R. Cox, and J. Best. *Application of Coiled Tubing Drilling Technology on a Deep Underpressured Gas Reservoir*. in *SPE/ICoTA North American Coiled Tubing Roundtable*. 1997. Society of Petroleum Engineers.
38. Cassee, U., et al. *True Hybrid Operations Combining Coiled Tubing Drilling and Conventional Rig Workover Techniques and Practices*. in *SPE/IADC Drilling Conference*. 2005. Society of Petroleum Engineers.
39. Weighill, G., H. Thoreby, and L. Myrholt, *Underbalanced coiled tubing drilling experience on the Ula Field.* SPE Production & Facilities, 1997. **12**(02): p. 67-72.
40. Van Venrooy, J., et al. *Underbalanced drilling with coiled tubing in Oman*. in *SPE/IADC Middle East Drilling Technology Conference*. 1999. Society of Petroleum Engineers.
41. Leising, L. and K. Newman, *Coiled-tubing drilling.* SPE drilling & completion, 1993. **8**(04): p. 227-232.
42. Guan, F., et al., *An Experimental Study of Flow Behavior of Coiled Tubing Drilling System.* Advances in Mechanical Engineering, 2014. **6**: p. 935159.
43. Kamyab, M., *Cuttings transportation in coiled tubing drilling for mineral exploration*. 2014.
44. Bizhani, M., F.E. Rodriguez Corredor, and E. Kuru, *Quantitative evaluation of critical*

conditions required for effective hole cleaning in coiled-tubing drilling of horizontal wells. SPE Drilling & Completion, 2016. **31**(03): p. 188-199.
45. Cho, H., S. Shah, and S. Osisanya, *A three-segment hydraulic model for cuttings transport in coiled tubing horizontal and deviated drilling.* Journal of Canadian Petroleum Technology, 2002. **41**(06).
46. Leising, L. and I. Walton, *Cuttings-transport problems and solutions in coiled-tubing drilling.* SPE drilling & completion, 2002. **17**(01): p. 54-66.
47. Peker, S.M. and S.S. Helvaci, *Solid-liquid two phase flow*. 2011: Elsevier.
48. Davies, L., D. Dollimore, and J. Sharp, *Sedimentation of supsensions: implications of theories of hindered settling.* Powder Technology, 1975. **13**(1): p. 123-132.
49. Davies, L. and D. Dollimore, *Sedimentation of suspensions: factors affecting the dispersion and hindered settling of calcium and other carbonates in a variety of liquids.* Powder Technology, 1978. **19**(1): p. 1-6.
50. Sadowski, Z., J. Mager, and J. Laskowski, *Hindered settling of coagulating suspensions.* Powder Technology, 1978. **21**(1): p. 73-79.
51. Turian, R., et al., *Characterization, settling, and rheology of concentrated fine particulate mineral slurries.* Powder Technology, 1997. **93**(3): p. 219-233.
52. Baldock, T., et al., *Settling velocity of sediments at high concentrations.* Coastal engineering, 2004. **51**(1): p. 91-100.
53. Richardson, J. and W. Zaki, *Sedimentation and fluidisation: Part I.* Chemical Engineering Research and Design, 1997. **75**: p. S82-S100.
54. Chhabra, R., *Wall effects on free-settling velocity of non-spherical particles in viscous media in cylindrical tubes.* Powder Technology, 1995. **85**(1): p. 83-90.
55. Chhabra, R., *Wall effects on terminal velocity of non-spherical particles in non-Newtonian polymer solutions.* Powder technology, 1996. **88**(1): p. 39-44.
56. Miyamura, A., S. Iwasaki, and T. Ishii, *Experimental wall correction factors of single solid spheres in triangular and square cylinders, and parallel plates.* International Journal of Multiphase Flow, 1981. **7**(1): p. 41-46.
57. Machač, I. and Z. Lecjaks, *Wall effect for a sphere falling through a non-Newtonian fluid in a rectangular duct.* Chemical engineering science, 1995. **50**(1): p. 143-148.
58. Chien, S.-F., *Settling velocity of irregularly shaped particles.* SPE Drilling & Completion, 1994. **9**(04): p. 281-289.
59. Clift, R., J.R. Grace, and M.E. Weber, *Bubbles, drops, and particles*. 2005: Courier Corporation.
60. Flemmer, R.L. and C. Banks, *On the drag coefficient of a sphere.* Powder Technology, 1986. **48**(3): p. 217-221.
61. Haider, A. and O. Levenspiel, *Drag coefficient and terminal velocity of spherical and nonspherical particles.* Powder technology, 1989. **58**(1): p. 63-70.
62. Khan, A. and J. Richardson, *The resistance to motion of a solid sphere in a fluid.* Chemical Engineering Communications, 1987. **62**(1-6): p. 135-150.
63. Turton, R. and O. Levenspiel, *A short note on the drag correlation for spheres.* Powder technology, 1986. **47**(1): p. 83-86.
64. Michell, S.J., *Fluid and Particle Mechanics: Chemical Engineering Division*. 2013: Elsevier.
65. Moore, P.L., *Drilling practices manual.* 1974.
66. Ghatage, S.V., et al., *Effect of turbulence on particle and bubble slip velocity.* Chemical Engineering Science, 2013. **100**: p. 120-136.
67. Galvin, K., S. Pratten, and G.N.T. Lam, *A generalized empirical description for particle slip velocities in liquid fluidized beds.* Chemical Engineering Science, 1999. **54**(8): p. 1045-1052.

68. Arsenijević, Z.L., et al., *Wall effects on the velocities of a single sphere settling in a stagnant and counter-current fluid and rising in a co-current fluid.* Powder Technology, 2010. **203**(2): p. 237-242.
69. Zhu, C., et al., *Experimental investigation of non-stationary motion of single small spherical particles in an upward flow with different velocities.* Powder Technology, 2015. **273**: p. 111-117.
70. Jourdan, G., et al. *Drag coefficient of a sphere in a non-stationary flow: new results*. in *Proceedings of the Royal Society of London A: Mathematical, Physical and Engineering Sciences*. 2007. The Royal Society.
71. Latto, B., G. Round, and R. Anzenavs, *Drag coefficients and pressure drops for hydrodynamically suspended spheres in a vertical tube with and without polymer addition.* The Canadian Journal of Chemical Engineering, 1973. **51**(5): p. 536-541.
72. Duduković, A.P. and S.K. Končar□Djurdjević, *The effect of tube walls on drag coefficients of coaxially placed objects.* AIChE Journal, 1981. **27**(5): p. 837-840.
73. Laskovski, D., P. Stevenson, and K. Galvin, *Lift and drag forces on an isolated cubic particle in pipe flow.* chemical engineering research and design, 2009. **87**(12): p. 1573-1581.
74. Bellani, G. and E.A. Variano, *Slip velocity of large neutrally buoyant particles in turbulent flows.* New Journal of Physics, 2012. **14**(12): p. 125009.
75. Fishwick, R., J. Winterbottom, and E. Stitt, *Explaining mass transfer observations in multiphase stirred reactors: particle-liquid slip velocity measurements using PEPT.* Catalysis today, 2003. **79**: p. 195-202.
76. Sun, B., et al., *Experimental study on the drag coefficient of single bubbles rising in static non-Newtonian fluids in wellbore.* Journal of Natural Gas Science and Engineering, 2015. **26**: p. 867-872.
77. Dewsbury, K., D. Karamanev, and A. Margaritis, *Dynamic behavior of freely rising buoyant solid spheres in non□Newtonian liquids.* AIChE journal, 2000. **46**(1): p. 46-51.
78. Karamanev, D.G. and L.N. Nikolov, *Free rising spheres do not obey Newton's law for free settling.* AIChE journal, 1992. **38**(11): p. 1843-1846.
79. MAEDA, M., S. IKAI, and A. UKON, *Pneumatic Conveying of Solids: Part 2, On Slip Velocities and Interaction between Wall and Particles in Vertical Lines.* Bulletin of JSME, 1974. **17**(108): p. 768-775.
80. Hussainov, M., et al., *Gas-solid flow with the slip velocity of particles in a horizontal channel.* Journal of aerosol science, 1996. **27**(1): p. 41-59.
81. Tallon, S., C.E. Davies, and B. Barry, *Slip velocity and axial dispersion measurements in a gas-solid pipeline using particle tracer analysis.* Powder technology, 1998. **99**(2): p. 125-131.
82. Arundel, P., et al., *Measurements of individual alumina particle velocities and the relative slip of different-sized particles in a vertical gas-solid suspension flow using a laser-anemometer system.* Journal of Physics D: Applied Physics, 1974. **7**(16): p. 2288.
83. Chhabra, R.P., *Bubbles, drops, and particles in non-Newtonian fluids*. 2006: CRC press.
84. Walker, S. and J. Li. *The effects of particle size, fluid rheology, and pipe eccentricity on cuttings transport*. in *SPE/ICoTA Coiled Tubing Roundtable*. 2000. Society of Petroleum Engineers.
85. Tomren, P., A. Iyoho, and J. Azar, *Experimental study of cuttings transport in directional wells.* SPE Drilling Engineering, 1986. **1**(01): p. 43-56.
86. Garcia-Hernandez, A.J., et al. *Determination of cuttings lag in horizontal and deviated wells*. in *SPE Annual Technical Conference and Exhibition*. 2007. Society of Petroleum Engineers.

87. Doron, P., D. Granica, and D. Barnea, *Slurry flow in horizontal pipes—experimental and modeling.* International Journal of Multiphase Flow, 1987. **13**(4): p. 535-547.
88. Krieger, I.M. and T.J. Dougherty, *A mechanism for non□Newtonian flow in suspensions of rigid spheres.* Transactions of the Society of Rheology, 1959. **3**(1): p. 137-152.
89. Quemada, D., *Models for rheological behavior of concentrated disperse media under shear.* Advances in rheology, 1984. **2**: p. 571-582.
90. Brinkman, H., *The viscosity of concentrated suspensions and solutions.* The Journal of Chemical Physics, 1952. **20**(4): p. 571-571.
91. Metzner, A., *Rheology of suspensions in polymeric liquids.* Journal of Rheology, 1985. **29**(6): p. 739-775.
92. Chong, J., E. Christiansen, and A. Baer, *Rheology of concentrated suspensions.* Journal of applied polymer science, 1971. **15**(8): p. 2007-2021.
93. Jeffrey, D.J. and A. Acrivos, *The rheological properties of suspensions of rigid particles.* AIChE Journal, 1976. **22**(3): p. 417-432.
94. Hoffman, R., *Discontinuous and dilatant viscosity behavior in concentrated suspensions. II. Theory and experimental tests.* Journal of Colloid and Interface Science, 1974. **46**(3): p. 491-506.
95. Konijn, B., O. Sanderink, and N. Kruyt, *Experimental study of the viscosity of suspensions: Effect of solid fraction, particle size and suspending liquid.* Powder technology, 2014. **266**: p. 61-69.
96. Becker, T., J. Azar, and S. Okrajni, *Correlations of mud rheological properties with cuttings-transport performance in directional drilling.* SPE Drilling Engineering, 1991. **6**(01): p. 16-24.
97. Munson, B.R., D.F. Young, and T.H. Okiishi, *Fundamentals of fluid mechanics.* New York, 1990. **3**(4).
98. Bourgoyne, A.T., et al., *Applied drilling engineering.* 1986.
99. Shahi, S. and E. Kuru, *An experimental investigation of settling velocity of natural sands in water using Particle Image Shadowgraph.* Powder Technology, 2015. **281**: p. 184-192.
100. Cheng, N.-S., *Simplified settling velocity formula for sediment particle.* Journal of hydraulic engineering, 1997. **123**(2): p. 149-152.
101. Kaye, B. and R. Boardman, *Proc. Symposium on Interaction between Fluids and Particles.* Inst. Chem. Engrs., London (June, 1962), 1962.
102. Koglin, B., *Statistical distribution of sedimentation rate in suspensions of low concentration.* Chemie Ingenieur Technik, 1971. **43**(13): p. 761-&.
103. Smith, T.N., *A model of settling velocity.* Chemical engineering science, 1998. **53**(2): p. 315-323.
104. Roscoe, R., *The viscosity of suspensions of rigid spheres.* British Journal of Applied Physics, 1952. **3**(8): p. 267.
105. Senapati, P., B. Mishra, and A. Parida, *Modeling of viscosity for power plant ash slurry at higher concentrations: Effect of solids volume fraction, particle size and hydrodynamic interactions.* Powder Technology, 2010. **197**(1): p. 1-8.
106. Rutgers, I.R., *Relative viscosity and concentration.* Rheologica Acta, 1962. **2**(4): p. 305-348.
107. Clark, R. and K. Bickham. *A mechanistic model for cuttings transport*. in *SPE Annual Technical Conference and Exhibition*. 1994. Society of Petroleum Engineers.
108. Lake, L.W. and J. Fanchi, *Petroleum Engineering Handbook vol. 1: General Engineering*. 2006, SPE.

109. *Brukunga mine site*. Available from: http://minerals.statedevelopment.sa.gov.au/mining/former_mines/brukunga_mine_site/.

Every reasonable effort has been made to acknowledge the owners of copyright material. I would be pleased to hear from any copyright owner who has been omitted or incorrectly acknowledged.

Appendix

Effect of the cuttings size and concentration on the fluid rheology

1. 0.15% XCD polymer fluid

Table - Cuttings effect (sand 0.2-0.3 mm) on fluid rheology.

Sand v%		0%		1%		2%		3%		4%		5%	
RPM	S.R. 1/s	SS (Pa)	Vis (cP)	SS (Pa)	Vis (cP)	SS (Pa)	Vis (cP)	SS (Pa)	Vis (cP)	SS (Pa)	Vis (cP)	SS (Pa)	Vis (cP)
600	1021.38	5.7	5.6	7.9	7.7	9.6	9.4	9.9	9.7	10.7	10.5	12.1	11.8
300	510.69	3.4	6.7	4.7	9.2	5.7	11.1	6.3	12.3	8.0	15.6	8.9	17.4
200	340.46	2.9	8.4	3.4	10.0	4.3	12.7	4.5	13.2	5.6	16.5	6.2	18.3
100	170.23	1.7	9.8	2.4	13.9	2.5	14.9	2.9	17.1	2.9	17.0	3.2	19.0
60	102.14	1.1	10.4	1.6	15.5	1.7	16.4	2.3	22.8	2.2	21.3	2.2	21.8
30	51.07	0.9	16.7	1.0	19.4	1.0	20.3	1.4	27.3	1.4	27.8	1.1	22.5
20	34.05	0.6	19.0	0.9	26.6	1.0	28.4	1.0	30.8	1.0	30.4	1.5	42.8
10	17.02	0.5	26.7	0.9	55.2	0.7	41.2	0.9	52.8	0.9	50.3	0.9	51.2
6	10.21	0.4	39.8	0.5	47.3	0.4	38.5	0.7	66.0	0.7	64.0	0.6	60.8
3	5.11	0.3	64.9	0.4	79.7	0.4	80.3	0.5	92.3	0.5	90.1	0.5	95.4
2	3.4	0.3	82.3	0.4	111.2	0.4	112.7	0.4	130.0	0.4	127.7	0.5	134.8
1	1.7	0.2	125.0	0.2	122.7	0.3	187.3	0.4	223.5	0.4	227.3	0.4	231.9

Table - Cuttings effect (sand 0.3-0.4 mm) on fluid rheology.

Sand v%		0%		1%		2%	
RPM	S.R. 1/s	SS (Pa)	Vis (cP)	SS (Pa)	Vis (cP)	SS (Pa)	Vis (cP)
600	1021.38	5.7	5.6	8.0	7.8	7.8	7.6
300	510.69	3.4	6.7	4.9	9.5	4.9	9.5
200	340.46	2.9	8.4	4.0	11.8	3.6	10.5
100	170.23	1.7	9.8	2.5	14.7	2.5	14.9
60	102.14	1.1	10.4	2.1	20.7	2.1	20.5
30	51.07	0.9	16.7	1.1	20.8	1.1	21.2
20	34.05	0.6	19	1.0	29.1	1.0	29.4
10	17.02	0.5	26.7	1.0	56.9	0.8	47.3
6	10.21	0.4	39.8	0.6	61.2	0.6	62.6
3	5.11	0.3	64.9	0.5	90.1	0.5	99.2
2	3.4	0.3	82.3	0.4	128.3	0.5	139.8
1	1.7	0.2	125	0.4	232.7	0.4	233.9

2. 0.2% XCD polymer fluid

Table - Cuttings effect (sand 0.2-0.3 mm) on fluid rheology.

Sand v%		0%		1%		2%		3%		4%		5%		8%		10%	
RPM	S.R. 1/s	SS (Pa)	Vis (cP)	SS (Pa)	Vis (cP)	SS (Pa)	Vis (cP)	SS (Pa)	Vis (cP)	SS (Pa)	Vis (cP)	SS (Pa)	Vis (cP)	SS (Pa)	Vis (cP)	SS (Pa)	Vis (cP)
600	1021.38	8.9	8.7	9.5	9.3	10.0	9.8	10.4	10.2	10.6	10.4	11.0	10.8	12.0	11.7	13.1	12.8
300	510.69	6.1	12.0	6.8	13.3	7.5	14.7	8.8	17.2	9.9	19.3	9.3	18.3	10.4	20.3	11.3	22.1
200	340.46	4.8	14.0	5.2	15.3	6.0	17.6	6.5	19.2	7.0	20.7	6.9	20.4	7.8	23.0	8.6	25.2
100	170.23	3.2	19.0	3.8	22.5	4.1	23.8	4.1	24.0	4.3	25.1	4.4	26.0	4.6	27.3	5.1	29.8
60	102.14	2.8	27.3	2.9	28.2	2.9	28.3	2.9	28.0	2.9	28.6	3.0	29.1	3.4	33.0	3.6	34.9
30	51.07	2.1	41.3	2.2	42.7	2.2	42.6	2.2	43.2	2.2	44.0	2.3	44.3	2.4	46.8	2.6	51.1
20	34.05	1.8	54.0	1.9	57.0	2.0	57.8	2.0	59.9	2.1	60.7	2.1	60.8	2.2	63.6	2.3	66.8
10	17.02	1.0	60.4	1.5	85.8	1.5	87.6	1.6	91.3	1.6	92.2	1.6	93.6	1.7	101.9	1.9	109.9
6	10.21	0.9	90.6	1.2	122.3	1.3	122.8	1.4	132.7	1.4	135.7	1.4	136.2	1.5	146.6	1.6	158.0
3	5.11	0.8	148.0	1.0	201.3	1.0	204.3	1.1	215.3	1.1	213.9	1.1	220.8	1.2	236.9	1.3	261.1
2	3.4	0.7	213.0	1.0	283.9	1.0	286.3	1.0	296.8	1.0	301.5	1.0	307.4	1.1	335.6	1.2	352.0
1	1.7	0.6	365.0	0.8	484.7	0.9	504.4	0.9	529.0	0.9	533.6	0.9	531.7	1.0	572.1	0.7	390.9

Table - Cuttings effect (sand 0.3-0.4 mm) on fluid rheology.

Sand v%		0%		1%		2%		3%		4%		5%		8%		10%	
RPM	S.R. 1/s	SS (Pa)	Vis (cP)	SS (Pa)	Vis (cP)	SS (Pa)	Vis (cP)	SS (Pa)	Vis (cP)	SS (Pa)	Vis (cP)	SS (Pa)	Vis (cP)	SS (Pa)	Vis (cP)	SS (Pa)	Vis (cP)
600	1021.38	8.9	8.7	9.6	9.4	9.6	9.4	10.0	9.8	10.1	9.9	10.0	9.8	10.7	10.5	11.0	10.8
300	510.69	6.1	12.0	6.7	13.1	7.0	13.8	7.5	14.6	8.1	15.9	7.2	14.1	9.1	17.9	8.6	16.8
200	340.46	4.8	14.0	5.4	15.8	5.6	16.4	5.9	17.4	6.3	18.4	5.7	16.8	7.0	20.5	6.3	18.4
100	170.23	3.2	19.0	3.8	22.2	3.8	22.5	3.9	23.2	4.0	23.5	3.8	22.5	4.1	24.2	3.9	23.0
60	102.14	2.8	27.3	2.9	28.0	2.8	27.9	2.9	28.2	2.8	27.3	2.8	27.9	2.9	28.5	2.9	28.5
30	51.07	2.1	41.3	2.0	38.4	2.0	38.6	2.0	39.0	2.0	39.3	2.0	39.9	2.0	40.1	2.1	41.2
20	34.05	1.8	54.0	1.8	51.7	1.8	51.9	1.8	52.4	1.8	51.5	1.8	53.5	1.8	54.0	1.9	54.6
10	17.02	1.0	60.4	1.4	82.4	1.4	82.0	1.4	83.1	1.4	82.6	1.4	83.0	1.4	84.5	1.5	85.7
6	10.21	0.9	90.6	1.2	121.2	1.2	121.0	1.3	122.6	1.3	124.9	1.2	122.2	1.3	125.3	1.3	127.0
3	5.11	0.8	148.0	1.0	194.8	1.0	199.5	1.1	207.4	1.1	214.2	1.0	200.9	1.1	211.7	0.1	27.6
2	3.4	0.7	213.0	0.9	259.7	0.9	272.2	1.0	283.7	1.0	294.3	0.9	267.5	1.0	289.3	1.0	302.0
1	1.7	0.6	365.0	0.6	359.8	0.6	372.5	0.7	408.2	0.8	444.3	0.7	403.5	0.7	430.7	0.8	468.7

Table - Cuttings effect (sand 0.4-0.5 mm) on fluid rheology.

Sand v%		0%		1%		2%		3%	
RPM	S.R. 1/s	SS (Pa)	Vis (cP)	SS (Pa)	Vis (cP)	SS (Pa)	Vis (cP)	SS (Pa)	Vis (cP)
600	1021.38	8.9	8.7	9.2	9.0	9.3	9.1	9.5	9.3
300	510.69	6.1	12.0	6.3	12.3	6.6	13.0	7.0	13.7
200	340.46	4.8	14.0	5.1	15.1	5.3	15.7	5.5	16.3
100	170.23	3.2	19.0	3.6	21.2	3.7	21.5	3.7	21.7
60	102.14	2.8	27.3	2.8	27.7	2.9	28.0	2.8	27.6
30	51.07	2.1	41.3	2.0	40.1	2.1	40.4	2.1	40.4
20	34.05	1.8	54.0	1.8	51.7	1.8	52.1	1.8	51.7
10	17.02	1.0	60.4	1.4	83.9	1.4	84.5	1.4	83.5
6	10.21	0.9	90.6	1.3	122.7	1.3	124.0	1.3	123.8
3	5.11	0.8	148.0	1.0	191.0	1.0	197.0	1.0	199.9
2	3.4	0.7	213.0	0.9	269.4	0.9	269.1	0.9	276.4
1	1.7	0.6	365.0	0.7	431.2	0.7	412.9	0.7	414.7

3. 0.25% XCD polymer fluid

Table - Cuttings effect (sand 0.2-0.3 mm) on fluid rheology.

Sand v%		0%		1%		2%		3%		4%		5%		8%		10%	
RPM	S.R. 1/s	SS (Pa)	Vis (cP)	SS (Pa)	Vis (cP)	SS (Pa)	Vis (cP)	SS (Pa)	Vis (cP)	SS (Pa)	Vis (cP)	SS (Pa)	Vis (cP)	SS (Pa)	Vis (cP)	SS (Pa)	Vis (cP)
600	1021.38	10.4	10.2	12.6	12.3	13.0	12.7	13.5	13.2	13.9	13.6	14.5	14.2	15.9	15.6	17.4	17
300	510.69	7.3	14.2	8.5	16.6	10.0	19.5	10.6	20.7	10.6	20.7	11.8	23.2	13.4	26.2	13.8	27
200	340.46	5.8	17	6.5	19.2	7.6	22.4	8.2	24.1	8.4	24.8	9.2	27.1	10.2	30.1	10.5	30.9
100	170.23	4.0	23.6	4.8	28.4	5.5	32.6	5.7	33.3	5.9	34.5	6.1	35.7	6.5	38.1	7.0	41
60	102.14	3.2	31.8	3.4	32.8	3.3	32.1	3.3	32.6	4.3	42.1	4.5	44.1	4.7	46.3	5.4	53.3
30	51.07	2.6	51.7	2.9	57.4	2.9	56.1	2.9	56.4	2.9	56.8	3.0	58.1	3.0	58.7	3.2	62.1
20	34.05	2.3	67.7	2.8	82.2	2.8	81.1	2.8	81.5	2.7	80.2	2.8	82.6	2.8	83.7	3.0	86.8
10	17.02	1.8	103	2.6	152.9	2.6	151.3	2.6	153.2	2.6	151.3	2.6	155.4	2.7	157.3	2.8	161.8
6	10.21	1.3	128	2.5	243.9	2.5	240.4	2.5	246.1	2.5	242.5	2.6	250.8	2.6	253.3	2.7	259.9
3	5.11	0.9	185	2.3	458.9	2.3	451.8	2.4	462.8	2.4	460.8	2.4	476.6	2.5	483.5	2.5	495.8
2	3.4	0.9	267	2.3	668.6	2.2	654.5	2.3	675.6	2.3	670.6	2.4	699.1	2.4	711.6	2.5	729.9
1	1.7	0.7	430	1.3	740	1.3	769.8	2.0	1200.5	2.1	1224.5	2.2	1319.8	2.3	1354.6	2.4	1391.2

Table - Cuttings effect (sand 0.3-0.4 mm) on fluid rheology.

Sand v%		0%		1%		2%		3%		4%		5%		8%		10%	
RPM	S.R. 1/s	SS (Pa)	Vis (cP)	SS (Pa)	Vis (cP)	SS (Pa)	Vis (cP)	SS (Pa)	Vis (cP)	SS (Pa)	Vis (cP)	SS (Pa)	Vis (cP)	SS (Pa)	Vis (cP)	SS (Pa)	Vis (cP)
600	1021.38	10.4	10.2	12.4	12.1	13.1	12.8	13.6	13.3	13.7	13.4	14.5	14.2	17.2	16.8	18.2	17.8
300	510.69	7.3	14.2	9.1	17.8	9.5	18.6	10.4	20.3	10.0	19.6	11.0	21.5	12.6	24.6	13.5	26.5
200	340.46	5.8	17	6.7	19.8	7.6	22.4	8.1	23.7	8.0	23.4	8.6	25.3	9.8	28.9	10.4	30.6
100	170.23	4.0	23.6	5.0	29.4	5.3	31.3	5.6	33.1	5.8	33.8	5.9	34.5	6.3	36.8	6.8	40
60	102.14	3.2	31.8	4.1	39.8	3.4	33.7	4.3	42	4.5	43.9	4.5	43.9	5.0	49.3	5.4	52.6
30	51.07	2.6	51.7	2.8	54.3	2.7	53.5	2.9	56.3	2.8	55.4	3.0	57.8	3.1	60.7	3.3	65.2
20	34.05	2.3	67.7	2.6	77.4	2.6	76.9	2.6	77.7	2.7	78.6	2.7	79.8	2.8	82.3	2.9	84.4
10	17.02	1.8	103	2.4	143.6	2.5	144.2	2.5	146.4	2.5	147.4	2.5	148.6	2.6	152.9	2.6	154.9
6	10.21	1.3	128	2.3	228.3	2.3	230	2.4	234.6	2.4	237.5	2.4	238.8	2.5	245.3	2.5	248.1
3	5.11	0.9	185	2.2	420.8	2.2	424.3	2.2	438.7	2.3	446.7	2.3	449.3	2.4	464.7	2.4	470.3
2	3.4	0.9	267	2.1	612.2	2.1	614.8	2.2	636.4	2.2	650.5	2.2	654.7	2.3	676.8	2.3	686.9
1	1.7	0.7	430	1.9	1139.9	1.9	1117.8	2.0	1170.9	2.1	1206.6	2.0	1205.2	2.2	1267.2	2.2	1296.8

Table - Cuttings effect (sand 0.4-0.5 mm) on fluid rheology.

Sand v%		0%		1%		2%		3%		4%		5%		8%	
RPM	S.R. 1/s	SS (Pa)	Vis (cP)	SS (Pa)	Vis (cP)	SS (Pa)	Vis (cP)	SS (Pa)	Vis (cP)	SS (Pa)	Vis (cP)	SS (Pa)	Vis (cP)	SS (Pa)	Vis (cP)
600	1021.38	10.4	10.2	12.3	12	12.8	12.5	13.0	12.7	14.5	14.2	14.3	14	16.5	16.2
300	510.69	7.3	14.2	8.3	16.2	9.3	18.3	9.5	18.6	10.6	20.8	10.4	20.4	11.5	22.5
200	340.46	5.8	17	6.4	18.8	7.3	21.3	7.4	21.7	8.2	24.1	7.9	23.2	8.6	25.3
100	170.23	4.0	23.6	4.6	26.8	4.9	28.7	4.9	28.8	5.0	29.6	5.1	29.9	5.7	33.3
60	102.14	3.2	31.8	3.4	33	3.5	34.7	3.6	35.1	3.5	34.7	3.7	36.2	4.2	41.5
30	51.07	2.6	51.7	2.7	53	2.8	54	2.8	54	2.8	55	2.8	55	2.9	56
20	34.05	2.3	67.7	2.5	72	2.5	73	2.6	75	2.6	75	2.6	75	2.6	77
10	17.02	1.8	103	2.1	125	2.2	130	2.3	133	2.4	141	2.5	146	2.5	149
6	10.21	1.3	128	2.0	194	2.1	201	2.1	210	2.3	223	2.3	225	2.5	248
3	5.11	0.9	185	1.5	303	1.6	314	1.7	325	1.7	330	1.7	341	1.8	357
2	3.4	0.9	267	1.7	512	1.8	525	1.8	536	1.9	559	1.9	554	1.9	566
1	1.7	0.7	430	1.3	745	1.3	760	1.3	756	1.3	774	1.3	784	1.3	788

Table - Cuttings effect (sand 0.5-0.6 mm) on fluid rheology.

Sand v%		0%		1%		2%		3%		4%	
RPM	S.R. 1/s	SS (Pa)	Vis (cP)	SS (Pa)	Vis (cP)	SS (Pa)	Vis (cP)	SS (Pa)	Vis (cP)	SS (Pa)	Vis (cP)
600	1021.38	10.4	10.2	12.8	12.5	14.4	14.1	14.6	14.3	14.7	14.4
300	510.69	7.3	14.2	9.7	19	10.9	21.4	11.3	22.2	11.5	22.6
200	340.46	5.8	17	7.8	23	8.2	24.1	8.5	25	8.4	24.8
100	170.23	4.0	23.6	4.6	27	4.9	28.5	5.6	33	6.5	38
60	102.14	3.2	31.8	4.1	40.5	4.2	41.2	4.3	41.7	4.6	45
30	51.07	2.6	51.7	3.6	70.3	3.7	72	3.8	73.8	4.1	80
20	34.05	2.3	67.7	3.2	93.8	3.3	96.5	3.4	100.5	3.3	97.4
10	17.02	1.8	103	2.5	147.8	2.5	144.9	2.8	161.8	3.7	220
6	10.21	1.3	128	2.3	227	2.3	230	2.4	232.7	2.3	227.5
3	5.11	0.9	185	1.8	357.7	1.8	356.5	2.0	397.5	2.0	384.4
2	3.4	0.9	267	1.7	506	1.7	505.6	1.9	562.2	1.7	511
1	1.7	0.7	430	1.5	893	1.5	882.5	1.6	953.5	1.5	897.1

Table - Cuttings effect (sand 0.6-0.71 mm) on fluid rheology.

Sand v%		0%		1%		2%	
RPM	S.R. 1/s	SS (Pa)	Vis (cP)	SS (Pa)	Vis (cP)	SS (Pa)	Vis (cP)
600	1021.38	10.4	10.2	13.2	12.9	13.8	13.5
300	510.69	7.3	14.2	9.7	19	11.7	23
200	340.46	5.8	17	8.2	24	10.2	30
100	170.23	4.0	23.6	5.4	32	6.5	38
60	102.14	3.2	31.8	3.9	37.7	4.6	45
30	51.07	2.6	51.7	3.4	67.1	3.5	68
20	34.05	2.3	67.7	2.9	86.4	3.3	95.9
10	17.02	1.8	103	2.2	130	2.2	130.5
6	10.21	1.3	128	2.0	200	2.9	280
3	5.11	0.9	185	1.8	350	1.5	295.9
2	3.4	0.9	267	1.4	400	1.3	395.9
1	1.7	0.7	430	1.1	670	1.2	692.3

4. **0.3% XCD polymer fluid**

Table - Cuttings effect (sand 0.2-0.3 mm) on fluid rheology.

Sand v%		0%		1%		2%		3%		4%		5%		8%		10%	
RPM	S.R. 1/s	SS (Pa)	Vis (cP)	SS (Pa)	Vis (cP)	SS (Pa)	Vis (cP)	SS (Pa)	Vis (cP)	SS (Pa)	Vis (cP)	SS (Pa)	Vis (cP)	SS (Pa)	Vis (cP)	SS (Pa)	Vis (cP)
600	1021.38	13.6	13.3	14.9	14.6	14.8	14.5	15.2	14.9	16.8	16.4	16.6	16.3	18.0	17.6	18.9	18.5
300	510.69	9.7	19	10.2	20	11.4	22.3	12.4	24.3	12.6	24.7	14.0	27.4	14.6	28.5	14.8	29
200	340.46	8.0	23.6	8.3	24.3	9.1	26.6	9.4	27.7	10.1	29.6	10.8	31.6	12.4	36.3	13.0	38.2
100	170.23	6.0	35	6.2	36.3	6.6	39	7.0	41.1	7.2	42.4	7.6	44.9	9.1	53.3	9.2	54.2
60	102.14	4.9	48	5.0	48.8	5.2	50.6	5.2	51	5.5	54	5.5	53.4	6.3	61.4	6.5	63.5
30	51.07	3.9	75.8	4.2	81.7	4.1	80.6	4.1	80.8	3.9	77.3	4.2	83.1	4.7	92	4.9	95.8
20	34.05	3.4	99	3.7	107.9	3.5	103.7	3.3	95.6	3.1	92.5	3.7	110.1	4.1	121.8	4.4	129.1
10	17.02	2.9	169	2.9	168.2	2.8	163	2.6	154.8	2.7	156.6	2.9	169.6	3.2	186.5	3.6	209.8
6	10.21	2.5	240	2.6	251.9	2.4	232.5	2.3	221.5	2.3	225.1	2.6	252.3	2.8	277.7	3.0	296.9
3	5.11	2.1	419	2.0	396	2.0	387.8	1.9	378.7	2.0	383.4	2.1	410.8	2.3	452	2.6	511.1
2	3.4	2.0	590	1.9	566.9	1.9	553.1	1.9	547.9	1.9	554.7	2.0	578.4	2.1	605	2.4	709
1	1.7	1.2	725	1.8	1047.4	1.7	1022.4	1.7	1020.6	1.8	1032.8	1.8	1052.1	1.9	1100	2.0	1182

Table - Cuttings effect (sand 0.3-0.4 mm) on fluid rheology.

Sand v%		0%		1%		2%		3%		4%		5%		8%		10%	
RPM	S.R. 1/s	SS (Pa)	Vis (cP)	SS (Pa)	Vis (cP)	SS (Pa)	Vis (cP)	SS (Pa)	Vis (cP)	SS (Pa)	Vis (cP)	SS (Pa)	Vis (cP)	SS (Pa)	Vis (cP)	SS (Pa)	Vis (cP)
600	1021.38	13.6	13.3	14.2	13.9	15.0	14.7	15.1	14.8	15.7	15.4	19.9	19.5	19.7	19.3	20.0	19.6
300	510.69	9.7	19	10.7	21	11.5	22.6	12.4	24.3	12.1	23.7	13.7	26.9	14.1	27.7	15.2	29.7
200	340.46	8.0	23.6	7.9	23.3	9.0	26.5	9.7	28.5	9.5	28	10.6	31.2	11.4	33.6	12.5	36.7
100	170.23	6.0	35	6.4	37.7	6.7	39.4	7.0	41.3	6.8	40	7.7	45.4	7.8	45.7	9.0	53
60	102.14	4.9	48	5.1	49.6	5.3	51.6	5.3	51.8	5.3	52	5.5	54.3	6.0	58.5	6.4	62.4
30	51.07	3.9	75.8	4.2	82.7	4.3	84.9	4.1	80.8	4.2	82	3.9	76.5	4.4	86.6	4.9	95.7
20	34.05	3.4	99	3.8	112.7	4.0	117.1	3.7	109.9	3.8	111.8	3.6	107	0.5	15.1	4.1	120.2
10	17.02	2.9	169	3.5	204.5	3.6	211.3	3.4	199.6	3.5	203.3	3.4	200	3.6	209.2	3.6	213
6	10.21	2.5	240	3.4	329	3.4	331.6	3.1	306.5	3.3	319.5	3.1	307	3.4	330	3.4	334
3	5.11	2.1	419	2.8	548	2.9	575	2.6	500.8	2.7	531	2.7	527	3.1	597	3.1	607
2	3.4	2.0	590	2.5	745	2.7	791	2.4	710.2	2.5	723	2.4	720	2.8	832	3.0	870
1	1.7	1.2	725	1.9	1133	2.0	1193	2.0	1150	2.0	1170	1.8	1070	2.5	1452	2.6	1554

Table - Cuttings effect (sand 0.4-0.5 mm) on fluid rheology.

Sand v%		0%		1%		2%		3%		4%		5%		8%		10%	
RPM	S.R. 1/s	SS (Pa)	Vis (cP)	SS (Pa)	Vis (cP)	SS (Pa)	Vis (cP)	SS (Pa)	Vis (cP)	SS (Pa)	Vis (cP)	SS (Pa)	Vis (cP)	SS (Pa)	Vis (cP)	SS (Pa)	Vis (cP)
600	1021.38	13.6	13.3	14.3	14	14.8	14.5	15.7	15.4	16.6	16.3	16.9	16.5	17.7	17.3	19.7	19.3
300	510.69	9.7	19	10.5	20.6	10.9	21.3	12.2	23.8	12.7	24.9	13.4	26.2	13.9	27.3	15.1	29.6
200	340.46	8.0	23.6	8.7	25.5	9.0	26.4	9.5	28	10.0	29.5	10.1	29.7	11.4	33.5	12.3	36.1
100	170.23	6.0	35	6.7	39.2	6.9	40.3	7.0	41.4	7.4	43.6	7.5	43.9	8.3	48.5	8.5	50.1
60	102.14	4.9	48	5.2	50.6	5.3	51.5	5.2	51	5.4	52.9	5.2	51.3	6.2	60.8	6.2	60.9
30	51.07	3.9	75.8	4.5	88.2	4.5	87.4	4.4	86.6	4.3	85.1	4.3	83.9	4.6	90.2	4.6	89.9
20	34.05	3.4	99	4.3	125.8	4.2	123.3	4.1	121.7	4.1	120.8	4.0	117.9	4.1	121.7	4.2	122
10	17.02	2.9	169	3.9	231.9	3.7	219.1	3.7	215.8	3.6	214.1	3.6	211.3	3.7	219.4	3.8	225.4
6	10.21	2.5	240	3.6	353.8	3.3	324.4	3.3	323.1	3.3	320	3.3	325.4	3.5	343.9	3.5	342.9
3	5.11	2.1	419	2.7	532.9	2.4	469.4	2.4	471	2.4	466	2.8	542.5	3.0	584.2	3.1	606.8
2	3.4	2.0	590	2.4	701.5	2.3	664.4	2.2	637.6	2.2	651	2.5	726	2.8	821.5	2.8	836
1	1.7	1.2	725	2.0	1201	1.9	1123	1.9	1139.5	1.9	1128.7	2.0	1160	2.1	1242.3	2.1	1256.9

Table - Cuttings effect (sand 0.5-0.6 mm) on fluid rheology.

Sand v%		0%		1%		2%		3%		4%		5%		8%	
RPM	S.R. 1/s	SS (Pa)	Vis (cP)	SS (Pa)	Vis (cP)	SS (Pa)	Vis (cP)	SS (Pa)	Vis (cP)	SS (Pa)	Vis (cP)	SS (Pa)	Vis (cP)	SS (Pa)	Vis (cP)
600	1021.38	13.6	13.3	14.3	14	14.6	14.3	15.3	15	16.3	16	17.0	16.6	19.9	19.5
300	510.69	9.7	19	11.3	22.1	11.0	21.5	12.8	25.1	14.5	28.3	15.3	30	17.9	35
200	340.46	8.0	23.6	8.7	25.6	8.9	26.2	9.8	28.9	10.1	29.6	10.9	32	12.3	36
100	170.23	6.0	35	6.7	39.6	6.8	40	6.9	40.5	6.9	40.6	8.3	48.7	9.1	53.2
60	102.14	4.9	48	5.6	54.6	5.4	52.4	6.1	60	5.4	53.3	5.3	52.3	6.3	61.3
30	51.07	3.9	75.8	4.3	84.7	4.1	81.1	4.2	82.7	4.5	88.8	4.3	84.2	4.4	86
20	34.05	3.4	99	4.0	116.8	3.8	112.7	3.9	115.3	3.9	116	3.8	112.8	4.0	118.2
10	17.02	2.9	169	3.6	210	3.4	199	3.4	199.2	3.5	204.6	3.4	201.2	3.4	201
6	10.21	2.5	240	3.3	321.6	3.5	341.2	3.3	320	3.2	312	3.1	300	3.1	299
3	5.11	2.1	419	2.8	540	2.6	509	2.6	509.5	2.7	533	2.8	550	2.6	517.6
2	3.4	2.0	590	2.2	644.5	2.4	700	2.4	715	2.6	750	2.3	677	2.2	650.6
1	1.7	1.2	725	2.0	1167	2.0	1167	1.7	1026	2.2	1286	2.0	1185	2.0	1191

Table - Cuttings effect (sand 0.6-0.71 mm) on fluid rheology.

Sand v%		0%		1%		2%		3%		4%	
RPM	S.R. 1/s	SS (Pa)	Vis (cP)	SS (Pa)	Vis (cP)	SS (Pa)	Vis (cP)	SS (Pa)	Vis (cP)	SS (Pa)	Vis (cP)
600	1021.38	13.6	13.3	13.8	13.5	15.9	15.6	16.3	16	18.8	18.4
300	510.69	9.7	19	11.7	23	13.3	26	15.3	30	15.3	30
200	340.46	8.0	23.6	9.1	26.8	10.0	29.3	10.2	30	11.9	35
100	170.23	6.0	35	6.2	36.6	6.5	38.4	6.9	40.8	7.5	44
60	102.14	4.9	48	5.3	52	5.6	54.4	5.6	55	5.3	52
30	51.07	3.9	75.8	4.0	78.7	4.1	80.7	4.5	87.6	4.0	78.8
20	34.05	3.4	99	3.4	100.3	3.5	103.4	3.9	114	3.9	113.7
10	17.02	2.9	169	2.9	168.5	2.9	172.5	3.0	178	3.0	173.5
6	10.21	2.5	240	2.6	257.5	2.6	253.6	2.9	281	3.1	300
3	5.11	2.1	419	2.3	441.3	2.4	468.5	2.2	425	2.0	400
2	3.4	2.0	590	2.9	842.3	2.9	850	2.0	600	3.1	900
1	1.7	1.2	725	1.5	905.3	1.9	1100	1.7	1000	2.1	1250

Table - Cuttings effect (sand 0.71-0.85 mm) on fluid rheology.

Sand v%		0%		1%	
RPM	S.R. 1/s	SS (Pa)	Vis (cP)	SS (Pa)	Vis (cP)
600	1021.38	13.6	13.3	14.3	14
300	510.69	9.7	19	11.5	22.5
200	340.46	8.0	23.6	9.2	27
100	170.23	6.0	35	7.2	42.1
60	102.14	4.9	48	6.1	60
30	51.07	3.9	75.8	4.6	90
20	34.05	3.4	99	3.6	105
10	17.02	2.9	169	4.2	245
6	10.21	2.5	240	2.9	280
3	5.11	2.1	419	2.6	500
2	3.4	2.0	590	2.9	850
1	1.7	1.2	725	2.1	1250

5. 0.35% XCD polymer fluid

Table - Cuttings effect (sand 0.2-0.3 mm) on fluid rheology.

Sand v%		0%		1%		2%		3%		4%		5%		8%		10%	
RPM	S.R. 1/s	SS (Pa)	Vis (cP)	SS (Pa)	Vis (cP)	SS (Pa)	Vis (cP)	SS (Pa)	Vis (cP)	SS (Pa)	Vis (cP)	SS (Pa)	Vis (cP)	SS (Pa)	Vis (cP)	SS (Pa)	Vis (cP)
600	1021.38	16.1	15.8	16.2	15.9	17.4	17	17.6	17.2	18.3	17.9	18.9	18.5	20.2	19.8	22.2	21.7
300	510.69	11.7	23	11.4	22.4	13.4	26.3	13.3	26	13.7	26.9	14.9	29.1	16.3	31.9	17.9	35
200	340.46	9.9	29	9.5	27.9	11.3	33.2	10.2	30	11.3	33.3	12.9	37.8	14.4	42.3	15.9	46.7
100	170.23	7.7	45	7.6	44.7	7.8	46	7.8	45.6	8.7	51.4	9.4	55.2	9.9	58	10.2	60
60	102.14	6.4	62.5	6.3	61.8	6.1	60	6.6	64.9	7.2	70.3	6.4	62.4	6.5	63.6	7.7	75
30	51.07	5.2	101	5.2	102.2	4.9	96.6	5.4	106.5	5.5	107	5.2	102.6	6.4	124.6	6.0	118
20	34.05	4.4	130	4.6	134.9	4.4	128.3	4.8	142	4.7	137.4	4.6	135	5.5	162.3	5.4	160
10	17.02	3.5	206	3.8	226	3.5	208.1	4.1	241	3.9	231	3.9	230	4.4	261.2	4.5	264
							232.5										
6	10.21	3.3	319	3.4	336	3.1	301	3.7	365	3.4	330	3.4	337	4.0	392.8	4.1	406
3	5.11	2.8	546	2.8	540	2.6	508	3.0	596	2.8	547	2.8	555	3.2	630.5	3.5	678
2	3.4	2.7	782	2.6	766	2.4	716	2.9	842	2.6	766	2.7	784	3.0	884.9	3.2	930
1	1.7	2.2	1320	2.2	1320	1.9	1136	2.4	1430	2.1	1227	2.2	1316	2.6	1502	2.7	1579

Table - Cuttings effect (sand 0.3-0.4 mm) on fluid rheology.

Sand v%		0%		1%		2%		3%		4%		5%		8%		10%	
RPM	S.R. 1/s	SS (Pa)	Vis (cP)	SS (Pa)	Vis (cP)	SS (Pa)	Vis (cP)	SS (Pa)	Vis (cP)	SS (Pa)	Vis (cP)	SS (Pa)	Vis (cP)	SS (Pa)	Vis (cP)	SS (Pa)	Vis (cP)
600	1021.38	16.1	15.8	16.0	15.7	16.5	16.2	17.9	17.5	18.1	17.7	18.9	18.5	20.2	19.8	21.7	21.2
300	510.69	11.7	23	11.4	22.4	12.0	23.5	13.3	26.1	14.1	27.7	14.1	27.7	15.3	30	16.5	32.4
200	340.46	9.9	29	9.5	28	9.5	28	11.2	32.8	11.7	34.3	11.7	34.5	13.2	38.7	14.0	41.2
100	170.23	7.7	45	7.7	45.1	7.2	42.2	8.5	49.8	8.8	51.6	8.6	50.5	10.1	59.3	10.2	60.2
60	102.14	6.4	62.5	6.1	60	6.0	59	6.4	63	6.8	66.7	6.5	63.7	8.1	79	8.2	80
30	51.07	5.2	101	5.2	101.7	5.1	100	5.2	101	5.1	100	5.2	101.3	6.1	120	6.5	128
20	34.05	4.4	130	4.4	130.4	4.4	130	4.3	126	4.3	126.3	4.5	132	4.6	136	5.4	158
10	17.02	3.5	206	3.8	220.5	3.8	221	3.6	213	3.5	208	3.7	216.5	4.3	252	4.4	259
6	10.21	3.3	319	3.2	310	3.2	318	3.2	309	3.3	319.5	3.4	329	3.8	372	3.9	378
3	5.11	2.8	546	2.6	509	2.5	498	2.4	460	2.3	450	2.6	505	3.3	637	3.2	635
2	3.4	2.7	782	1.8	517	2.3	691	2.2	637	2.3	665	2.3	671	2.9	866	3.0	875
1	1.7	2.2	1320	1.6	963	1.7	997	1.6	927	1.6	926	1.8	1049	1.6	927	2.3	1345.5

Table - Cuttings effect (sand 0.4-0.5 mm) on fluid rheology.

Sand v%		0%		1%		2%		3%		4%		5%		8%		10%	
RPM	S.R. 1/s	SS (Pa)	Vis (cP)	SS (Pa)	Vis (cP)	SS (Pa)	Vis (cP)	SS (Pa)	Vis (cP)	SS (Pa)	Vis (cP)	SS (Pa)	Vis (cP)	SS (Pa)	Vis (cP)	SS (Pa)	Vis (cP)
600	1021.38	16.1	15.8	17.0	16.6	17.2	16.8	17.7	17.3	18.2	17.8	18.5	18.1	20.3	19.9	23.2	22.7
300	510.69	11.7	23	12.0	23.4	12.4	24.2	12.9	25.2	13.7	26.8	14.1	27.6	14.8	29	17.4	34
200	340.46	9.9	29	10.2	30.1	10.3	30.2	10.8	31.6	11.5	33.7	11.6	34.1	12.3	36.2	14.5	42.5
100	170.23	7.7	45	7.8	45.6	8.0	47.1	7.1	41.5	8.7	51.2	8.7	51.1	9.7	57.1	11.1	65
60	102.14	6.4	62.5	6.8	66.7	6.9	67.9	7.0	68.4	7.3	71.4	6.9	67.8	7.8	76	8.8	86
30	51.07	5.2	101	5.6	110	5.7	112.2	5.7	112.3	5.8	113.3	5.4	105.5	5.9	115	6.7	132
20	34.05	4.4	130	5.0	147.5	5.0	148	5.0	147	5.0	148	4.9	142.8	5.0	148	5.9	173
10	17.02	3.5	206	4.3	251	4.3	253.5	4.3	250	4.3	250	4.1	242	4.3	252	5.1	300
6	10.21	3.3	319	3.9	381	4.0	394	4.0	392	4.0	388	3.8	377	4.0	388	4.5	440
3	5.11	2.8	546	3.2	626	3.2	636	3.2	635	3.3	647	3.1	615	3.1	616	3.9	772
2	3.4	2.7	782	2.9	856.5	3.0	876.5	2.9	861	2.9	865	2.9	845	2.9	855	3.9	1147
1	1.7	2.2	1320	2.4	1419.2	2.5	1448	2.4	1389	2.3	1380	2.3	1334	2.3	1361	3.0	1738

Table - Cuttings effect (sand 0.5-0.6 mm) on fluid rheology.

Sand v%		0%		1%		2%		3%		4%		5%		8%		10%	
RPM	S.R. 1/s	SS (Pa)	Vis (cP)	SS (Pa)	Vis (cP)	SS (Pa)	Vis (cP)	SS (Pa)	Vis (cP)	SS (Pa)	Vis (cP)	SS (Pa)	Vis (cP)	SS (Pa)	Vis (cP)	SS (Pa)	Vis (cP)
600	1021.38	16.1	15.8	18.5	18.1	17.4	17	17.8	17.4	18.2	17.8	21.4	21	22.5	22	22.5	22
300	510.69	11.7	23	12.9	25.3	13.8	27	14.6	28.5	14.8	29	16.3	32	16.3	32	16.9	33
200	340.46	9.9	29	10.3	30.3	11.1	32.5	11.1	32.5	11.4	33.6	12.1	35.4	13.3	39	13.3	39
100	170.23	7.7	45	7.8	46	7.9	46.7	8.9	52.5	9.1	53.4	10.4	61	9.5	56	9.7	57
60	102.14	6.4	62.5	6.7	65.2	6.8	67	7.3	71	7.4	72	7.0	69	7.2	70.4	7.3	71
30	51.07	5.2	101	5.3	103	5.6	110	5.4	105	5.5	107	5.6	110	5.7	111	5.6	110
20	34.05	4.4	130	4.7	139	4.9	145	4.6	136.3	4.7	139	4.8	140	5.0	148	4.8	142
10	17.02	3.5	206	4.1	243	4.3	250	4.0	237	4.0	236.5	4.3	252	4.4	256	4.1	240
6	10.21	3.3	319	3.8	372	3.9	386	3.7	360	3.7	363	3.6	349	3.8	376	3.8	372
3	5.11	2.8	546	2.7	532	3.2	618	2.7	530	2.7	535	2.7	536	3.4	662	3.4	659
2	3.4	2.7	782	2.9	850	2.9	850	2.9	867	3.1	900	2.5	740	2.7	795	3.1	924
1	1.7	2.2	1320	2.4	1400	2.4	1400	2.2	1300	2.3	1350	2.2	1322	2.6	1500	2.6	1500

Table - Cuttings effect (sand 0.6-0.71 mm) on fluid rheology.

Sand v%		0%		1%		2%		3%		4%		5%	
RPM	S.R. 1/s	SS (Pa)	Vis (cP)	SS (Pa)	Vis (cP)	SS (Pa)	Vis (cP)	SS (Pa)	Vis (cP)	SS (Pa)	Vis (cP)	SS (Pa)	Vis (cP)
600	1021.38	16.1	15.8	16.9	16.5	18.4	18	18.6	18.2	21.7	21.2	23.5	23
300	510.69	11.7	23	12.2	23.8	13.7	26.8	14.3	28	17.1	33.5	16.6	32.5
200	340.46	9.9	29	10.4	30.5	11.3	33.2	11.5	33.7	11.6	34	12.9	38
100	170.23	7.7	45	7.7	45.3	9.4	55.5	8.3	48.5	9.2	54	9.9	58
60	102.14	6.4	62.5	6.5	64	6.9	68	7.3	71.2	6.8	67	7.0	69
30	51.07	5.2	101	5.6	109	5.7	111	5.7	111	6.0	118	6.1	119
20	34.05	4.4	130	5.4	159	5.3	155	5.7	166	5.3	156	5.5	161
10	17.02	3.5	206	4.3	250	4.2	249	4.5	265	4.6	270	4.7	275

Table - Cuttings effect (sand 0.71-0.85 mm) on fluid rheology.

Sand v%		0%		1%		2%		3%	
RPM	S.R. 1/s	SS (Pa)	Vis (cP)	SS (Pa)	Vis (cP)	SS (Pa)	Vis (cP)	SS (Pa)	Vis (cP)
600	1021.38	16.1	15.8	18.1	17.7	18.4	18	20.4	20
300	510.69	11.7	23	15.3	30	15.8	31	18.4	36
200	340.46	9.9	29	12.3	36	11.9	35	13.3	39
100	170.23	7.7	45	8.3	49	8.3	49	11.7	69

Table - Cuttings effect (sand 0.85-0.1 mm) on fluid rheology.

Sand v%		0%		1%		2%	
RPM	S.R. 1/s	SS (Pa)	Vis (cP)	SS (Pa)	Vis (cP)	SS (Pa)	Vis (cP)
600	1021.38	16.1	15.8	18.6	18.2	21.4	21
300	510.69	11.7	23	14.3	28	19.4	38
200	340.46	9.9	29	10.6	31	13.6	40
100	170.23	7.7	45	7.8	46	8.9	52

6. 0.4% XCD polymer fluid

Table - Cuttings effect (sand 0.2-0.3 mm) on fluid rheology.

Sand v%		0%		1%		2%		3%		4%		5%		8%		10%	
RPM	S.R. 1/s	SS (Pa)	Vis (cP)	SS (Pa)	Vis (cP)	SS (Pa)	Vis (cP)	SS (Pa)	Vis (cP)	SS (Pa)	Vis (cP)	SS (Pa)	Vis (cP)	SS (Pa)	Vis (cP)	SS (Pa)	Vis (cP)
600	1021.38	17.5	17.1	18.4	18	18.4	18	18.8	18.4	19.4	19	19.9	19.5	22.0	21.5	22.2	21.7
300	510.69	13.3	26	14.0	27.5	14.0	27.4	14.5	28.4	15.2	29.7	16.4	32.1	17.6	34.4	18.5	36.2
200	340.46	11.5	33.8	11.8	34.6	11.7	34.5	12.0	35.1	13.3	39.1	14.0	41	15.5	45.6	16.2	47.6
100	170.23	9.4	55	9.6	56.6	9.7	56.9	9.6	56.4	10.7	62.8	11.5	67.4	12.7	74.5	13.6	80
60	102.14	8.1	79.6	8.3	81.5	8.4	82.2	8.3	81.7	9.2	90.4	9.7	95	10.7	105	11.4	112
30	51.07	6.7	131.5	6.8	133.6	6.8	134	6.8	133	7.6	149	7.7	151	8.8	173	9.4	184
20	34.05	6.4	189.4	6.5	190.5	6.5	192	6.4	188	6.8	200.5	6.8	199	7.7	226	8.0	236
10	17.02	5.3	311.2	5.2	304.1	5.2	304	5.2	304	6.2	362	6.1	361	6.6	385	6.7	394
6	10.21	4.9	477.2	4.8	470	4.9	478	4.9	484	5.1	503	5.1	498	6.2	604	6.3	621
3	5.11	4.2	825.9	4.3	843	4.3	844	4.3	850	4.8	935	4.7	923	5.0	977	0.5	100
2	3.4	3.9	1145.8	3.9	1134	3.8	1122	3.8	1125	4.5	1325	4.5	1317	4.8	1425	4.9	1447
1	1.7	3.4	1976.3	3.3	1963	3.4	1978	3.4	1983	3.5	2048	3.5	2050	4.3	2530	4.5	2654

Table - Cuttings effect (sand 0.3-0.4 mm) on fluid rheology.

Sand v%		0%		1%		2%		3%		4%		5%		8%		10%	
RPM	S.R. 1/s	SS (Pa)	Vis (cP)	SS (Pa)	Vis (cP)	SS (Pa)	Vis (cP)	SS (Pa)	Vis (cP)	SS (Pa)	Vis (cP)	SS (Pa)	Vis (cP)	SS (Pa)	Vis (cP)	SS (Pa)	Vis (cP)
600	1021.38	17.5	17.1	17.7	17.3	18.1	17.7	18.4	18	19.1	18.7	19.3	18.9	19.9	19.5	21.7	21.2
300	510.69	13.3	26	13.5	26.4	13.9	27.2	14.6	28.5	14.8	29	15.4	30.2	16.8	32.8	18.5	36.2
200	340.46	11.5	33.8	11.3	33.2	11.6	34	12.5	36.6	12.6	37.1	13.0	38.3	14.0	41.2	15.8	46.4
100	170.23	9.4	55	9.2	54.3	9.4	55.5	9.8	57.5	10.0	58.6	10.3	60.5	11.1	65.4	12.9	75.9
60	102.14	8.1	79.6	8.1	79.7	8.2	80.5	8.6	84.4	8.8	86.2	8.9	87	9.2	89.6	10.6	104
30	51.07	6.7	131.5	6.6	130	6.8	134	7.1	140	7.3	142	7.1	140	7.8	152	8.7	170
20	34.05	6.4	189.4	5.8	169	6.0	175	6.4	188	6.6	193	6.6	195	7.0	205	7.6	224
10	17.02	5.3	311.2	4.9	290	5.1	299	5.1	299	5.5	323	5.6	331	5.9	346	6.5	384
6	10.21	4.9	477.2	4.6	454	4.8	470	4.7	465	4.9	477	4.8	467	5.1	495	5.4	529
3	5.11	4.2	825.9	4.4	855	4.5	883	4.4	860	4.5	882	4.3	850	4.6	902	4.8	940
2	3.4	3.9	1145.8	4.3	1250	4.4	1286	4.3	1258	4.3	1274	4.2	1225	4.4	1295	4.6	1360
1	1.7	3.4	1976.3	3.8	2250	4.1	2394	3.9	2292	4.0	2345	3.7	2200	4.1	2417	4.3	2500

Table - Cuttings effect (sand 0.4-0.5 mm) on fluid rheology.

Sand v%		0%		1%		2%		3%		4%		5%		8%		10%	
RPM	S.R. 1/s	SS (Pa)	Vis (cP)	SS (Pa)	Vis (cP)	SS (Pa)	Vis (cP)	SS (Pa)	Vis (cP)	SS (Pa)	Vis (cP)	SS (Pa)	Vis (cP)	SS (Pa)	Vis (cP)	SS (Pa)	Vis (cP)
600	1021.38	17.5	17.1	17.7	17.3	18.5	18.1	18.6	18.2	18.7	18.3	19.1	18.7	20.3	19.9	20.9	20.5
300	510.69	13.3	26	13.6	26.6	14.9	29.1	14.9	29.1	15.1	29.5	15.8	31	17.4	34	18.4	36
200	340.46	11.5	33.8	11.3	33.3	12.6	37.1	12.6	36.9	12.8	37.5	12.8	37.5	14.6	43	15.0	44
100	170.23	9.4	55	9.3	54.4	10.1	59.2	9.7	56.7	10.0	58.9	10.0	59	11.2	66	11.9	70
60	102.14	8.1	79.6	8.2	80	8.7	85	8.3	81.6	8.8	85.7	8.8	86.4	9.6	94	10.0	98
30	51.07	6.7	131.5	7.0	138	7.4	144	7.3	142	7.3	142	7.4	144	8.0	157	8.2	161
20	34.05	6.4	189.4	6.5	190	6.8	199	6.6	195	6.6	193	6.7	196	7.2	210	7.6	224
10	17.02	5.3	311.2	5.5	323	5.6	330	5.6	327	5.5	324	5.7	332	6.1	358	6.3	372
6	10.21	4.9	477.2	5.1	496	5.2	514	5.2	510	5.1	504	5.3	515	5.4	529	5.6	550
3	5.11	4.2	825.9	4.1	812	4.3	849	4.2	826	4.2	815	4.9	963	4.8	945	5.1	990
2	3.4	3.9	1145.8	3.9	1156	4.0	1180	3.9	1160	3.9	1149	4.1	1210	4.3	1266	5.1	1500
1	1.7	3.4	1976.3	3.6	2130	3.6	2136	3.6	2120	3.6	2097	3.6	2140	4.3	2500	4.7	2750

Table - Cuttings effect (sand 0.5-0.6 mm) on fluid rheology.

Sand v%		0%		1%		2%		3%		4%		5%		8%		10%	
RPM	S.R. 1/s	SS (Pa)	Vis (cP)	SS (Pa)	Vis (cP)	SS (Pa)	Vis (cP)	SS (Pa)	Vis (cP)	SS (Pa)	Vis (cP)	SS (Pa)	Vis (cP)	SS (Pa)	Vis (cP)	SS (Pa)	Vis (cP)
600	1021.38	17.5	17.1	17.9	17.5	18.3	17.9	18.6	18.2	19.3	18.9	19.8	19.4	20.7	20.3	22.0	21.5
300	510.69	13.3	26	14.6	28.5	14.8	29	14.9	29.1	15.5	30.4	16.9	33	17.9	35	20.9	41
200	340.46	11.5	33.8	11.6	34.1	11.7	34.5	12.0	35.3	12.4	36.3	12.6	37	12.9	38	15.3	45
100	170.23	9.4	55	9.2	54.1	9.3	54.7	9.6	56.3	10.4	61	10.2	60	10.7	63	11.7	69
60	102.14	8.1	79.6	8.0	78.6	8.2	80	8.3	81.5	8.6	84	8.1	79	8.7	85	9.3	91
30	51.07	6.7	131.5	6.7	131	6.9	135	6.9	136	7.4	145	6.9	135	7.5	147	7.1	140
20	34.05	6.4	189.4	6.2	181	6.3	185	6.0	177	6.8	200	6.9	203	6.3	186	6.6	195
10	17.02	5.3	311.2	5.5	324	5.6	328	5.6	330	5.7	334	5.3	310	5.8	338	5.4	320

Table - Cuttings effect (sand 0.6-0.71 mm) on fluid rheology.

Sand v%		0%		1%		2%		3%		4%		5%		8%	
RPM	S.R. 1/s	SS (Pa)	Vis (cP)	SS (Pa)	Vis (cP)	SS (Pa)	Vis (cP)	SS (Pa)	Vis (cP)	SS (Pa)	Vis (cP)	SS (Pa)	Vis (cP)	SS (Pa)	Vis (cP)
600	1021.38	17.5	17.1	17.9	17.5	18.9	18.5	19.9	19.5	20.9	20.5	23.0	22.5	25.5	25
300	510.69	13.3	26	13.3	26	15.3	30	16.9	33	17.9	35	19.4	38	22.0	43
200	340.46	11.5	33.8	11.2	33	11.9	35	12.6	37	12.9	38	13.6	40	18.7	55
100	170.23	9.4	55	9.4	55	10.0	59	10.4	61	9.1	53.5	10.7	63	15.3	90
60	102.14	8.1	79.6	8.7	85	9.0	88	8.8	86	8.9	87	8.7	85		
30	51.07	6.7	131.5	6.7	131	7.1	140	6.9	135	7.1	140				
20	34.05	6.4	189.4	6.1	180	5.9	173	6.6	195						
10	17.02	5.3	311.2	6.4	375	5.0	292								

Table - Cuttings effect (sand 0.71-0.85 mm) on fluid rheology.

Sand v%		0%		1%		2%		3%		4%		5%	
RPM	S.R. 1/s	SS (Pa)	Vis (cP)	SS (Pa)	Vis (cP)	SS (Pa)	Vis (cP)	SS (Pa)	Vis (cP)	SS (Pa)	Vis (cP)	SS (Pa)	Vis (cP)
600	1021.38	17.5	17.1	18.4	18	19.4	19	22.0	21.5	23.5	23	25.5	25
300	510.69	13.3	26	15.8	31	15.3	30	17.9	35	20.4	40	21.4	42
200	340.46	11.5	33.8	11.2	33	11.9	35	13.6	40	15.3	45	20.4	60
100	170.23	9.4	55	9.5	56	11.9	70	13.6	80	15.3	90		

Table - Cuttings effect (sand 0.85-1 mm) on fluid rheology.

Sand v%		0%		1%		2%		3%	
RPM	S.R. 1/s	SS (Pa)	Vis (cP)	SS (Pa)	Vis (cP)	SS (Pa)	Vis (cP)	SS (Pa)	Vis (cP)
600	1021.38	17.5	17.1	18.4	18	22.5	22	23.5	23
300	510.69	13.3	26	14.3	28	17.4	34	15.3	30
200	340.46	11.5	33.8	11.6	34	12.3	36	13.6	40
100	170.23	9.4	55	9.9	58	9.5	56	10.2	60